FORM, SORM and Simulation Techniques for Nonlinear Random Vibrations

by

Heonsang Koo and Armen Der Kiureghain

Report No. UCB/SEMM-2003/01

Structural Engineering, Mechanics & Materials
Department of Civil & Environmental Engineering
University of California, Berkeley

February 2003

ABSTRACT

Approximate solution methods for nonlinear random vibration problems are developed using computational tools of the time-invariant structural reliability theory. The basic framework of the approach is composed of: (1) representation of the input stochastic excitation in terms of a finite number of random variables, (2) formulation of each response statistic of interest in terms of one or more limit-state functions of the random variables, and (3) estimation of the response statistic using computational reliability tools.

An important step in the proposed approach is the finding of the design point, which is the point on the limit-state surface that is nearest to the origin in a transformed standard normal space. This point is usually found by solving a constrained optimization problem, requiring repeated computations of the limit-state function and its gradient. In this report, a new method for determining the excitation corresponding to the design point is presented. The basic idea starts from the finding that, for a linear oscillator subjected to a stationary Gaussian white-noise excitation, the "design-point excitation" is a linear function of the unit-impulse response function of the oscillator. Inspired by this idea, we investigate the dynamic characteristics of nonlinear oscillators by observing their free vibration motion and its mirror image. It is shown that for a nonlinear elastic single-degree-of-freedom (SDOF) oscillator subjected to a stationary Gaussian white noise, the design-point excitation is identical to the excitation that generates the mirror image of the free vibration response, when the oscillator is released from the target threshold. This idea is extended to general nonlinear systems, including systems having hysteretic behavior and multi-degree-of-freedom systems subjected to non-white and non-stationary excitation, for an approximate solution of the design-point excitation. The design-point excitation is the most likely realization of the stochastic excitation to produce a target response threshold.

The accuracy and effectiveness of solution tools such as the first-order reliability method (FORM), the second-order reliability method (SORM), and various sampling techniques are investigated in the context of nonlinear random vibration analysis. FORM is found to produce fairly accurate results for most moderately nonlinear random

vibration problems, particularly for high thresholds. SORM is found to produce unreliable results for certain nonlinear random vibration problems, because of rapid changes in the curvatures of the limit-state surface near the design point. Importance sampling using design points and sampling on the orthogonal plane are investigated as simulation techniques. Both are found to be far more efficient than the crude Monte Carlo simulation method. Sampling on the orthogonal plane is found to be at least as efficient as the importance sampling method; additionally, this method is effective for computing the mean out-crossing rate.

Simulation methods for computing the first-excursion probability of nonlinear random vibration response are investigated. Through discretization of the time axis, the first-excursion problem is represented as a series-system reliability problem and the corresponding probability is approximately computed by importance sampling and by sampling on the orthogonal plane. The method can account for broad classes of system nonlinearity, as well as for uncertainty in system properties. It is found that the sampling on the orthogonal plane is at least as efficient as the importance sampling method.

Lastly, an approximate representation of a narrowband Gaussian process in terms of discretized envelope and phase processes is explored. The Nataf distribution model is used to approximately describe the second- and higher-order joint distributions of the envelope and phase processes. With this formulation, the narrowband process can be represented with a relatively small number of random variables, which is convenient for simulation and FORM analysis. However, it is found that the adopted Nataf distribution introduces too large an error for reliability analysis by FORM.

The new methods developed in this report for FORM and sampling solution of random vibration problems significantly improve our ability to solve nonlinear problems, for which practical solution techniques are presently unavailable.

Table of Contents

List of Figures

List of Tables

Acknowledgement

Financial support from the Taisei Chair is acknowledged. The first author also acknowledges financial support from the Ministry of Construction and Transportation in Korean Government.

1 Introduction

1.1 Motivation

The analysis of structural response under dynamic loading is a major topic in structural engineering. The primary goal of the analysis lies in the prediction of failure conditions, so that the structure can be designed to prevent failures, or to minimize the likelihood of their occurrence. Since structures are designed to sustain much severe levels of load than under normal operating conditions, it is crucial to account for structural behavior near the failure states. Considering that structural failures usually occur under grossly nonlinear domains, it is essential to account for nonlinearity in the structural response to dynamic loading. Another aspect that must be considered is randomness in loads and uncertainty in structural properties. Examples of randomness can be observed in loads arising from natural phenomena, such as wind and earthquakes. Furthermore, uncertainty is present in such structural characteristics as material properties and member sizes. To properly account for the randomness in loads and uncertainty in structural characteristics, a probabilistic approach to the analysis of structural response to dynamic loading is necessary.

Nonlinear random vibration incorporates the above two aspects: nonlinearity and randomness. In nonlinear random vibration problems, the responses of a nonlinear vibrating system are determined probabilistically, when the system parameters and/or input excitation are described as random quantities. Nonlinear random vibration is useful in predicting the responses of structures such as buildings or bridges under earthquake or wind loading. Several solution methods have been developed for nonlinear random vibration problems. Most existing methods, unfortunately, are either computationally too expensive or are highly restrictive in their domains of application. A brief review of the most popular of these methods is presented in Section 1.2.

In this report, a recently developed solution method (Der Kiureghian and Li 1996a and 1996b) for nonlinear random vibration problems is investigated and further

developed. The basic idea is to convert the time-variant random vibration problem into a time-invariant structural reliability problem through a reformulation of the problem. To do that, we first discretize the continuous-parameter input random process and describe it by a finite number of random variables. One or more limit-state functions are then introduced to describe the reliability statistic of interest in the random vibration problem. With this reformulation, solution tools of classical structural reliability theory, such as the first- and second-order reliability methods (FORM and SORM) and various simulation techniques, can be used to solve the problem.

It turns out that, as in structural reliability, FORM provides a fairly good approximation for the random vibration problem near the tail regions of the underlying distributions. Furthermore, SORM and simulation techniques can be used to improve the FORM solution. As already demonstrated by Der Kiureghian and Li (1996a, 1996b) and Der Kiureghian (2000), the method can handle a wide variety of random vibration problems, including problems involving nonlinear systems, non-Gaussian excitation, and uncertain systems. It allows consideration of a variety of reliability measures, including statistics of crossing rates and the first-excursion probability. Furthermore, the method provides additional information in the form of the most likely realization of the excitation and the corresponding response with respect to any given event.

A crucial step of the proposed solution approach is to find the design point, which is the point on the limit-state surface that is nearest to the origin in the standard normal space. This is the point at which approximations to the limit-state surface are constructed, or based on which sampling distributions are selected. This point is usually found by solving a constrained optimization problem. Experience reveals that for a nonlinear problem, the time taken to find this solution increases in proportion to the degree of nonlinearity of the limit-state function and the number of random variables. Considering that several hundred random variables are typically generated as a result of the discretization of the input process, an efficient method for solving the nonlinear optimization problem is essential if the proposed method is to be effective in practice.

The motivation behind the present study has come from the need for improving the efficiency in solving the optimization problem to find the design point of a nonlinear random vibration problem. Such improvement will contribute to this method becoming a

practical method for solving nonlinear random vibration problems. Along the way, a number of other related problems have been identified and solved, as described in the following section

1.2 Objective and Scope

The objective of this report is to improve and further develop the first-order reliability method (FORM) as a solution technique for nonlinear random vibration problems, and to develop tools for refinement of the FORM solution. In addition to FORM, important sampling using design points and sampling in orthogonal plane are developed as solution techniques for nonlinear random vibration. Applications of these methods to a number of nonlinear random vibration problems are investigated, where important response statistics such as crossing rates and the first-excursion probability are determined and compared with either exact or Monte Carlo solutions. The problem of efficiently discretizing a narrow-band process through discretizing its envelope and phase processes is also explored.

The main step in solving a random vibration problem by FORM is the finding of the design point. As mentioned earlier, this requires solving a constrained optimization problem, which typically requires iterative numerical solutions of the dynamic response and its gradient. It is shown in this report that, for special classes of problems, the design point can be found by utilizing the dynamic characteristics of the system and without engaging iterative calculations to solve the optimization problem. This class includes linear or nonlinear elastic oscillators subjected to Gaussian white noise excitation.

In an early study having a different objective, Drenick (1970) found that the so called 'critical excitation' of a linear single-degree-of-freedom (SDOF) oscillator can be obtained directly from the mirror image of the unit impulse response function of the oscillator. The critical excitation is the excitation that causes a vibrating system to achieve maximum response for a given input energy norm. This result is based on the fact that the response of a linear system can be represented by a convolution integral of the excitation and the unit impulse response function of the system, i.e.

$x(t) = \int_0^t f(\tau)h(t-\tau)d\tau$, where $x(t)$ is the response of the system, $f(t)$ is the excitation, and $h(t)$ is the impulse response function. If the time axis is discretized, $x(t)$ can be seen as the inner product of two vectors resulting from the discretization of $f(\tau)$ and $h(t-\tau)$. Since the inner product of two vectors is maximized when they lie in the same direction, the maximum response is achieved when $f(\tau)$ is proportional to $h(t-\tau)$, which is the mirror image of the unit impulse response function. This idea has been used by Shinozuka (1970) in finding the critical excitation for a frequency band-limited excitation, and also extended to stochastic problems by Iyengar and Manohar (1987), Srinivasan *et al.* (1991), and Manohar and Sarkar (1995).

Quite independently, Der Kiureghian (2000) and Au and Beck (2001) found that the mirror-image of the unit-impulse response function also coincides with the design point of a linear system subjected to a Gaussian white noise, when it is treated in the context of FORM analysis. Unfortunately, this idea holds only for linear systems, since the convolution integral used above is the result of the superposition principle, which is one of the important characteristics of linear systems. For nonlinear problems, superposition does not work and the unit-impulse response function does not completely characterize the system. Therefore, the design point must be found through an iterative numerical algorithm. Considering that most problems related to structural safety are nonlinear, improvement in the efficiency of finding the design point is important for the convenient use of the first-order reliability method.

In this report a method is developed to directly find the design point or a point in its close neighborhood, without directly solving the required optimization problem. The idea behind the method comes from the solution of the design point for linear systems. As mentioned above, for a linear system, the design point is closely related to the unit-impulse response function, which represents the dynamic characteristic of the system. The design point of a nonlinear system is also related to its dynamic characteristics. However, for a nonlinear system the response to a unit impulse does not completely characterize the system. Instead, we find that the free vibration motion of a nonlinear vibrating system with prescribed initial conditions contains the requisite information about the system characteristics that is necessary for determining the design point. This is

reasonable, since a vibrating system behaves according to its own characteristic when there is no external intervention.

Based on the above idea, it is shown that for an elastic nonlinear SDOF system subjected to a Gaussian white noise excitation, the design point can be obtained directly from a single analysis of the free vibration response of the system with prescribed initial conditions. It is also shown that this idea can be extended to find a good approximation of the design point in general nonlinear problems, including hysteretic oscillators and multi-degree-of-freedom systems.

After finding the design point, we can readily calculate the FORM probability approximation. SORM or simulation techniques, such as importance sampling or sampling on the orthogonal plane, can be used for refinement of the FORM solution. However, experience shows that SORM is not a good refinement method for nonlinear random vibration problems due to the complex behavior of the limit-state surface near the design point. We also find that the directional simulation technique (Bjerager 1988) is not an efficient method for solving random vibration problems that typically involve large numbers of random variables.

In this report, the importance sampling method (Melchers 1989, Engelund and Rackwitz 1993) and the sampling on the orthogonal plane method (Hohenbichler and Rackwitz 1988, Engelund and Rackwitz 1993) are used as refinement tools of the FORM solution. These methods utilize the design point in different ways. While the design point is used as the center of the sampling density in the importance sampling method, the sampling on the orthogonal plane method takes the direction of the design point to set up the sampling plane. It is shown that the sampling on the orthogonal plane method is superior or at least equivalent to the importance sampling method in efficiency. It is also shown that the sampling on the orthogonal plane method can be effectively used in estimating the mean out-crossing rate.

Recently, Au and Beck (2001) developed an efficient simulation method for computing the first-excursion probability for linear systems. In this report, this method is extended to nonlinear problems that are characterized either by nonlinear systems, systems subjected to non-Gaussian excitation, or uncertain systems. After discretizing the time axis, the first-excursion problem can be interpreted as a series system reliability

problem made of a large number of components, each representing the state of the system at a discrete point in time. In the efficient simulation method developed by Au and Beck (2001), the sampling density is constructed as the sum of conditional normal densities, each defined over the failure domain of a component. For a linear problem, this can be done easily, since the limit-state surface for each component is a hyperplane, which is completely defined by the corresponding design point. This is not the case for nonlinear problems. In this report, we extend the Au and Beck method to nonlinear problems by implementing two simple modifications in their method and using the orthogonal plane sampling technique.

Lastly, an idea for efficient discretization of narrowband Gaussian processes is explored in this report. The idea is to represent the process in terms of discretized forms of its envelope and phase processes. Since the envelope and phase processes are much more slowly varying than the narrowband process itself, a relatively crude grid of time points is sufficient to accurately represent these processes than it would if the process itself were to be discretized. However, in order to discretize the envelope and phases processes, one needs higher-order probability distributions of these non-Gaussian processes. Although it is theoretically possible to derive these higher-order distributions, use of joint distributions beyond the second order is impractical. In this study we explore the possibility of using the Nataf distribution to describe the envelope and phase processes, in which case all the higher-order distributions are easily defined. With this approach, it turns out that the number of points necessary to discretize the narrowband process can be reduced by a factor of 10 or 20. However, the approximation introduced by the assumption of the Nataf distribution turns out to be too crude. The conclusion from this study is that, while the method can be used to efficiently simulate narrowband processes, it cannot be used with confidence to solve random vibration problems involving narrowband input processes.

1.3 Review of the State of the Arts

In this section, existing methods for the analysis of nonlinear random vibration are briefly reviewed. Also reviewed are recent developments related to FORM as a solution method of random vibration problems.

The existing solution methods for nonlinear random vibration problems include the Fokker-Planck-Kolmogorov (FPK) equation, stochastic averaging, equivalent linearization, equivalent nonlinearization, moment closure, the perturbation method and Monte Carlo simulation. Since Caughey (1971), a number of publications that cover comprehensive reviews of the methods of nonlinear random vibration have appeared (Roberts 1981, 1984, Roberts and Dunne 1988, Nigam 1983, Spanos and Lutes 1986, Roberts and Spanos 1990, Soong and Grigoriu 1993, Lin and Cai 1995, Lutes and Sarkani 1997, To 2000). Here, this literature is briefly reviewed in the context of application to structural engineering problems.

The method of the FPK equation is based on the theory of continuous Markov processes. It can be shown that the response of a system subjected to Gaussian white noise excitation can be represented as a Markov vector. Based on this finding, the PFK equation describes the probability density function of the response as a function of time. Solution methods of the FPK equation are described in several texts on random vibration (Nigam 1983, Soong and Grigoriu 1993, Soize 1994, Lin and Cai 1995, Lutes and Sarkani 1997, To 2000). Caughey and Ma (1982) have discussed the class of problems that can be solved by the FPK equation. Unfortunately, the class of problems exactly solvable by an appropriate FPK equation is quite limited. Due to the limitation in its application and the mathematical complexity of the formulation, the PFK equation method is not popular in structural engineering applications.

The stochastic averaging method (Stratonovitch 1964, Roberts 1986, 1989, Roberts and Spanos 1986, To 2000) has been widely used for problems involving lightly damped SDOF oscillators under wide-band random excitations. In this approach, the response process is decoupled into amplitude and phase processes, and a one-dimensional FPK equation is derived for each process. Reduction of the dimension in the FPK equation from two to one greatly simplifies the computation. The method is especially

useful in estimating reliability statistics of the first-excursion type (Roberts 1989). However, there are considerable difficulties in applying this method to systems with more than one degree of freedom.

The equivalent linearization method (Caughey 1963, Atalik and Utku 1976, Wen 1980, Baber and Wen 1981, Roberts and Spanos 1990) is widely used for the approximate solution of nonlinear random vibration problems due to its simplicity and adaptability to multi-degree-of-freedom systems. The main idea is to replace the nonlinear dynamical system by a linear system such that the mean square error in the response is minimized. The response statistics within the medium threshold region (say within one or two standard deviations of the mean) tend to match with exact results fairly well. However, the method fails to provide the effect of nonlinearity in the tail region. It has been shown that the error in the probability distribution increases exponentially after a threshold two or three times the standard deviation (Schueller and Bucher 1986). The method is useful in estimating the overall behavior of the response of a nonlinear system, but it is not appropriate for estimating the statistics of extreme response thresholds that are of interest in reliability studies. Nevertheless, this method remains one of the few methods that are applicable to structural engineering problems. Later in this report, we make comparisons of solutions obtained by this method with those obtained by the proposed FORM and sampling methods.

The equivalent nonlinearization method (Lutes 1970, Caughey 1986, Lin 1988, Zhu and Yu 1989) is a generalization of the equivalent linearization method. The basic idea is to replace the nonlinear system with another nonlinear system, for which an exact solution is available. The method partly makes up for the deficiency of the equivalent linearization method, providing improved solutions. However, the range of application of the method is quite restricted due to the limited number of nonlinear problems for which exact solutions are available.

In the moment closure technique (Kraichan 1962, Crandall 1973, 1980, 1985 Iyengar and Dash 1978), equations for the statistical moments of the response are derived either from the equation of motion or from the FPK equation. Since the moments generally have an infinite hierarchy of coupled equations, a closure technique has to be applied to obtain an approximate solution under an appropriate assumption on the

distribution. Though the accuracy can be improved by increasing the order of the closure, the complexity of the moment equations dramatically increases as the order of the closure or the number of degrees of freedom of the system increases.

The perturbation method (Crandall 1963) is used for the solution of weakly nonlinear systems. In this method, the solution of the nonlinear problem is represented by a series of solutions of linear random vibration problems. A small parameter is used to characterize the order of nonlinearity. In general, the calculations are lengthy and rapidly become prohibitive as the order of nonlinearity increases.

The Monte Carlo simulation method (Shinozuka 1972) can be applied to nonlinear random vibration problems without theoretical limitations. When applied to random vibration problems, this method requires that the continuous input excitation process be represented in a discrete form, a requirement that is shared by the proposed FORM approach investigated in this report. In general, higher accuracy is achieved by increasing the number of simulations. However, if a direct sampling approach is used, an enormous number of sample functions must be generated in order to accurately estimate statistics associated with high response thresholds. Though this method lacks computational efficiency, with increasing computer power and speed, it is becoming more popular. Furthermore, this method often provides the only available benchmark for checking the accuracy of approximate methods. Finally, the efficiency of the Monte Carlo simulation method can be drastically improved by using special sampling techniques. In this report, such improved sampling techniques, including importance sampling and sampling on the orthogonal plane, are investigated in connection with nonlinear random vibration problems.

The first-order reliability method (FORM) is a widely used approximate technique for solution of structural reliability problems that are defined in terms of random variables. Li and Der Kiureghian (1995) and Der Kiureghian and Li (1996a, 1996b) were the first to use this method to solve random vibration problems. As mentioned earlier, this method requires a discrete representation of the input excitation process, such that the random vibration problem can be defined in terms of random variables. More recently, Der Kiureghian (2000) used this formulation to make geometric interpretations of linear random vibration problems in the space of the discretized random

variables and to investigate the accuracy of FORM and SORM solutions for response to non-Gaussian excitation. Au and Beck (2000) used a similar approach to compute the first-excursion probability of a linear system subjected to a Gaussian excitation. Bucher (2000) and Macke (2000) used the design point obtained from the FORM solution of the random vibration problem to construct an importance sampling technique. A detailed description of this method is presented in Chapter 2. Further investigation, development and improvement of these methods are the main objectives of this report.

In the author's experience, finding the design point is the most critical step in the FORM solution of random vibration problems. Though independently developed, the procedure to find the design point has an analogy with that of the critical excitation originally introduced by Drenick (1970). Several researches, including Shinozuka (1970), Drenick (1973), Abdelrahman *et al.* (1978), Wang and Yun (1979), Iyengar and Manohar (1987), Srinivasan *et al.* (1991), and Takewaki (2002) have also contributed to this topic. Among these researchers, only Drenick (1977) and Takewaki (2002) addressed nonlinear problems. In these works, nonlinear systems are linearized in an appropriate sense and approximate solutions of the critical excitation are obtained. Considering that high accuracy is required in finding the design point, the approximate approaches that are used to obtain the critical excitations of nonlinear systems are found not to be useful in the FORM solution of nonlinear random vibration problems. Instead, new approaches for various classes of nonlinear problems are developed in this report.

1.4 Organization of the Report

Following this introductory chapter, the general methodology of the reliability formulation of random vibration problems is presented in Chapter 2. Topics presented include a brief review of FORM and SORM, reliability formulation of random vibration problems, discretization of a continuous-parameter random process, and specific formulations for several reliability statistics of interest.

The critical step in FORM is to find the design point. In Chapter 3, the design point excitation and the mirror image excitation of various dynamic systems are investigated as part of a strategy for finding the design point. A simple idea for

determining two design points needed for estimating the mean out-crossing rate is also presented.

Chapter 4 is devoted to the development and assessment of various methods for approximate solution of nonlinear random vibration problems by time-invariant reliability methods. As refinement to FORM estimates, importance sampling using design points and sampling on the orthogonal plane are considered. Several numerical examples are used to investigate the adequacy of FORM as a solution tool for nonlinear random vibration problems. The FORM solutions are compared with exact solutions, where such solutions are available, the solution obtained by the equivalent linearization method, and solutions obtained by simulation.

In Chapter 5, we consider the first-excursion probability problem for nonlinear systems. The efficient sampling method developed for a linear system by Au and Beck (2000) is extended to nonlinear problems. The method of sampling on the orthogonal plane is used for this purpose. An example is presented to demonstrate the efficiency and accuracy of the proposed method.

In chapter 6, we explore the possibility of representing a narrowband process in terms of discretized envelope and phase processes. Various properties of a narrowband process and its envelope and phase processes are investigated. The Nataf distribution is used to construct approximate joint distributions for the envelope and phase processes. The accuracy of this representation in the context of FORM analysis is investigated.

Chapter 7 presents a summary of the major findings of this study and describes areas where further study is needed.

2 Structural Reliability Formulation of Random Vibration Problems

2.1 Introduction

In this chapter, we describe how random vibration problems can be formulated and solved by the methods of structural reliability. First, a brief review is made of the methods of structural reliability, such as the first- and second-order reliability methods, FORM and SORM, algorithms for finding the design point, and reliability sensitivity measures. We then consider several important random vibration problems and formulate them as structural reliability problems following the earlier formulations of Der Kiureghian and Li (1996a and 1996b). A necessary step in this formulation is a discrete representation of the continuous stochastic input process, which we describe in some detail. The chapter ends with a brief discussion of available numerical methods for computing the response and its gradient for nonlinear dynamic systems.

2.2 Review of Structural Reliability Methods

The methods of structural reliability aim at computing the probability of failure of a structural system. The structural reliability problem is defined in terms of a set of basic random variables $\mathbf{x} = (x_1, \cdots, x_n)$ that describe the uncertain quantities affecting the state of the structure, and a set of m limit-state functions $g_k(\mathbf{x}, \theta)$, $k = 1, 2, \ldots, m$, that describe the failure event of interest, where $\theta = (\theta_1, \cdots, \theta_p)$ denotes a set of p deterministic parameters. The structural system is seen as composed of components, and the k-th limit-state function is defined such that $\{g_k(\mathbf{x}, \theta) \le 0\}$ denotes the event of failure of the k-th component in the outcome space of the random variables $\mathbf{x}$. The probability of failure of the system, denoted p_f, is given by

$$p_f = \int_{\mathcal{D}} f(\mathbf{x}) d\mathbf{x} \tag{2.1}$$

where $f(\mathbf{x})$ denotes the joint probability density function of $\mathbf{x}$, and $\mathcal{D}$ is the failure domain defined in terms of the limit-state functions $g_k(\mathbf{x},\theta)$, $k = 1, 2, \ldots, m$. Depending on how the failure domain is defined, the structural reliability problem falls into one of the following four categories:

- A structural "component" reliability problem is one in which the failure domain is defined by a single limit-state function, i.e.,

$$\mathcal{D} \equiv \{g(\mathbf{x},\theta) \le 0\} \tag{2.2}$$

- A structural "series system" reliability problem is one in which the failure domain is defined as the union of component failure events, i.e.,

$$\mathcal{D} \equiv \left\{ \bigcup_{k=1}^{m} g_k(\mathbf{x},\theta) \le 0 \right\} \tag{2.3}$$

  where m is the number of components in the series system. Thus, a series system fails if any of its components fail.

- A structural "parallel system" reliability problem is one in which the failure domain is defined as the intersection of component failure events, i.e.,

$$\mathcal{D} \equiv \left\{ \bigcap_{k=1}^{m} g_k(\mathbf{x},\theta) \le 0 \right\} \tag{2.4}$$

  where m is the number of components in the parallel system. Thus, a parallel system fails if every one of its components fails.

- A structural "general system" reliability problem is one in which the failure domain is defined in terms of both unions and intersections of component failure events. In general, such systems can be formulated either in terms of a series system of parallel subsystems (cut-set formulation), or in terms of a parallel system of series subsystems (link-set formulation). The former formulation leads to the definition

$$\mathcal{D} \equiv \left\{ \bigcup_{K} \bigcap_{k \in C_K} g_k(\mathbf{x},\theta) \le 0 \right\} \tag{2.5}$$

  where C_K is the K-th cut set, which is the index set of any subset of components whose joint failure constitutes failure of the system

For most structural reliability problems, an analytical evaluation of the integral in (2.1) is impossible and, therefore, numerical methods have been developed for approximate analysis. The first- and second-order reliability methods, commonly known as FORM and SORM, are widely used as approximate solution tools for such analysis. In the following section, these methods and their related topics are briefly described. More detailed development of these methods can be found in Ditlevsen and Madsen (1996).

2.2.1 FORM and SORM

FORM and SORM are approximate methods for computing the probability integral (2.1). In these methods, the limit-state surface $g_k(\mathbf{x},\theta)=0$ for each component is replaced by a first- or second-order approximating surface, respectively. The approximation is carried out at a point, known as the design point, which is the point on the surface $g_k(\mathbf{x},\theta)=0$ that is nearest to the origin in a transformed standard normal space.

FORM approximates the limit-state surface of each component as a tangential hyperplane at the design point. For a component reliability problem, the accuracy of FORM is primarily dictated by the nonlinearity of the limit-state surface around the design point. This is because the dominant contribution to the probability integral in (2.1) comes from the neighborhood of this point, where the probability density (in the standard normal space) achieves its maximum value. On the other hand, SORM approximates the limit-state surface as a hyperboloid, which can reflect the nonlinearity around the design point up to the second order. For nonlinear problems, SORM usually gives a better approximation than FORM.

For FORM or SORM analysis, we transform the random variables $\mathbf{x}$ into standard normal random variables $\mathbf{u}$ through a suitable one-to-one mapping T: $\mathbf{x} \rightarrow \mathbf{u}$. The limit-state functions $g_k(\mathbf{x},\theta)$, $k=1,2,\ldots,m$, are accordingly transformed such that $G_k(\mathbf{u},\theta) = g_k[T^{-1}(\mathbf{u}),\theta]$. The design points $\mathbf{u}_k^*$, $k=1,2,\ldots,m$, are obtained by solving the constrained optimization problems

$$\mathbf{u}_k^* = \arg\min \left\{ \|\mathbf{u}\| : \mathbf{u} \in \mathcal{D} \cap G_k(\mathbf{u},\theta)=0 \right\}, \quad k=1,2,\ldots,m \tag{2.6}$$

After finding the design points, we replace the limit-state surfaces $G_k(\mathbf{u},\theta)=0$, $k=1,2,\ldots,m$, by the first order (in FORM) or second order (in SORM) approximating surfaces at the design points.

In FORM, the k-th approximating surface is a hyperplane defined by

$$G_k(\mathbf{u},\theta) \cong \nabla_{\mathbf{u}} G_k^{\mathrm{T}}(\mathbf{u}-\mathbf{u}_k^*) = \left\|\nabla_{\mathbf{u}} G_k\right\|(\beta_k - \boldsymbol{\alpha}_k^{\mathrm{T}}\mathbf{u}) \tag{2.7}$$

where $\nabla_{\mathbf{u}} G_k$ denotes the gradient vector of $G_k(\mathbf{u},\theta)=0$ with respect to $\mathbf{u}$ evaluated at the design point $\mathbf{u}_k^*$, $\boldsymbol{\alpha}_i = -\nabla_{\mathbf{u}} G_k / \left\|\nabla_{\mathbf{u}} G_k\right\|$ is the normalized negative gradient vector, and β_k is the distance of the hyper-plane from the origin. For the component reliability problem in (2.2), the first order approximation of p_f is given by

$$p_f \cong \Phi(-\beta) \tag{2.8}$$

where β is the reliability index obtained above and $\Phi(\cdot)$ is the standard normal distribution function. For the series and parallel system problems, the first order solutions are given by

$$p_{fs} \cong 1 - \Phi_m(\boldsymbol{\beta},\mathbf{R}) \tag{2.9}$$

$$p_{fp} \cong \Phi_m(-\boldsymbol{\beta},\mathbf{R}) \tag{2.10}$$

where subscripts s and p respectively refer to the "series" and "parallel" system, and $\Phi_m(\boldsymbol{\beta},\mathbf{R})$ denotes the m-variate standard normal distribution with zero means, unit variances and correlation matrix $\mathbf{R}$ at the point $\boldsymbol{\beta}^{\mathrm{T}} = [\beta_1,\cdots,\beta_m]$. The element i,j of the correlation matrix is given by $\rho_{ij} = \boldsymbol{\alpha}_i^{\mathrm{T}}\boldsymbol{\alpha}_j$. For $m = 2$, i.e., systems with two components, one can show that

$$\Phi_2(\beta_1,\beta_2,\rho_{12}) = \Phi(\beta_1)\Phi(\beta_2) + \int_0^{\rho_{12}} \varphi_2(\beta_1,\beta_2,\rho)\mathrm{d}\rho \tag{2.11}$$

where $\varphi_2(\beta_1,\beta_2,\rho)$ is the bi-variate standard normal probability density function with zero means, unit variances and correlation ρ.

In SORM, the surfaces are replaced by approximating parabolic surfaces fitted at the design points $\mathbf{u}_k^*$, $k=1,2,\ldots,m$, (Breitung 1984, Der Kiureghian *et al* 1987, Der Kiureghian and De Stefano 1991). Due to the difficulty in incorporating the multiple

parabolic surfaces, however, SORM is usually used for component problems only. For a component reliability problem, Breitung (1984) has suggested the following formula

$$p_f \cong \Phi(-\beta)\prod_{i=1}^{n-1}\frac{1}{\sqrt{1+\beta\kappa_i}} \tag{2.12}$$

where κ_i denote the principal curvatures of the limit-state surface at the design point, taken positive when the surface curves away from the origin near the design point. More accurate formulae for the SORM approximation have been suggested subsequently (Hohenbichler and Rackwitz 1988, Tvedt 1990).

2.2.2 Algorithm for Finding the Design Point

In solving (2.6), we can first solve the optimization problem for each component

$$\mathbf{u}_k^* = \arg\min\ \left\{\|\mathbf{u}\| : G_k(\mathbf{u},\theta) = 0\right\} \tag{2.13}$$

and check if the solution of (2.13) belongs to the failure domain $\mathcal{D}$ of the system. If the solution point of (2.13) is not in the failure domain $\mathcal{D}$, some additional work has to be done to find the correct design point for the component in a system. Here, we describe a solution algorithm for (2.13).

Among several optimization algorithms that can solve (2.13) (see Liu and Der Kiureghian 1991 for a review), the improved HL-RF algorithm developed by Zhang and Der Kiureghian (1994) is known to be especially efficient. Here, we briefly describe this algorithm.

Let $\mathbf{u}_j$ be the point at j-th iteration. Then, the updated point $\mathbf{u}_{j+1}$ is obtained by solving the following recursive equation.

$$\mathbf{u}_{j+1} = \mathbf{u}_j + \lambda_j \mathbf{d}_j \tag{2.14}$$

where $\mathbf{d}_j$ is a search direction given by

$$\mathbf{d}_j = \left[\nabla_{\mathbf{u}_j} G^{\mathrm{T}}\mathbf{u}_j - G(\mathbf{u}_j,\theta)\right]\frac{\nabla_{\mathbf{u}_j} G}{\left\|\nabla_{\mathbf{u}_j} G\right\|^2} - \mathbf{u}_j \tag{2.15}$$

and λ_j is a step size obtained from

$$\lambda_j = \arg\min_{\lambda \in (0,1]} \left\{ m(\mathbf{u}_j + \lambda \mathbf{d}_j) - m(\mathbf{u}_j) \right\} \tag{2.16}$$

in which $m(\cdot)$ is the merit function

$$m(\mathbf{u}_j) = \frac{1}{2}\left\|\mathbf{u}_j\right\|^2 + c_j \left| G(\mathbf{u}_j, \theta) \right| \tag{2.17}$$

where $c_j > 0$ is a penalty parameter. It has been shown by Zhang and Der Kiureghian (1994) that the search direction (2.15) is a descent direction of the merit function (2.17) provided $c_j > \left\|\mathbf{u}_j\right\| / \left\|\nabla G(\mathbf{u}_j, \theta)\right\|$ is selected at each iteration.

2.2.3 Sensitivity Analysis

Sensitivity analysis aims to measure the partial derivative of the failure probability with respect to parameters θ, which appear in the limit-state function or the probability distribution $f(\mathbf{x})$. Sensitivity measures are useful for many purposes, including for identification of important sources of uncertainty and for optimal design. General description of sensitivity analysis can be found in Bjerager and Krenk (1989) and Ditlevsen and Madsen (1996). Here, sensitivity analysis is discussed within the scope of our study, where sensitivity measures are used to primarily to estimate the probability density function of a response quantity.

The sensitivity of the failure probability with respect to the parameter θ of the limit-state function is given by

$$\frac{\partial P[g(\mathbf{x},\theta) \le 0]}{\partial \theta} \cong \frac{\partial \Phi(-\beta)}{\partial \theta} = -\varphi(\beta)\frac{\partial \beta}{\partial \theta} \tag{2.18}$$

where

$$\frac{\partial \beta}{\partial \theta} = \frac{1}{\left\|\nabla_u G\right\|}\frac{\partial G(\mathbf{u}^*, \theta)}{\partial \theta} \tag{2.19}$$

If $R(\mathbf{x})$ denotes a response quantity, the cumulative distribution function of R at a threshold θ can be obtained by solving the reliability problem

$$g(\mathbf{x},\theta) = R(\mathbf{x}) - \theta \tag{2.20}$$

The value of the probability density function of R at the threshold θ can be obtained from (2.18) as the sensitivity with respect to θ. The cumulative distribution function and

probability density function of the response quantity for a range of the threshold values can be approximately constructed by repeatedly solving the reliability and sensitivity problems for selected values of the threshold θ. This is rather cumbersome, because we have to perform a new FORM analysis for each value of the parameter r.

For a small change of the parameter, we can roughly estimate the probability density of the response quantity by using the sensitivity measure for the original parameter value. Suppose that the parameter θ of the limit-state function is increased by $\Delta\theta$, that is, $\tilde{\theta} = \theta + \Delta\theta$. The probability density of the response quantity for the new threshold $\tilde{\theta}$ can be represented by the sensitivity measure of the failure probability, i.e.,

$$\frac{\partial P[g(x,\tilde{\theta}) \le 0]}{\partial \tilde{\theta}} \cong \frac{\partial \Phi(-\tilde{\beta})}{\partial \tilde{\theta}} = -\varphi(\tilde{\beta})\frac{\partial \tilde{\beta}}{\partial \tilde{\theta}} \tag{2.21}$$

For the new reliability index $\tilde{\beta}$, we make the first order approximation

$$\tilde{\beta} \cong \beta + \frac{\partial \beta}{\partial \theta}\Delta\theta \tag{2.22}$$

and for the new sensitivity measure $\partial\tilde{\beta}/\partial\tilde{\theta}$, we use the original value as

$$\frac{\partial \tilde{\beta}}{\partial \tilde{\theta}} \cong \frac{\partial \beta}{\partial \theta} \tag{2.23}$$

We can justify (2.23) on two grounds. First, the rate of change of the sensitivity measure is relatively slow compared to that of the reliability index. Secondly, as evident in (2.21), the influence of the sensitivity measure $\partial\tilde{\beta}/\partial\tilde{\theta}$ on the probability density is linear while that of the reliability index is exponential. Thus, the probability density function for the new parameter value $\tilde{\theta}$ can be obtained approximately as

$$\frac{\partial P[g(x,\tilde{\theta}) \le 0]}{\partial \tilde{\theta}} \cong -\varphi(\beta + \frac{\partial \beta}{\partial \theta}\Delta\theta)\frac{\partial \beta}{\partial \theta} \tag{2.24}$$

When the probability density function is estimated over a wide range of thresholds, we can greatly reduce the number of the sensitivity analysis using (2.24). However, since this is a rough approximation, the acceptable range of the perturbation has to be determined based on the degree of accuracy required.

2.3 Reliability Formulation of Random Vibration Problems

Consider a general random vibration problem defined by the stochastic differential equation

$$\mathbf{L}[\mathbf{x}(t), \mathbf{v}] = \mathbf{P}\mathbf{f}(t) \tag{2.25}$$

where t denotes the time, $\mathbf{L}$ is a differential operator, $\mathbf{x}(t)$ is the response vector such as generalized displacements or internal forces, $\mathbf{v}$ is a vector of time-invariant system parameters that characterize the mass, damping, restoring force, or member capacities of the system, $\mathbf{P}$ is a load distribution matrix, and $\mathbf{f}(t)$ is a vector of input processes, e.g., components of ground motion. In random vibration problems, our concern lies in estimating the statistics of the response processes for prescribed probabilistic descriptions of $\mathbf{v}$ and $\mathbf{f}(t)$.

Many response statistics of interest in random vibration are formulated in terms of the excursions of the response vector $\mathbf{x}(t)$ into a failure domain defined as

$$\mathcal{D} = \{\mathbf{x}(t), \mathbf{v} : g[\mathbf{x}(t), \mathbf{v}] \le 0\} \tag{2.26}$$

where $g[\mathbf{x}(t), \mathbf{v}]$ is a limit-state function. For example, the probability that a response $\mathbf{x}(t)$ will exceed a threshold x_0 at time t is defined by the failure domain $\{x(t) \ge x_0\}$ with the corresponding limit-state function $g = x_0 - x(t)$. Other specific examples are described in Section 2.5.

Figure 2.1 illustrates a realization of the response process $\mathbf{x}(t)$ in the outcome space of $(\mathbf{x}, \mathbf{v})$. The same process is represented in terms of the limit-state function in Figure 2.2. We can see that out-crossings of the vector process $\mathbf{x}(t)$ in Figure 2.1 coincide with down-crossings of the limit-state function below zero in Figure 2.2. To solve problems of this type by the methods of structural reliability, it is necessary to represent the input random processes in a discrete form in terms of a finite number of random variables.

The proposed solution procedure for random vibration problems by use of the structural reliability method can be summarized as follows:

- Represent each input process $f(t)$ in terms of a finite number of random variables, say $\mathbf{f} = (f_1, \cdots, f_n)$, where n is the resolution of the discrete representation. Together with random variables $\mathbf{v}$ describing the system properties, these define the basic random variables of the problem, $\mathbf{y} = (\mathbf{f}, \mathbf{v})$. Detailed description of this discrete representation is given in Section 2.4.
- Formulate the random vibrations problem in terms of one or more limit-state functions suitable for structural reliability analysis. Specific examples are described in Section 2.5.
- Use an appropriate structural reliability method to solve the problem. In this study, we investigate the use of FORM, SORM and various importance sampling techniques for this purpose.

2.4 Discrete Representation of Stochastic Excitation

As mentioned at the previous section, in order to solve random vibration problems by the methods of structural reliability, the input processes must be represented in terms of a finite number of random variables. There are several methods available for discrete representation of random processes. In this section, several of these methods are reviewed, including a method that is particularly appropriate for modeling earthquake ground motions.

For a Gaussian process $f(t)$ with a mean function $\mu(t)$, virtually all existing discrete representation methods lead to the form

$$f(t) = \mu(t) + \sum_{i=1}^{n} u_i s_i(t) = \mu(t) + \mathbf{s}(t)^{\mathrm{T}} \mathbf{u} \tag{2.27}$$

where $\mathbf{u} = [u_1, \cdots, u_n]^{\mathrm{T}}$ is a vector of standard normal variables, $\mathbf{s}(t) = [s_1(t), \cdots, s_n(t)]^{\mathrm{T}}$ is a vector of deterministic basis functions dependent on the covariance structure of the process, and n is a measure of the resolution of the representation (Der Kiureghian 2000). The main difference between various representation methods lies in the selection of the basis functions. The following are examples of the basis functions when the random process is represented in the form of (2.27):

- The Karhunen-Loève expansion method (Loève 1977) depends on the spectral decomposition of the covariance function of the process. The basis functions in this case are represented by $s_i(t) = \sqrt{\lambda_i}\Psi_i(t)$, where λ_i and $\Psi_i(t)$ are the i-th eigenvalue and eigenfunction associated with the covariance function of the process.
- The expansion optimal linear estimation (EOLE) method (Li and Der Kiureghian 1993) combines an optimal linear estimation representation with spectral decomposition. The basis functions in this case are represented by $s_i(t) = \boldsymbol{\Psi}_i^{\mathrm{T}}\boldsymbol{\Sigma}_{f(t)\mathbf{F}} / \sqrt{\lambda_i}$, where λ_i and $\boldsymbol{\Psi}_i$ are the i-th eigenvalue and eigenvector associated with the covariance matrix of an n-vector $\mathbf{F}$ containing the values of $f(t)$ at selected time points t_i, $i = 1, \cdots, n$, and $\boldsymbol{\Sigma}_{f(t)\mathbf{F}}$ denotes the vector of covariances of $f(t)$ with $\mathbf{F}$.
- The orthogonal series expansion method (Zhang and Ellingwood 1994) is similar to the Karhunen-Loeve expansion but employs a set of orthogonal functions that are not necessarily eigenfunctions. The basis function is represented by $s_i(t) = \sqrt{\lambda_i}\varphi_i(t)$, where λ_i and $\varphi_i(t)$ are computed from the orthogonal functions and the covariance function of the process.
- In a representation using trigonometric polynomials (Hasofer 1987, Grigoriu 1993), the basis function has the form of $\mathbf{s}^{\mathrm{T}}(t) = \boldsymbol{\alpha}_n(t)^{\mathrm{T}}\mathbf{L}$, where $\boldsymbol{\alpha}_n(t)$ denotes a vector of simple trigonometric functions and $\mathbf{L}$ is a lower-triangular matrix related to the covariance function of the process.

One can show that other discretization methods such as linear regression (Ditlevsen 1996) can also be written in the form of (2.27). A recent in-depth review of the above discretization methods can be found in Sudret and Der Kiureghian (2002).

Another method that is particularly well suited to modeling earthquake ground motions represents the process in terms of the response of a filter to a train of random pulses (Der Kiureghian 2000). The pulses may represent intermittent ruptures at the fault, whereas the filter may represent the medium through which the waves travel. If the pulses are Gaussian and the filter is linear, the process $f(t)$ is Gaussian. This representation can also be written in the form of (2.27).

Suppose that the process $f(t)$ is the response of a linear filter to a white noise excitation $W(t)$. Rather than discretizing $f(t)$ directly, we can discretize $W(t)$. Let t_i, $i = 1, 2, \ldots, n$, denote a set of closely and equally spaced time points at intervals $\Delta t = t_{i+1} - t_i$ and define a sequence of random pulses with magnitudes

$$w_i = \int_{t_{i-1}}^{t_i} W(t)dt \qquad i = 1, 2, \ldots, n \tag{2.28}$$

One can show that w_i are statistically independent Gaussian random variables with zero mean and constant variance

$$\sigma^2 = 2\pi S_o \Delta t \tag{2.29}$$

where S_o is the intensity of the white noise. The sequence w_i, $i = 1, 2, \ldots, n$, represents $W(t)$ in the discrete form of a random pulse train. The response of the linear filter to this pulse train is also of the form (2.27), with the basis functions

$$s_i(t) = \sigma h_f(t - t_i) \tag{2.30}$$

where $h_f(t)$ is the impulse response function of the filter.

Consider, for example, a second-order filter subjected to a pulse train defined by

$$\ddot{x}_f(t) + 2\zeta_f \omega_f \dot{x}_f(t) + \omega_f^2 x_f(t) = -\sum_{i=1}^{n} w_i \delta(t - t_i) \tag{2.31}$$

where $x_f(t)$ defines the displacement of the filter, ω_f and ζ_f represent the natural frequency and the damping ratio of the filter, respectively, and $\delta(\cdot)$ denotes the Dirac delta function. The absolute acceleration response of the filter is given by

$$f(t) = -2\zeta_f \omega_f \dot{x}_f(t) - \omega_f^2 x_f(t) \tag{2.32}$$

It can be easily verified that the impulse response function for this response of the filter (2.31) is

$$h_f(t) = -\left[\frac{\omega_f}{\sqrt{1-\zeta_f^2}} \sin\left(\omega_f t\sqrt{1-\zeta_f^2}\right) + 2\zeta_f \omega_f \cos\left(\omega_f t\sqrt{1-\zeta_f^2}\right)\right] \exp\left(-\zeta_f \omega_f t\right) \tag{2.33}$$

The above characterization defines a stationary process. Earthquake motions, however, are typically non-stationary in both time and frequency domains. To account for

temporal non-stationarity, we multiply the pulse train by a deterministic modulating function $q(t)$. The discrete representation in (2.27) becomes

$$f(t) = q(t)\left\{\mu(t) + \sum_{i=1}^{n} u_i s_i(t)\right\} \tag{2.34}$$

For typical earthquakes, $q(t)$ tends to gradually increase to a constant plateau and then decrease to zero at termination of the motion.

To account for spectral non-stationarity, one can change the filter properties with time. However, a simpler approach is to use multiple filters each with its own modulating function. Hence, we write the most general discrete form of the input process as

$$f(t) = \sum_{k} q_k(t)\left\{\mu(t) + \sum_{i=1}^{n} u_i s_{ik}(t)\right\} \tag{2.35}$$

where $q_k(t)$ denotes the modulating function for the k-th filter and $s_{ik}(t)$ denotes the basis function obtained from (2.30) for the k-th filter. By proper selection of filter properties and modulating functions, almost any kind of temporal and spectral non-stationarity can be modeled.

Figure 2.3 shows an example of the non-stationary excitation generated using (2.35). Figure 2.3a shows the time modulation functions for two filters, whose system properties are $\omega_{f1} = 5\pi$ rad/sec, and $\zeta_{f1} = 0.4$ for the first filter and $\omega_{f2} = 2\pi$ rad/sec and $\zeta_{f2} = 0.2$ for the second filter. Figure 2.3b shows a sample of a train of pulses with $\Delta t = 0.02$ sec approximating the white noise with the intensity $S_o = 1$ (m/sec^2)^2/(rad/sec). We have used (2.33) for the impulse response functions of the two filters to generate the non-stationary excitation in Figure 2.3c. This resembles the actual pattern of earthquake accelerograms, in which the primary wave with high frequency content appears first and is followed by the secondary waves having low frequency content.

For non-Gaussian processes, representation by a linear relation shown in (2.27) is not possible. The non-Gaussian process is defined as a nonlinear function of the vector **u**. Several methods of representation in terms of standard normal variables are available, depending on the manner in which the process is defined. If the process is defined in terms of a set of non-Gaussian random variables, then the Rosenblatt transformation (Hohenbichler and Rackwitz 1981) can be used to transform these variables into standard

normal variables. If the process is defined by a nonlinear translation of a Gaussian process (Liu and Der Kiureghian 1986, Grigoriu 1995), then the underlying Gaussian process can be represented in the form of (2.27). Examples of discretized non-Gaussian processes can be found in Der Kiureghian (2000).

2.5 Reliability Statistics of Random Vibration Response

We can think of many reliability statistics in random vibration problems. Here, we present several important reliability statistics associated with the excursions of $\mathbf{x}(t)$ into the failure domain $\mathcal{D}$ discussed in Section 2.3. These are primarily based on Der Kiureghian and Li (1996a).

2.5.1 Probability Distribution of a Response Function

Suppose that the probability distribution of a function $h[\mathbf{x}(t)]$ of the response vector $\mathbf{x}(t)$ at time t is of interest. We define the limit-state function

$$g[\mathbf{x}(t), \mathbf{v}, \theta] = h[\mathbf{x}(t)] - \theta \tag{2.36}$$

where θ is a selected threshold. The reliability solution gives the cumulative distribution function of $h[\mathbf{x}(t)]$ at the threshold θ, i.e.,

$$F_h(\theta) = P\{g[\mathbf{x}(t), \mathbf{v}, \theta] \le 0\} \tag{2.37}$$

Furthermore, the probability density function of $h[\mathbf{x}(t)]$ is obtained as the sensitivity of the above solution with respect to θ, i.e.,

$$f_h(\theta) = \frac{\partial P\{g[\mathbf{x}(t), \mathbf{v}, \theta] \le 0\}}{\partial \theta} \tag{2.38}$$

As described in Section 2.2.3, this sensitivity is easily computed in FORM. The complete distribution of $h[\mathbf{x}(t)]$ is obtained by solving the problem for the relevant range of θ values. In particular, using $h = x(t)$, we obtain the probability distribution of the scalar response quantity $x(t)$ at time t.

2.5.2 Mean Out-crossing Rate

As mentioned earlier, the rate of out-crossings of $\mathbf{x}(t)$ into a component failure domain $\mathcal{D} = \{g[\mathbf{x}(t), \mathbf{v}] \leq 0\}$ per unit time is identical to the rate of down-crossings of $g[\mathbf{x}(t), \mathbf{v}]$ below the zero level (see Figure 2.1 and Figure 2.2). Based on a well known result by Rice (1944,1945), the mean value of this rate can be written as

$$\nu(t) = -\int_{-\infty}^{0} \dot{g} f_{g\dot{g}}(0, \dot{g}, t) d\dot{g} \tag{2.39}$$

where $f_{g\dot{g}}(g, \dot{g}, t)$ is the joint probability density function of $g[\mathbf{x}(t), \mathbf{v}]$ and $\dot{g}[\mathbf{x}(t), \mathbf{v}]$ at time t. Unfortunately, Rice's formula (2.39) is difficult to compute when the system is nonlinear or the response $\mathbf{x}(t)$ is non-Gaussian.

Alternatively, the mean out-crossing rate can be written in the form (Hagen and Tvedt 1991)

$$\nu(t) = \lim_{\delta t \to 0} \frac{P\{g[\mathbf{x}(t), \mathbf{v}] > 0 \cap g[\mathbf{x}(t + \delta t), \mathbf{v}] \leq 0\}}{\delta t} \tag{2.40}$$

In the above expression, the numerator denotes the probability that the response is inside the safe domain at time t and inside the failure domain $\mathcal{D}$ at a slightly later time, $t + \delta t$. Clearly, one or more out-crossing events must have occurred during the interval δt. For a sufficiently small δt, the probability of two or more out-crossings is negligible in relation to the probability of a single out-crossing. Hence, the intersection probability in the numerator is essentially equal to the probability of one out-crossing within δt. The mean number of events within δt can be written as

$$\nu(t)\delta t = 0 \times P(0 \text{ crossing}) + 1 \times P(1 \text{ crossing}) + O(\delta t^2) \tag{2.41}$$

Neglecting the higher-order terms and dividing the both sides by δt, we obtain (2.40).

From the standpoint of the structural reliability analysis, the formulation of (2.40) is far simpler than that of (2.39). In (2.40), the mean out-crossing rate can be evaluated by solving a parallel-system reliability problem with two components having the limit-state functions

$$G_1(\mathbf{u}) = -g[\mathbf{x}(t), \mathbf{v}] \tag{2.42}$$

$$G_2(\mathbf{u}) = g[\mathbf{x}(t + \delta t), \mathbf{v}] \tag{2.43}$$

The first order approximation of (2.43) is given by

$$g[\mathbf{x}(t+\delta t),\mathbf{v}] \cong g[\mathbf{x}(t),\mathbf{v}] + \nabla_x g[\mathbf{x}(t),\mathbf{v}]\dot{\mathbf{x}}(t)\delta t \tag{2.44}$$

This is practically identical to (2.43) and more convenient since the limit-state function is composed of the responses at the same time as in (2.42).

In Figure 2.4, the failure domain of the parallel system problem in the numerator of (2.40) is shown together with its FORM approximation in the standard normal space. If we know the design points of the individual components and their correlation, we can analytically evaluate the FORM solution using (2.11). Since the time perturbation δt is small, the correlation of the two events is very close to -1, and therefore, computation has to be performed with high precision for an accurate result. In Section 3.9, we introduce a simple procedure that can easily solve this problem by shifting the design point of the first component in time.

2.5.3 First-Excursion Probability

The probability of excursion during an interval $(0,T)$, can be represented by

$$P_T = P\{\min_{0<t\le T} g[\mathbf{x}(t),\mathbf{v}] \le 0\} \tag{2.45}$$

This is equal to the probability of failure, if a single excursion into $\mathcal{D}$ causes the failure of the system. It is well known (Lin 1967) that the probability in (2.45) is bounded by

$$P\{\min_{0<t\le T} g[\mathbf{x}(t),\mathbf{v}] \le 0\} \le \int_0^T \nu(t)dt \tag{2.46}$$

This upper bound always provides a conservative estimate of the failure probability. Furthermore, if the system variables $\mathbf{v}$ are deterministic and the out-crossing events can be assumed to constitute Poisson events, an approximation to the probability of interest is given by

$$P\{\min_{0<t\le T} g[\mathbf{x}(t),\mathbf{v}] \le 0\} \cong 1 - \exp\left[-\int_0^T \nu(t)dt\right] \tag{2.47}$$

The above is often used as an approximation of the true probability of failure. This approximation works well if the out-crossing events are statistically independent, a

condition that is approximately satisfied when the events are rare and do not occur in clusters.

Although it provides an insight into the problem, this approach is not efficient for non-stationary problems, since for such problems the out-crossing rate must be evaluated for many points in time. In Chapter 5, we describe an efficient simulation method for computing the first-excursion probability that has recently been proposed by Au and Beck (2001) for linear systems, and extend it to solve the first-excursion probability for nonlinear random vibration problems.

2.5.4 Cumulative Excursion Time

The duration of time spent in domain $\mathcal{D}$ during an interval $(0,T)$ is called the cumulative excursion time. This time period can be formulated as

$$\eta(t) = \int_0^T I\{-g[\mathbf{x}(t), \mathbf{v}]\}dt \tag{2.48}$$

where $I\{\cdot\}$ is the indicator function with $I\{a\} = 0$ for $a < 0$ and $I\{a\} = 1$ for $a \geq 0$.

For a given T, $\eta(T)$ is a random variable. Here, we are interested in its mean and variance. Taking expectation, we have

$$\begin{aligned} \mathrm{E}[\eta(t)] &= \mathrm{E}\left\{\int_0^T I\{-g[\mathbf{x}(t), \mathbf{v}]\}dt\right\} \\ &= \int_0^T \mathrm{E}\{I\{-g[\mathbf{x}(t), \mathbf{v}]\}\}dt \\ &= \int_0^T P\{g[\mathbf{x}(t), \mathbf{v}] \leq 0\}dt \end{aligned} \tag{2.49}$$

It is seen that the mean of the occupancy time is given in terms of the component reliability problem defined in (2.2). All we have to do is to solve the reliability problem for a sequence of time points and evaluate the integral (2.49) numerically.

The mean square of the occupancy time is obtained as follows:

$$\mathrm{E}[\eta^2(t)] = \mathrm{E}\left\{\int_0^T\int_0^T I\{-g[\mathbf{x}(t_1), \mathbf{v}]\}I\{-g[\mathbf{x}(t_2), \mathbf{v}]\}dt_1dt_2\right\}$$

$$= \int_0^T \int_0^T \mathrm{E}\{I\{-g[\mathbf{x}(t_1),\mathbf{v}]\} I\{-g[\mathbf{x}(t_2),\mathbf{v}]\}\} dt_1 dt_2$$

$$= \int_0^T \int_0^T P\{g[\mathbf{x}(t_1),\mathbf{v}] \le 0 \cap g[\mathbf{x}(t_2),\mathbf{v}] \le 0\} dt_1 dt_2 \tag{2.50}$$

For each pair of t_1 and t_2, the integrand in (2.50) requires the solution of a parallel-system reliability problem with the two limit-state functions

$$G_1(\mathbf{u},t_1) = g[\mathbf{x}(t_1),\mathbf{v}] \tag{2.51}$$

$$G_2(\mathbf{u},t_2) = g[\mathbf{x}(t_2),\mathbf{v}] \tag{2.52}$$

The mean square is computed by solving this problem for all pairs of t_1 and t_2 within the interval $(0,T)$, followed by a numerical evaluation of the double integral in (2.50). The variance is computed from the well known relation $\mathrm{var}[\eta(T)] = \mathrm{E}[\eta^2(T)] - \mathrm{E}^2[\eta(T)]$.

2.5.5 Duration of a Single Excursion

The duration of an excursion after the occurrence of an out-crossing at time t is defined as

$$D(t) = \inf\{\tau - t > 0 : g[\mathbf{x}(\tau),\mathbf{v}] > 0\} \tag{2.53}$$

where $\inf\{x : f(x) > 0\}$ denotes the smallest value of x for which the function $f(x)$ is positive. For a given t, $D(t)$ is clearly a random variable. The exact statistics of this random variable are difficult to obtain. However, a good approximation of its mean is derived below.

Let $\eta(t,\Delta t)$ denote the occupancy time in $\mathcal{D}$ during the small interval $(t,t+\Delta t)$ and ΔN denote the number of out-crossing events during the same interval. The time-averaged duration of the each excursion is $D(t) = \eta(t,\Delta t)/\Delta N$. Noting that $\mathrm{E}[\Delta N] = \nu(t)\Delta t$, we have

$$\mathrm{E}[D(t)] = \mathrm{E}\left\{\frac{\eta(t,\Delta t)}{\Delta N}\right\} \cong \frac{\mathrm{E}[\eta(t,\Delta t)]}{\nu(t)\Delta t} \tag{2.54}$$

where we have taken the first order approximation for the mean of the ratio. From (2.41), it should be clear that for small Δt, $\mathrm{E}[\eta(t,\Delta t) \cong P\{g[\mathbf{x}(t),\mathbf{v}] \le 0\}\Delta t$. Thus,

$$\mathrm{E}[D(t)] \cong \frac{P\{g[\mathbf{x}(t),\mathbf{v}] \le 0\}}{\nu(t)} \tag{2.55}$$

Both terms on the right-hand side have been discussed earlier in Section 2.5.1 and 2.5.2, respectively. Specifically, the numerator requires a component reliability analysis and the denominator requires a parallel system reliability analysis with two components.

2.5.6 Cumulative Area of Excursion

The cumulative area of excursion of the scalar process $g[\mathbf{x}(t),\mathbf{v}]$ during an interval $(0,T)$, is defined by

$$A(T) = -\int_0^T \min\{g[\mathbf{x}(t),\mathbf{v}],0\}dt \tag{2.56}$$

We are interested in the mean value of this area. Taking expectation, we have

$$\begin{aligned}\mathrm{E}[A(T)] &= -\int_0^T \mathrm{E}\{\min\{g[\mathbf{x}(t),\mathbf{v}],0\}\}dt \\ &= -\int_0^T \int_{-\infty}^0 \theta f_g(\theta,t)d\theta dt\end{aligned} \tag{2.57}$$

where $f_g(\theta,t)$ is the probability density function of $g[\mathbf{x}(t),\mathbf{v}]$ and can be written as

$$f_g(\theta,t) = \frac{\partial P\{g[\mathbf{x}(t),\mathbf{v}] - \theta \le 0\}}{\partial\theta} \tag{2.58}$$

Substituting the above relation in (2.57) and replacing θ by $-\theta$, we obtain

$$\mathrm{E}[A(T)] = -\int_0^T \int_0^\infty \theta \frac{\partial P\{g[\mathbf{x}(t),\mathbf{v}] + \theta \le 0\}}{\partial\theta} d\theta dt \tag{2.59}$$

The partial derivative in the integrand is the sensitivity of a component reliability problem with the limit-state function

$$G(\mathbf{u},t,\theta) = g[\mathbf{x}(t),\mathbf{v}] + \theta \tag{2.60}$$

To compute the mean of the cumulative excursion area, we solve the component reliability sensitivities for a grid of θ and t values followed by numerical evaluation of the double integral (2.59).

2.6 Evaluation of the Limit-state Function and its Gradient

As described in Section 2.2, several structural reliability methods require repeated evaluations of the limit-state function and its gradient. In our application, the limit-state function is expressed in terms of the responses of a nonlinear vibrating system. Furthermore, the gradient of the limit-state function involves the Jacobian of the response vector with respect to the random variables. Evaluation of the response can be done using conventional numerical integration methods, such as the Newmark method (Newmark 1959, Chopra 1995) or the Runge-Kutta method (Lambert 1991). For evaluation of the Jacobian, the direct differentiation method (DDM) (Tsay and Arora 1990, Zhang and Der Kiureghian 1993 and 1997, Li and Der Kiureghian 1995, Butcher 2000) is an efficient tool. Below, we briefly describe the DDM for nonlinear dynamic response.

Consider a second-order stochastic differential equation describing the motion of a nonlinear oscillator

$$\mathbf{Q}[\ddot{\mathbf{x}}(t), \dot{\mathbf{x}}(t), \mathbf{x}(t), \mathbf{v}] = \mathbf{P}\mathbf{F}(t) \tag{2.61}$$

where $\mathbf{Q}$ is a nonlinear function vector composed of the system parameters $\mathbf{v}$ and the system responses $\ddot{\mathbf{x}}(t)$, $\dot{\mathbf{x}}(t)$, and $\mathbf{x}(t)$, $\mathbf{P}$ is an influence matrix, and $\mathbf{F}(t) = \{F_1(t), F_2(t), \cdots\}$ is the excitation vector. Suppose that the excitation processes $\mathbf{F}(t)$ are represented in a discrete form in terms of a vector of random variables $\mathbf{f}$. Then, the gradient of the response with respect to the random variables $\mathbf{y} = (\mathbf{f}, \mathbf{v})$ can be obtained by directly differentiating the above equation of motion. Let $y \in \mathbf{y}$ be a member of this set of random variables. The governing equation for the derivative of the displacement vector $\mathbf{s}(t) = \partial \mathbf{x}(t) / \partial y$ is given by

$$\frac{\partial \mathbf{Q}}{\partial \ddot{\mathbf{x}}}\ddot{\mathbf{s}} + \frac{\partial \mathbf{Q}}{\partial \dot{\mathbf{x}}}\dot{\mathbf{s}} + \frac{\partial \mathbf{Q}}{\partial \mathbf{x}}\mathbf{s} = \frac{\partial \mathbf{P}\mathbf{F}}{\partial y} - \frac{\partial \mathbf{Q}}{\partial \mathbf{v}}\frac{\partial \mathbf{v}}{\partial y} \tag{2.62}$$

In the above equation, $\partial \mathbf{Q} / \partial \ddot{\mathbf{x}}$, $\partial \mathbf{Q} / \partial \dot{\mathbf{x}}$ and $\partial \mathbf{Q} / \partial \mathbf{x}$ can be obtained by linearization of the response at the time of interest. Therefore, the Jacobian of the responses can be calculated by solving the time variant linear equations in (2.62). Specific implementations of this

approach can be found in Zhang and Der Kiureghian (1993) and (1997) and Li and Der Kiureghian (1995).

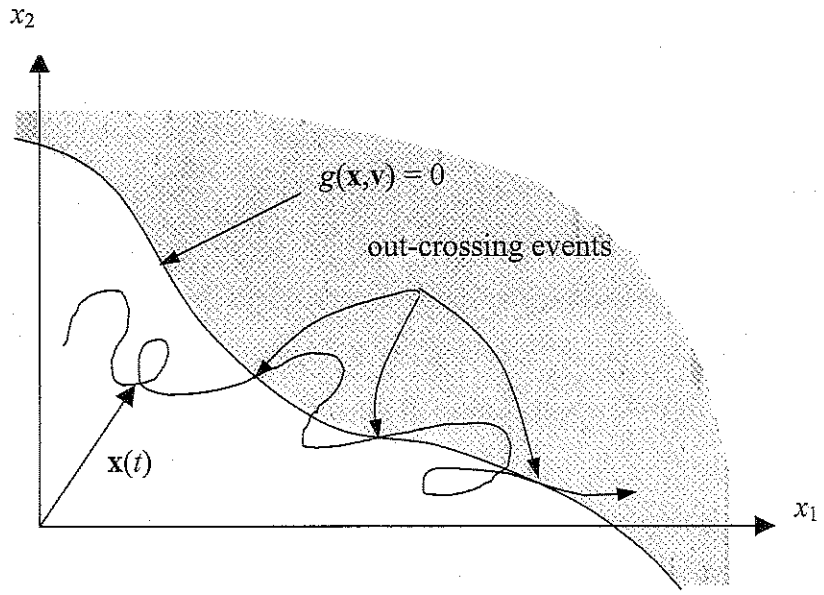

Figure 2.1. Excursions of the response vector into a failure domain.

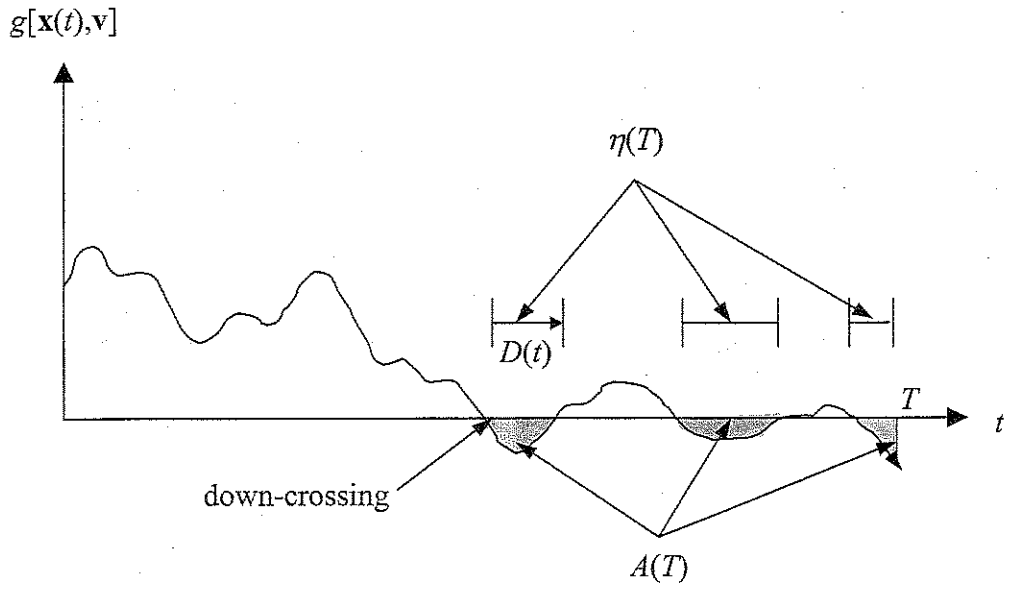

Figure 2.2. Down-crossings of $g[\mathbf{x}(t),\mathbf{v}]$ and various response statistics.

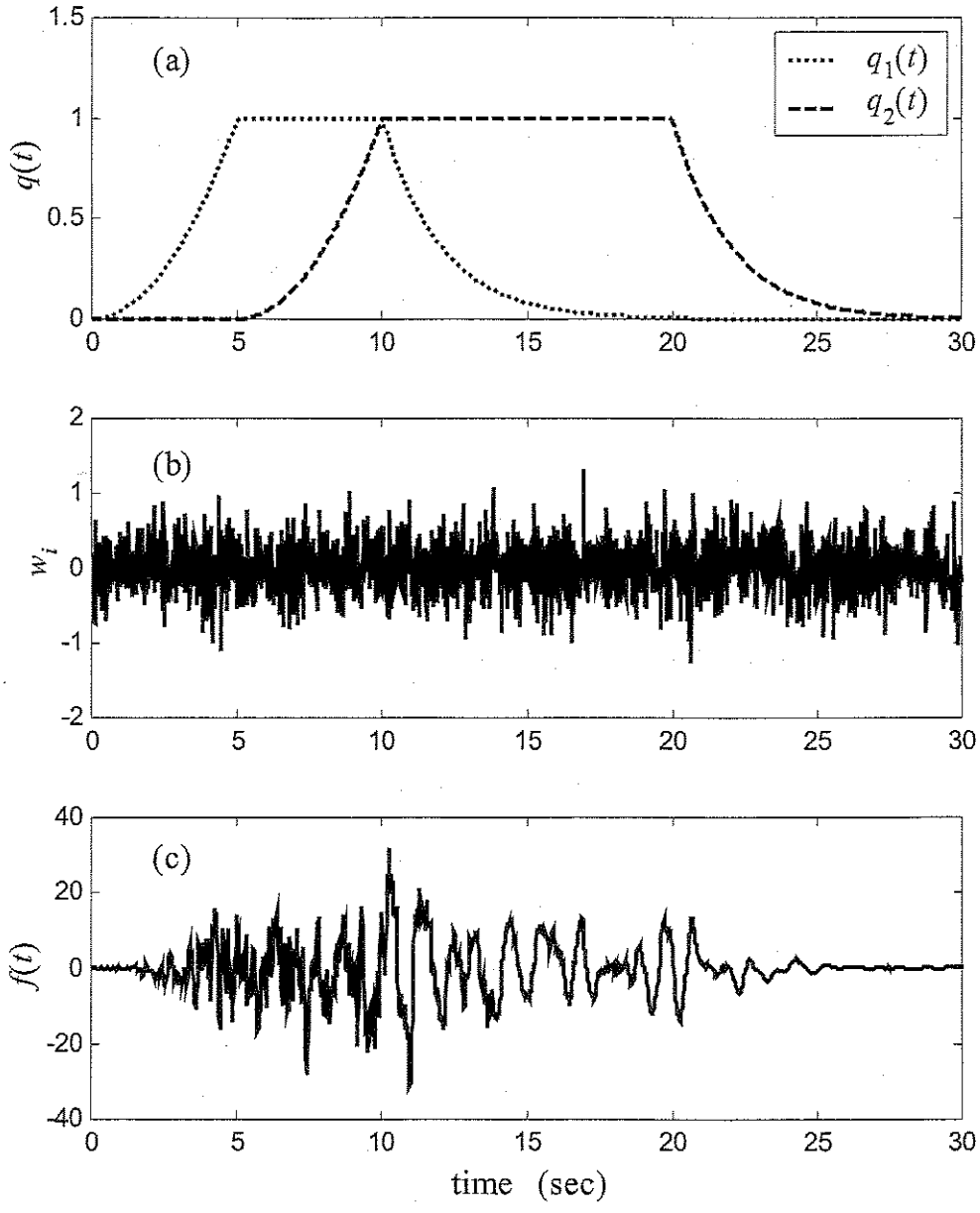

Figure 2.3. (a) Time modulation functions, (b) random sample of pulse train w_i (c) random sample of the excitation $f(t)$.

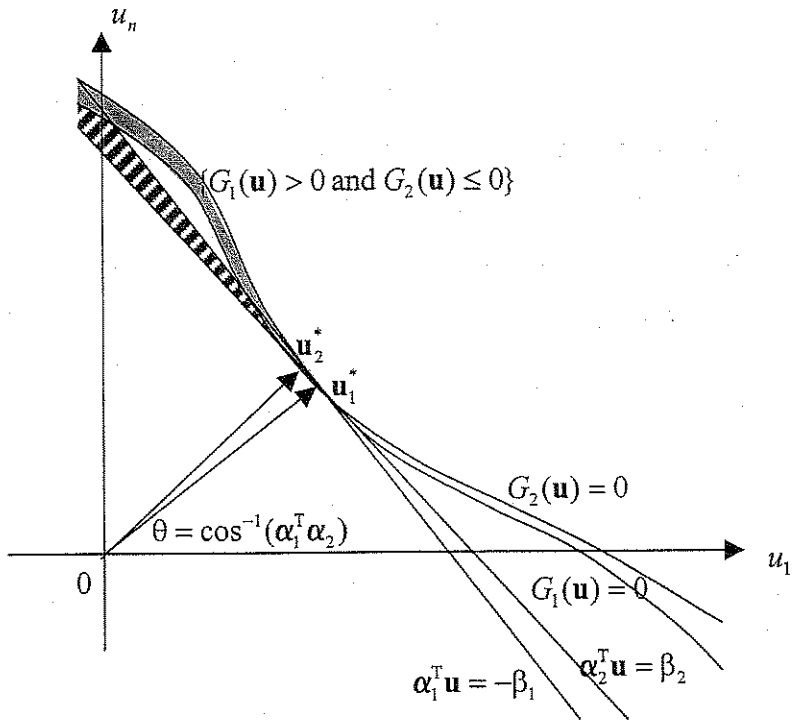

Figure 2.4. Failure domain of the parallel system for computing the mean out-crossing rate.

3 Design Point Excitation

3.1 Introduction

In the previous chapter, we presented the general form of the reliability formulation of random vibration problems. As described there, analytical solutions are not available for most structural reliability problems, and the random vibration problems are no exception. Therefore, we must pursue approximate solution techniques, such as FORM, SORM and simulation, especially with importance sampling. A key step in these solution techniques is the finding of the design point, which, as defined in the previous chapter, is the point on the limit-state surface nearest to the origin in the standard normal space. In structural reliability, the design point is usually found by solving a constrained optimization problem (see Section 2.2). Several specially designed algorithms to solve the design-point problem have been developed (Liu and Der Kiureghian 1991, Zhang and Der Kiureghian 1994, Abdo and Rackwitz 1990). These algorithms typically are iterative and involve repeated evaluations of the limit-state function and its gradient.

One characteristic of the random vibration problem formulated as a structural reliability problem is the large number of random variables, which result from the representation of the continuous stochastic input process in a discrete form. Typically, one may have several hundred or thousand random variables. Considering that the time required to solve an optimization problem usually depends on the degree of nonlinearity of the objective and constraint functions as well as the number of variables involved, one can expect that finding the design point for a nonlinear random vibration problem by the direct use of optimization methods can be prohibitively costly. Furthermore, if there is no recourse but to use these methods, significant advantage can be gained by having a good starting point for the iterative scheme.

In this chapter, we discuss the design point for random vibration problems and the corresponding realization of the excitation, i.e., the design point excitation. As described in Chapter 2, the design point is the most likely realization (in the standard normal space)

of the random variables for the failure event of interest. Likewise, the design point excitation represents the most likely realization (in the standard normal space) of the stochastic excitation process for the failure event of interest. Rather than resorting to an optimization algorithm to find the design point, we try to obtain the solution by considering the dynamic characteristics of the vibrating system. We find that for linear and certain elastic nonlinear systems, an exact solution of the design point can be found without resorting to iterative calculations. For more general nonlinear systems, we are able to obtain good approximations of the design point, which subsequently can be used as a "warm" starting point in an iterative optimization algorithm to find the exact solution.

The idea is based on the finding that, for a linear oscillator subjected to Gaussian excitation, the design point can be directly obtained from the unit impulse response function of the oscillator without resorting to iterative optimization calculations (Drenik 1970, Shinozuka 1970, Der Kiureghian 2000, Au and Beck 2001). The unit impulse response function is a fundamental characteristic of a linear dynamic system. This suggests that the dynamic characteristics of a system play an important role in finding the design point. As it is well known, impulse response functions do not exist for nonlinear systems and, therefore, a direct generalization of the above idea to nonlinear systems is not possible. However, it turns out that nonlinear systems have other characteristics, which can be exploited to obtain the design point. In particular, the free vibration response of a nonlinear system contains information about the system that can be used to find an exact or approximate solution of the design point.

For given nonzero initial conditions, we can observe the free vibration of a system by numerically integrating the differential equations governing the motion of the system. Considering that the free vibration response is a natural behavior of the system without any external intervention, we see that one aspect of the dynamic characteristic of the system is realized in the free vibration motion. Furthermore, for many oscillators, the vibration response under the design point excitation shows a trend similar to the mirror image of the free vibration that is obtained by reversing the time order of the free vibration motion.

Based on this observation, we study the mirror image of the free vibration motion of the system and the excitation that generates a response identical to such a motion. This excitation is hereafter called the "mirror image excitation." By comparing the design point excitation with the mirror image excitation, we find that for nonlinear elastic systems subjected to Gaussian white noise, the mirror image excitation is identical to the design point excitation.

This idea is extended to the case of general nonlinear systems, including hysteretic systems, multi-degree-of-freedom systems, and systems subjected to non-white or non-stationary excitations. Though for these systems the mirror image excitation does not give the exact design point, it leads us to a point in the neighborhood of the design point, so that we have a "warm" starting point for a subsequent iterative solution by an optimization algorithm. Other topics discussed in this chapter are the design point for systems with uncertain properties, and a simple approach for determining the design points of the two components of a parallel system that are used for computing the mean out-crossing of random vibration response of nonlinear systems.

3.2 Design Point Excitation

Consider the stochastic differential equation of a vibrating system given as

$$\mathbf{M}\ddot{\mathbf{x}}(t) + \mathbf{C}\dot{\mathbf{x}}(t) + \mathbf{R}[\mathbf{x}(t), \dot{\mathbf{x}}(t)] = \mathbf{P}f(t) \tag{3.1}$$

where $\mathbf{M}$ and $\mathbf{C}$ are the mass and damping matrices, respectively, $\mathbf{R}[\mathbf{x}(t), \dot{\mathbf{x}}(t)]$ is a restoring force vector, $\mathbf{P}$ is a load distribution vector, and $f(t)$ is a stochastic excitation process. As described in Chapter 2, in a random vibration problem we are usually interested in the probability measure $P\{g[\mathbf{x}(t), \dot{\mathbf{x}}(t)] \le 0\}$, where $g[\mathbf{x}(t), \dot{\mathbf{x}}(t)]$ is a limit-state function. We assume g is continuously differentiable with respect to $\mathbf{x}(t)$ and $\dot{\mathbf{x}}(t)$. Note that t appears as a fixed parameter in this problem.

To solve this problem using the reliability formulation, the first step is to discretize the continuous stochastic excitation process $f(t)$ so that it is represented in terms of a finite number of basic random variables $\mathbf{v}$ (see Section 2.4). The response vectors $\mathbf{x}(t)$ and $\dot{\mathbf{x}}(t)$ and, therefore, the limit-state function $g[\mathbf{x}(t), \dot{\mathbf{x}}(t)]$ are then

implicit functions of $\mathbf{v}$, i.e., $g[\mathbf{x}(t),\dot{\mathbf{x}}(t)]=\tilde{g}(\mathbf{v},t)$. The next step is to find the design point by solving the optimization problem

$$\min \left\{\|\mathbf{u}\| : G(\mathbf{u},t)=0\right\} \tag{3.2}$$

where $\mathbf{u}=\mathbf{T}(\mathbf{v})$ is the standard normal vector obtained by transforming $\mathbf{v}$ (see Section 2.4), and $G(\mathbf{u},t)=\tilde{g}[\mathbf{T}^{-1}(\mathbf{u}),t]$ is the limit-state function in the standard normal space. Let $\mathbf{u}^*(t)$ be the solution of the above problem. As described in Chapter 2, after we find the design point, we can apply FORM, SORM, or importance sampling to approximately compute the probability measure $P\{g[\mathbf{x}(t),\dot{\mathbf{x}}(t)]\le 0\}$. We will do this in Chapter 4. Here we want to focus on the properties of the design point and the corresponding excitation.

Having found the design point, we can generate the corresponding excitation $f^*(t)$ in terms of the realization $\mathbf{v}^*(t)=\mathbf{T}^{-1}[\mathbf{u}^*(t)]$ of the basic random variables. This realization of the excitation is known as "the design point excitation" (Der Kiureghian 2000). It has maximum likelihood among all possible realizations of the excitation process that give rise to the event $\{g[\mathbf{x}(t),\dot{\mathbf{x}}(t)]\le 0\}$, provided variables $\mathbf{v}$ are normal. If $\mathbf{v}$ are non-normal, the design point excitation has nearly maximum likelihood with respect to the given event. In most cases, it is easy to convert the design point $\mathbf{u}^*(t)$ to the design point excitation or vice versa by simple transformations.

It should be clear that finding the design point or the design point excitation is a crucial step in solving the random vibration problem by reliability analysis. Due to the complexity of the problem, the level of optimality pursued for (3.2) is confined to the first order necessary conditions:

$$\nabla\|\mathbf{u}\|+\lambda\nabla G(\mathbf{u})=0 \tag{3.3a}$$

$$G(\mathbf{u})=0 \tag{3.3b}$$

where λ is the Lagrange multiplier. We have dropped t in the above, since it is a constant in the limit-state function. As described in section 2.2.1, there are several algorithms available for solving this problem. However, these algorithms tend to be time consuming due to the non-linearity of the problem and the large number of random variables involved.

In many applications, the excitation can be assumed to be Gaussian. In addition, if the excitation is white noise or broadband, the response pattern of a linear single-degree-of-freedom (SDOF) oscillator under the design point excitation shows a harmonic behavior with a frequency matching the natural frequency of the oscillator. Though the response of a general nonlinear system is not as simple as that of the linear SDOF oscillator, it is still related to the dynamic characteristics of the system. In the following section, we turn our attention to the free vibration and its mirror image motion. This helps us understand the dynamic characteristics of a vibrating system. We develop the mirror image excitation that generates the mirror image of the free vibration motion.

3.3 Mirror Image Excitation

Consider the differential equation of a nonlinear elastic SDOF oscillator

$$m\ddot{x}(t) + c\dot{x}(t) + R[x(t)] = f(t) \tag{3.4}$$

where m is the mass, c is the damping coefficient, $R[x(t)]$ is the elastic restoring force represented by an algebraic function of $x(t)$, and $f(t)$ is the excitation function. We are interested in determining the excitation that produces a response resembling the mirror image of the free vibration motion of the oscillator.

Suppose the system undergoes free vibration with initial conditions $x_F(0) = x_0$ and $\dot{x}_F(0) = \dot{x}_0$. Its motion is governed by the differential equation

$$m\ddot{x}_F(t) + c\dot{x}_F(t) + R[x_F(t)] = 0 \tag{3.5}$$

where the subscript F denotes the response in free vibration. In general, there is no closed-form formula for the response of a nonlinear oscillator, and we have to use a numerical integration algorithm to compute the response of the oscillator (see Section 2.6). Let $x_F(t_n)$ and $\dot{x}_F(t_n)$ denote the free vibration responses at time t_n.

Now, imagine that the mirror image motion of the free vibration, denoted $x_I(t)$, occurs as shown in Figure 3.1. The initial conditions are the same as the responses of the system at time t_n, i.e. $x_I(0) = x_F(t_n)$ and $\dot{x}_I(0) = -\dot{x}_F(t_n)$, where the subscript I denotes the mirror image of the free vibration. The negative sign in the velocity indicates that the

vibration occurs in the opposite direction of the free vibration. At time t_n, the system reaches the same state as the initial condition of the free vibration, i.e. $x_I(t_n) = x_0$ and $\dot{x}_I(t_n) = -\dot{x}_0$. It is clear that we need to apply a special excitation to generate the mirror image response of the free vibration. We call this excitation "the mirror image excitation (of free vibration)".

The mirror image excitation can be found by considering how the energy is dissipated during the free vibration and its mirror image motion. For the system in (3.5), energy dissipation occurs only through the damping force. The following three cases are instructive in understanding the role of the damping force: free vibration without damping, free vibration with damping, and free vibration with negative damping. These cases are described by the equations

$$m\ddot{x}(t) + R[x(t)] = 0 \tag{3.6}$$

$$m\ddot{x}(t) + c\dot{x}(t) + R[x(t)] = 0 \tag{3.7}$$

$$m\ddot{x}(t) - c\dot{x}(t) + R[x(t)] = 0 \tag{3.8}$$

When released from the same non-zero initial conditions, the vibration patterns of the above three systems will be different. For the system (3.6) with no damping, no energy will be dissipated and therefore the system will vibrate periodically with no decay in its amplitude and it will periodically return to its initial state. If there is positive damping as in (3.7), the amplitude of vibration will gradually decrease due to the effect of the damping and will diminish to zero after a sufficiently long time. If there is negative damping as in (3.8), the amplitude of vibration will be amplified in a manner exactly opposite to the case with positive damping. Although a system with negative damping is not realistic, the concept is useful in deriving the mirror image excitation.

The reverse analogy between systems (3.7) and (3.8) can be seen more clearly if one treats the damping force as an external load exerted on the undamped system. Moving the damping force to the right side of (3.7), we have the external load $f(t) = -c\dot{x}(t)$ that works against the direction of motion, while in (3.8) the external load $f(t) = c\dot{x}(t)$ amplifies the motion of the system by working in the same direction as the motion.

Because a real system does not have negative damping, we can make the system in (3.8) realistic by adding twice the damping force to both sides of the equation, yielding

$$m\ddot{x}(t) + c\dot{x}(t) + R[x(t)] = 2c\dot{x}(t) \tag{3.9}$$

Now, (3.9) is mathematically identical to (3.8) and also physically acceptable. The right side of (3.9) is the excitation that generates the mirror image of the free vibration response of the system in (3.7). Based on this idea, we can generate the mirror image excitation of the free vibration in (3.5) as

$$f(t) = 2c\dot{x}_I(t) = -2c\dot{x}_F(t_n - t) \tag{3.10}$$

If we apply the above excitation to the oscillator with the initial conditions $x_I(0) = x_F(t_n)$ and $\dot{x}_I(0) = -\dot{x}_F(t_n)$, the system vibrates along the mirror image of the free vibration and reaches the state $x_I(t_n) = x_F(0) = x_0$ and $\dot{x}_I(t_n) = -\dot{x}_F(0) = -\dot{x}_0$ at time t_n.

It is insightful to examine the free vibration motion and its mirror image from an energy viewpoint. Let E_0 denote the total initial energy of the system at the start of the free vibration motion. After time t_n, the amount of energy dissipated during the free vibration is

$$E_d(t_n) = \int_{C_F} c\dot{x}_F dx_F = \int_0^{t_n} c\dot{x}_F^2(\tau) d\tau \tag{3.11}$$

where C_F is the displacement path during the free vibration. The energy remaining in the system at time t_n, say $E_F(t_n)$, is the difference of the initial energy and the dissipated energy, i.e. $E_F(t_n) = E_0 - E_d(t_n)$. Now, the mirror image excitation is applied to the system and, after time t_n, the system recovers the initial state of the free vibration motion. From (3.10), the work done by the mirror image excitation during this motion is

$$W = \int_{C_I} 2c\dot{x}_I dx_I = \int_0^{t_n} 2c\dot{x}_I^2(\tau) d\tau \tag{3.12}$$

where C_I is the displacement path during the mirror image motion. The amount of energy dissipated during this motion is the same as that during the free vibration motion. Comparing (3.11) and (3.12), it is clear that half of the input energy has been dissipated

during the mirror image vibration and the remaining half has been stored in the system. The amount of energy stored in the system under the mirror image excitation at time t_n is

$$E_I(t_n) = E_F(t_n) + W - E_d(t_n) = E_F(t_n) + E_d(t_n) = E_0 \tag{3.13}$$

which is identical to the initial energy of the system in the free vibration motion.

So far, we have considered a system with nonlinearity in the elastic restoring force. We can generalize the mirror image excitation to more general nonlinear elastic systems. For example, consider a general elastic SDOF system defined by the differential equation

$$m\ddot{x}(t) + \varphi[x(t), \dot{x}(t)]\dot{x}(t) + R[x(t)] = f(t) \tag{3.14}$$

where the damping coefficient c has been replaced by an algebraic function $\varphi[x(t), \dot{x}(t)]$ of the displacement and velocity at the given time and other parameters are as before. If $\varphi[x(t), \dot{x}(t)]$ is symmetric with respect to both $x(t)$ and $\dot{x}(t)$, i.e., replacing $x(t)$ by $-x(t)$ or $\dot{x}(t)$ by $-\dot{x}(t)$ does not affect the value of $\varphi[x(t), \dot{x}(t)]$, using the same procedure as before, we obtain the mirror image excitation of the free vibration as

$$f(t) = -2\varphi[x_F(t_n - t), \dot{x}_F(t_n - t)]\dot{x}_F(t_n - t) \tag{3.15}$$

where $x_F(t)$ and $\dot{x}_F(t)$ denote the displacement and velocity in the free vibration motion.

One can extend the above concept to a hysteretic system such as an elasto-plastic oscillator. In this case, however, we must consider other types of energy dissipation as well. In a hysteretic system, the energy-dissipation occurs in two ways: one with the damping force, as before, and the other with the hysteretic resistance. Furthermore, the energy dissipation due to the hysteretic resistance works differently under the mirror image excitation from that under the free vibration motion. Therefore, more caution is required in finding the mirror image excitation of general nonlinear systems. This topic is addressed in Section 3.6.

Using a similar idea, we can also generate the mirror image excitation for multi-degree-of-freedom (MDOF) systems. However, unlike an SDOF system, the energy dissipation in an MDOF system occurs at multiple locations and, therefore, the mirror image excitation generated according to this idea may not be useful. Later, we make an

approximation for MDOF systems based on the assumption that a fixed shape, e.g., the fundamental mode shape, dominates the response.

In the following sections, we examine the relation of the mirror image excitation and the design point excitation for specific systems.

3.4 Linear Oscillator Subjected to Gaussian Excitation

For a linear oscillator, a closed-form solution of the design point excitation is readily available (Der Kiureghian 2000, Au and Beck 2001). In this section, rather than deriving the solution itself, we discuss how the design point excitation can be related to the mirror image excitation of the linear oscillator. Though many of the properties that hold for linear systems are not valid for nonlinear systems, the results in this section are useful in gaining insight into the dynamic characteristics of general nonlinear systems.

Consider the stochastic differential equation of a linear SDOF oscillator

$$m\ddot{x}(t) + c\dot{x}(t) + kx(t) = f(t) \tag{3.16}$$

where m is the mass, c is the damping coefficient, k is the stiffness, and $f(t)$ is a random excitation. Suppose $f(t)$ is Gaussian with zero mean. Then, using a discretization method, $f(t)$ can be represented in terms of a linear function of a vector of independent standard normal random variables $\mathbf{u} = [u_1, \cdots, u_n]^{\mathrm{T}}$, as described in Section 2.4, i.e. $f(t) = \mathbf{s}^{\mathrm{T}}(t)\mathbf{u}$, where $\mathbf{s}(t) = [s_1(t), \cdots, s_n(t)]^{\mathrm{T}}$ is a vector of shape functions.

To determine the probability distribution of the response at time t_n, we consider the limit-state function $G(\mathbf{u}) = x_0 - x(\mathbf{u}, t_n)$, where the dependence of the response on the standard normal variables $\mathbf{u}$ is explicitly shown. The design point $\mathbf{u}^*$ is obtained as the solution of the constraint optimization problem

$$\mathbf{u}^* = \arg\min\left\{ \|\mathbf{u}\| :\ G(\mathbf{u}) = x_0 - x(\mathbf{u}, t_n) = 0 \right\} \tag{3.17}$$

Solving (3.17), one obtains

$$\mathbf{u}^* = x_0 \frac{\mathbf{a}(t_n)}{\|\mathbf{a}(t_n)\|^2} \tag{3.18}$$

where $\mathbf{a}(t) = [a_1(t) \cdots a_n(t)]^T$ and

$$a_i(t) = \int_0^t s_i(\tau) h(t-\tau) d\tau \tag{3.19}$$

where $h(t) = \frac{1}{m\omega_d} \exp[-\zeta\omega_n t] \sin(\omega_d t)$ is the unit impulse response function of the oscillator, $\omega_n = \sqrt{k/m}$ is the natural frequency of the oscillator, $\omega_d = \omega_n \sqrt{1-\zeta^2}$, and ζ is the damping ratio (Der Kiureghian 2000).

Now, suppose that the excitation is a Gaussian white noise with intensity S_o. Then, the basis functions $s_i(t)$ can be represented by $s_i(t) = \sigma\delta(t-t_i)$, where $\sigma = \sqrt{2\pi S_o \Delta t}$, $\Delta t = t_i - t_{i-1}$, $i = 1, \cdots, n$, and $\delta(t)$ is the Dirac delta function (see Section 2.4). In this case, (3.18) reduces to

$$u_i^* = x_0 \frac{h(t_n - t_i)}{\sigma \sum_{n=1}^{n} h(t_n - t_i)^2}; \quad i = 1, \cdots, n \tag{3.20}$$

The corresponding design point excitation, $f^*(t)$, is given by

$$f^*(t) = \mathbf{s}^T \mathbf{u}^* = \sum_{i=1}^{n} x_0 \frac{h(t_n - t_i)\delta(t - t_i)}{\sum_{j=1}^{n} h(t_n - t_j)^2} \tag{3.21}$$

where $\delta(t)$ is the Dirac delta function as defined earlier. Due to discretization of the white noise, the design point excitation in (3.21) is represented in the form of a train of pulses. For convenience, we will rewrite (3.21) in the discrete form

$$f_i^* = x_0 \frac{h_i}{\sum_{i=1}^{n} h_i^2} \tag{3.22}$$

where $f_i^* = f^*(t_i)$ and $h_i = h(t_n - t_i)$, $i = 1, \cdots, n$. In the following, it is shown how the design point excitation in (3.22) can be related to the mirror image excitation of the free vibration motion.

Suppose that the linear SDOF oscillator undergoes free vibration with the initial conditions $x(0) = x_0$ and $\dot{x}(0) = 0$. These initial conditions are identical to the conditions

that the oscillator must achieve at $t = t_n$ in response to the design point excitation. The displacement condition, $x(0) = x_0$, is the same as the constraint in (3.17). The velocity condition, $\dot{x}(0) = 0$, corresponding to $\dot{x}(t_n) = 0$ for the response to the design point excitation, is essential for the oscillator to have minimum energy at the prescribed threshold. Under the Gaussian white noise excitation, the design point excitation can be interpreted as a realization of the excitation that puts the system at the threshold x_0 at $t = t_n$ with the minimum energy required. A non-zero velocity at $t = t_n$ would imply that the excitation is superfluous. Therefore, the solution of (3.17) satisfies the additional constraint $G_2(\mathbf{u}) = \dot{x}(\mathbf{u}, t_n) = 0$, though it is not explicitly stated.

Under free vibration with the above initial conditions, the displacement of the oscillator at time t is

$$x_F(t) = \frac{x_0 \omega_n}{\omega_d} \exp[-\zeta \omega_n t] \cos(\omega_d t - \phi) \tag{3.23}$$

where $\phi = \tan^{-1} \frac{\zeta \omega_n}{\omega_d}$. The subscript F is to indicate that the response is in free vibration. The corresponding velocity is proportional to the impulse response function $h(t)$, i.e.,

$$\dot{x}_F(t) = -\omega_n^2 x_0 \frac{1}{\omega_d} \exp[-\zeta \omega_n t] \sin(\omega_d t) = -k x_0 h(t) \tag{3.24}$$

Substituting $h(t) = -\dot{x}_F(t)/k x_0$ into (3.22), we have

$$f_i^* = -\frac{k x_0^2 \dot{x}_F(t_n - t_i)}{\sum_{i=1}^{i=n} \dot{x}_F(t_n - t_i)^2} \tag{3.25}$$

The above relation shows that the design point excitation of a linear system under a Gaussian white noise excitation is proportional to the mirror image of the velocity of the system undergoing free vibration starting from the target threshold x_0 as the initial condition. Multiplying the numerator and denominator of (3.25) by $c\Delta t$ and using the identity $\sum_{i=1}^{i=n} c\dot{x}_F(t_n - t_i)^2 \Delta t = \sum_{i=1}^{i=n} c\dot{x}_F(t_i)^2 \Delta t$, we can rewrite (3.25) as

$$f_i^* = -\frac{kx_0^2 c\dot{x}_F(t_n - t_i)\Delta t}{\sum_{i=1}^{i=n} c\dot{x}_F(t_i)^2 \Delta t} \tag{3.26}$$

In the numerator, $P(x_0) = kx_0^2$ is twice the initial potential energy stored in the system. Assuming that the time interval Δt is small, the term $\sum_{i=1}^{i=n} c\dot{x}_F(t_i)^2 \Delta t$ in the denominator is approximately equal to the dissipated energy $E_d(t_a) = \int_0^{t_n} c\dot{x}_F(\tau)^2 d\tau$ during the free vibration. Thus, we can rewrite (3.26) as

$$f_i^* = -2c\dot{x}_F(t_n - t_i)\Delta t \frac{P(x_0)}{E_d(t_n)} \tag{3.27}$$

We can see that the design point excitation is proportional to the mirror image of the velocity, or the damping force of the free vibration. Furthermore, as t_n increases, the dissipated energy $E_d(t_n)$ approaches the initial potential energy $P(x_0)$ and (3.27) simplifies to

$$f_i^* = -2c\dot{x}_F(t_n - t_i)\Delta t \quad \text{for large } t_n \tag{3.28}$$

The above expression is the discrete form of the mirror image excitation in (3.10) since $x_I(t) = x_F(t_n - t)$ and $\dot{x}_I(t) = -\dot{x}_F(t_n - t)$. Therefore, the design point excitation of a linear oscillator subjected to a Gaussian white noise is identical to the mirror image excitation of the free vibration motion when the oscillator is released from the target threshold.

3.5 Nonlinear Elastic SDOF Oscillator

It was shown in the preceding section that for a linear oscillator subjected to a Gaussian white noise, the design point excitation is the same as the mirror image excitation of the free vibration motion. In this section, it is shown that the same property applies to a nonlinear elastic SDOF oscillator subjected to a stationary Gaussian white noise

excitation. This idea is extended to problems with filtered or/and non-stationary excitations for an approximate solution of the design point excitation.

3.5.1 Stationary Gaussian White Noise

Consider the differential equation governing the response of a nonlinear elastic SDOF oscillator

$$m\ddot{x}(t) + c\dot{x}(t) + R[x(t)] = f(t) \tag{3.29}$$

where m is the mass, c is the damping coefficient, $R[x(t)]$ is a nonlinear elastic restoring force, and $f(t)$ is a Gaussian white noise. In order to find the design point excitation, we must solve the optimization problem of (3.2). The excitation $f(t)$ can be represented in a discrete form as a pulse vector $\mathbf{f} = (f_1, \cdots, f_n)^{\mathrm{T}}$, where $f_i = \sigma u_i$ or $\mathbf{f} \sim \mathrm{N}(\mathbf{0}, \sigma^2\mathbf{I})$, in which $\sigma = \sqrt{2\pi S_o \Delta t}$. In this case, the excitation vector $\mathbf{f}$ is a multiple of the standard normal vector $\mathbf{u}$ and, therefore, solving (3.2) is equivalent to solving

$$\min \|\mathbf{f}\|^2 \text{ subject to } g(\mathbf{f}) = x_0 - x(\mathbf{f}, t_n) = 0 \tag{3.30}$$

For convenience, we have used the norm square instead of the norm itself. This is fine because minimizing the norm square is the same as minimizing the norm. The excitation obtained for the above problem is the design point excitation and also the optimal excitation in the square norm sense.

Instead of directly solving the optimization problem (3.30), we solve the modified problem

$$\min \|\mathbf{f}\|^2 \text{ subject to } g(\mathbf{f}) = P(x_0) - P(x(\mathbf{f}, t_n)) = 0 \tag{3.31}$$

where $P(x)$ is the potential energy stored in the system. (For example, if the system is linear, $P(x) = kx^2/2$.) We have replaced the threshold constraint by the potential energy constraint, which slightly relaxes the feasibility condition. To make sure that we have the same solution as the original problem, we need to have the additional condition that $x(\mathbf{f}, t_n) \geq 0$ when $x_0 \geq 0$ and $x(\mathbf{f}, t_n) \leq 0$ when $x_0 \leq 0$. However, we suppress this constraint because it can be implicitly satisfied. As mentioned earlier, for the design point excitation, the velocity of the system at time t_n must be zero. Hence, the kinetic energy

of the system is zero at t_n and this explains the reason why solving (3.31) leads to the solution of (3.30). Similar to (3.3), the first order optimality conditions of (3.31) are

$$\nabla\|\mathbf{f}\|^2 + \lambda\nabla g(\mathbf{f}) = 0 \tag{3.32a}$$

$$g(\mathbf{f}) = 0 \tag{3.32b}$$

where λ is a Lagrange multiplier

Now, we will show that the mirror image excitation of the free vibration motion of the oscillator satisfies the optimality conditions in (3.32). First, consider the free vibration of the system with the initial conditions $x_F(0) = x_0$ and $\dot{x}_F(0) = 0$. Let $P(x_0)$ denote the corresponding potential energy. Note that the initial conditions of the free vibration motion are set to satisfy the constraints in (3.30) and (3.31) including the implicit constraint that the velocity be zero at time t_n. Suppose that the responses at time t_n are $x_F(t_n) = x_n$ and $\dot{x}_F(t_n) = \dot{x}_n$. Suppose time t_n is sufficiently large for these responses of the damped system to be negligible. Then, the amount of energy dissipated during the free vibration motion is

$$E_d(t_n) = \int_0^{t_n} c\dot{x}_F^2(\tau)d\tau \cong P(x_0) \tag{3.33}$$

Second, consider the mirror image excitation as in Section 3.3, i.e.,

$$f(t) = 2c\dot{x}_I(t) \tag{3.34}$$

where $\dot{x}_I(t) = -\dot{x}_F(t_n - t)$ is the mirror image velocity of the free vibration motion. When subjected to this excitation, after time t_n the oscillator recovers the initial conditions of the free vibration, i.e., $x(t_n) = x_0$ and $\dot{x}(t_n) = 0$. The work done by the mirror image excitation during this motion is

$$W = \int_0^{t_n} 2c\dot{x}_I^2(\tau)d\tau \tag{3.35}$$

Considering that the amount of energy dissipated during this motion is the same as that during the free vibration motion, the energy stored in the system after time t_n is

$$P(x(t_n)) = W - E_d(t_n) = \int_0^{t_n} c\dot{x}_I^2(\tau)d\tau \tag{3.36}$$

Again, we represent the mirror image excitation in the discrete form $\mathbf{f} = (f_1, \cdots, f_n)^{\mathrm{T}}$, where $f_i = \int_{t_{i-1}}^{t_i} f(\tau)d\tau \cong 2c\dot{x}_I(t_i)\Delta t = 2c\dot{x}_{I,i}\Delta t,\ i = 1, \cdots, n,$ and $\Delta t = t_n / n$.

We now examine the optimality conditions in (3.32). For the gradient of $\nabla\|\mathbf{f}\|^2$, we have

$$\frac{\partial}{\partial f_i}\|\mathbf{f}\|^2 = 2f_i = 4c\dot{x}_{I,i}\Delta t, \quad i = 1, \cdots, n \tag{3.37}$$

Using (3.36) and the discrete time interval, we can write the constraint $g(\mathbf{f}) = 0$ as

$$g(\mathbf{f}) = P(x_0) - \sum_{i=1}^{n} c\dot{x}_{I,i}^2 \Delta t$$

$$= P(x_0) - \sum_{i=1}^{n} \frac{f_i^2}{4c\Delta t} = 0 \tag{3.38}$$

The corresponding gradient is

$$\frac{\partial}{\partial f_i} g(\mathbf{f}) = -\frac{f_i}{2c\Delta t} = -\dot{x}_{I,i} \tag{3.39}$$

Both gradients in (3.37) and (3.39) are proportional to the velocity term $\dot{x}_I$ and, therefore, the optimality condition in (3.32a) is satisfied. The optimality condition in (3.32b) is satisfied by virtue of (3.33) and (3.36) and the equality $\int_0^{t_n} c\dot{x}_F^2(\tau)d\tau = \int_0^{t_n} c\dot{x}_I^2(\tau)d\tau$.

Thus, for a nonlinear elastic SDOF system subjected to a stationary Gaussian white noise, the design point excitation is identical to the mirror image excitation of the free vibration motion with the target threshold as the initial condition. Furthermore, as shown in Section 3.3, the mirror image excitation is proportional to the velocity response in the free vibration motion. Therefore, we can find the design point excitation simply by observing the free vibration motion from the target threshold and using the mirror image of the velocity response in free vibration.

Example 3.1

Consider the equation of motion of a Duffing oscillator

$$m\ddot{x}(t) + c\dot{x}(t) + k[x(t) + \gamma x(t)^3] = f(t) \tag{3.40}$$

where m is the mass, c is the damping coefficient, k is the linear stiffness, γ is the nonlinearity parameter, and $f(t)$ is the excitation process. For this oscillator, when the excitation is a Gaussian white noise, the design point excitation is identical to the mirror image excitation. Here, we compute the mirror image excitation from the velocity of the free vibration motion.

For the numerical evaluation, the parameter values m = 1 Kg, $c = 0.2\pi$ N·sec/m, $k = (2\pi)^2$ N/m, and γ = 1 are considered. For the excitation $f(t)$, the Gaussian white noise with intensity S_o = 1 N^2/(rad/sec) is idealized as a train of Gaussian random pulses as in Section 2.4 with $\Delta t = 0.025$ sec, and the response is evaluated at time t_n = 10 sec, which is sufficient time to achieve stationarity in the response of the system. We consider the limit-state function $g = 3\sigma_o - x(t_n)$, where $\sigma_o^2 = \pi S_o/(ck)$ denotes the mean square stationary response of the linear oscillator with $\gamma = 0$.

For the free vibration motion, the oscillator is released with the initial conditions $x(0) = 3\sigma_o$ and $\dot{x}(0) = 0$. Figure 3.2(a) shows the mirror image of the velocity in the free vibration motion. Using (3.34), we compute the mirror image excitation as shown in Figure 3.2(b), which is identical to the design point excitation.

Example 3.2

Consider a nonlinear elastic oscillator described by

$$m\ddot{x}(t) + c[\dot{x}^2(t) + (k/m)x^2(t)]\dot{x}(t) + kx(t) = f(t) \tag{3.41}$$

where m is the mass, c is the damping coefficient, and k is the stiffness, and $f(t)$ is the excitation function. This example is an elastic SDOF oscillator, whose damping value changes depending on the magnitude of the total energy. Specifically, the damping coefficient increases in proportion to the total of the kinetic and potential energy in the oscillator.

We compute the mirror image excitation from the velocity of the free vibration motion. Numerical values of the system parameters considered are m = 1 Kg, c = 1 N·sec/m, and k = 100 N/m. A white noise excitation with intensity S_o = 100 N^2/(rad/sec)

is considered, which is idealized as a train of Gaussian random pulses with $\Delta t = 0.01\,\text{sec}$. The duration of the excitation is set as t_n = 10 sec, and we use the limit-state function $g = 3\sigma - x(t_n)$, where $\sigma^2 = (1/k)\sqrt{mS_o/c}$ is the mean square response of the nonlinear oscillator (Lutes and Sarkani 1997).

The oscillator is released with the initial conditions $x(0) = 3\sigma$ and $\dot{x}(0) = 0$. Figure 3.3(a) shows the mirror image of the velocity in the free vibration motion. We observe that in the early stage of the free vibration, the amplitude reduces rapidly and, after a short while, the amplitude stabilizes as if the oscillator is undamped. This is because the damping value changes in proportion to the energy level. When the total energy stored in the oscillator is sufficiently small, the magnitude of damping is almost negligible and the oscillator behaves like an undamped system. Using (3.15), we compute the mirror image excitation, which is shown in Figure 3.3(b). This is identical to the design point excitation for the limit-state function under consideration.

3.5.2 Stationary Filtered Gaussian Excitation

The results obtained in the previous section strictly apply when the excitation is a Gaussian white noise. For problems with more general excitations, such as non-white, non-stationary or non-Gaussian excitations, one must resort to the iterative optimization algorithm described in Section 2.2.2. However, in such an algorithm, starting from a point near the solution often helps reduce the number of iterations. In this section, we describe how the idea of the mirror image excitation can be used to find a good starting point when the excitation is a stationary filtered Gaussian process. The following section addresses the case of a non-stationary Gaussian excitation.

As described in Section 2.4, a non-white stationary excitation can be considered as the response of a filter to a Gaussian white noise. Unlike a Gaussian white noise, the filtered excitation is correlated and, therefore, the original optimality conditions in the standard normal space given in (3.3) must be considered in finding the design point.

It is instructive to review the structure of the optimality conditions in (3.3). These optimality conditions consist of two parts: first, the direction of the design point should be in line with the gradient of the limit-state function at the design point and, second, the

design point should be on the limit-state surface. If we have an approximate direction of the design point, we can easily find a point along that direction that is on the limit-state surface and, thereby, satisfy the second condition. This point can be used as a starting point for the iteration. We now consider the direction of the design point.

Let $u_i \sim N(0,1)$, $i=1,\cdots,n$, denote the standard normal random variables and $f(t)$ denote the filtered excitation as defined in (2.27). Recall that $f(t_j)=\sum_{i=1}^{j} u_i h_f(t_j-t_i)$, where $h_f(t)$ is the unit-impulse response function of the filter. For convenience, we represent the excitation $f(t)$ by a train of pulses f_j, $j=1,\cdots,n$, where $f_j=\int_{t_{j-1}}^{t_j} f(\tau)d\tau$. As mentioned above, the random variables f_j, $j=1,\cdots,n$, are correlated.

Consider the gradient $\nabla G(\mathbf{u})$ of the limit-state function at the design point in the standard normal space. In reliability analysis, the normalized negative gradient vector $\boldsymbol{\alpha}=-\nabla G/\|\nabla G\|$ plays an important role, as it defines the direction vector of the design point. Using the chain rule, we can write for the elements of the gradient vector

$$\frac{\partial G}{\partial u_i}=\sum_{j=1}^{n}\frac{\partial G}{\partial f_j}\frac{\partial f_j}{\partial u_i} \qquad i=1,\cdots,n \tag{3.42}$$

The term $\partial G/\partial f_j$ represents the derivative of the limit-state function with respect to the excitation pulses f_j, and the term $\partial f_j/\partial u_i$ represents the derivative of the excitation pulse f_j with respect to the standard normal pulse u_i.

For $G(\mathbf{u})=x_0-x(\mathbf{u},t_n)$, the term $\partial G/\partial f_j$ represents the derivative of the negative response $-x(\mathbf{u},t_n)$ with respect to the magnitude of the pulse load at time t_j. In general, this derivative conveys information about the dynamic characteristics of the system. For a linear oscillator, the derivative is indeed the mirror image of the negative unit impulse response function, i.e.,

$$\frac{\partial G}{\partial f_j}=-h(t_n-t_j) \qquad j=1,\cdots,n \tag{3.43}$$

where $h(t)$ is the unit impulse response function of the oscillator. For a nonlinear oscillator, the system properties continuously change depending on the response of the oscillator at the given time and, therefore, a specific form of the response is required to compute the derivative. A response that is close to the response to the design point excitation is desirable because finding the design point excitation is the purpose of the analysis. Here, we use the mirror image of the free vibration motion of the oscillator released with the initial conditions of $x(0) = x_0$ and $\dot{x}(0) = 0$ as the response to compute the derivative. The mirror image of the free vibration motion is identical to the response to the design point excitation for a stationary Gaussian white noise. One can expect that the response to the design point excitation for a filtered Gaussian excitation will not be very different from the mirror image of the free vibration motion, though it will depend on the filter properties. One advantage of using the mirror image of the free vibration motion is that the derivative is proportional to the negative mirror image excitation. From (3.37) and (3.39), we have

$$\frac{\partial G}{\partial f_j} \propto -f_j \qquad j = 1, \cdots, n \tag{3.44}$$

where f_j, $j = 1, \cdots, n$, are the mirror image excitation in pulse form, i.e., $f_j = \int_{t_{j-1}}^{t_j} f(t)dt$.

The partial derivatives $\partial f_j / \partial u_i$ are easily computed for a linear filter. Specifically,

$$\frac{\partial f_j}{\partial u_i} = \begin{cases} h_f(t_j - t_i) & i \le j \\ 0 & \text{otherwise} \end{cases} \tag{3.45}$$

where $h_f(t)$ is the unit impulse response function of the filter.

Having computed the partial derivatives, we estimate the direction of the gradient vector at the design point by substituting the derivatives into (3.42). Given the direction vector $\alpha = -\nabla G / \|\nabla G\|$, the next step is to find the point $\mathbf{u} = \beta\alpha$ by solving for β in $G(\beta\alpha) = 0$. For most problems, this can be easily done by the secant method. For a linear system, this leads to an exact solution of the design point. For a nonlinear system, it leads to an approximate solution, which often is sufficiently accurate for practical purposes.

Example 3.3

Consider the Duffing oscillator of Example 3.1. All parameters are as before, except that the excitation is now a filtered Gaussian white noise specified by

$$f(t) = \ddot{x}_f(t) + W(t) = -2\zeta_f \omega_f \dot{x}_f(t) - \omega_f^2 x_f(t) \tag{3.46}$$

where $x_f(t)$ is the response of the filter. Numerical values for filter parameters are set as $\omega_f = 5\pi$ rad/sec and $\zeta_f = 0.6$. The impulse response function of this filter is given in (2.33) of Chapter 2. The Gaussian white noise with the intensity $S_o = 1$ N^2/(rad/sec) is idealized with the time step $\Delta t = 0.025$ sec as before. The limit-state function is $g = 3\sigma_o - x(t_n)$, where $\sigma_o^2 = \pi S_o/(ck)$ is the mean square response of the linear oscillator with $\gamma = 0$ in (3.40).

Figure 3.4 compares the unit direction vectors α of the exact design point and of the approximate design point obtained by the method described above. The inner product of these two vectors is computed as 0.989. We can see that the direction obtained by this method is extremely close to the direction of the exact design point. This direction vector can now be used to find a corresponding point on the limit-state surface as a close approximation to the design point.

3.5.3 Non-stationary Filtered Gaussian Excitation

We now consider a non-stationary Gaussian excitation, which is obtained by time modulating a stationary process (see Section 2.4 for details).

It is instructive to examine the statistical properties of the random pulses f_j obtained by the discretization of the excitation process in the form $f_j = \int_{t_{j-1}}^{t_j} f(\tau)d\tau$. For a stationary Gaussian white noise, the excitation pulses are statistically independent and identically distributed. In this case, the design point can be found directly from the mirror image excitation, as described before. For a stationary Gaussian non-white excitation, the excitation pulses are identically distributed but not statistically independent. In the previous section, we showed that in this case, the design point or a close approximation

to it can be obtained by incorporating the correlation between pulses into the mirror image excitation. Recall that the correlation is incorporated in terms of the derivative $\partial f_j / \partial u_i$ as shown in (3.42) and (3.45). In the case of a non-stationary excitation, if the time-modulation function is directly applied to a stationary Gaussian white noise, the excitation pulses are statistically independent but not identically distributed. On the other hand, if the time-modulation function is applied to a stationary Gaussian non-white excitation, then we have correlated excitation pulses that are not identically distributed. In both cases, the excitation pulses are not identically distributed, and we must properly account for this to find a good approximation of the design point.

Here, we use a simple approach. First, we assume that the excitation is stationary and find the design point excitation or its approximation by use of the mirror image excitation, as described in Section 3.5.1 and 3.5.2. Second, we apply the time-modulation function to the excitation obtained under the stationarity assumption. This gives us an approximate direction vector α, which can be used to find the design point by solving $G(\beta\alpha) = 0$.

In this method, the non-stationarity is incorporated in a rather crude manner. Numerical experiments show that this method may or may not work well depending on the shape of the time modulation function. Furthermore, if the excitation has both temporal and spectral non-stationarity (for example, by use of multiple filters with different modulating functions), this approach may not work well. The following example provides an indication of the effectiveness of this method.

Example 3.4

In this example, a non-stationary Gaussian excitation is applied to the Duffing oscillator of Example 3.3. All conditions are as before, except that the following modulating function is applied to the stationary excitation to achieve a non-stationarity input:

$$\begin{aligned} q(t) &= t^2/25 && 0 \le t < 5 \\ &= 1 && 5 \le t < 10 \\ &= \exp[-(t-10)/2] && 10 \le t \end{aligned}$$

We set the time parameter in the limit-state function as t_n = 5, 10, and 12 sec and examine the unit direction vectors of the design point and its approximation. Figure 3.5 compares the vectors α of the exact design point and its approximate point obtained by the proposed method for the three cases. We see that for the case with t_n = 5 sec, where t_n is within the upslope of the time-modulation function, the computed direction vector α is not quite accurate (the inner product with the exact value of α is 0.798), but good enough to be used as an "educated" starting point for an iterative solution. For t_n = 10 sec, we obtain an excellent approximation of the direction vector (the inner product of the two vectors is 0.983). When t_n is in the down slope of the time-modulation function, as in part (c) of Figure 3.5, the approximate direction vector α tends to be far from the exact direction of the design point (the inner product of two vectors is 0.130).

In most applications, particularly in earthquake engineering, our interest is in reliability during the strong motion phase of the earthquake. This example shows that the proposed method provides good results on this segment of the non-stationary excitation.

3.6 Hysteretic SDOF Oscillator

One characteristic of a hysteretic system is that there remains a permanent deformation after a free vibration motion if the initial displacement is beyond the yield point. Due to this effect, the mirror image excitation of the free vibration motion of a hysteretic oscillator is not necessarily the same as the design point excitation for the response to a stationary Gaussian white noise. However, it has been observed in numerical examples that the mirror image excitation shows a similar pattern to the design point excitation. Furthermore, for mildly hysteretic systems, those two excitations are almost identical. In this section, we develop the mirror image excitation for the case of an oscillator having the Bouc-Wen hysteresis model.

Consider the equation of motion of a hysteretic oscillator represented by the Bouc-Wen model (Bouc 1963, Wen 1976)

$$m\ddot{x}(t) + c\dot{x}(t) + k[\alpha x(t) + (1-\alpha)z(t)] = f(t) \tag{3.47}$$

$$\dot{z}(t) = -\gamma|\dot{x}(t)||z(t)|^{n-1} z(t) - \beta|z(t)|^{n} \dot{x}(t) + A\dot{x}(t) \tag{3.48}$$

where m is the mass, c is the damping coefficient, k is the stiffness, α is a parameter controlling the degree of hysteresis, and $z(t)$ is the hysteretic term governed by the nonlinear differential equation in (3.48), where γ, β, A and n are parameters that control the shape and amplitude of the hysteresis loop. Suppose that we have the limit-state function $G(\mathbf{u}) = x_0 - x(\mathbf{u}, t_n)$, such that at the design point $x(t_n) = x_0$ and $\dot{x}(t_n) = 0$. Let $z(t_n) = z_0$ be the value of the hysteretic response at the design point. We know that, similarly to the velocity response, we must have $\dot{z}(t_n) = 0$. The hysteretic term z_0 is usually unknown but we can determine it while seeking the response of the mirror image excitation of the free vibration. The response of the mirror image motion can be computed in the following manner.

First, we compute the free vibration response with the initial conditions $x_F(0) = x_0$, $z_F(0) = z_0$ and $\dot{x}_F(0) = \dot{z}_F(0) = 0$ where z_0 is a small trial value. The subscript F indicates the free vibration response. By reversing the time order of the displacement $x_F(t)$ and velocity $\dot{x}_F(t)$ of the free vibration response, we obtain the response of the mirror image motion, i.e., $x_I(t) = x_F(t_n - t)$ and $\dot{x}_I(t) = -\dot{x}_F(t_n - t)$, where the subscript I indicates the response of the mirror image motion. The mirror image response of the hysteretic term, denoted $z_I(t)$, cannot be obtained by reversing the free vibration response $z_F(t)$, since the hysteretic term under the mirror image motion works differently from that under the free vibration. To obtain the hysteretic response for the mirror image motion, we must solve the first order differential equation

$$\dot{z}_I(t) = -\gamma|\dot{x}_I(t)||z_I(t)|^{n-1} z_I(t) - \beta|z_I(t)|^{n} \dot{x}_I(t) + A\dot{x}_I(t) \tag{3.49}$$

with the initial condition $z_I(0) = 0$. If $z_I(t_n)$ is different from the assumed value $z_F(0) = z_0$, set $z_0 = z_I(t_n)$ and repeat the above analysis. Depending on the degree of nonlinearity, three to seven iterations usually produce convergence.

Having computed the mirror image response of the free vibration, we can now compute the corresponding mirror image excitation. This excitation consists of damping and hysteretic parts as follows:

$$f(t) = 2c\dot{x}_I(t) + f_{\text{hys}}[x_I(t), \dot{x}_I(t), z_I(t)] \tag{3.50}$$

The damping part of the excitation, $2c\dot{x}_I(t)$, is the same as that for elastic problems described in Section 3.3. The hysteretic part $f_{\text{hys}}[x_I(t), \dot{x}_I(t), z_I(t)]$ can be obtained from the hysteretic loops of the free vibration and its mirror image. Figure 3.6 shows the half cycles of the hysteretic loops of the free vibration and its mirror image. The velocities at the maximum points a and b are zero. The hysteretic term $z_F[x(t)]$ is that of the free vibration from a to b and the hysteretic term $z_I[x(t)]$ is that of its mirror image from b to a. The straight line $z_L[x(t)]$ represents the case of no hysteretic energy loss. When the system undergoes free vibration from a to b, the energy loss due to hysteretic resistance is $\int_{x_a}^{x_b} k(1-\alpha)[z_F(t) - z_L(t)]dx$. In the mirror image of the free vibration, the hysteretic energy loss is $\int_{x_b}^{x_a} k(1-\alpha)[z_I(t) - z_L(t)]dx$. The total input energy required to compensate the hysteretic energy loss in the mirror image excitation is the sum of the two energy losses, i.e. $\int_{x_b}^{x_a} k(1-\alpha)[z_I(t) - z_F(t)]dx$. Therefore, the hysteretic part of the mirror image excitation is

$$f_{\text{hys}}[x(t), \dot{x}(t), z(t)] = k(1-\alpha)[z_I(t) - z_F(t)] \tag{3.51}$$

For convenience, one may use $f_{\text{hys}}[x(t), \dot{x}(t), z(t)] \approx 2k(1-\alpha)[z_I(t) - z_L(t)]$ with a negligible loss in accuracy

Example 3.5

Consider the SDOF Bouc-Wen oscillator in (3.47) and (3.48). The oscillator is subjected to a Gaussian white noise excitation with intensity $S_o = 1\,\text{N}^2/(\text{rad/sec})$. The damping coefficient is set as $c = 0.3\pi$ N·sec/m and the linear stiffness is set as $k = (3\pi)^2$ N/m. For other parameters, numerical values are set as $n = 1$, $A = 1$ and $\gamma = \beta = 1/2\sigma_o$, where $\sigma_o^2 = \pi S_o/(ck)$ is the mean square response of the linear ($\alpha = 1$) oscillator. The white noise excitation is idealized as a train of Gaussian random pulses with $\Delta t = 0.02$ sec. The

limit-state function $G(\mathbf{u},t_n)=x_0-x(\mathbf{u},t_n)$ is considered with $t_n=8\,\text{sec}$. We consider two cases for the hysteresis parameter α: α = 0.5 for a mildly hysteretic oscillator, and α = 0.1 for a strongly hysteretic oscillator.

Figure 3.7 shows the exact and approximate design point hysteretic loops for mildly and strongly hysteretic parameters. For the mildly hysteretic oscillator with α = 0.5, the approximate response obtained from the mirror image of the free vibration motion is very close to the exact design point response, while for the strongly hysteretic system with α = 0.1, the approximate design point response is not as accurate. This affects the approximate solution to the design point. As shown in Figure 3.8, for the mildly hysteretic oscillator, the unit direction vector $\boldsymbol{\alpha}$ for the approximate design point practically coincides with the direction vector $\boldsymbol{\alpha}$ for the exact design point (the inner product of the two unit vectors is 0.986). For the strongly hysteretic system, the approximate solution of the $\boldsymbol{\alpha}$ vector is considerably different from the exact direction (the inner product of the two vectors is 0.790). For strongly hysteretic systems, the results obtained by this analysis can be used as a good starting point for the iterative algorithm to find the exact design point.

3.7 MDOF System

As mentioned in the introduction, for an MDOF system we cannot directly find the design point using the mirror image excitation, even for a linear system subjected to stationary Gaussian white noise excitation. In many cases, however, the mirror image excitation can still be used to find a rough approximation of the design point or a good starting point for an iterative solution.

Consider the differential equation of a nonlinear MDOF system

$$\mathbf{M}\ddot{\mathbf{x}}(t)+\mathbf{C}\dot{\mathbf{x}}(t)+\mathbf{R}[\mathbf{x}(t)]=\mathbf{f}(t) \tag{3.52}$$

where $\mathbf{M}$ is the $m\times m$ positive definite mass matrix, $\mathbf{C}$ is the $m\times m$ positive definite damping matrix, $\mathbf{R}[\mathbf{x}(t)]$ is an $m\times 1$ vector of nonlinear restoring forces, and $\mathbf{f}(t)$ is an $m\times 1$ vector of excitations. We restrict our attention to an excitation in the form of a base

motion, in which case $\mathbf{f}(t) = \mathbf{M}\mathbf{P}\ddot{u}_g(t)$, where the influence vector $\mathbf{P}$ represents the displacements at the degrees of freedom of the structure resulting from static application of a unit base motion, and $\ddot{u}_g(t)$ is the acceleration of the base.

In order to obtain an approximation of the design point for the MDOF system, we assume a dominant vibration shape for the system. For example, we can assume the vibration shape as the first mode of the linear system obtained by the initial stiffness properties of the system. We then set the initial conditions of the system consistent with the assumed vibration shape such that the limit-state function is satisfied, i.e., such that $g[\mathbf{x}_F(0)] = 0$ and $\dot{\mathbf{x}}_F(0) = 0$. Then, we perform free vibration analysis and compute the mirror image excitation. If the system is elastic, an approximation of the design point excitation is

$$\mathbf{f}(t) = -2\mathbf{C}\dot{\mathbf{x}}_F(t_n - t) = 2\mathbf{C}\dot{\mathbf{x}}_I(t) \tag{3.53}$$

where $\dot{\mathbf{x}}_I(t)$ is the mirror image of the velocity of the free vibration motion. The corresponding base acceleration is

$$\ddot{u}_g(t) = \frac{\mathbf{P}^{\mathrm{T}}\mathbf{M}^{-1}\mathbf{f}(t)}{\mathbf{P}^{\mathrm{T}}\mathbf{P}} \tag{3.54}$$

For a hysteretic system, similarly to (3.50), we can write the approximate solution as

$$\mathbf{f}(t) = 2\mathbf{C}\dot{\mathbf{x}}_I(t) + \mathbf{f}_{\mathrm{hys}}[\mathbf{x}_I(t), \dot{\mathbf{x}}_I(t), \mathbf{z}_I(t)] \tag{3.55}$$

Example 3.6

Consider a two-degree-of-freedom Bouc-Wen structure (see Figure 3.9) defined by

$$\mathbf{M}\ddot{\mathbf{x}}(t) + \mathbf{C}\dot{\mathbf{x}}(t) + \mathbf{K}\left[\begin{Bmatrix}\alpha_1 d_1(t)\\ \alpha_2 d_2(t)\end{Bmatrix} + \begin{Bmatrix}(1-\alpha_1)z_1(t)\\ (1-\alpha_2)z_2(t)\end{Bmatrix}\right] = \mathbf{M}\mathbf{1}\ddot{u}_g(t) \tag{3.56}$$

$$\dot{z}_i(t) = -\gamma_i\left|\dot{d}_i(t)\right|\left|z_i(t)\right|^{n-1} z_i(t) - \beta_i\dot{d}_i(t)\left|z_i(t)\right|^n + A_i\dot{d}_i(t) \qquad i = 1, 2 \tag{3.57}$$

where $\mathbf{M}$ is the mass matrix, $\mathbf{C}$ is the damping coefficient matrix, $\mathbf{K}$ is the linear stiffness matrix, $d_1(t) = x_1(t)$, $d_2(t) = x_2(t) - x_1(t)$ are the inter-story drifts, $z_i(t)$, $i = 1, 2$, are hysteretic components of the response, and $\ddot{u}_g(t)$ is the ground acceleration. We set the

system parameters as $\mathbf{M} = m\begin{bmatrix} 2 & 0 \\ 0 & 1 \end{bmatrix}$, $\mathbf{C} = c\begin{bmatrix} 6 & -2 \\ -2 & 2 \end{bmatrix}$, $\mathbf{K} = k\begin{bmatrix} 2 & 0 \\ 0 & 1 \end{bmatrix}$, where parameter values are m = 1 Kg, c = 1 N·sec/m, and k = 10 N/m, and the parameters of the hysteretic model as $A_1 = A_2 = 1$, $\gamma_1 = \beta_1 = 1/2\sigma_{d1o}$, and $\gamma_2 = \beta_2 = 1/2\sigma_{d2o}$, where σ_{d1o} and σ_{d2o} are the standard deviations of the interstory drifts of the linear system (α_1 = α_2 = 1) numerically estimated as 0.562 and 0.481, respectively. In (3.56), **1** is a 2-vector of ones. The ground acceleration $\ddot{u}_g(t)$ is given as a stationary Gaussian white noise with intensity $S_o = 1$ (m/sec)^2/(rad/sec), which is idealized as a train of Gaussian random pulses with $\Delta t = 0.025$ sec. The limit-state function is set as $g = 3\sigma_{d2o} - d_2(t_n)$ with $t_n = 12$ sec. Two cases are examined: (a) $\alpha_1 = \alpha_2 = 0.5$ for a mildly hysteretic system, and (b) $\alpha_1 = \alpha_2 = 0.1$ for a strongly hysteretic system.

Figure 3.10 compares the exact and approximate estimates of the unit direction vector $\boldsymbol{\alpha}$ for the design point. For the mildly nonlinear system with $\alpha_1 = \alpha_2 = 0.5$, the approximation is excellent with the two vectors practically coinciding (the inner product of the two vectors equals 0.998). For the strongly nonlinear system with $\alpha_1 = \alpha_2 = 0.1$, the approximation is poor (the inner product of two vectors equals 0.674), but a good starting point for an iterative solution of the design point.

3.8 Uncertainties in System Parameters

One advantage of the reliability methods used in this study is that one can easily handle system uncertainties. In the reliability formulation, we already deal with a large number of random variables to represent the continuous input process in a discrete form. Incorporating the system uncertainties is accomplished by simply adding a few more random variables. Although this process will increase the computational work, the randomness in the system parameters does not affect the basic framework of the method.

When system parameters are modeled as random variables, nonlinearity is introduced into the limit-state function. Even a linear system subjected to a Gaussian excitation becomes a nonlinear problem, if there is randomness in system parameters.

Therefore, we have to solve for the design point using the iterative algorithm described in Section 2.2.2. However, we can reduce the needed computational effort by using the mirror image excitation at the initial stage of the analysis. For this purpose, we may use the mean or other reasonable values of the system parameters to generate the mirror image excitation. This approach is illustrated in the following example.

Example 3.7

Consider the Duffing oscillator of Example 3.1 with the same excitation. Here, the system parameters ω and ζ are considered as random variables having independent lognormal distributions with means 2π rad/sec and 0.05, respectively equal coefficients of variation δ, for which we consider the three cases $\delta = 0$ (deterministic system), $\delta = 0.05$ and $\delta = 0.1$. The results of the analysis are summarized in Table 3.1 and Figure 3.11. Table 3.1 lists the design point coordinates of the system parameters along with the corresponding reliability indices for each case. Figure 3.10 shows the exact design point excitations for the three systems. It can be seen that the design point excitations are rather different, but the solution for the deterministic system can serve as a good starting point for iterative solution of the design point for the random systems.

The randomness in system parameters increases the uncertainty in the response of the system, flattening the probability density function of the response variables in the tail region and significantly reducing the reliability index. When tail behavior of the probability density function is of interest in the system response, the system uncertainties, if present, must be considered.

3.9 Estimation of the Mean Out-crossing Rate

In Section 2.5.2, we showed that the mean out-crossing rate can be obtained by solving

$$\nu(t) = \lim_{\delta t \to 0} \frac{P\{g[\mathbf{x}(t), \mathbf{v}] > 0 \cap g[\mathbf{x}(t+\delta t), \mathbf{v}] \le 0\}}{\delta t}$$

$$\cong \frac{P\{g[\mathbf{x}(t), \mathbf{v}] > 0 \cap g[\mathbf{x}(t+\delta t), \mathbf{v}] \le 0\}}{\delta t} \quad \text{for small } \delta t \qquad (3.58)$$

The numerator in (3.58) is a parallel system reliability problem with two components. In FORM, this is approximated by

$$P\{g[\mathbf{x}(t),\mathbf{v}]>0 \cap g[\mathbf{x}(t+\delta t),\mathbf{v}]\le 0\} \cong \Phi(\beta_1,\beta_2,\rho) \tag{3.59}$$

where β_1 and β_2 are the reliability indices for the events $g_1 = g[\mathbf{x}(t),\mathbf{v}]>0$ and $g_2 = g[\mathbf{x}(t+\delta t),\mathbf{v}]\le 0$, respectively.

For an accurate result, we must make the perturbation δt as small as possible. However, the two events are only δt apart in time with opposite inequality signs. Therefore, if we use too small a δt, the correlation coefficient between the two linearized events becomes almost -1, and this causes singularity in the probability integration of (2.11). In practice, $\delta t = \Delta t/10$ or $\delta t = \Delta t/100$, where Δt is the interval used in discretizing the excitation, is sufficiently small for a reliable result. Still, the correlation coefficient is very close to -1 and, therefore, high computational precision is required to obtain a stable result. Since the correlation coefficient is equal to the inner product of the unit α vectors of the two design points, this also means that accurate estimation of the design points is necessary for this analysis

If we use the relation of the two limit-state functions, however, we can easily solve the problem. Observe that the second limit-state function in (3.57) is almost identical to the first one, except that it is slightly shifted in time and has the inequality sign in the opposite direction. Suppose that we have found the design point excitation of the first component, say $f_1(t)$. Let β_1 and α_1 denote the corresponding reliability index and normalized negative gradient vector. For sufficiently small δt, we can approximate the design point excitation of the second component by shifting the first design point in time by δt, i.e., $f_2(t) = f_1(t+\delta t)$ as shown in Figure 3.12 for an example case.

For a stationary excitation, the above procedure produces the exact result, since the design point excitations at different target times have the same shape but are shifted in time. For a non-stationary excitation, the procedure is not exact, since the probabilistic structure of the process changes in time. However, the approximation produces sufficiently accurate result if δt is much smaller than the time scale of change of the probabilistic structure of the non-stationary process. This condition is easily satisfied in

practical problems. With this approximation, the reliability index of the second component is $\beta_2 \approx -\beta_1$, and the corresponding normalized negative gradient vector α_2 is obtained by shifting α_1 in time by δt. This simple approach is advantageous in that we can get stable and consistent results without having to compute the design points with high precision. Furthermore, for the case with $\beta = \beta_1 = -\beta_2$ and ρ close to -1, the probability integral in (2.11) simplifies to

$$\Phi_2(\beta, -\beta, \rho) \cong \frac{1}{2\pi} \exp\left(-\frac{\beta^2}{2}\right)\left[\sin^{-1}(\rho) - \sin^{-1}(-1)\right] \tag{3.60}$$

where $\rho = \alpha_1^T \alpha_2$. See Appendix A for the derivation of this result.

Example 3.8

We estimate the up-crossing rate for the displacement response of the Duffing oscillator of Example 3.4 above the threshold of $3\sigma_o$, where $\sigma_o^2 = \pi S_o /(ck)$ is the mean-square response of the linear oscillator with $\gamma = 0$ in (3.40). All parameter values are the same as described in Example 3.4. The time increment for computing the up-crossing rate is selected as $\delta t = \Delta t / 100$ sec.

Figure 3.13 compares the mean up-crossing rate obtained by this simple method with the exact result based on a complete FORM analysis of the parallel system. For the exact analysis, the program CALREL (Liu, *et al.* 1989) was used. It is observed that the proposed simple method for computing the mean up-crossing rate produces an excellent result.

Table 3.1. Design point system coordinates for Duffing oscillator with deterministic and random parameters.

Case	Reliability Index	Design Point Values	
		ω	ζ
Deterministic system $\delta = 0$	3.755	2π	0.05
Random System $\delta = 0.05$	3.601	$0.958 \times 2\pi$	0.978×0.05
Random System $\delta = 0.10$	3.326	$0.907 \times 2\pi$	0.940×0.05

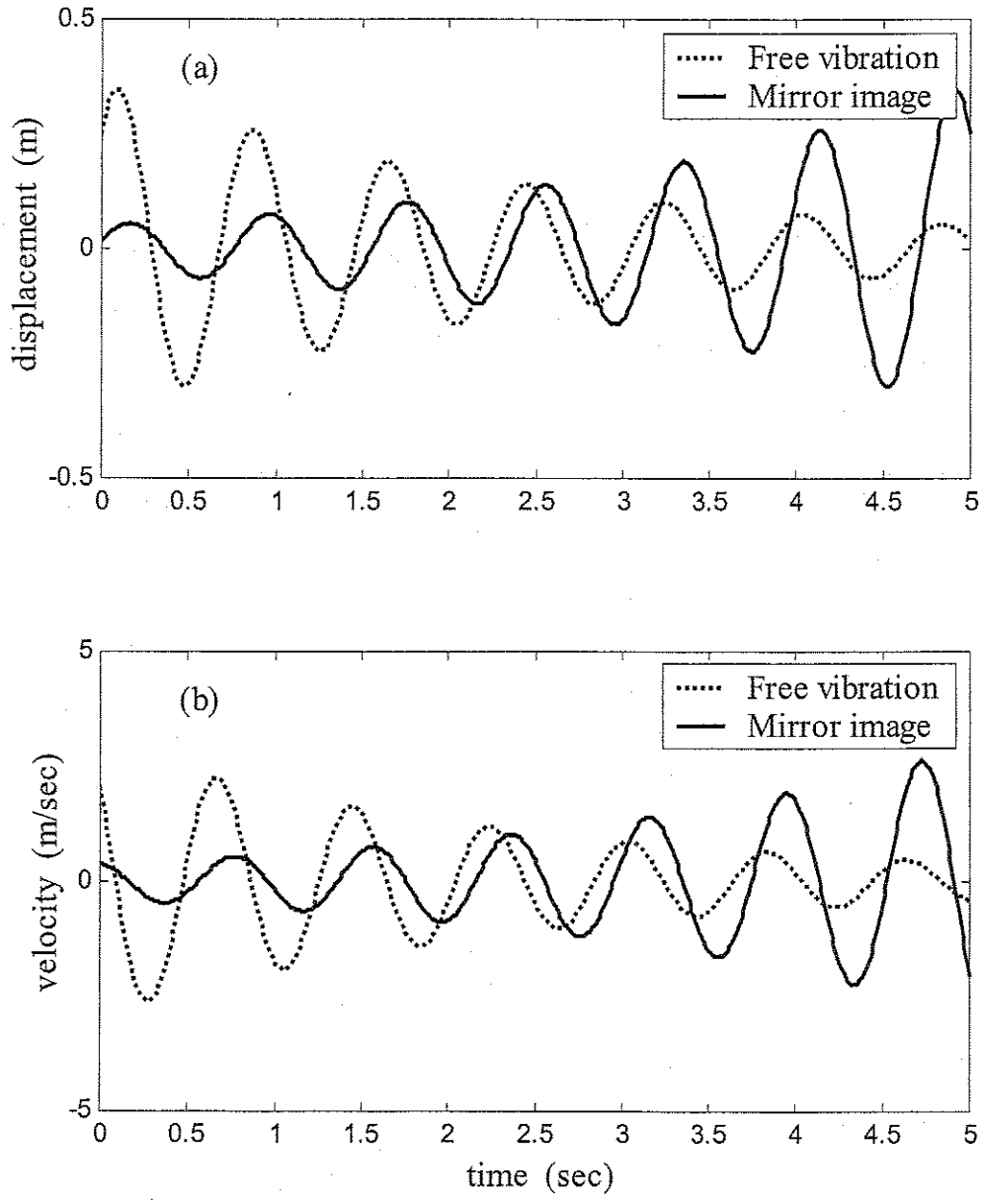

Figure 3.1. Free vibration responses and their mirror images: (a) displacement (b) velocity.

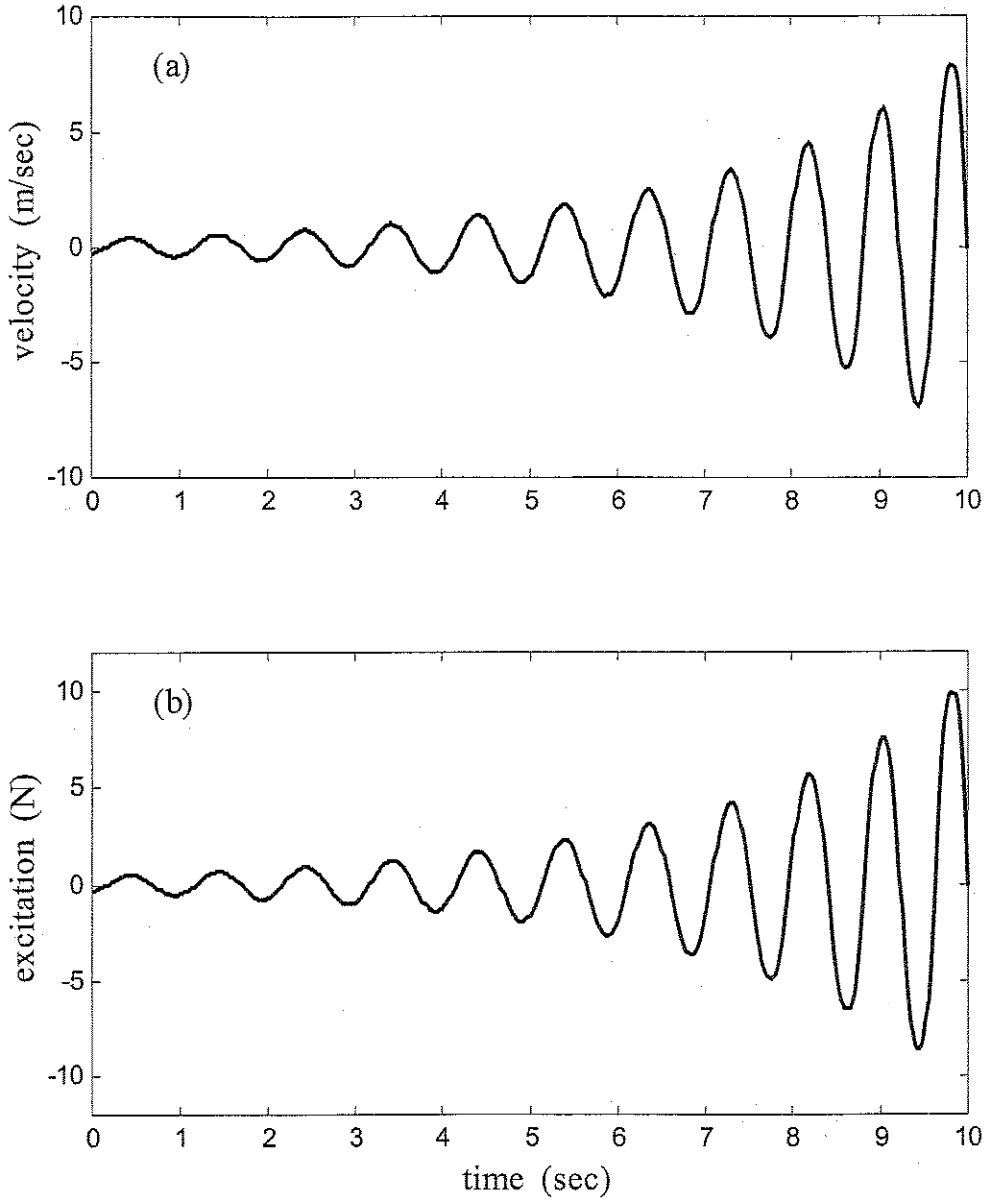

Figure 3.2. Results for the Duffing oscillator: (a) mirror image of velocity response in free vibration, (b) mirror image excitation.

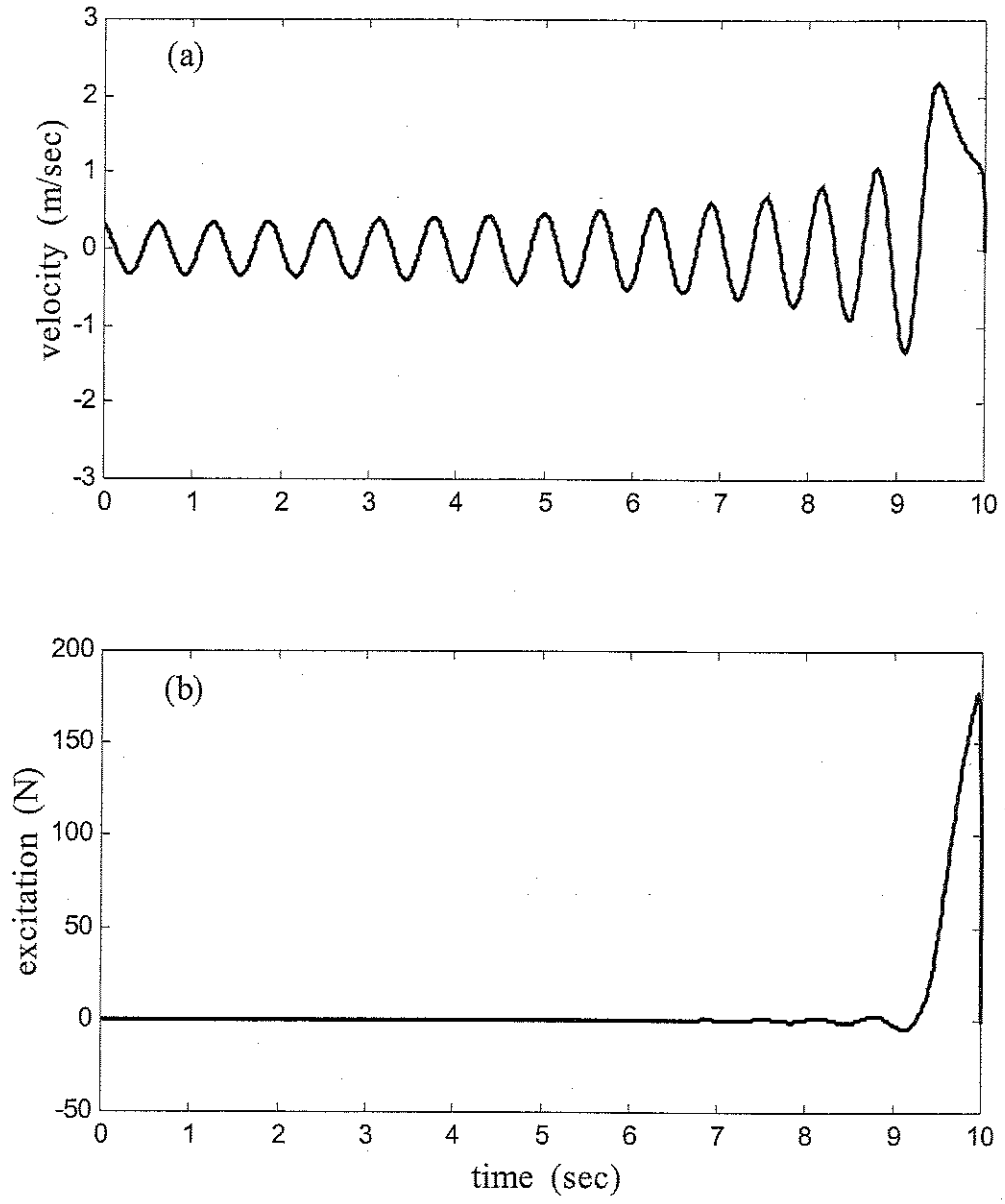

Figure 3.3. Results for elastic oscillator with nonlinear damping: (a) mirror image of velocity response in free vibration, (b) mirror image excitation.

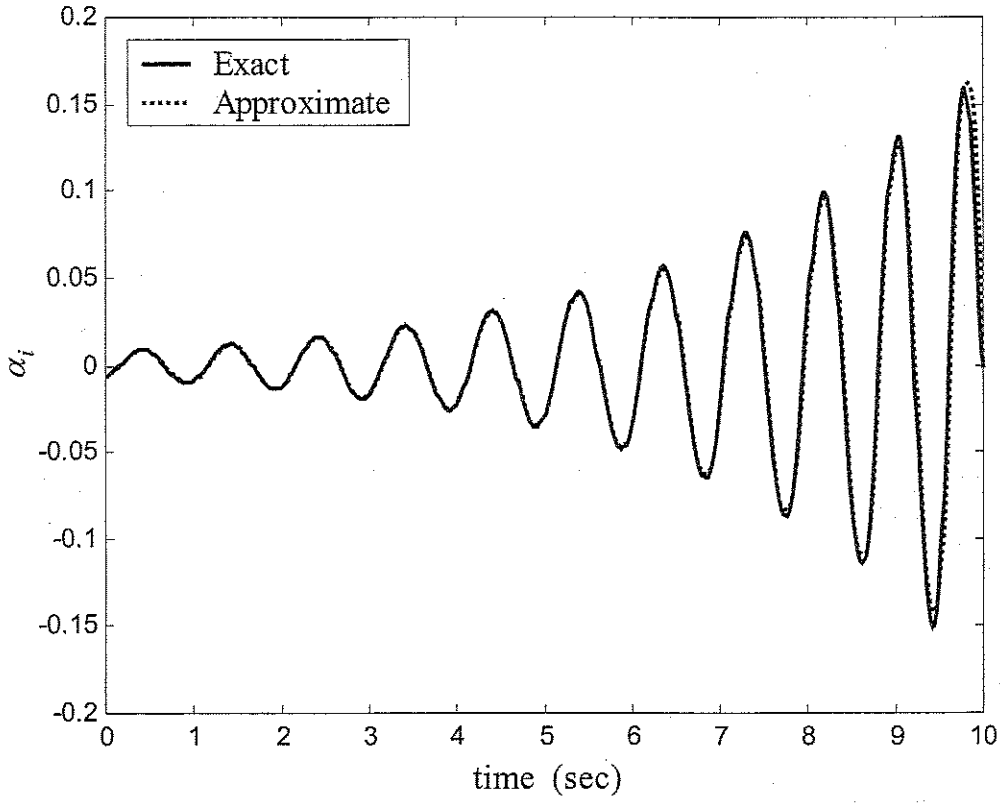

Figure 3.4. Exact and approximate $\boldsymbol{\alpha}$ vectors at the design point for the response of a Duffing oscillator to a filtered stationary Gaussian excitation.

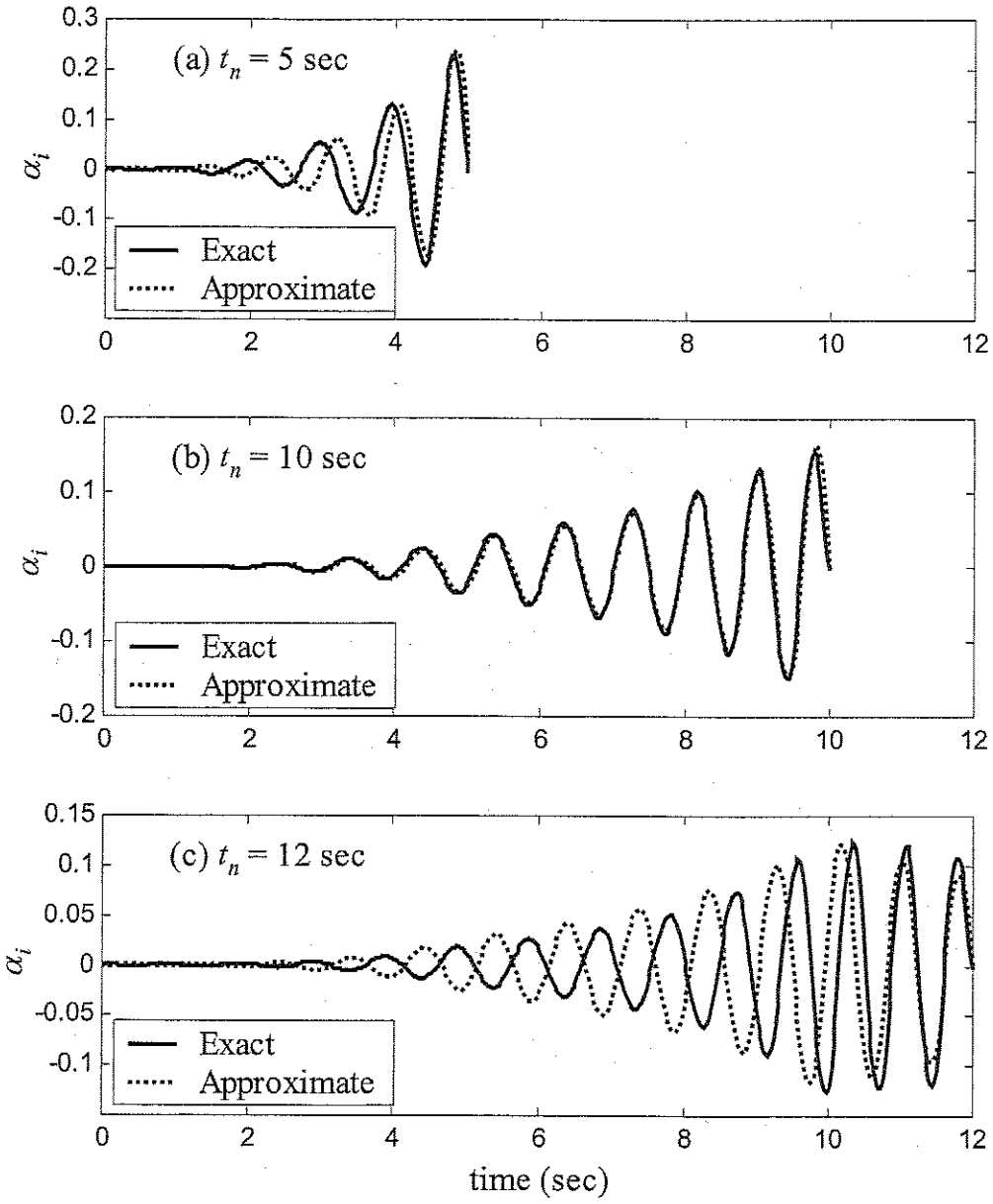

Figure 3.5. Exact and approximate α vectors at the design point for the response of a Duffing oscillator to a non-stationary filtered excitation for selected time points t_n.

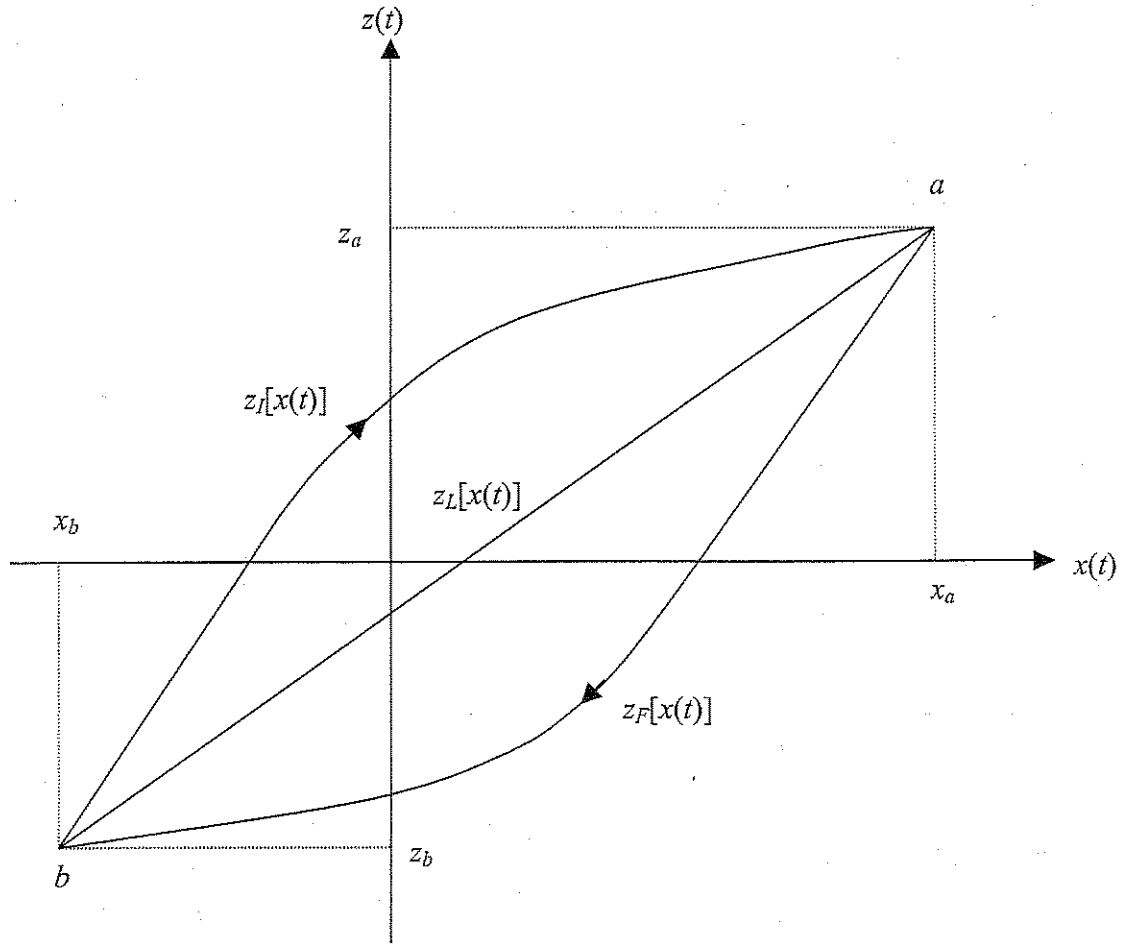

Figure 3.6. Energy dissipating mechanism of a hysteretic oscillator.

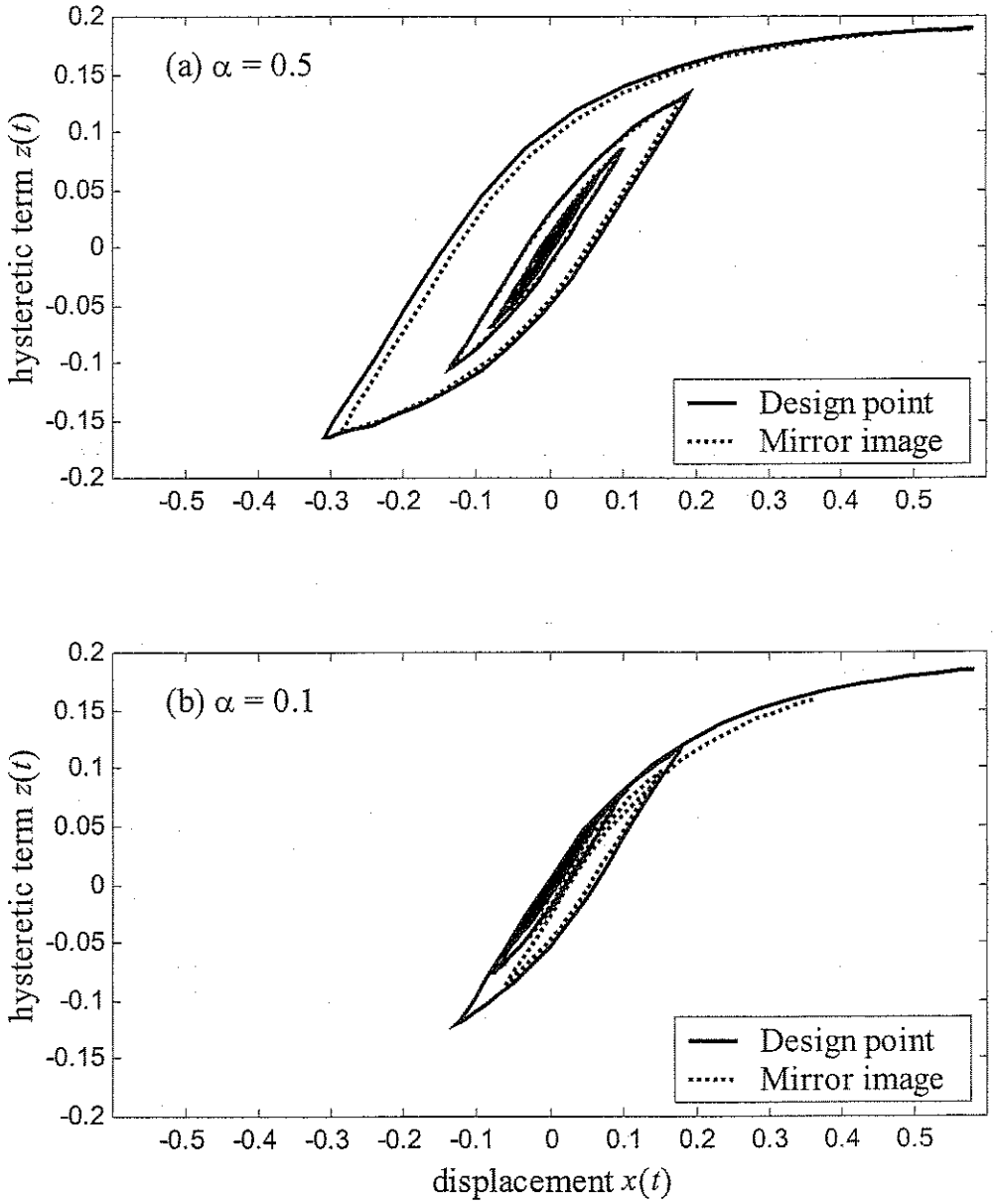

Figure 3.7. Exact and approximate design point hysteresis loops for Bouc-Wen oscillator.

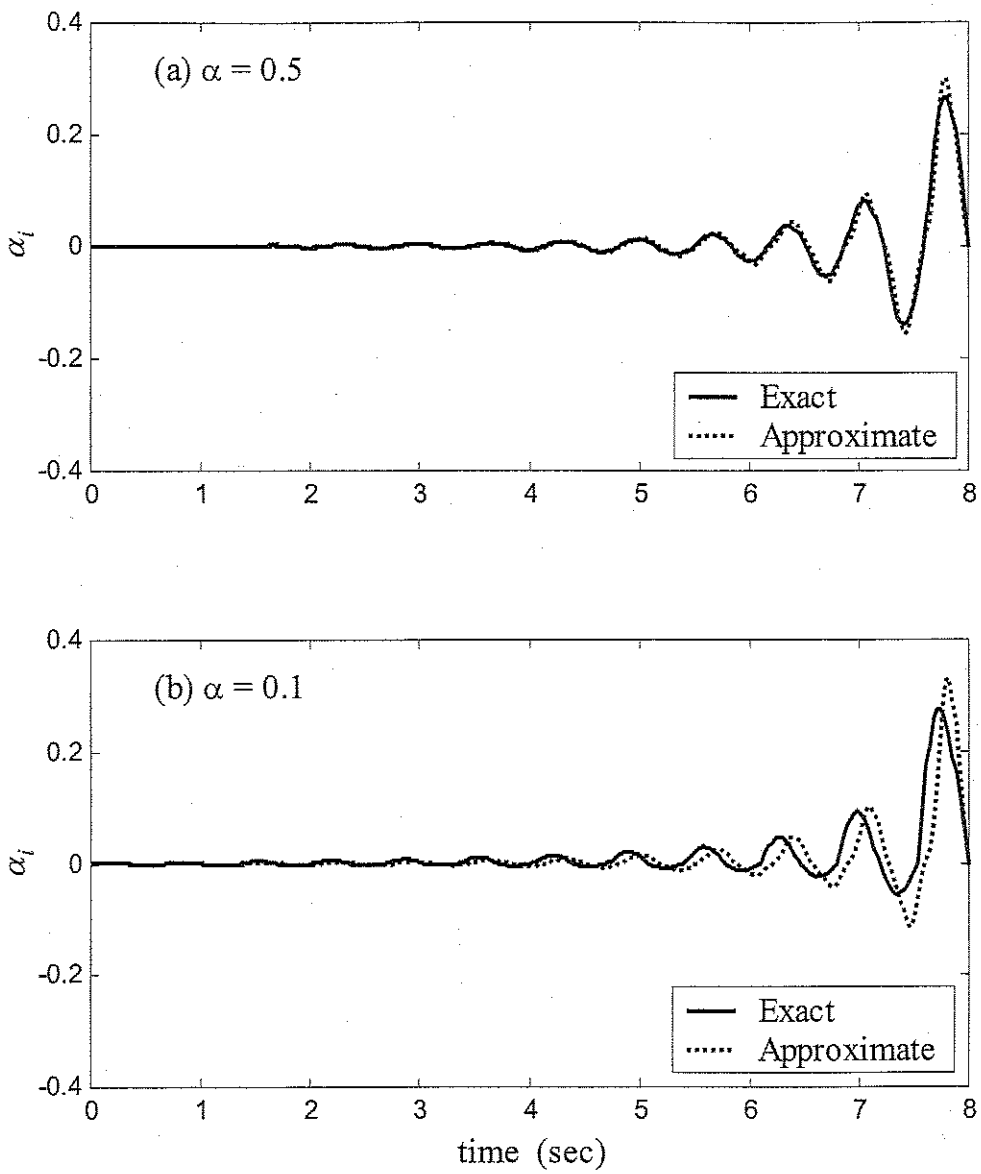

Figure 3.8. Exact and approximate α vectors at the design point for the response of a Bouc-Wen oscillator to a Gaussian white noise excitation.

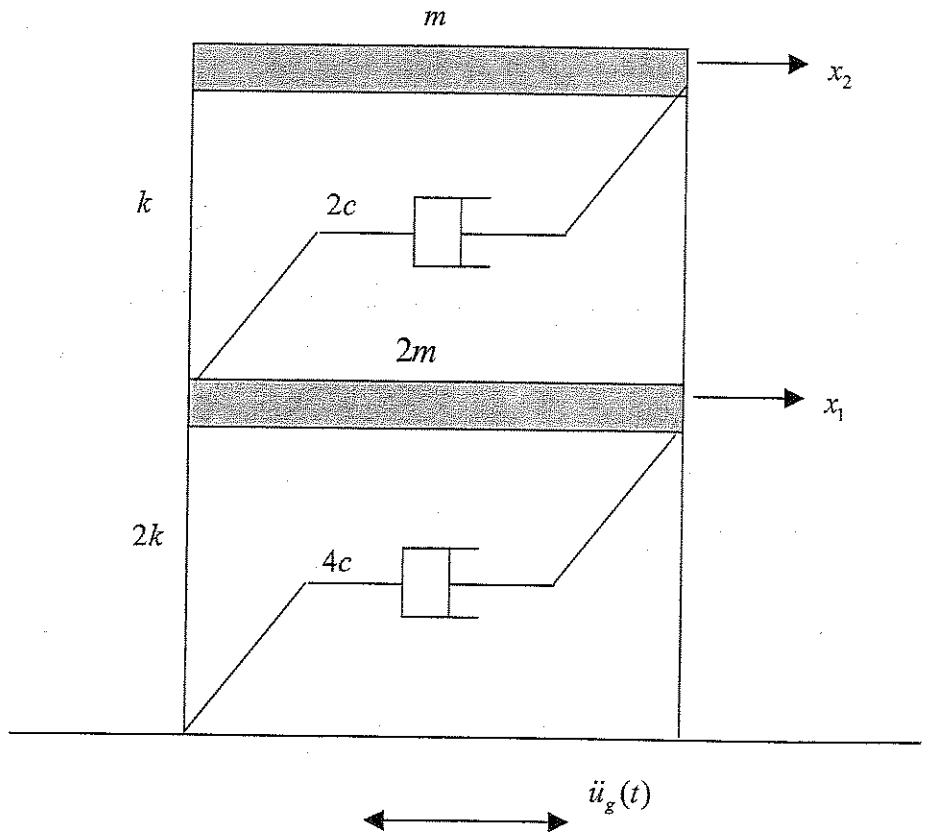

Figure 3.9. A two-degree-of-freedom Bouc-Wen structure.

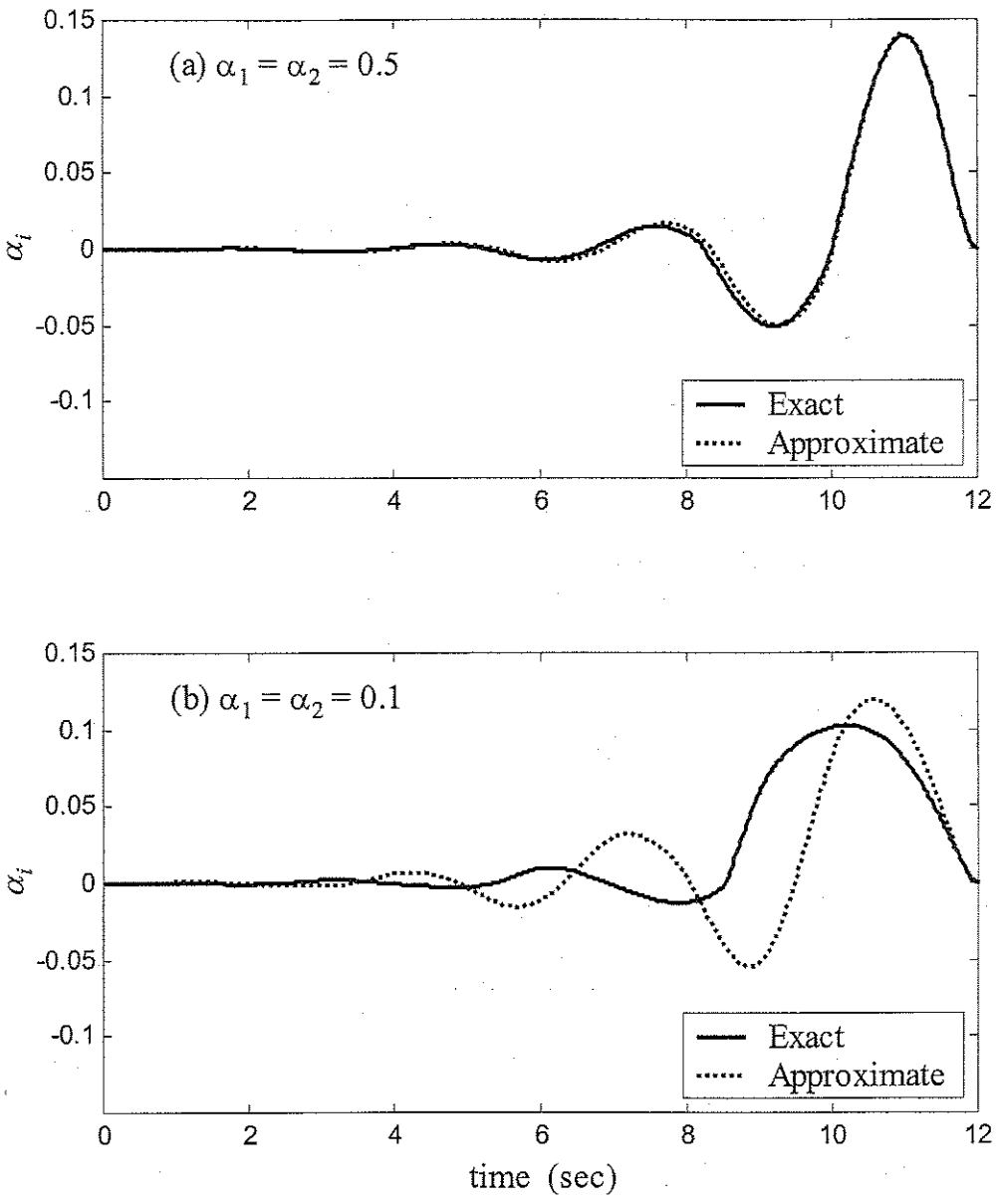

Figure 3.10. Exact and approximate $\boldsymbol{\alpha}$ vectors at the design point for the response of a two-degree-of-freedom Bouc-Wen structure to a Gaussian white noise excitation.

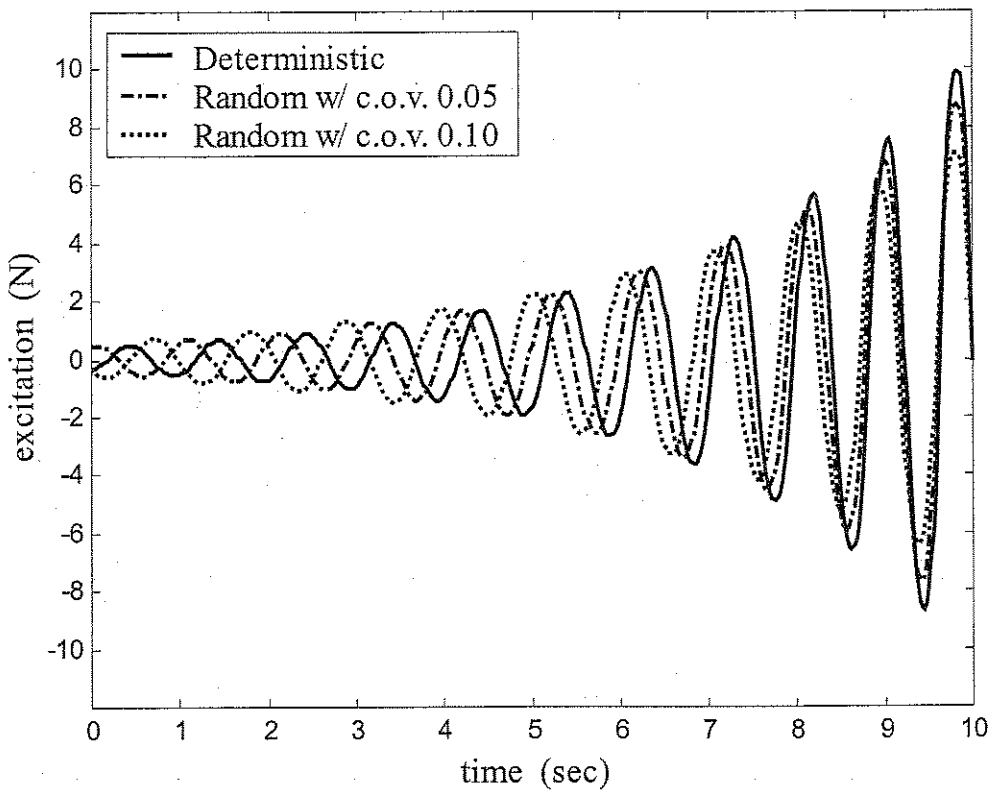

Figure 3.11. Design point excitations for a Duffing oscillator with deterministic and random parameters.

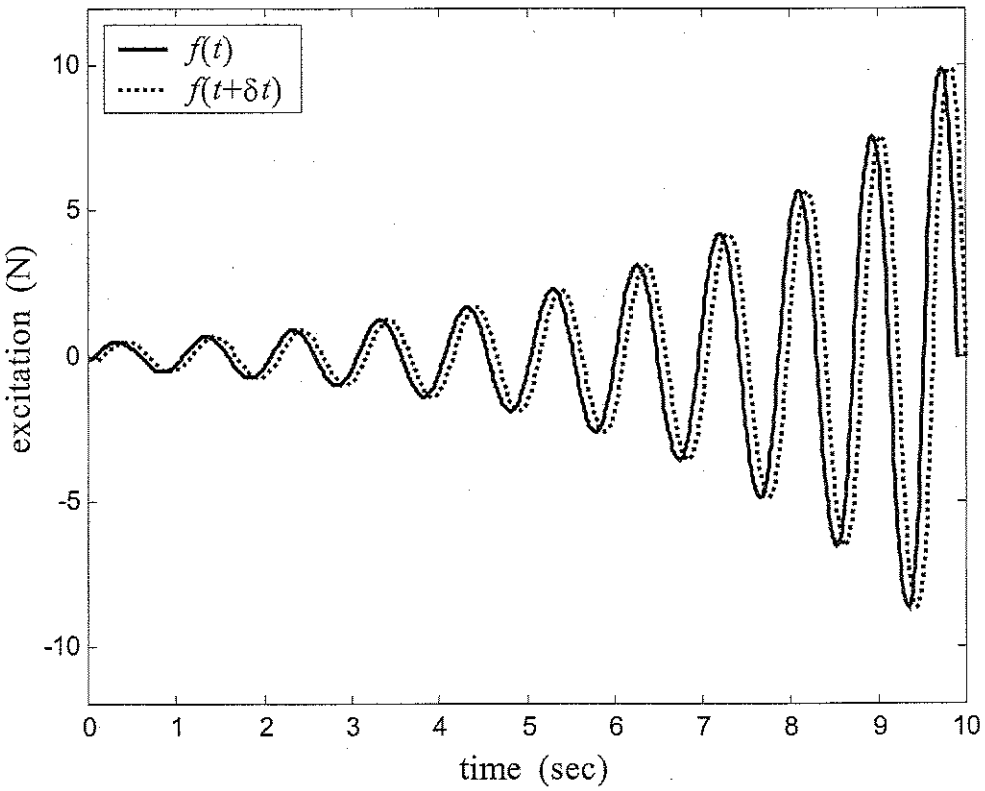

Figure 3.12. Design point excitation $f(t)$ and its time-shifted version $f(t+\delta t)$.

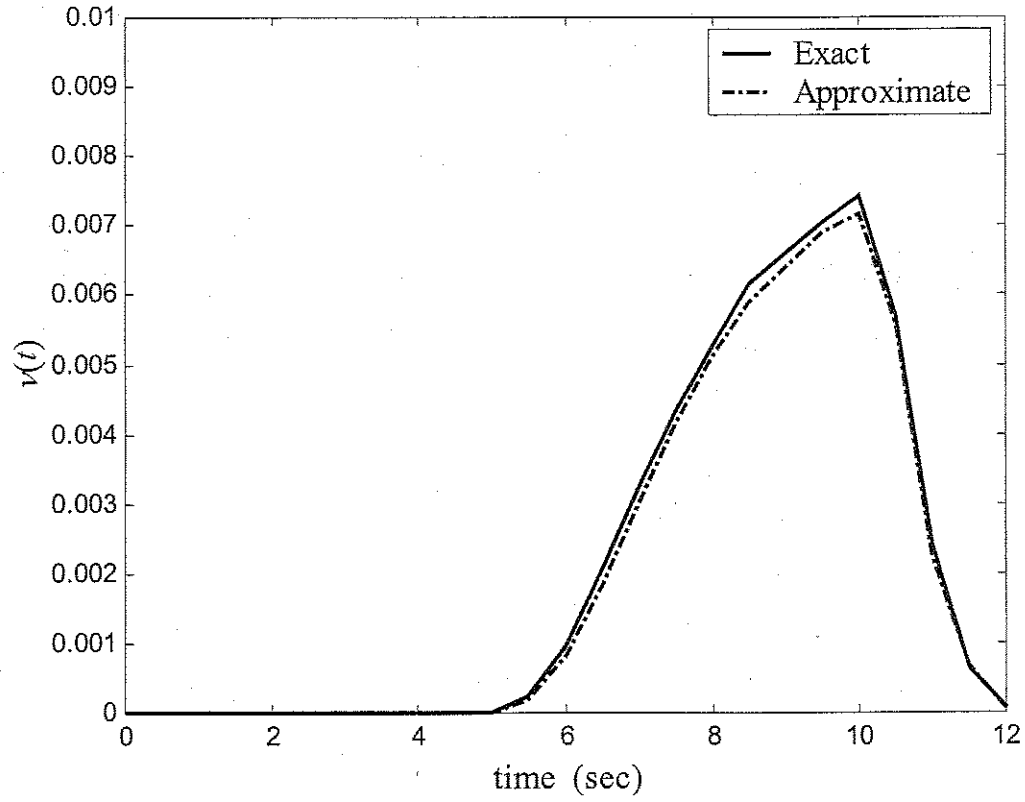

Figure 3.13. Exact and approximate FORM estimates of the mean up-crossing rate for a Duffing oscillator.

4 Computational Methods

4.1 Introduction

The ultimate goal of reliability analysis is to estimate the failure probability given by the integral in (2.1). This is also the case in solving random vibration problems by means of reliability analysis, as described in Section 2.3 of Chapter 2. For most structural reliability problems, however, analytic solutions are not available and, accordingly, computational methods must be used to find the solution.

In the previous chapter, we discussed efficient methods for finding the design point for random vibration problems. Based on the design point, we can estimate the failure probability using several approximate methods, such as FORM, SORM and various simulation techniques. In this chapter, we discuss these approximate solution methods in the context of random vibration problems.

4.2 FORM (First-Order Reliability Method)

FORM approximates the limit-state surface by a tangential hyper plane at the design point. In the case of a component reliability problem, the first-order approximation of the failure probability is

$$P_f \cong P_{f1} = \Phi(-\beta) \tag{4.1}$$

where β is the reliability index, denoting the distance from the origin to the design point in the standard normal space. For a linear system subjected to a Gaussian excitation, the limit-state surface for a scalar response quantity exceeding a specified threshold is a hyper plane and, therefore, FORM provides an exact solution. Though FORM is the simplest among the approximation methods described here, its accuracy is often good for most mildly nonlinear systems. For such systems, FORM can be used for estimating the probability of a scalar response quantity exceeding a high threshold, because FORM provides an asymptotically exact result for small probabilities (Breitung 1984).

It is useful to compare FORM with the equivalent linearization method (ELM), which is popular as a solution method for nonlinear random vibration problems. Though these methods both employ linearization, they are different in the object of linearization. ELM (see Roberts and Spanos 1990) linearizes the system in such a manner that the error in the response, i.e., the difference between the responses of the actual and linearized systems, is minimized in the mean square sense. On the other hand, FORM linearizes the limit-state surface $G(\mathbf{u}) = 0$ at the design point, which has the highest probability density in the failure region $\{G(\mathbf{u}) \leq 0\}$ in the standard normal space. The linearized problem here does not necessarily correspond to a physically realizable linear system. The linearization is carried out for the purpose of computing the probability of interest, e.g., the probability that the response at a given time will exceed a specified threshold, or the probability of the parallel system involved in computing the mean up-crossing rate.

The overall performance of the ELM is good for threshold values of the order of one standard deviation from the mean. As the threshold approaches the tail region, however, the error in the ELM estimate increases rapidly. It has been reported that for a Duffing oscillator subjected to a Gaussian white noise excitation, the probability density estimated by the ELM is 250 times greater than the exact one for a threshold equal to three times the standard deviation (Hampl 1986).

On the other hand, the FORM approximation is not strongly affected by the threshold level. In FORM, we find the design point for each individual threshold value and estimate the corresponding probability by assuming the limit-state surface is a hyper plane. The error in the FORM estimate is due to the approximation of the limit-state surface. For most problems, the limit-state surface changes in a smooth way as the threshold increases. For this reason, the error in FORM is usually stable and consistent over a wide range of threshold values. Our experience shows that generally FORM tends to be less accurate than the ELM in the high probability density region, and more accurate in the tail region. Thus, FORM is advantageous in estimating reliability statistics that relate to the tail behavior of the probability distribution. In addition, FORM provides insight into the problem by identifying the design point excitation, which is the most likely excitation to produce the failure event of interest.

4.3 SORM (Second-Order Reliability Method)

In SORM, we make a second-order approximation of the limit-state surface by fitting a paraboloid at the design point in the standard normal space. The paraboloid is constructed either by fitting to the principal curvatures of the limit-state surface at the design point (Breitung 1984), or by fitting to a set of points selected on the limit-state surface in the neighborhood of the design point (Der Kiureghian *et al.* 1987). A second-order approximation of the failure probability is then given by (Breitung 1984)

$$P_f \cong P_{f2} \cong \Phi(-\beta)\prod_{i=1}^{n-1}\frac{1}{\sqrt{1+\beta\kappa_i}} \tag{4.2}$$

where β is the reliability index and κ_i are the principal curvatures of the approximating paraboloid.

For reliability problems with nonlinear limit-state surfaces, SORM usually provides better accuracy than FORM. However, our experience shows that this is not necessarily the case for random vibration problems. SORM solutions obtained by estimating the principal curvatures at the design point may not be necessarily better than the FORM solutions, particularly if the SORM approximation is based on fitting to the principal curvatures at the design point. One reason for this can be observed in Figure 4.1, which shows the intersection of the limit-state surface with the plane (u_1, u_n) in the standard normal space for the oscillator with nonlinear damping in Example 3.2 (Section 3.5.1). In this problem, the major principal curvature at the design point is estimated as 2.5, which is quite large. As one moves away from the design point, the curvature decreases rapidly and even changes its sign a small distance away from the design point. Obviously, a parabolic fitting to the curvatures of this surface would not lead to a good approximation. This and many other examples that we have explored have led us to conclude that SORM is not an effective approximation method for random vibration problems.

4.4 Simulation Techniques

Random vibration problems formulated as structural reliability problems are high dimensional integration problems, and simulation techniques can be effectively used as solution tools. General description of simulation techniques can be found in the classical text by Rubinstein (1981). Here, we describe three simulation methods that are used in solving structural reliability problems. These are the design-point importance sampling method, the directional simulation method, and the sampling on the orthogonal plane method. Of these methods, we find that the first and the last are more effective in solving random vibration problems. We then make comparisons of the efficiencies and accuracies of the design-point importance sampling method and the sampling on the orthogonal plane method for a series of example problems.

4.4.1 Importance sampling

The basic idea of importance sampling is that we replace the original probability density function of the random variables by an appropriate sampling density function, which makes the sampling more efficient. This method fits well into the structural reliability problem, since the design point can serve as a control point for selecting the sampling density. Importance sampling conducted in the standard normal space for a component problem is based on the following derivation:

$$\begin{aligned} P[G(\mathbf{u}) \le 0] &= \int_{G(\mathbf{u})\le 0} \varphi(\mathbf{u}) d\mathbf{u} \\ &= \int_{\mathbf{u}} I[-G(\mathbf{u})]\varphi(\mathbf{u}) d\mathbf{u} \\ &= \int_{\mathbf{u}} I[-G(\mathbf{u})]\frac{\varphi(\mathbf{u})}{f(\mathbf{u})} f(\mathbf{u}) d\mathbf{u} \\ &= \mathrm{E}_{f(\mathbf{u})}\left[I[-G(\mathbf{u})]\frac{\varphi(\mathbf{u})}{f(\mathbf{u})} \right] \end{aligned} \tag{4.3}$$

In the above, $f(\mathbf{u})$ is an appropriate sampling density and $I[\cdot]$ is the indicator function with $I[a]=0$ for $a<0$ and $I[a]=1$ for $a \ge 0$. To be unbiased, $f(\mathbf{u})$ must be nonzero

wherever $I[\cdot]=1$. Furthermore, to be efficient, the variance of $I[-G(\mathbf{u})]\varphi(\mathbf{u})/f(\mathbf{u})$ must be minimized. This can be achieved by minimizing the number of samples with $I[\cdot]=0$ and by making $f(\mathbf{u})$ proportional to $\varphi(\mathbf{u})$.

We define the random quantity in (4.3) as

$$q = I[-G(\mathbf{u})]\frac{\varphi(\mathbf{u})}{f(\mathbf{u})} \tag{4.4}$$

Then, the probability of failure can be estimated as the sample mean of q, i.e.,

$$\hat{P}_f = \frac{1}{N}\sum_{k=1}^{N} q_k \tag{4.5}$$

where $\hat{P}_f$ is the estimate of the probability of failure. The uncertainty in the estimate $\hat{P}_f$ can be measured by its coefficient of variation, which is given by

$$\delta_{\hat{P}_f} = \frac{1}{\sqrt{N}}\delta_q \tag{4.6}$$

where δ_q is the coefficient of variation of the samples of q. The above relation shows that the variation of $\hat{P}_f$ is small when the variation of q is small. The efficiency of the importance sampling method is determined by the size of the coefficient of variation of q.

In structural reliability analysis, the sampling density $f(\mathbf{u})$ is usually assumed to be a normal distribution centered at the design point $\mathbf{u}^*$. For this purpose, we do not need to find the exact design point. An approximate estimate of $\mathbf{u}^*$ can be sufficiently good. When applied to random vibration problems, importance sampling can be effectively used in estimating the probability distribution of the response described in Section 2.5.1. However, it is not efficient in estimating the up-crossing rate, which involves a parallel system reliability problem produced by perturbation of the limit-state function, as described in Section 2.5.2. Since the domain of integration in this case is a narrow wedge (see Figure 2.4 in Chapter 2), most samples produced with a normal sampling density fall in the region with $I[\cdot]=0$ and, hence, the coefficient of variation of the samples of q remains large.

4.4.2 Directional Simulation

The directional simulation belongs to the class of conditional simulation. In conditional simulation (Ayyub and Chia 1992), the set of random variables $\mathbf{x}$ is divided into two subsets, say $\mathbf{x} = (\mathbf{y},\mathbf{z})$, and the probability integration is represented by

$$p_f = \int_{\mathcal{D}} f(\mathbf{x})d\mathbf{x}$$

$$= \int P[(\mathbf{z},\mathbf{y}) \in \mathcal{D}|\mathbf{y}] f(\mathbf{y})d\mathbf{y} \tag{4.7}$$

where $f(\mathbf{x})$ is the probability density function of $\mathbf{x}$ and $\mathcal{D}$ is the failure domain of interest. In (4.4), $P[(\mathbf{z},\mathbf{y}) \in \mathcal{D}|\mathbf{y}]$ is the conditional probability of failure for given $\mathbf{y}$. This conditional probability is solved analytically, and simulation is performed for the reduced set of random variables $\mathbf{y}$. For efficient simulation, we can use the importance sampling in this conditional simulation.

In directional simulation (Bjerager 1988), we represent the random vector $\mathbf{u}$ in the n dimensional standard normal space as $\mathbf{u} = R\mathbf{a}$, where $\mathbf{a} = \mathbf{u}/\|\mathbf{u}\|$ and $R = \|\mathbf{u}\|$. Due to the rotational symmetry of the standard normal space, the unit random vector $\mathbf{a}$ is uniformly distributed on the unit sphere centered at the origin and the norm square R^2 has the chi-square distribution with n degrees of freedom, i.e. $R^2 = \chi_n^2(r^2)$. Furthermore, $\mathbf{a}$ and R are statistically independent. It follows that the probability integration can be represented as

$$P[G(\mathbf{u}) \le 0] = \int P[G(R\mathbf{a}) \le 0|\mathbf{a}] f(\mathbf{a})d\mathbf{a} \tag{4.8}$$

where

$$P[G(R\mathbf{a}) \le 0|\mathbf{a}] = 1 - \chi_n^2[r(\mathbf{a})^2] \tag{4.9}$$

where $r(\mathbf{a})$ is the distance from the origin to the limit-state surface in direction $\mathbf{a}$, which is obtained by solving $G(r\mathbf{a}) = 0$. As in (4.4), we can define the random quantity

$$q = 1 - \chi_n^2[r(\mathbf{a})^2] \tag{4.10}$$

and compute the mean and coefficient of variation of the estimate of the failure probability using (4.5) and (4.6), respectively.

To improve the efficiency of the method, directional simulation can be conducted with importance sampling, i.e.,

$$P[G(\mathbf{u}) \le 0] = \int P(G(R\mathbf{a}) \le 0 | \mathbf{a}) \frac{f(\mathbf{a})}{h(\mathbf{a})} h(\mathbf{a}) d\mathbf{a} \tag{4. 11}$$

where the probability density function $h(\mathbf{a})$ is chosen with a higher density in the direction towards the design point in an appropriate way. In practical application, the directional importance sampling is combined with the original directional simulation method to make sure that the simulation covers all directions and the estimate of the failure probability is unbiased.

The directional simulation method is particularly efficient for special classes of problems. For example, it works well for problems with spherical or nearly spherical limit-state surfaces. In general, however, the directional simulation method is not efficient for high dimensional problems, since the number of directions to simulate grows rapidly with the dimension. Random vibration problems are inevitably high dimensional due to discretization of a random process, which produces a large number of random variables. For this reason, the directional simulation method is no longer pursued in this study.

4.4.3 Sampling on the Orthogonal Plane

In Section 4.4.1, we used the design point as the center of the sampling density of the importance sampling method. In Section 4.4.2, we mentioned that the direction of the design point can be used as a guide for selecting the sampling density in directional importance sampling. The sampling method on the orthogonal plane uses the design point in a different way.

Suppose that we have found the design point $\mathbf{u}^*$ and the corresponding negative gradient normal vector $\boldsymbol{\alpha}$. Let $\mathbf{u}' = (u_1', \cdots, u_n')$ be an orthonormal transformation of a point $\mathbf{u}$ in the standard normal space, such that the axis u_n' coincides with $\boldsymbol{\alpha}$. We make the assumption that, in the transformed space, the limit-state surface $G(\mathbf{u}') = 0$ can be written in the form $u_n' = h(\mathbf{u}_{n-1}')$ where $\mathbf{u}_{n-1}' = (u_1', \cdots, u_{n-1}')$ and $h(\mathbf{u}_{n-1}')$ is a single-valued

function for any selection of its argument. This assumption may not hold for some problems. For example, spherically-shaped limit-state surface does not satisfy this assumption. However, for practical purposes, it is sufficient that this assumption hold over a reasonable neighborhood of the design point, say within a radius of 3 in the standard normal space.

In this method, we first simulate the $n-1$ dimensional standard normal vector $\mathbf{u}'_{n-1} = (u'_1, \cdots, u'_{n-1})$ on the orthogonal plane $u'_n = \boldsymbol{\alpha}^{\mathrm{T}}\mathbf{u} = 0$ and then evaluate the function $u'_n = h(\mathbf{u}'_{n-1})$, which is the distance from the orthogonal plane to the limit-state surface. Figure 4.2 shows the overall picture of how the simulation is performed. The mathematical derivation of the method is as follows:

$$\begin{aligned} P[G(\mathbf{u}'_n) \le 0] &= \int_{G(\mathbf{u}'_n)\le 0} \varphi(\mathbf{u}'_n)d\mathbf{u}'_n \\ &= \int_{h(\mathbf{u}'_{n-1})\le u'_n} \varphi(u'_n)\varphi(\mathbf{u}'_{n-1})du'd\mathbf{u}'_{n-1} \\ &= \int_{\mathbf{u}'_{n-1}} \left[\int_{h(\mathbf{u}'_{n-1})}^{\infty} \varphi(u'_n)du'_n \right] \varphi(\mathbf{u}'_{n-1})d\mathbf{u}'_{n-1} \\ &= \int_{\mathbf{u}'_{n-1}} \Phi\left[-h(\mathbf{u}'_{n-1})\right]\varphi(\mathbf{u}'_{n-1})d\mathbf{u}'_{n-1} \\ &= \mathrm{E}_{\varphi(\mathbf{u}'_{n-1})}\left[\Phi[-h(\mathbf{u}'_{n-1})]\right] \end{aligned} \tag{4.12}$$

where $\mathrm{E}_{\varphi(\mathbf{u}'_{n-1})}[\cdot]$ denotes the expectation of the argument with respect to the distribution $\varphi(\mathbf{u}'_{n-1})$. As in (4.4), we define the random quantity

$$q = \Phi[-h(\mathbf{u}'_{n-1})] \tag{4.13}$$

and compute the mean and coefficient of variation of the estimate of the failure probability from (4.5) and (4.6), respectively.

The steps in this algorithm can be summarized as follows:

1. Simulate the n dimensional standard normal vector $\mathbf{u}_n$.
2. Compute $\mathbf{u}'_{n-1}$ by projecting $\mathbf{u}_n$ onto the orthogonal plane $\boldsymbol{\alpha}^{\mathrm{T}}\mathbf{u} = 0$.
3. Compute $u'_n = h(\mathbf{u}'_{n-1})$ by solving $G(\mathbf{u}'_{n-1}, u'_n) = 0$.
4. Compute q as in (4.13).

5. Repeat the above for a sample q_k, $k = 1, \ldots, N$, where N denotes the sample size, and use (4.5) and (4.6) to compute the mean and coefficient of variation of the failure probability estimate.

This method is comparable to the directional simulation in the sense that the failure probability is computed by taking the sample average of the conditional probability for each sample. In this method, however, simulation is performed in the orthogonal plane parallel to the tangential hyper plane of the design point. Therefore, simulation occurs only in the direction parallel to the vector $\boldsymbol{\alpha}$, and furthermore, each sample has the standard normal distribution.

Compared to important sampling, the drawback of this method is that we have to evaluate the limit-state function repeatedly for each simulation to locate the point on the limit-state surface, while in importance sampling only one evaluation of the limit-state function is performed for each simulation. According to our experience, using the secant method four to five iterations are sufficient to find the point on the limit-state surface for a given point on the orthogonal plane. For strongly nonlinear problems, the distance to the limit-state surface for a simulated point on the orthogonal plane can be very different from the distance to the tangent hyper plane at the design point, which is equal to the reliability index β. If the distance is much greater than β, we can approximate q by zero. For example, if $\beta = 3$ with $\Phi(-3) = 1.34\text{E}{-3}$ and the computed distance is greater than 5 which corresponds to $\Phi(-5) = 2.87\text{E}{-7}$, it is meaningless to find the exact value of q, because the conditional probability of failure in that direction is less than one thousandth of the conditional probability of failure in the direction of the design point. In such a case , we can set q equal to 0 with little loss of accuracy .

In this method, it is not necessary to have found the exact design point, as long as the assumption regarding a unique solution of u'_n in $G(\mathbf{u}'_{n-1}, u'_n) = 0$ is satisfied. However, the accuracy of the computed design point and the nonlinearity of the limit-state surface affect the coefficient of variation of the probability estimate in (4.6). The following examples demonstrate these effects.

Example 4.1

To see the effect of the accuracy of the design point, consider a simple two-dimensional linear problem in the standard normal space, as shown in Figure 4.3. For this problem, if we use the exact orthogonal plane, all computed distances to the limit-state surface will be equal to β and the coefficient of variation of the q values in (4.13) will be zero. Now, suppose we have an approximate design point, $\mathbf{u}^*_{\text{approx}}$, with the corresponding normalized negative gradient vector $\boldsymbol{\alpha}_{\text{approx}}$ and orthogonal plane $\boldsymbol{\alpha}^{\mathrm{T}}_{\text{approx}}\mathbf{u} = 0$, see Figure 4.3. In this case, the values of q computed from (4.13) will be different for each simulation and q will have a non-zero coefficient of variation, thus leading to a less efficient simulation result. As a specific example, Figure 4.4 shows the coefficient of variation of q as a function of the distance between the true and the approximate design points for the case when $\beta = 3$. We can see that the coefficient of variation of q increases linearly with the distance of the approximate design point from the true design point. One can also see that any nonlinearity in the limit-state surface will increase the coefficient of variation of q and, hence, decrease the efficiency of this sampling method. For this reason, this sampling method is more efficient for mildly nonlinear problems than for strongly nonlinear problems.

Example 4.2

To examine the efficiency of this method in solving random vibration problems, we consider Example 3.5 of Section 3.6 concerning a hysteretic Bouc-Wen oscillator subjected to a Gaussian white noise excitation. Of interest is the probability that the response at $t_n = 8$ sec will exceed the threshold x_0. All parameters values are as described in Example 3.5. We use two methods for this purpose: (a) sampling on the orthogonal plane, and (b) design point importance sampling. Table 4.1 lists the solutions by these two methods as well as the FORM solution for two values of the nonlinearity parameter α and the three threshold levels $x_0 = 2\sigma_o$, $x_0 = 3\sigma_o$ and $x_0 = 4\sigma_o$, where σ_o is the root-mean-square of the linear oscillator ($\alpha = 1$), see Example 3.5. The case with $\alpha = 0.5$ corresponds to a mildly nonlinear oscillator, whereas the case with $\alpha = 0.1$ corresponds to a strongly nonlinear oscillator. Also listed in Table 4.1 are the number of simulations in each sampling method as well as the number of g-function evaluations (in

parenthesis) for the orthogonal plane sampling method. Note that the number of g-function evaluations in the design point importance sampling is the same as the number of simulations.

As can be seen in Table 4.1, the results by the two vastly different sampling methods are in close agreement, but different from the FORM results, particularly for the strongly nonlinear oscillator. This points to the nonlinearity of the limit-state surface. The results in Table 4.1 clearly show that, for this example, the orthogonal plane sampling method is more efficient than the design point importance sampling method in terms of the number of simulations. Even if we include the additional number of g-function evaluations necessary for finding the distance to the limit-state surface for each sample, the orthogonal plane sampling method is more efficient than the design point importance sampling method.

One advantage of the orthogonal plane sampling method is that it is effective in computing the mean out-crossing rate. The formula for the mean out-crossing rate, as described in Chapter 2, is

$$\nu(t) \cong \frac{P\{g[\mathbf{x}(t)] > 0 \cap g[\mathbf{x}(t+\delta t)] \le 0\}}{\delta t} \qquad \text{small } \delta t \tag{4.14}$$

The intersection of the two events in (4.14) forms a thin curved wedge, as illustrated in Figure 4.5. If we conduct importance sampling with the sampling density centered at the design points, very few samples will fall in the intersection domain. Furthermore, it is not easy to construct a sampling density that is more appropriate for this kind of a domain. For this reason, the importance sampling method is not an effective solution method for this problem. On the other hand, the orthogonal plane sampling method is effective for this problem, as described below.

Let $u'_n = h_1(\mathbf{u}'_{n-1})$ for $G_1(\mathbf{u}') = g[\mathbf{x}(t)] = 0$ and $u'_n = h_2(\mathbf{u}'_{n-1})$ for $G_2(\mathbf{u}') = g[\mathbf{x}(t+\delta t)] = 0$. We define the random quantity q as

$$q = \{\Phi[-h_2(\mathbf{u}'_{n-1})] - \Phi[-h_1(\mathbf{u}'_{n-1})]\} I[h_1(\mathbf{u}'_{n-1}) - h_2(\mathbf{u}'_{n-1})] \tag{4.15}$$

where $I[a] = 1$ if $a \ge 0$ and $I[a] = 0$ if $a < 0$. One can easily verify that the above value of q is equal to the conditional probability of the intersection event in the numerator of (4.14) for the direction corresponding to the simulated point on the orthogonal plane. The

probability of the intersection event can now be estimated as the sample mean of q as in (4.5). The coefficient of variation of the estimate is obtained using (4.6).

It is observed that in using the orthogonal plane sampling method to compute the mean out-crossing rate, the only additional work required is to find the distance to the second limit-state surface, $g[\mathbf{x}(t+\delta t)]=0$, which is a perturbation of the limit-state surface, $g[\mathbf{x}(t)]=0$. Since the solutions of u_n' for the two surfaces are close to each other, the first solution can be used as a good starting point for iterative solution of the second distance. With this approach, the additional work needed to estimate the mean out-crossing rate is trivial.

4.5 Example Applications

In this section we present a series of example applications for random vibration reliability analysis of nonlinear dynamical systems. The goal is twofold: (a) to demonstrate applications of the proposed methods, and (b) to examine the accuracy of the proposed methods. When possible, comparisons are made with exact solutions available in the literature. Furthermore, in several examples, comparisons are made with results obtained by the Equivalent Linearization Method, ELM.

4.5.1 Duffing Oscillator

The Duffing oscillator is described by the differential equation

$$m\ddot{x}(t)+c\dot{x}(t)+k[x(t)+\gamma x(t)^3]=f(t) \tag{4.16}$$

where m, c and k are the system parameters and γ represents a measure of nonlinearity of the oscillator. The response of this oscillator is characterized by a nonlinear elastic behavior. When considering the probability that the response at a given time will exceed a specified threshold, the design point excitation for this oscillator, when it is subjected to a Gaussian white noise input, can be obtained with a single free vibration analysis, as described in Chapter 3. For non-white or non-stationary excitations, iterative calculations

are necessary to find the design point. A good starting point for such calculations can be obtained by use of the mirror image excitation, as described in Chapter 2.

Two examples are considered with different excitation patterns. In the first example, the oscillator is subjected to a Gaussian white noise. The complementary probability distribution and the mean up-crossing rate for a range of threshold values are estimated by FORM and compared with the exact solution and with results obtained by the ELM. In the second example, we consider a non-stationary input in the form of a time-modulated, filtered Gaussian white noise. For this example, several reliability statistics introduced in Section 2.5 are estimated.

Example 4.3

Assume $f(t)$ in (4.16) is a stationary Gaussian white noise with intensity S_o. An exact solution for the joint probability density function of the response and its time derivative is given by (see Lutes and Sarkani 1997)

$$f(x,\dot{x}) = B\exp\left\{-\frac{c}{2\pi S_o}\left[m\dot{x}^2 + k(x^2 + \gamma x^4/2)\right]\right\} \tag{4.17}$$

where B is a normalizing constant. The ELM result for the response of this oscillator is a zero-mean Gaussian process with the mean square $\sigma^2 = \pi S_o/(ck_{eq})$, where $k_{eq} = (\pi S_o/c)[6\gamma/(\sqrt{1+12\gamma\pi S_o/ck}-1)]$ (Lutes and Sarkani 1997).

For the numerical evaluation, the parameter values are set as m = 1 Kg, $c = 0.2\pi$ N·sec/m, k = $(2\pi)^2$ N/m, and γ = 1. The white noise excitation with intensity S_o = 1 N^2/(rad/sec) is idealized as a train of Gaussian random pulses as in Section 2.4 with Δt = 0.025 sec, and the response is evaluated at time t_n = 10 sec, which is sufficient time to achieve stationarity in the response of the oscillator. The perturbation time increment for computing the out-crossing rate in (2.40) is selected as $\delta t = \Delta t/100$ sec.

Figure 4.6 shows the computed complementary cumulative distribution function of the response as a function of the normalized threshold x/σ_o, where $\sigma_o^2 = \pi S_o/(ck)$ is the mean-square of the linear oscillator, i.e., the case with $\gamma = 0$. Four different results are shown in the figure: (a) the exact solution obtained by numerically integrating (4.17),

shown as a solid line, (b) the ELM approximation, shown as a dashed line, (c) the FORM approximation, shown as a dash-dotted line, and, for the purpose of a reference, (d) the result for a linear oscillator with $\gamma = 0$, shown as a dotted line. The distribution based on the ELM approximation and for the linear oscillator are Gaussian. The exact solution and the approximation based on FORM are non-Gaussian distributions. The large difference between the exact result and the result for the linear oscillator points to the extent of nonlinearity in the system. The results in Figure 4.6 clearly show that the ELM approximation is good at low thresholds, whereas the FORM approximation is superior to the ELM at the higher thresholds. We can see this more clearly in Figure 4.7, which shows plots of the approximate to exact cumulative probability for ELM and FORM.

Figure 4.8 shows plots of the computed mean up-crossing rate as a function of the normalized threshold x/σ_o. Again, four results are shown: (a) the exact result (solid line), obtain by use of (4.17) in Rice's well known formula, (b) the ELM approximation (dashed line), (c) the FORM approximation (dash-dotted line), and, for the purpose of a reference, (d) the result for the linear oscillator (dotted line). Figure 4.9 shows the ratios of the approximate to exact mean up-crossing rates based on ELM and FORM approximations. Trends in Figure 4.8 and Figure 4.9 are similar to those observed for the complementary cumulative distribution function in Figure 4.6 and Figure 4.7 with FORM showing even better accuracy here.

It is important to note that the FORM result for each threshold in Figure 4.6 is based on a single free vibration analysis of the oscillator. Furthermore, the FORM estimate for the mean up-crossing rate at each threshold level is obtained by time-shifting the design point excitation obtained from the free vibration analysis.

Example 4.4

We now apply a time-modulated, Gaussian, filtered-white noise excitation to the Duffing oscillator. The parameters of the oscillator are as in Example 4.3. The excitation is obtained as

$$f(t) = q(t)\hat{f}(t) \tag{4.18a}$$

where

$$\hat{f}(t) = \ddot{x}_f(t) + W(t) = -2\zeta_f \omega_f \dot{x}_f(t) - \omega_f^2 x_f(t) \tag{4.18b}$$

where $W(t)$ is a white noise process, ω_f and ζ_f are the filter frequency and damping ratio, respectively, and $x_f(t)$ is the response of the filter. The white noise with intensity S_o = 1 N^2/(rad/sec) is discretized in the same manner as in Example 4.3. The filter parameters are set as $\omega_f = 5\pi$ rad/sec and $\zeta_f = 0.6$. The modulating function in (4.18a) is specified as

$$\begin{aligned} q(t) &= t^2/25 && t \le 5 \\ &= 1 && 5 < t \le 10 \\ &= \exp[-(t-10)/2] && 10 < t \end{aligned} \tag{4.19}$$

Reliability analysis is performed for the limit-state function $g = 3\sigma_o - x(t)$, where $\sigma_o^2 = \pi S_o/(ck)$. No exact solution of this problem is available.

Figure 4.10 shows the probability of the response exceeding the specified threshold as a function of time, as computed by FORM using the exact design point for each value of t. For reference, a scaled plot of $q(t)$ is shown as a dotted line. It is seen that the probability of exceeding the specified threshold has a shape resembling $q(t)$, but with a time delay. The highest value of the probability occurs near $t = 10$ sec, which is the termination point of the strong phase of the input excitation.

Figure 4.11 shows the mean up-crossing rate for the specified threshold as a function of time, as computed by FORM by time-shifting the design point obtained from the above analysis. Remarkably, the plots for the exceedance probability and the mean up-crossing rate are nearly identical in shape.

Other interesting statistics of the response process are obtained as follows:

An upper bound to the probability of a first excursion above the threshold $3\sigma_o$ is obtained from (2.46) by integrating the mean up-crossing rate in time. This is essentially equal to the area underneath the mean up-crossing rate curve in Figure 4.11. The result is $P_T \le 2.50\text{E}{-2}$. This upper bound estimate is 37% larger than the result of $\hat{P}_T$ = 1.83E–2 obtained by Monte Carlo simulation with a coefficient of variation of 0.05.

The mean and standard deviation of the cumulative excursion time above the threshold $3\sigma_o$ are obtained by use of (2.49) and (2.50). The mean is equal to the area underneath the probability curve in Figure 4.10 and equals $E[\eta(12)] = 0.00234$ sec. The mean-square is obtained by solving a series of parallel system problems for a grid of time points, followed by integration in time, as in (2.50). The result by FORM is $E[\eta^2(12)] = 0.00120$ sec^2. This gives the standard deviation $\sigma_{\eta(12)} = 0.035$ sec, which is much larger than the mean, indicating vast uncertainty in the cumulative excursion time.

The mean duration of a single excursion above the threshold of $3\sigma_o$ is estimated from (2.55) by dividing the probability estimates in Figure 4.10 by the corresponding mean up-crossing estimates in Figure 4.11. Over the time period 5 ~ 12 sec, the mean duration of a single excursion above the specified threshold varies from 0.063 sec to 0.095 sec.

To estimate the mean of the cumulative excursion area as in (2.59), we need to compute the probability sensitivity measure $-dP/d\theta$ over a wide range of parameter values θ for all discrete time points t_i, $i = 1, \cdots, n$. If we compute the sensitivity measure for each value of θ at each time t_i by performing the sensitivity analysis, the amount of work will be enormous. Rather than computing these values individually from the sensitivity analysis, we will use the formula (2.24), which can approximately estimate the sensitivity measure without performing the sensitivity analysis. To check the accuracy of the approximation, we computed the reliability index β and the corresponding sensitivity measure $-dP/d\theta$ for the threshold values $3.5\sigma_o$ and $4\sigma_o$ at time $t = 10$ sec from FORM analysis and compared the results with the approximate values obtained from (2.24). Figure 4.12 and Figure 4.13 show how well the approximate values fit the values obtained by performing the sensitivity analysis individually. The mean of the cumulative excursion area estimated by this method is $E[A(12)] = 0.000153$ m·sec. Since the mean cumulative excursion time is $E[\eta(12)] = 0.00234$ sec, the mean depth of excursion above the threshold $3\sigma_o$ is roughly 0.000153/0.00234 = 0.0654 m.

The above examples serve to demonstrate the many different statistics of a random vibration response that one can compute with the proposed method.

4.5.2 Elastic SDOF Oscillator with Nonlinear Damping

Consider a nonlinear elastic oscillator described by

$$m\ddot{x}(t) + c[\dot{x}^2(t) + (k/m)x^2(t)]\dot{x}(t) + kx(t) = f(t) \tag{4.20}$$

where m, c and k are the system parameters. As can be seen, the damping force for this oscillator changes depending on the magnitude of the total energy. When the excitation $f(t)$ is a zero-mean, stationary Gaussian white noise of intensity S_o, the exact joint probability density function of the response and its derivative is given by (Lutes and Sarkani 1997)

$$f(x,\dot{x}) = B\exp\left(\frac{-c(m\dot{x}^2 + kx^2)^2}{4m\pi S_o}\right) \tag{4.21}$$

where B is a normalizing constant. The ELM result for the response of this oscillator is a zero-mean Gaussian process with the mean square $\sigma^2 = \pi S_o/(c_{eq}k)$, where $c_{eq} = 2\sqrt{c\pi S_o/m}$ (Lutes and Sarkani 1997).

Example 4.5

In this example, the oscillator in (4.20) is subjected to a Gaussian white noise. We compute the complementary probability distribution function and the mean up-crossing rate for a range of threshold values with FORM and compare the results with the exact solution and the results obtained by the ELM. As an improvement on FORM, the orthogonal plane sampling is performed.

Numerical values are assigned as m = 1 Kg, c = 1 N·sec/m, and k = 100 N/m. The white noise excitation S_o = 100 N^2/(rad/sec) is idealized as a train of Gaussian random pulses with Δt = 0.01 sec. The duration of the excitation is set as 10 sec. The time increment for the mean up-crossing rate in (2.40) is set at $\delta t = \Delta t/100$ sec.

Figure 4.14 and Table 4.2 show the results for the complementary cumulative distribution function as a function of the normalized threshold x/σ, where

$\sigma^2 = (1/2k)\sqrt{m\pi S_o / c}$ is the mean-square response of the nonlinear oscillator. Four different results are shown in Figure 4.14: (a) the exact solution obtained by numerically integrating (4.21), shown as a solid line, (b) the ELM approximation, shown as a dashed line, (c) the FORM approximation, shown as a dash-dotted line, and, as an example of the improvement on FORM, (d) the result of the orthogonal plane sampling with c.o.v. = 0.05, shown as open circle marks (see Table 4.2 for the number of simulations). As in Duffing oscillator, the ELM approximation is good at low thresholds, whereas the FORM approximation is superior to the ELM at the higher thresholds. We can see this more clearly in Figure 4.15, which shows plots of the approximate to exact cumulative probability for ELM and FORM. The estimates based on orthogonal plane sampling are in close agreement with the exact results.

Figure 4.16 and Table 4.3 show the computed mean up-crossing rate as a function of the normalized threshold x/σ. Again, four results are shown: (a) the exact result (solid line), obtain by use of (4.21) in Rice's well known formula, (b) the ELM approximation (dashed line), (c) the FORM approximation (dash-dotted line), and, as an improvement on FORM, (d) the result the orthogonal plane sampling with c.o.v. = 0.1, shown as a circle (see Table 4.3 for the number of simulations). Figure 4.17 shows the ratios of the approximate to exact mean up-crossing rates based on ELM and FORM approximations. Trends in Figure 4.16 and Figure 4.17 are similar to those observed for the complementary cumulative distribution function in Figure 4.14 and Figure 4.15.

As in the case of the Duffing oscillator, the FORM result for each threshold in Figure 4.14 is based on a single free vibration analysis of the oscillator, and the FORM estimate for the mean up-crossing rate at each threshold level is obtained by time-shifting the design point excitation obtained from the free vibration analysis. As shown in Table 4.2 and Table 4.3, we can easily improve the FORM solution with a relatively small number of simulations using the orthogonal plane sampling method.

4.5.3 SDOF Hysteretic Oscillator

Consider a SDOF hysteretic oscillator having the Bouc-Wen constitutive model

$$m\ddot{x}(t) + c\dot{x}(t) + k[\alpha x(t) + (1-\alpha)z(t)] = f(t) \tag{4.22}$$

$$\dot{z}(t) = -\gamma|\dot{x}(t)||z(t)|^{n-1} z(t) - \beta|z(t)|^n \dot{x}(t) + A\dot{x}(t) \tag{4.23}$$

where m, c and k are the system parameters, $z(t)$ is an auxiliary variable that represents the hysteretic component of the restoring force, and α is a parameter that controls the degree of hysteresis. In (4.23), γ, β, n and A are parameters that can be adjusted to match an observed hysteretic loop. No exact solutions for the response of this oscillator are available. The solution by ELM can be obtained numerically, as described in Wen (1980).

Example 4.6

Consider the hysteretic oscillator in (4.22) subjected to a Gaussian white noise excitation of intensity S_o = 1 N^2/(rad/sec). The system parameters are set as m = 1 Kg, c = 3 N·sec/m, and $k = (3\pi)^2$ N/m. Numerical values assigned to the other parameters are α = 0.1, n = 1, A = 1 and $\gamma = \beta = 1/(2\sigma_o)$, where $\sigma_o^2 = \pi S_o/(ck)$ is the mean-square of the linear oscillator with α = 1. The white noise excitation is idealized as a train of Gaussian random pulses with Δt = 0.02 sec. Time t_n = 8 sec is used to achieve stationarity in the response.

Figure 4.18 and Table 4.4 show the results for the complementary cumulative distribution function of the response as a function of the normalized threshold x/σ_o. Shown in the figure are the "exact" result (solid line) obtained by the orthogonal plane sampling with c.o.v. = 0.05 (see Table 4.4 for the number of simulations), the ELM approximation (dashed line), and the FORM approximation (dash-dotted line). We see that the FORM result performs superior to the ELM result at moderate to high thresholds.

Figure 4.19 and Table 4.5 show the results for the mean up-crossing rate as a function of the normalized threshold x/σ_o. The orthogonal plane sampling is used for simulation of the mean up-crossing rate with c.o.v. = 0.10 (see Table 4.5 for the number of simulations). The nature of the results is similar to those in Figure 4.18.

4.5.4 Two-Degree-of-Freedom Bouc-Wen Structure

Consider a two-degree-of-freedom Bouc-Wen structure (see Figure 3.9)

$$\mathbf{M}\ddot{\mathbf{x}}(t)+\mathbf{C}\dot{\mathbf{x}}(t)+\mathbf{K}\left[\begin{Bmatrix}\alpha_1 d_1(t)\\ \alpha_2 d_2(t)\end{Bmatrix}+\begin{Bmatrix}(1-\alpha_1)z_1(t)\\ (1-\alpha_2)z_2(t)\end{Bmatrix}\right]=\mathbf{M}\mathbf{1}\ddot{u}_g(t) \tag{4.24}$$

$$\dot{z}_i(t)=-\gamma_i\left|\dot{d}_i(t)\right|z_i(t)\Big|^{n-1}z_i(t)-\beta_i\dot{d}_i(t)\left|z_i(t)\right|^n+A_i\dot{d}_i(t)\quad i=1,2 \tag{4.25}$$

where $\mathbf{M}$ is the mass matrix, $\mathbf{C}$ is the damping coefficient matrix, $\mathbf{K}$ is the linear stiffness matrix, $d_1(t)=x_1(t)$, $d_2(t)=x_2(t)-x_1(t)$ are the inter-story drifts, $z_i(t)$, $i=1, 2$, are hysteretic components of the response, and $\ddot{u}_g(t)$ is the ground acceleration. We set the system parameters as $\mathbf{M}=\begin{bmatrix}2 & 0\\ 0 & 1\end{bmatrix}$kg, $\mathbf{C}=\begin{bmatrix}6 & -2\\ -2 & 2\end{bmatrix}$N·sec/m, $\mathbf{K}=\begin{bmatrix}20 & 0\\ 0 & 10\end{bmatrix}$N/m, and the parameters related to the hysteretic behavior are set as $A_1=A_2=1$, $\gamma_1=\beta_1=1/(2\sigma_{d1o})$, and $\gamma_2=\beta_2=1/(2\sigma_{d2o})$, where σ_{d1o} and σ_{d2o} are the standard deviations of the interstory drifts of the linear system ($\alpha_1=\alpha_2=1$). In (4.24), $\mathbf{1}$ is a 2-vector of ones. We examine two cases for the ground acceleration $\ddot{u}_g(t)$ – one with a stationary Gaussian white noise, and the other with a non-stationary Gaussian excitation.

Example 4.7

In this example, we consider the case when the oscillator is subjected to a stationary Gaussian white noise. The white noise excitation with the intensity S_o = 1 $(\text{m/sec}^2)^2/(\text{rad/sec})$ idealized as a train of Gaussian random pulses with Δt = 0.025sec, and the response is evaluated at time t_n = 12 sec, which is sufficient time to achieve stationarity. The perturbation time increment for computing the outcrossing rate in (2.40) is selected as $\delta t = \Delta t/20$ sec. The root-mean-square responses for the linear system are σ_{d1o} = 0.562 m and σ_{d2o} = 0.481 m.

Figure 4.20, Table 4.6 and Table 4.7 show the results for the complementary cumulative distribution functions of the two inter-story drifts, where simulation by the orthogonal plane sampling with c.o.v. = 0.05, FORM, and ELM are compared (see Table

4.6 and Table 4.7 for the number of simulations). Trends are as seen for the SDOF oscillators: ELM provides good results for low thresholds, whereas the FORM provides superior results at high thresholds (low probabilities).

Figure 4.21, Table 4.8 and Table 4.9 show the results for the mean up-crossing rates for the two inter-story drift responses, where simulation by the orthogonal plane sampling with c.o.v. = 0.10, ELM, and FORM are compared (see Table 4.8 and Table 4.9 for the number of simulations). Trends are similar to those observed in Figure 4.20 for the cumulative distribution.

Example 4.8

In this example, the system is subjected to a non-stationary, Gaussian, filtered-white-noise excitation, which is produced in the same manner as in Example 4.4. The white noise with intensity S_o = 1 $(\text{m/sec}^2)^2/(\text{rad/sec})$ is discretized as in Example 4.7. The numerical values for the filter parameters are set as $\omega_f = 2\pi$ rad/sec and $\zeta_f = 0.6$. The modulating function $q(t)$ is as in (4.19). The reliability analysis is performed for the limit-state function $g = 6\sigma_{dio} - d_i(t)$, $i = 1, 2$.

Figure 4.22 and Figure 4.23 show the probabilities of the responses exceeding the thresholds $6\sigma_{dio}$, i = 1, 2 and the corresponding mean up-crossing rates over time, respectively. For reference, a scaled plot of $q(t)$ is shown as a dotted line. The upper bounds of the first excursion probabilities estimated by using (2.46) are $P_{T_1} \approx$ 5.20E–2 for the inter story drift D_1 and $P_{T2} \approx$ 1.09E–2 for the interstory drift D_2. These results compare favorably with Monte Carlo simulation results of $\hat{P}_{T_1}$ = 5.41E–2 and $\hat{P}_{T_2}$ = 1.16E–2, respectively, which are obtained with c.o.v. = 0.05. The reason that the results obtained using (2.46) are slightly smaller than the simulation results can be explained by observing the trend of the mean up-crossing rate shown in Figure 4.21, where the FORM solution tends to be slightly smaller than the simulation.

Table 4.1. Comparison of simulation methods with Bouc-Wen oscillator (c.o.v. = 0.05).

Parameter	Threshold	FORM	Ortho. Plane. Sampl.		Importance sampling	
			Probability	Samples	Probability	Samples
$\alpha = 0.5$	$2\sigma_o$	8.41E–3	5.75E–3	229 (1,031)	5.49E–3	1,972
	$3\sigma_o$	1.98E–4	1.30E–4	330 (1,454)	1.39E–4	4,547
	$4\sigma_o$	1.88E–6	1.40E–6	490 (2,370)	1.31E–6	4,409
$\alpha = 0.1$	$2\sigma_o$	1.23E–2	1.78E–2	1,057 (3,822)	1.93E–2	7,794
	$3\sigma_o$	8.40E–4	1.30E–3	2,274 (7,750)	1.28E–3	21,695
	$4\sigma_o$	4.61E–5	6.48E–5	4,433 (15,039)	6.27E–5	19,373

Numbers in parentheses indicate the number of evaluations of the limit-state function in the orthogonal plane sampling method.

Table 4.2. Comparison of probability values $P[X > x]$ for response of elastic SDOF oscillator with nonlinear damping (c.o.v. = 0.05 for simulation).

x/σ	Exact	ELM	FORM	Orthogonal Plane Sampling	
				$\hat{P}$	Samples
0.5	3.30E–1	2.98E–1	4.60E–1	3.23E–1	327 (1,458)
1.0	1.78E–1	1.44E–1	3.45E–1	1.72E–1	324 (1,500)
1.5	6.87E–2	5.55E–2	1.85E–1	6.80E–2	563 (2,674)
2.0	1.48E–2	1.68E–2	5.53E–2	1.34E–2	885 (4,166)
2.5	1.23E–3	3.96E–3	6.34E–3	9.58E–4	1,610 (7,335)
3.0	2.38E–5	7.19E–4	1.66E–4	1.52E–5	2,348 (10,219)
3.5	5.61E–8	1.00E–4	5.28E–7	2.25E–8	2,796 (11,048)

Numbers in parentheses indicate the number of evaluations of the limit-state function in the orthogonal plane sampling method.

Table 4.3. Comparison of mean up-crossing rates $\nu(t)$ for response of elastic SDOF oscillator with nonlinear damping (c.o.v. = 0.1 for simulation).

x/σ	Exact	ELM	FORM	Orthogonal Plane Sampling	
				$\hat{\nu}(t)$	Samples
0.5	1.47	1.38	1.65	1.47	340 (3,348)
1.0	1.11	0.91	1.80	1.27	221 (1,760)
1.5	5.88E–1	4.47E–1	1.45	6.93E–1	339 (2,771)
2.0	1.76E–1	1.67E–1	6.22E–1	2.61E–1	353 (2,958)
2.5	2.01E–2	4.68E–2	9.90E–2	2.22E–2	797 (6,749)
3.0	5.25E–4	9.92E–3	3.47E–3	5.06E–4	744 (6,348)
3.5	1.63E–6	1.59E–3	1.40E–5	9.98E–7	1,443 (7,935)

Numbers in parentheses indicate the number of evaluations of the limit-state function in the orthogonal plane sampling method.

Table 4.4. Comparison of probability values $P[X > x]$ for response of Bouc-Wen oscillator (c.o.v. = 0.05 for simulation).

x/σ_o	ELM	FORM	Orthogonal Plane Sampling	
			$\hat{P}$	Samples
0.2	4.08E–1	4.14E–1	4.02E–1	294 (1,102)
0.4	3.20E–1	3.24E–1	3.49E–1	289 (1,087)
0.6	2.42E–1	2.41E–1	2.59E–1	394 (1,482)
0.8	1.75E–1	1.72E–1	1.78E–1	463 (1,732)
1.0	1.22E–1	1.18E–1	1.47E–1	521 (1,973)
1.2	8.07E–2	7.90E–2	9.79E–2	549 (2,032)
1.4	5.12E–2	5.14E–2	6.75E–2	729 (2,698)
1.6	3.10E–2	3.25E–2	4.74E–2	1,002 (3,665)
1.8	1.79E–2	2.03E–2	3.08E–2	870 (3,163)
2.0	9.81E–3	1.23E–2	1.78E–2	1,446 (5,168)
2.2	5.13E–3	7.35E–3	1.07E–2	1,614 (5,709)
2.4	2.55E–3	4.37E–3	6.58E–3	1,988 (7,115)
2.6	1.21E–3	2.55E–3	3.67E–3	1,639 (5,726)
2.8	5.44E–4	1.52E–3	2.24E–3	2,248 (7,759)
3.0	2.32E–4	8.40E–4	1.30E–3	2,274 (7,750)
3.2	9.44E–5	4.76E–4	7.22E–4	4,061 (1,4000)
3.4	3.64E–5	2.63E–4	3.65E–4	2,179 (7,490)
3.6	1.33E–5	1.50E–4	2.12E–4	3,216 (10,928)
3.8	4.64E–6	8.26E–5	1.20E–4	4,231 (14,315)
4.0	1.53E–6	4.61E–5	6.48E–5	4,433(15,039)

Numbers in parentheses indicate the number of evaluations of the limit-state function in the orthogonal plane sampling method.

Table 4.5. Comparison of mean up-crossing rates $\nu(t)$ for response of Bouc-Wen oscillator (c.o.v. = 0.10 for simulation).

x/σ_o	ELM	FORM	Orthogonal Plane Sampling	
			$\hat{\nu}(t)$	Samples
0.2	9.49E–1	1.43	1.01	260 (1,560)
0.4	8.75E–1	1.30	9.78 E–1	353 (2,140)
0.6	7.63E–1	1.10	7.42 E–1	323 (1,933)
0.8	6.31E–1	8.83E–1	6.82 E–1	283 (1,664)
1.0	4.94E–1	6.68E–1	5.59 E–1	373 (2,203)
1.2	3.66E–1	4.90E–1	3.78 E–1	341 (1,963)
1.4	2.57E–1	3.43E–1	2.68 E–1	346 (1,967)
1.6	1.71E–1	2.34E–1	2.00 E–1	505 (2,852)
1.8	1.08E–1	1.54E–1	1.66 E–1	673 (3,839)
2.0	6.41E–2	1.01E–1	9.64 E–2	888 (5,019)
2.2	3.62E–2	6.30E–2	6.90 E–2	1,222 (6,868)
2.4	1.94E–2	3.88E–2	3.81 E–2	2,017 (11,084)
2.6	9.80E–3	2.38E–2	2.51 E–2	2,425 (13,399)
2.8	4.70E–3	1.44E–2	1.52 E–2	3,504 (19,152)
3.0	2.13E–3	8.32E–3	8.32 E–3	1,689 (9,224)
3.2	9.17E–4	4.90E–3	5.55 E–3	4,657 (25,062)
3.4	3.74E–4	2.83E–3	2.70 E–3	2,718 (14,659)
3.6	1.44E–4	1.63E–3	1.65 E–3	3,060 (16,515)
3.8	5.26E–5	9.27E–4	7.46 E–4	1,395 (7,527)
4.0	1.82E–5	5.23E–4	5.72 E–4	6,165 (32,887)

Numbers in parentheses indicate the number of evaluations of the limit-state function in the orthogonal plane sampling method.

Table 4.6. Comparison of probability values $P[D_1 > d_1]$ for the inter-story drift D_1 of two-degree-of-freedom Bouc-Wen system (c.o.v. = 0.05 for simulation).

d_1/σ_{do1}	ELM	FORM	Orthogonal Plane Sampling	
			$\hat{P}$	Samples
0.3	4.35E–1	3.97E–1	4.54E–1	232 (844)
0.6	3.72E–1	3.26E–1	4.24E–1	206 (627)
0.9	3.12E–1	2.70E–1	3.56E–1	266 (982)
1.2	2.56E–1	2.26E–1	3.23E–1	203 (707)
1.5	2.07E–1	1.90E–1	2.80E–1	304 (1,086)
1.8	1.64E–1	1.60E–1	2.58E–1	245 (840)
2.1	1.27E–1	1.33E–1	2.17E–1	252 (855)
2.4	9.58E–2	1.11E–1	1.80E–1	304 (1,026)
2.7	7.09E–2	9.23E–2	1.66E–1	254 (857)
3.0	5.13E–2	7.60E–2	1.26E–1	333 (1,087)
3.3	3.63E–2	6.24E–2	1.25E–1	371 (1,218)
3.6	2.51E–2	5.10E–2	8.90E–2	355 (1,138)
3.9	1.69E–2	4.11E–2	7.35E–2	427 (1,369)
4.2	1.11E–2	3.31E–2	6.84E–2	536 (1,725)
4.5	7.17E–3	2.65E–2	5.22E–2	515 (1,649)
4.8	4.50E–3	2.10E–2	3.85E–2	394 (1,248)
5.1	2.76E–3	1.65E–2	3.25E–2	491 (1,558)
5.4	1.65E–3	1.29E–2	2.61E–2	447 (1,426)
5.7	9.63E–4	1.01E–2	1.88E–2	434 (1,362)
6.0	5.48E–4	7.78E–3	1.54E–2	598 (1,864)

Numbers in parentheses indicate the number of evaluations of the limit-state function in the orthogonal plane sampling method.

Table 4.7. Comparison of probability values $P[D_2 > d_2]$ for the inter-story drift D_2 of two-degree-of-freedom Bouc-Wen system (c.o.v. = 0.05 for simulation).

d_2/σ_{do2}	ELM	FORM	Orthogonal Plane Sampling	
			$\hat{P}$	Samples
0.3	4.13E–1	3.86E–1	4.20E–1	302 (1,058)
0.6	3.29E–1	2.94E–1	3.75E–1	274 (1,003)
0.9	2.54E–1	2.27E–1	3.45E–1	248 (899)
1.2	1.89E–1	1.77E–1	2.91E–1	284 (1,020)
1.5	1.35E–1	1.39E–1	2.19E–1	377 (1,363)
1.8	9.26E–2	1.09E–1	1.96E–1	394 (1,397)
2.1	6.11E–2	8.51E–2	1.39E–1	380 (1,317)
2.4	3.86E–2	6.62E–2	1.26E–1	480 (1,648)
2.7	2.34E–2	5.11E–2	1.04E–1	549 (1,858)
3.0	1.36E–2	3.91E–2	6.98E–2	575 (1,900)
3.3	7.56E–3	2.96E–2	5.75E–2	726 (2,375)
3.6	4.02E–3	2.23E–2	4.50E–2	975 (3,166)
3.9	2.05E–3	1.66E–2	3.50E–2	975 (3,169)
4.2	9.95E–4	1.22E–2	2.55E–2	1,190 (3,800)
4.5	4.62E–4	8.92E–3	1.70E–2	1,314 (4,123)
4.8	2.05E–4	6.42E–3	1.22E–2	1,181 (3,701)
5.1	8.69E–5	4.58E–3	7.20E–3	809 (2,511)
5.4	3.52E–5	3.24E–3	5.87E–3	1,054 (3,256)
5.7	1.36E–5	2.26E–3	4.20E–3	1,913 (5,900)
6.0	5.01E–6	1.57E–3	2.85E–3	1,952 (5,980)

Numbers in parentheses indicate the number of evaluations of the limit-state function in the orthogonal plane sampling method.

Table 4.8. Comparison of mean up-crossing rates $\nu(t)$ for the inter-story drift D_1 of two-degree-of-freedom Bouc-Wen system (c.o.v. = 0.10 for simulation).

d_1/σ_{do1}	ELM	FORM	Orthogonal Plane Sampling	
			$\hat{\nu}(t)$	Samples
0.3	1.71E–1	3.00E–1	1.16E–1	290 (1,662)
0.6	1.65E–1	2.47E–1	1.59E–1	239 (1,300)
0.9	1.54E–1	2.09E–1	1.18E–1	259 (1,449)
1.2	1.40E–1	1.77E–1	1.18E–1	240 (1,374)
1.5	1.24E–1	1.51E–1	1.12E–1	242 (1,371)
1.8	1.07E–1	2.78E–1	1.10E–1	225 (1,237)
2.1	9.03E–2	1.09E–1	9.07E–2	227 (1,265)
2.4	7.40E–2	9.24E–2	9.84E–2	264 (1,455)
2.7	5.90E–2	7.82E–2	8.21E–2	266 (1,476)
3.0	4.58E–2	6.63E–2	7.42E–2	266 (1,451)
3.3	3.46E–2	5.54E–2	6.02E–2	301 (1,636)
3.6	2.55E–2	4.60E–2	5.51E–2	233 (1,255)
3.9	1.83E–2	3.83E–2	4.89E–2	258 (1,367)
4.2	1.27E–2	3.15E–2	4.06E–2	327 (1,697)
4.5	8.66E–3	2.57E–2	3.23E–2	370 (1,918)
4.8	5.73E–3	2.08E–2	3.02E–2	484 (2,522)
5.1	3.69E–3	1.68E–2	2.00E–2	428 (2,168)
5.4	2.32E–3	1.35E–2	2.05E–2	394 (2,025)
5.7	1.41E–3	1.07E–2	1.57E–2	312 (1,586)
6.0	8.41E–4	8.44E–3	1.16E–2	424 (2,119)

Numbers in parentheses indicate the number of evaluations of the limit-state function in the orthogonal plane sampling method.

Table 4.9. Comparison of mean up-crossing rates $\nu(t)$ for the inter-story drift D_2 of two-degree-of-freedom Bouc-Wen system (c.o.v. = 0.10 for simulation).

d_2/σ_{do2}	ELM	FORM	Orthogonal Plane Sampling	
			$\hat{\nu}(t)$	Samples
0.3	1.78E–1	3.09E–1	1.19E–1	262 (1,506)
0.6	1.66E–1	2.54E–1	1.12E–1	202 (1,201)
0.9	1.47E–1	2.01E–1	1.22E–1	171 (1,027)
1.2	1.24E–1	1.59E–1	1.05E–1	249 (1,440)
1.5	9.92E–2	1.24E–1	8.75E–2	252 (1,478)
1.8	7.59E–2	9.85E–2	7.56E–2	277 (1,588)
2.1	5.53E–2	7.78E–2	6.03E–2	299 (1,658)
2.4	3.83E–2	6.15E–2	6.23E–2	395 (2,182)
2.7	2.53E–2	4.84E–2	4.98E–2	447 (2,399)
3.0	1.59E–2	3.77E–2	4.17E–2	380 (2,052)
3.3	9.54E–3	2.92E–2	3.16E–2	406 (2,152)
3.6	5.45E–3	2.23E–2	2.69E–2	422 (2,211)
3.9	2.96E–3	1.70E–2	1.56E–2	504 (2,508)
4.2	1.53E–3	1.28E–2	1.53E–2	538 (2,772)
4.5	7.56E–4	9.53E–3	1.04E–2	413 (2,063)
4.8	3.55E–4	7.05E–3	9.43E–3	438 (2,200)
5.1	1.59E–4	5.14E–3	6.78E–3	526 (2,581)
5.4	6.76E–5	3.70E–3	4.33E–3	635 (3,126)
5.7	2.74E–5	2.64E–3	3.06E–3	502 (2,410)
6.0	1.06E–5	1.86E–3	2.43E–3	830 (3,946)

Numbers in parentheses indicate the number of evaluations of the limit-state function in the orthogonal plane sampling method.

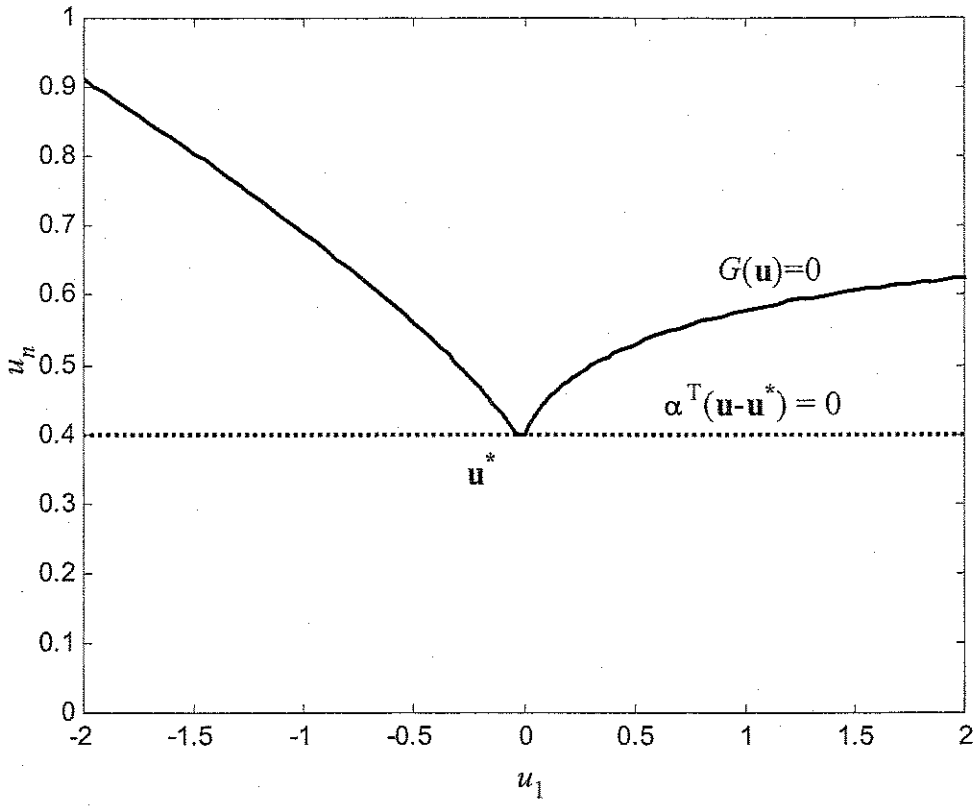

Figure 4.1. Shape of limit-state surface along first principal axis for the system with nonlinear damping.

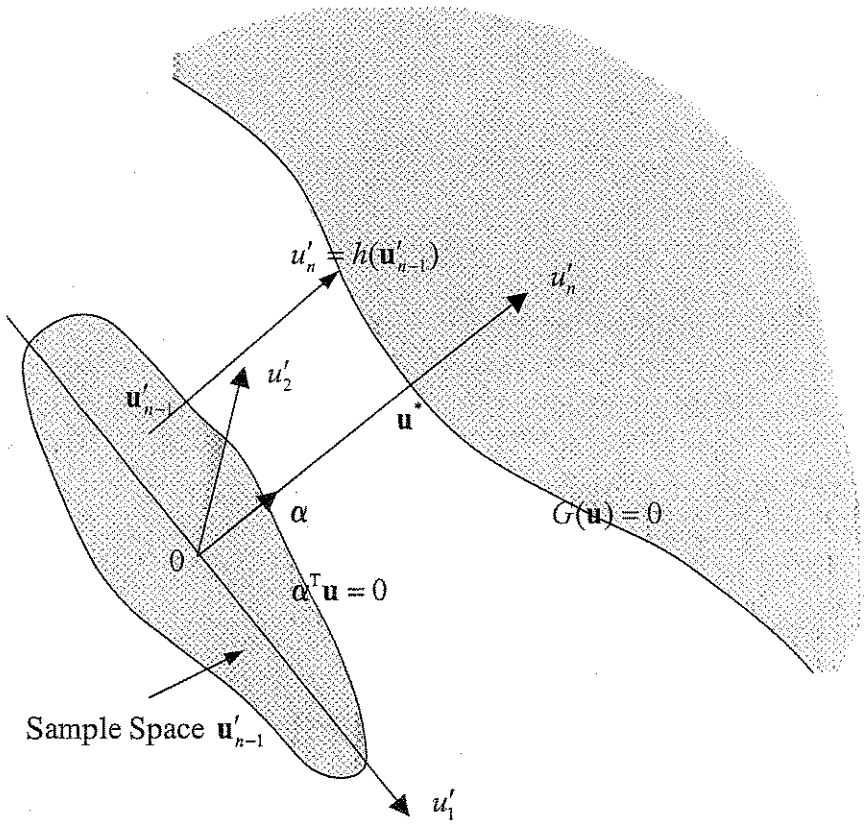

Figure 4.2. Sampling in the orthogonal plane.

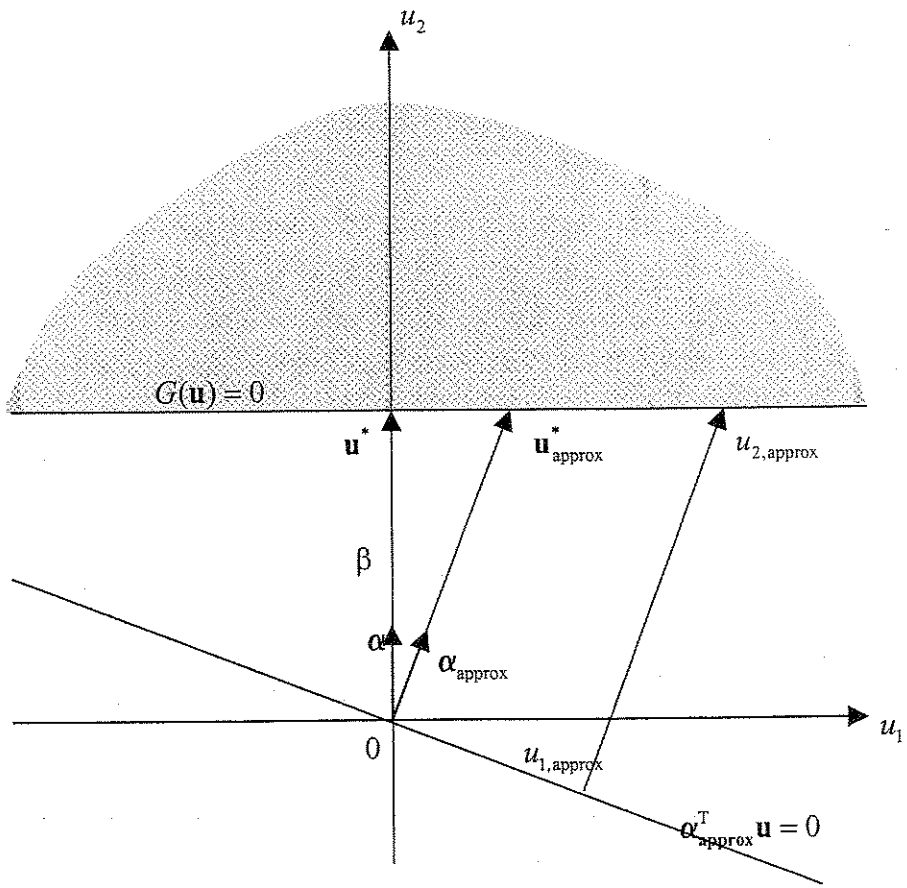

Figure 4.3. Orthogonal plane sampling with approximate design point.

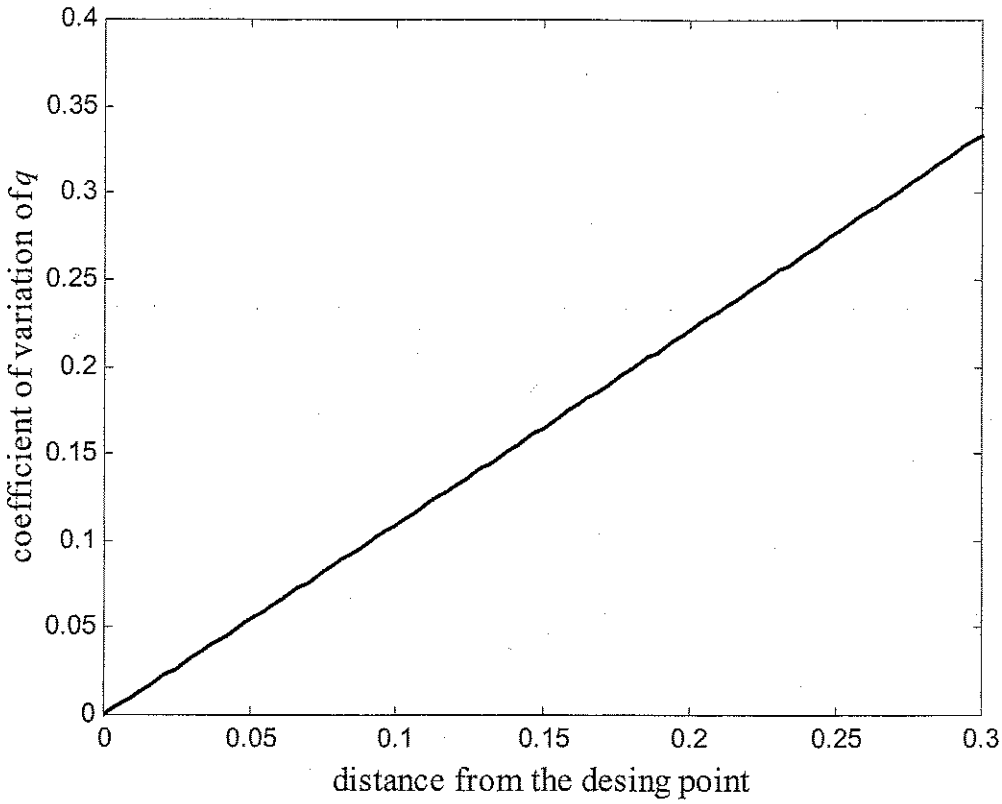

Figure 4.4. Relation between distance from design point and coefficient of variation of q.

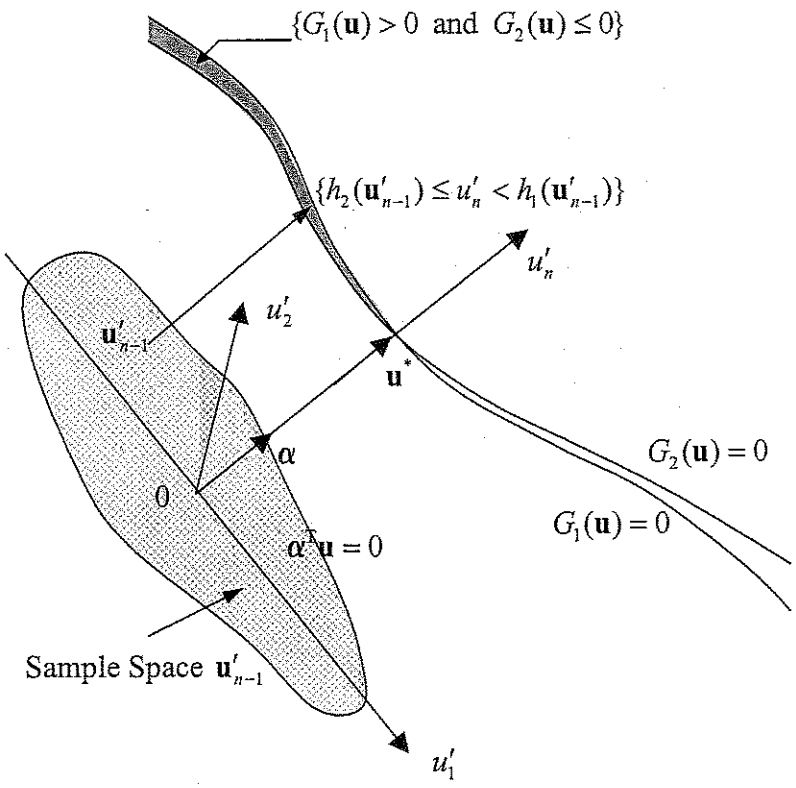

Figure 4.5. Simulation of the mean out-crossing rate by sampling in the orthogonal plane.

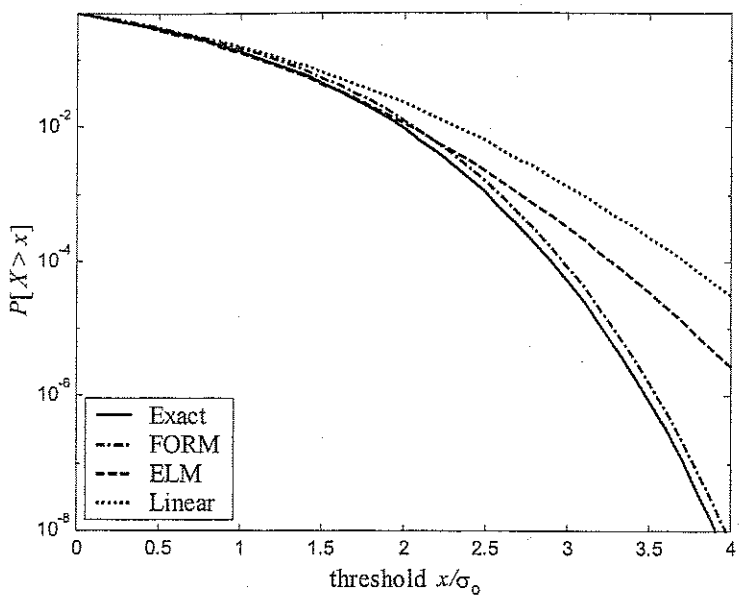

Figure 4.6. Complementary distribution function of response of Duffing oscillator.

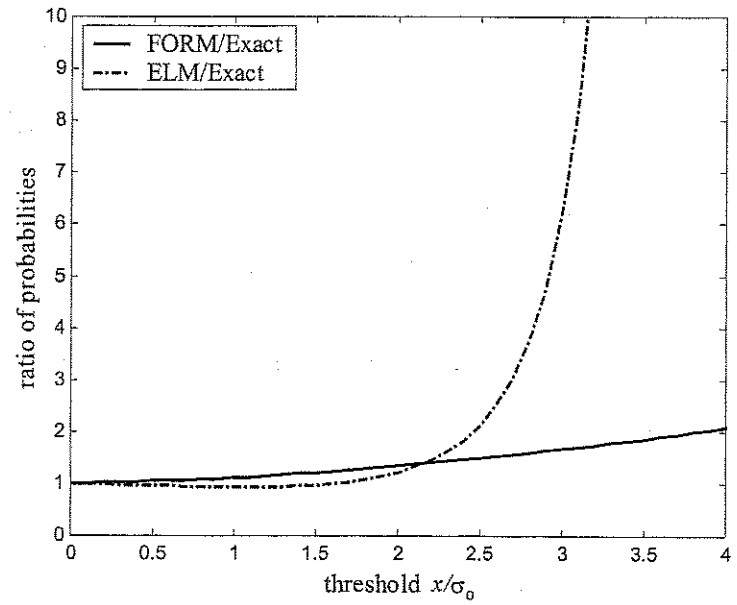

Figure 4.7. Comparison of relative errors for response of Duffing oscillator.

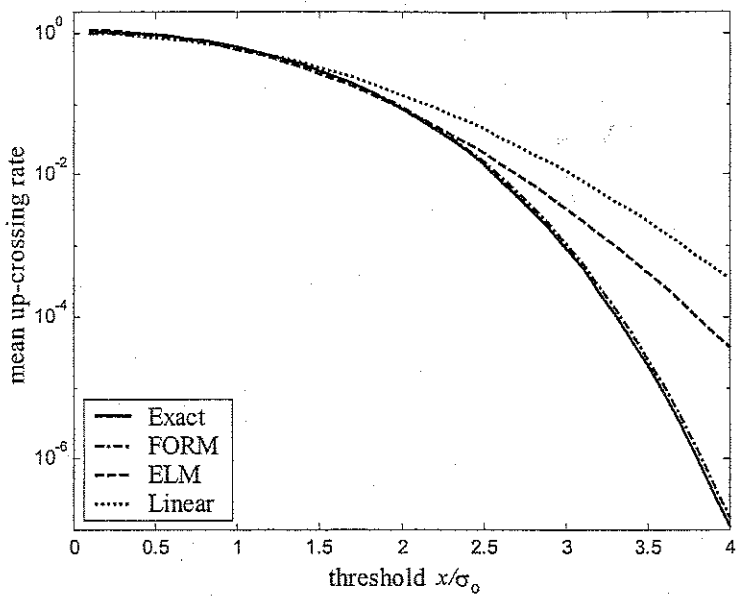

Figure 4.8. Stationary mean up-crossing rate of Duffing oscillator.

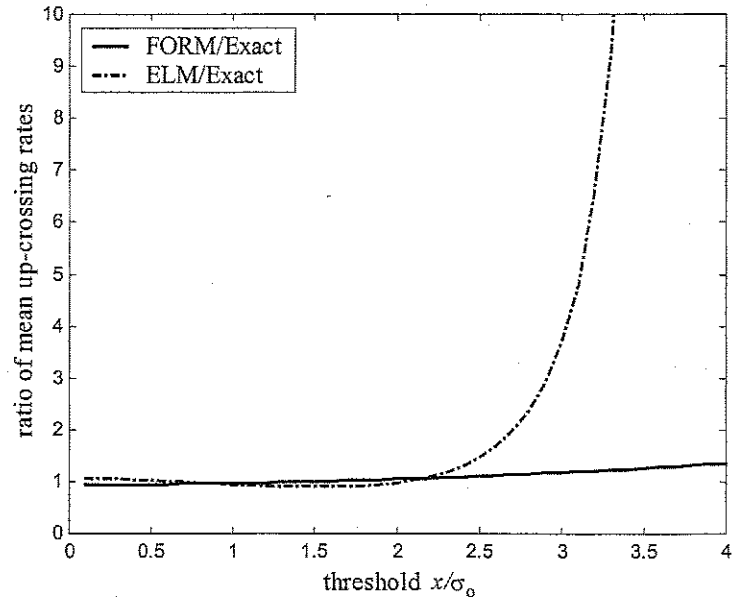

Figure 4.9. Comparison of relative errors of mean up-crossing rate of Duffing oscillator.

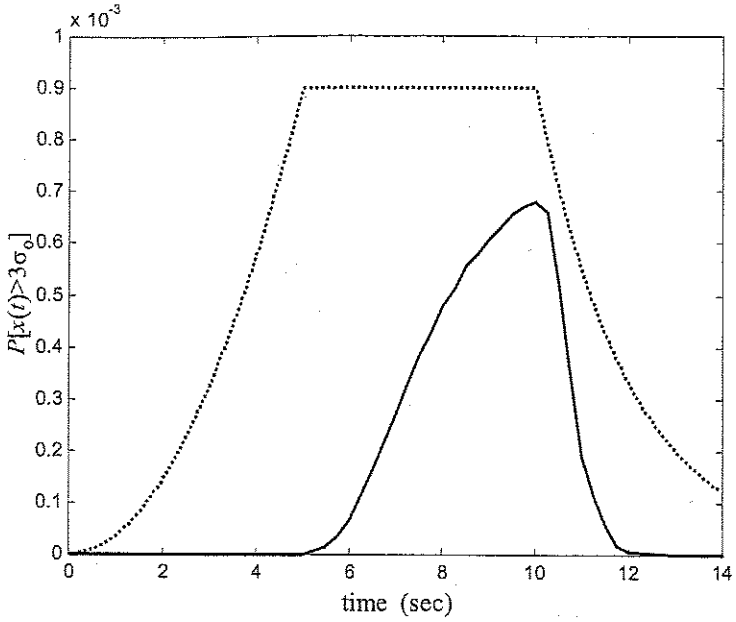

Figure 4.10. Probability of response exceeding threshold $3\sigma_o$ for Duffing oscillator subjected to non-stationary Gaussian excitation.

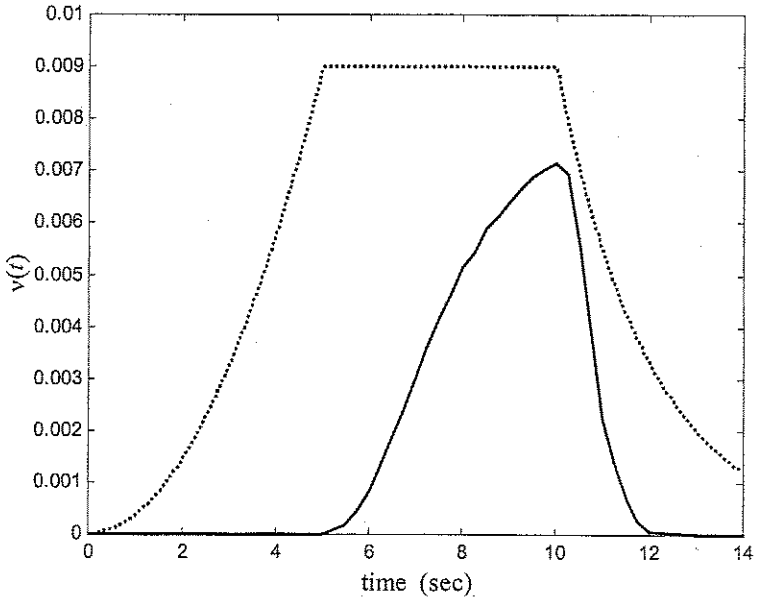

Figure 4.11. Mean rate of up-crossing threshold $3\sigma_o$ for Duffing oscillator subjected to nonstationary Gaussian excitation.

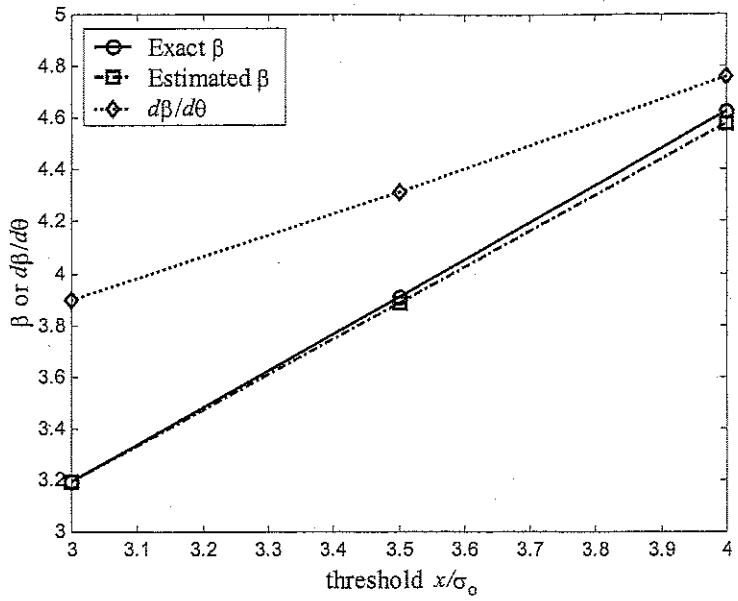

Figure 4.12. Comparison of exact and approximate reliability indices.

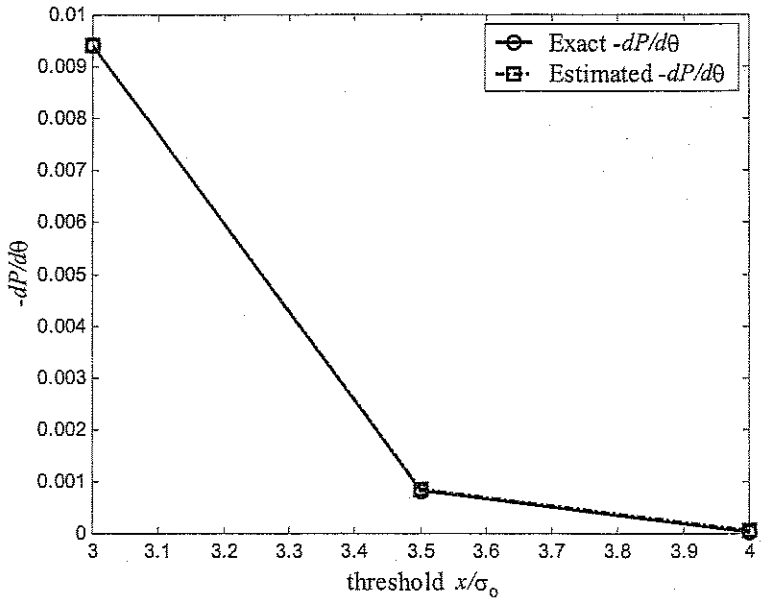

Figure 4.13. Comparison of exact and approximate estimates of first-order probability density approximation.

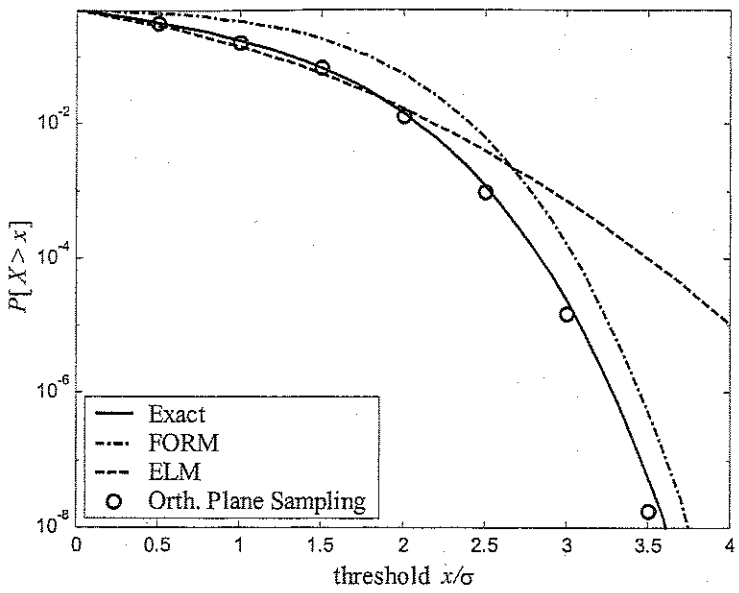

Figure 4.14. Complementary distribution function of response of elastic SDOF oscillator with nonlinear damping.

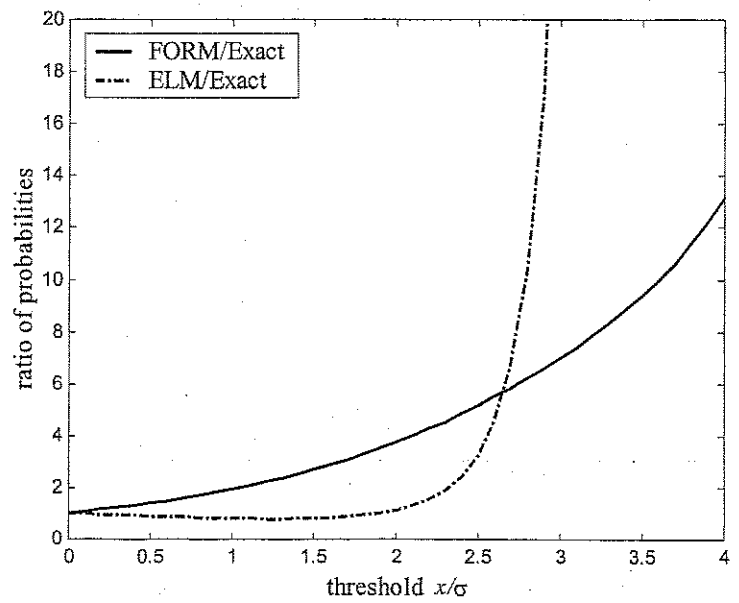

Figure 4.15. Comparison of relative errors for response of elastic SDOF oscillator with nonlinear damping.

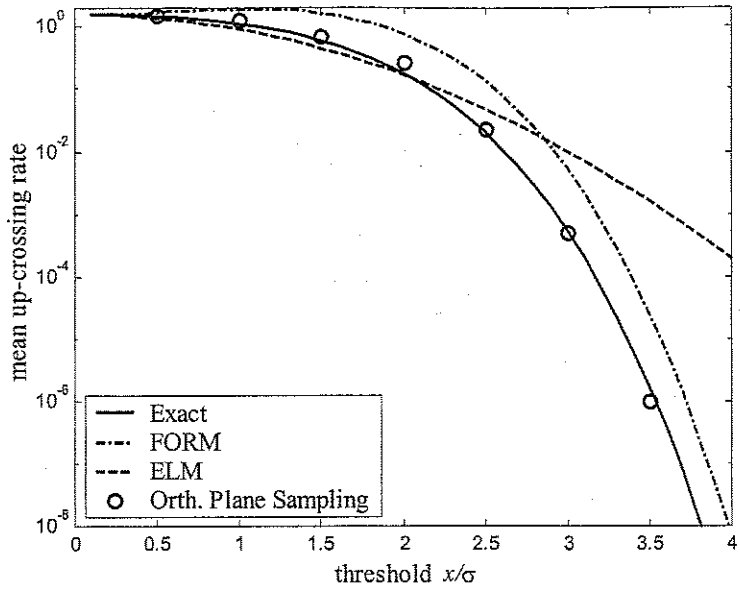

Figure 4.16. Stationary mean up-crossing rate of an elastic SDOF oscillator with nonlinear damping.

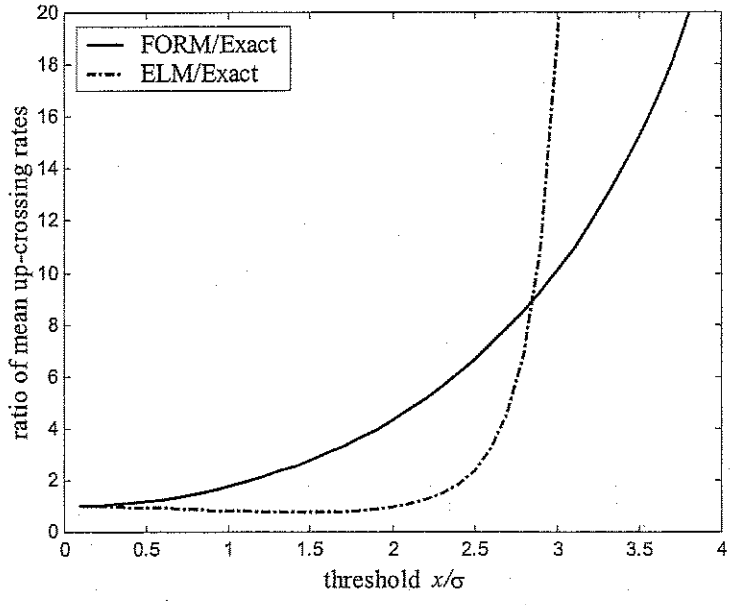

Figure 4.17. Comparison of relative errors of mean up-crossing rate of elastic SDOF oscillator with nonlinear damping.

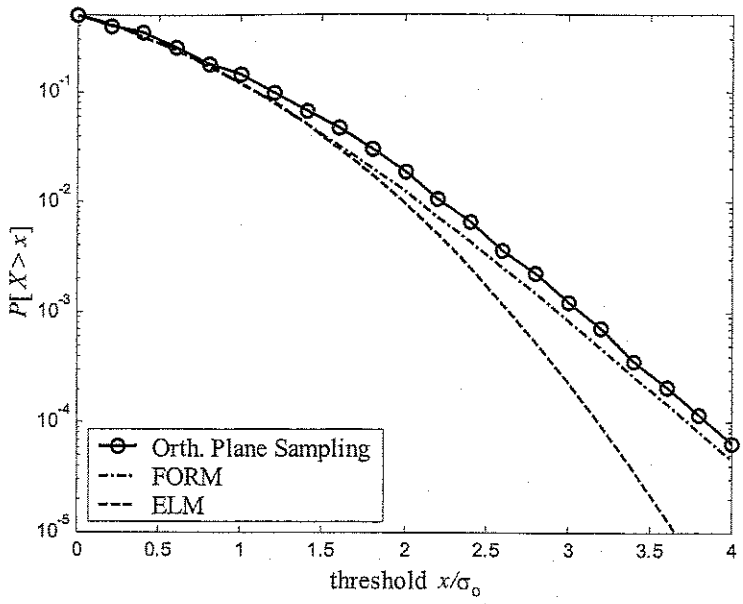

Figure 4.18. Complementary distribution function of the response of Bouc-Wen Oscillator (c.o.v. = 0.05 for simulation).

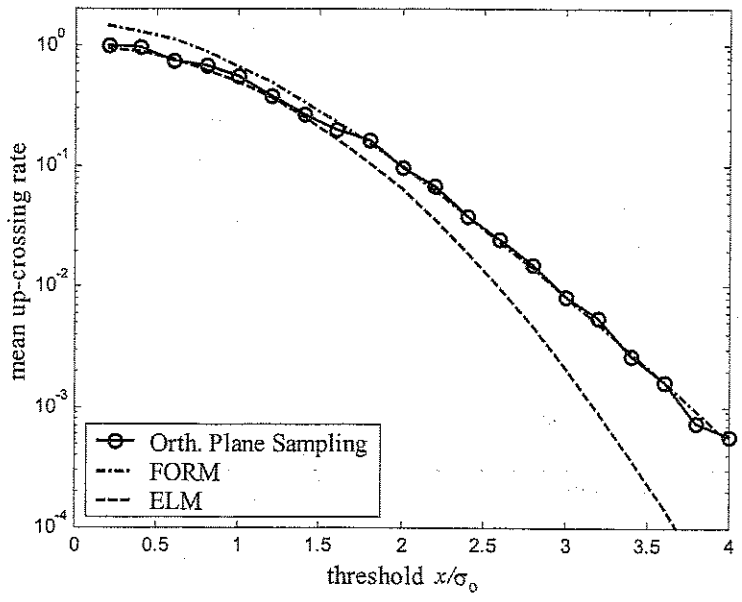

Figure 4.19. Stationary mean up-crossing rate of Bouc-Wen Oscillator (c.o.v. = 0.1 for simulation).

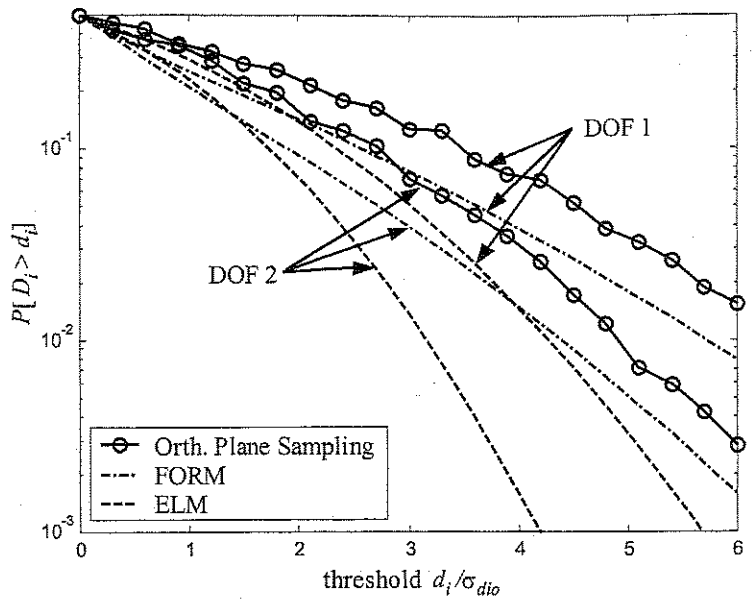

Figure 4.20. Complementary distribution functions of the inter-story drifts of two-degree-of-freedom Bouc-Wen System (c.o.v. = 0.05 for simulation).

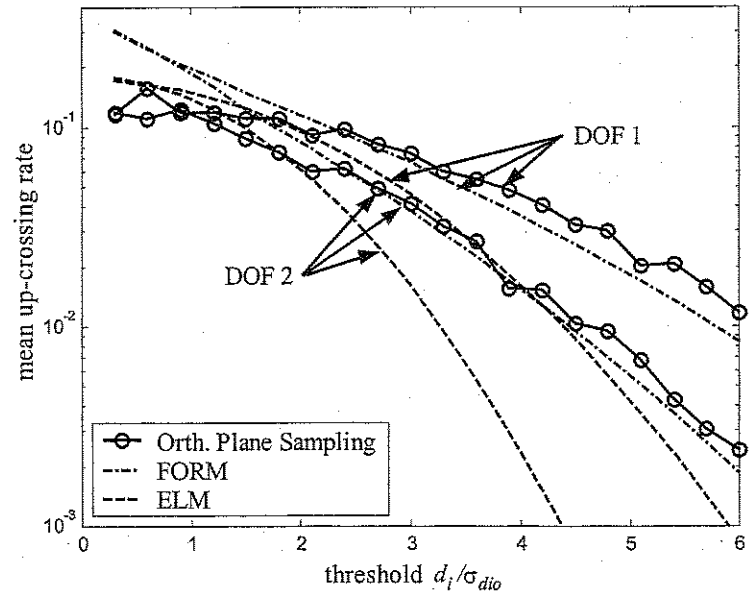

Figure 4.21. Stationary mean up-crossing rates of the inter-story drifts of two-degree-of-freedom Bouc-Wen system (c.o.v. = 0.1 for simulation).

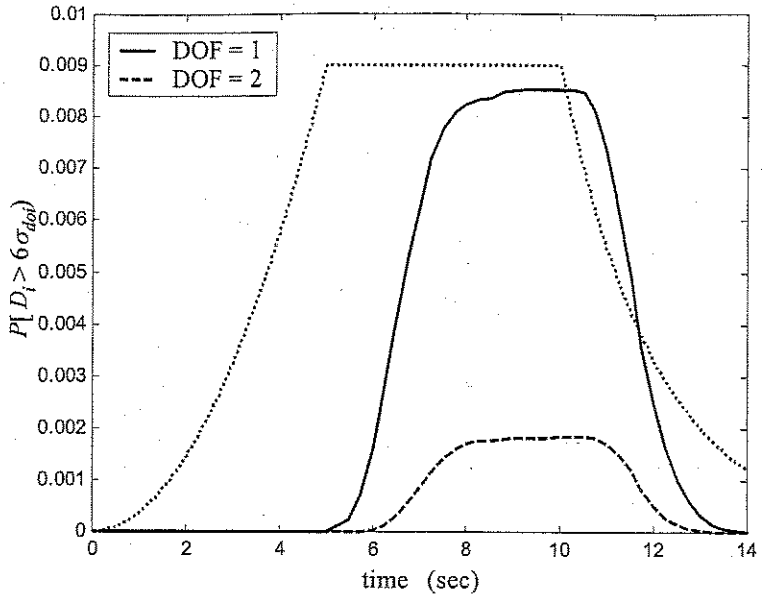

Figure 4.22. Probability of inter-story drifts exceeding threshold $6\sigma_{dio}$, $i = 1, 2$, for two-degree-of-freedom Bouc-Wen system subjected to non-stationary Gaussian excitation.

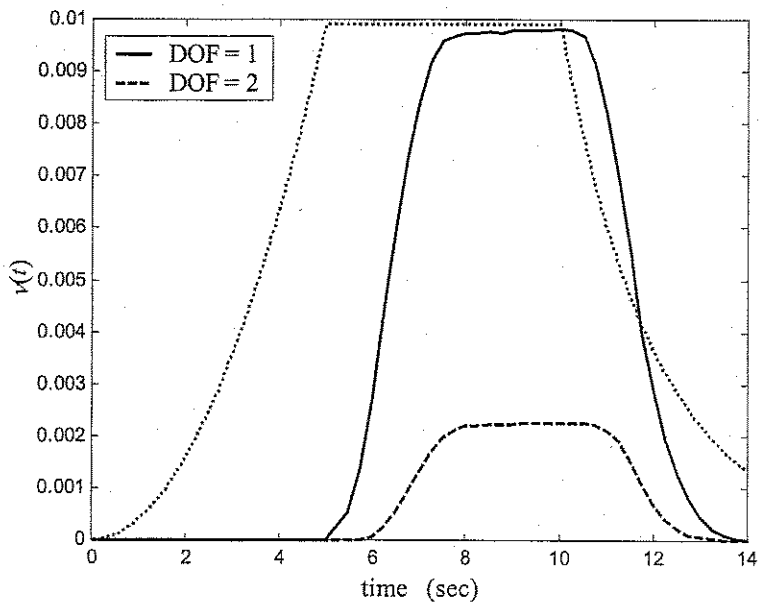

Figure 4.23. Mean rates of inter-story drifts up-crossing the threshold $6\sigma_{dio}$, $i = 1, 2$, for two-degree-of-freedom Bouc-Wen system subjected to a non-stationary Gaussian excitation.

5 Simulation of First-Excursion Probability

5.1 Introduction

The first-excursion probability is one of the most important reliability statistics in random vibrations. Unfortunately, no general solution procedure is available for this problem, except under restrictive conditions when the response can be treated as a one-dimensional Markov process (Lin and Cai, 1995). For this reason, approximate solutions are pursued for most engineering applications.

In Chapter 2, we have reviewed an approximate method based on the out-crossing rate. In general, we can estimate the upper bound of the First-excursion probability by integrating the out-crossing rate over the duration of the response. In order to apply this method to nonstationary problems, however, the out-crossing rates have to be evaluated for many time points during the period under consideration, which makes the method rather costly. Even if we have computed the out-crossing rates accurately, we can at best get an upper bound.

An alternative approach for solving this problem is Monte Carlo simulation. As is well known, this approach is versatile but computationally inefficient, especially for small probability problems. In structural reliability, importance sampling is widely used to improve the efficiency of the crude Monte Carlo simulation method.

Recently, Au and Beck (2001) proposed an efficient importance sampling method for simulation of the first-excursion probability of a linear system subjected to a Gaussian excitation. They first transformed the first-excursion problem into a series-system reliability problem by discretizing the time axis into small intervals $\Delta t = t_{i+1} - t_i$, $i = 1, \cdots, n$, where n is the number of time steps, or components of the system. They then approximated the first-excursion probability as the probability of the union of the failure events in all the time-point components. They used a sampling density composed of standard normal probability density functions conditioned on the failure event in each

time step (component), say $p(\mathbf{u}|E_i)$, $i=1,\cdots,n$, where $\mathbf{u}$ is the standard normal vector and E_i is the failure event of the i-th component. They showed that this sampling density is highly efficient for simulation of the first-excursion probability of a linear system with deterministic parameters and subjected to Gaussian excitation.

In this chapter, we extend the importance sampling method proposed by Au and Beck (2001) to nonlinear random vibration problems, including systems with uncertain parameters. A two-degree-of-freedom Bouc-Wen structure in Section 4.5.4 is used to demonstrate the method. The efficiency and accuracy of the method are compared with those of a conventional importance sampling method and the crude Monte Carlo simulation method.

5.2 Problem Formulation

Consider the First-excursion probability for an interval $(0,T)$,

$$P_T = P\{\min_{0<t\le T} g[\mathbf{x}(t),\mathbf{v}] \le 0\} \tag{5.1}$$

where $g(\cdot)$ is a limit-state function described in terms of a response vector $\mathbf{x}(t)$ and a vector of system parameters $\mathbf{v}_1$. It is assumed that the input excitation process is discretized (see Der Kiureghian 2000), such that its randomness is represented in terms of a vector of random variables $\mathbf{v}_2$. Thus, the response $\mathbf{x}(t)$ is an implicit function of the vector of random variables $\mathbf{v}=(\mathbf{v}_1,\mathbf{v}_2)$ that collectively define the random nature of the input process and the system. As is common in reliability analysis, a probability-preserving transformation $\mathbf{u}=\mathbf{T}(\mathbf{v})$ is used, such that $\mathbf{u}$ is a vector of standard normal variables. The limit-state function is then written as $g[\mathbf{x}(\mathbf{v}_1,\mathbf{v}_2,t),\mathbf{v}_1] = g(\mathbf{v},t) = g[\mathbf{T}^{-1}(\mathbf{u}),t] = G(\mathbf{u},t)$.

The problem in (5.1) can be reformulated as a series-system reliability problem by considering a set of closely and equally spaced time points t_i, $i=1,\cdots,n$, with $\Delta t = t_{i+1}-t_i$, $t_1=0$ and $t_n=T$. The number of time steps, n, determines the number of components of the series system. (This number is not necessarily equal to the number of

time steps used in discretizing the input excitation.) For convenience, let $G_{\min}(\mathbf{u}) = \min_{0<t\le T} G(\mathbf{u},t)$ and $G_i(\mathbf{u}) = G(\mathbf{u},t_i)$, $i=1,\cdots,n$. Then, $G_i(\mathbf{u}) \ge G_{\min}(\mathbf{u})$, $i=1,\cdots,n$, and we can write

$$P_T = P[G_{\min}(u) \le 0] \ge P\left[\bigcup_{i=1}^{n} G_i(\mathbf{u}) \le 0\right] \tag{5.2}$$

Thus, the series-system probability provides a lower bound to the first-excursion probability. This bound can be improved by selecting a dense grid of time points (small Δt), as described below. Figure 5.1 depicts the above concept in the space of the standard normal random variables $\mathbf{u}$. The failure domains of the individual components (time points) collectively approximate the failure domain of the series system, i.e., the domain of the first-excursion event.

As mentioned above, the lower bound in (5.2) can be improved by selecting a dense grid of time points. However, too dense a grid is not necessary, since component events for the successive time points are closely correlated and additional points in between will not contribute to the probability on the right side of (5.2). Numerical experiments reveal that, for practical purposes, it is sufficient that the correlation coefficient between the linearized limit-state functions for two neighboring time points be no less than about 0.9. In the first-order reliability method (FORM), this correlation coefficient is given by the scalar product of the unit direction vectors towards the design points of the corresponding limit-state surfaces, i.e., $\rho_{i,i+1} = \boldsymbol{\alpha}_i^T \boldsymbol{\alpha}_{i+1}$, see Figure 5.1. Efficient methods for finding the design point for the individual components are developed in Chapter 3 and Koo and Der Kiureghian (2001). In the following, we denote the design point for the i-th component as $\mathbf{u}_i^*$.

The probability in (5.2) can be written as

$$P\left[\bigcup_{i=1}^{n} G_i(\mathbf{u}) \le 0\right] = \int_{\mathbf{u}} I\left[\max_{i=1,\ldots,n}\left(-G_i(\mathbf{u})\right)\right]\varphi(\mathbf{u})d\mathbf{u}$$

$$= \mathrm{E}_{\varphi(\mathbf{u})}\left\{I\left[\max_{i=1,\ldots,n}\left(-G_i(\mathbf{u})\right)\right]\right\} \tag{5.3}$$

where $I[a]=1$ for $a \geq 0$ and $I[a]=0$ for $a<0$, $\varphi(\cdot)$ is the standard normal probability density function, and $E_{\varphi(\cdot)}\{\cdot\}$ denotes the expectation with respect to $\varphi(\cdot)$. It is clear that for any random realizations $\mathbf{u}_k$, $k=1,\cdots,N$, generated according to $\varphi(\cdot)$, the probability of interest can be computed as the sample mean of the corresponding indicator values I_k, $k=1,\cdots,N$, where N denotes the sample size. Let

$$q(\mathbf{u}) = I\left[\max_{i=1,\ldots,n}\left(-G_i(\mathbf{u})\right)\right] \tag{5.4}$$

and $q_k = q(\mathbf{u}_k)$. Then, an unbiased estimate of the First-excursion probability is

$$\hat{P}_T = \frac{1}{N}\sum_{k=1}^{N} q_k \tag{5.5}$$

A measure of uncertainty of this estimate is given by the coefficient of variation

$$\delta_{\hat{P}_T} = \frac{1}{\sqrt{N}}\delta_q \tag{5.6}$$

where δ_q is the sample coefficient of variation of q_k, $k=1,\cdots,N$.

When the first-excursion probability is small, most of the simulated points $\mathbf{u}_k$ fall within the safe domain, where $q_k = 0$. In that case, the number of simulations N must be very large to achieve reasonable accuracy. To improve the efficiency of the simulation, it is common to use importance sampling (Rubinstein 1981). Equation (5.3) is written as

$$\begin{aligned} P\left[\bigcup_{i=1}^{n} G_i(\mathbf{u}) \leq 0\right] &= \int_{\mathbf{u}} I\left[\max_{i=1,\ldots,n}\left(-G_i(\mathbf{u})\right)\right]\frac{\varphi(\mathbf{u})}{f(\mathbf{u})} f(\mathbf{u})d\mathbf{u} \\ &= \mathrm{E}_{f(\mathbf{u})}\left\{I\left[\max_{i=1,\ldots,n}\left(-G_i(\mathbf{u})\right)\right]\frac{\varphi(\mathbf{u})}{f(\mathbf{u})}\right\} \end{aligned} \tag{5.7}$$

where $f(\mathbf{u})$ is a sampling density and $\mathrm{E}_{f(\mathbf{u})}\{\cdot\}$ denotes the expectation with respect to $f(\mathbf{u})$. Setting

$$q(\mathbf{u}) = I\left[\max_{i=1,\ldots,n}\left(-G_i(\mathbf{u})\right)\right]\frac{\varphi(\mathbf{u})}{f(\mathbf{u})} \tag{5.8}$$

the estimate of the first-excursion probability can now be obtained from (5.5) – (5.6) by simulating a sample $\mathbf{u}_k$, $k=1,\cdots,N$, according to the sampling distribution $f(\mathbf{u})$ and

computing the corresponding sample of $q(\mathbf{u})$ from (5.8). One can show that the estimate in (5.5) is unbiased, as long as $f(\mathbf{u}) \neq 0$ for any $\mathbf{u}$ in the failure domain, i.e., for $\mathbf{u} \in \{\min_{i=1,\cdots,n} G_i(\mathbf{u}) \leq 0\}$. Furthermore, the coefficient of variation of the estimate will be small, if $f(\mathbf{u})$ is only non-zero in the failure domain and if it is proportional to $\varphi(\mathbf{u})$ in the failure domain of the system.

As should be clear, the main issue in importance sampling is the choice of the sampling density $f(\mathbf{u})$. In the following, we describe two choices of the sampling density: a commonly used sampling density constructed by use of the design points, and a sampling density proposed by Au and Beck (2001) based on conditional distributions. The latter is extended to nonlinear reliability problems.

5.3 Importance Sampling Distribution

A natural way of constructing an importance sampling distribution for a series system is to compose it from importance sampling distributions of the individual components. Let $f_i(\mathbf{u})$, $i = 1, \cdots, n$, denote selected importance sampling distributions for the components of the system. The sampling distribution for the series system may then be constructed as

$$f(\mathbf{u}) = \sum_{i=1}^{n} w_i f_i(\mathbf{u}) \tag{5.9}$$

where w_i, $i = 1, \cdots, n$, with $w_i > 0$ and $w_1 + \cdots + w_n = 1$, are a set of weight factors. Each factor w_i may be taken proportional to a measure of importance of the corresponding component of the system, say its probability of failure.

A widely used choice for the individual component sampling distribution is the standard Gaussian probability density centered at the corresponding design point (Shueller and Stix 1987). Combining this with (5.9) yields (Melchers 1989)

$$f(\mathbf{u}) = \sum_{i=1}^{n} w_i \varphi(\mathbf{u} - \mathbf{u}_i^*) \tag{5.10}$$

This method usually performs far better than the crude Monte Carlo simulation method. However, it is not as efficient as is possible because of two reasons: (a) as much as half

or more of the simulated points $\mathbf{u}_k$ may fall within the safe domain, where $q_k = 0$, (b) the function $\varphi(\mathbf{u} - \mathbf{u}_k^*)$ is far from being proportional to the probability density function $\varphi(\mathbf{u})$ in the failure domain. Improvements in the choice of the importance sampling distribution can be made on both grounds.

Au and Beck (2001) devised a sampling distribution for linear systems having deterministic parameters and subjected to Gaussian excitation in such a way that the sampling density has the same shape as the original probability density function in the failure domain, at least at the component level. According to their formulation,

$$f(\mathbf{u}) = \sum_{i=1}^{n} w_i p(\mathbf{u}|E_i) \tag{5.11}$$

where $E_i = \{G_i(\mathbf{u}) \le 0\}$ is the failure event at time t_i (component i) and $p(\mathbf{u}|E_i)$ is the conditional probability density function of $\mathbf{u}$ given the failure event E_i. The latter can be written as

$$p(\mathbf{u}|E_i) = \frac{\varphi(\mathbf{u}) I[-G_i(\mathbf{u})]}{p_i} \tag{5.12}$$

where $p_i = P(E_i)$. For the weight factors w_i, Au and Beck (2001) selected

$$w_i = \frac{p_i}{\sum_{j=1}^{n} p_j} \tag{5.13}$$

Substituting (5.12) and (5.13) in (5.11) and the latter in (5.8), we have

$$q(\mathbf{u}) = \frac{\sum_{j=1}^{n} p_j}{\sum_{j=1}^{n} I[-G_j(\mathbf{u})]} \tag{5.14}$$

The estimate of the first-excursion probability can now be obtained from (5.5) – (5.6) by simulating a sample $\mathbf{u}_k$, $k = 1, \cdots, N$, according to the sampling distribution in (5.11) – (5.13) and computing the corresponding sample of $q(\mathbf{u})$ from (5.14). In deriving the expression in (5.14), we have dropped the indicator function $I[\max_{i=1,\cdots,n}\{-G_i(\mathbf{u})\}]$ that

appears in (5.8) because it is always equal to unity for the selected sampling density. This, in fact, is an important advantage of this choice of the sampling distribution.

5.4 Application to Linear and Nonlinear Systems

So far, we have not made any assumption regarding the linearity or nonlinearity of the vibrating system, or the Gaussian or non-Gaussian nature of the input excitation. Neither have we specified whether the system parameters are deterministic or random. Therefore, if we can simulate samples of $\mathbf{u}$ according to the distribution in (5.11) and accurately compute the statistic $q(\mathbf{u})$ in (5.14), then we can use the above approach for estimation of the first-excursion probability of general dynamical systems, possibly with random properties, subjected to Gaussian or non-Gaussian excitation. Au and Beck (2001) used this approach to estimate the first-excursion probability for linear, deterministic systems subjected to Gaussian excitation. Their method is described in the following sub-section. Subsequently, we extend their method to general nonlinear problems, which may involve nonlinear dynamical systems, non-Gaussian excitation, or uncertain system properties.

5.4.1 Linear System Subjected to Gaussian Excitation

For a linear system subjected to a Gaussian excitation, the failure domain of the i-th component is the half space separated by the hyperplane $\alpha_i^{\mathrm{T}}(\mathbf{u}-\mathbf{u}_i^*)=0$, where $\mathbf{u}_i^*$ is the design point and α_i is the unit vector in the direction of the design point (see Figure 5.2). Let $\mathbf{u}'=(u_1',\cdots,u_n')$ be an orthonormal transformation of $\mathbf{u}$ such that the u_n' axis coincides with α_i. We can express the failure event E_i as $u_n' \geq \beta_i$, where $\beta_i = \alpha_i^T \mathbf{u}_i^*$ is the reliability index of the i-th component. The variables $u_1',\cdots,u_{n-1}'$ are clearly independent of E_i. Thus, we can write

$$p(\mathbf{u}|E_i) = p(\mathbf{u}'|E_i)$$

$$= \varphi(u_1',\ldots,u_{n-1}'|E_i)\varphi(u_n'|u_1',\ldots,u_{n-1}',E_i)$$

$$= \varphi(u'_1,...,u'_{n-1})\varphi(u'_n|u'_n \geq \beta_i) \tag{5.15}$$

It is seen that the conditional probability density function is the product of the $n-1$ dimensional normal density function $\varphi(u'_1,...,u'_{n-1})$ and the truncated normal density function $\varphi(u'_n|u'_n \geq \beta_i)$. Furthermore, the individual component failure probabilities are given by $p_i = \Phi(-\beta_i)$, where $\Phi(\cdot)$ is the standard normal cumulative probability function.

Following Au and Beck (2001), simulation of a sample $\mathbf{u}_k$, $k = 1,\cdots,N$, according to $f(\mathbf{u})$ in (5.11) – (5.13) can be carried out in the following manner:

a) Compute the design point $\mathbf{u}_i^*$, the unit direction vector $\boldsymbol{\alpha}_i$, the reliability index β_i, and the probability $p_i = \Phi(-\beta_i)$ for each time-point component i, $i = 1,\cdots,n$. It is noted that, for linear systems, closed form solution of the design point is available (see Der Kiureghian 2000).

b) Randomly select a time-point component according to the discrete probabilities w_i, $i = 1,\cdots,n$, in (5.13). Suppose that the i-th component is selected with the corresponding unit direction reliability $\boldsymbol{\alpha}_i$ and reliability index β_i.

c) Simulate a standard normal vector $\mathbf{u} = (u_1,\cdots,u_n)$.

d) Simulate a uniform variable U on [0, 1] and compute

$$d = \Phi^{-1}\left[U + (1-U)\Phi(\beta_i)\right] \tag{5.16}$$

e) Compute

$$\begin{aligned} \mathbf{u}_k &= (\mathbf{u} - \boldsymbol{\alpha}_i^{\mathrm{T}}\mathbf{u}\boldsymbol{\alpha}_i) + d\boldsymbol{\alpha}_i \\ &= \mathbf{u} + (d - \boldsymbol{\alpha}_i^{\mathrm{T}}\mathbf{u})\boldsymbol{\alpha}_i \end{aligned} \tag{5.17}$$

The first expression in (5.17) can be interpreted as the following two-step simulation (see Figure 5.2): (a) the simulated vector $\mathbf{u}$ is projected on the orthogonal plane $\boldsymbol{\alpha}_i^{\mathrm{T}}\mathbf{u} = 0$, yielding a random point according to $\varphi(u'_1,...,u'_{n-1})$, and (b) the truncated normal variable d is simulated according to $\varphi(u'_n|u'_n \geq \beta_i)$. The sum of the two vectors $\mathbf{u} - \boldsymbol{\alpha}_i^{\mathrm{T}}\mathbf{u}\boldsymbol{\alpha}_i$ and

$d\alpha_i$ yields a vector, which is always in the failure domain of the component and has the distribution in (5.15).

5.4.2 Extension to Nonlinear Problems

For general nonlinear problems that involve nonlinear dynamical systems, non-Gaussian excitation, or random system properties, it is not so easy to compute the component probabilities p_i, which are needed in (5.14). Furthermore, simulation according to the conditional density $p(\mathbf{u}|E_i)$ is problematic, since we do not have a closed form expression of this distribution. Here, we make two assumptions to proceed with an approximate solution approach.

The first assumption concerns the geometry of the failure domain of the individual components in the standard normal space. We assume that any line perpendicular to the plane $\boldsymbol{\alpha}_i^{\mathrm{T}}\mathbf{u} = 0$, where $\boldsymbol{\alpha}_i$ is the unit direction vector for the design point of component i, intersects the limit-state surface $G_i(\mathbf{u}) = 0$ of the corresponding component in at most one point. When there is no intersection, we assume the point is at infinite distance on either side of the plane, depending on the sign of $G_i(\mathbf{u}) = 0$. Under this assumption, we can represent the limit state surface $G_i(\mathbf{u}) = 0$ as an explicit function of the points on the orthogonal plane $\boldsymbol{\alpha}_i^{\mathrm{T}}\mathbf{u} = 0$, i.e. $u'_n = h_i(u'_1, \cdots, u'_{n-1})$, where $\mathbf{u}' = (u'_1, \cdots, u'_n)$ is the orthonormal transformation of $\mathbf{u}$ defined in Section 5.4.1. For a linear system subjected to a Gaussian excitation, as discussed in Section 5.4.1, this assumption holds strictly. In that case, the limit-state surface $G_i(\mathbf{u}) = 0$ is a plane parallel to the orthogonal plane $\boldsymbol{\alpha}_i^{\mathrm{T}}\mathbf{u} = 0$ and, therefore, $G_i(\mathbf{u}) = 0$ can be written as $u'_n = \beta_i$, where β_i is the distance between the two planes. For nonlinear problems, there is no guarantee that the assumption holds. For practical purposes, however, it is sufficient if the assumption holds in the neighborhood of the design point $\mathbf{u}_i^*$.

The second assumption is that the FORM approximations $\Phi(-\beta_i)$, $i=1,\cdots,n$, for the time-point component probabilities are proportional to the corresponding exact probabilities p_i, $i=1,\cdots,n$. This assumption strictly holds for stationary random vibration problems, where the probabilistic definition of the response is invariant with respect to a shift in the time origin. For non-stationary processes, this assumption introduces an approximation in the proposed method. However, considering the case of stationary processes, this approximation is not expected to be critical, particularly if the first-excursion event is associated with a nearly stationary, strong-motion phase of the non-stationary excitation. This is the case, for example, for most far-field earthquake ground motions.

Based on the first assumption, we can represent the conditional density function of $\mathbf{u}$ given the failure of the i-th component, $p(\mathbf{u}|E_i)$, in a manner similar to (5.15). Specifically,

$$\begin{aligned} p(\mathbf{u}|E_i) &= p(\mathbf{u}'|E_i) \\ &= p(u_1',\ldots,u_{n-1}'|E_i)\,p(u_n'|u_1',\ldots,u_{n-1}',E_i) \end{aligned} \tag{5.18}$$

Using Bayes' rule, the first density function on the right side can be written as

$$p(u_1',\ldots,u_{n-1}'|E_i) = \varphi(u_1',\ldots,u_{n-1}')\frac{\Phi[-h_i(u_1',\cdots,u_{n-1}')]}{p_i} \tag{5.19}$$

where $h_i(u_1',\cdots,u_{n-1}')$ is the distance of the point $(u_1',\cdots,u_{n-1}',0)$ on the orthogonal plane from the limit-state surface $G_i(\mathbf{u})=0$, as shown in Figure 5.3. The second term on the right-hand side of (5.18) is the truncated normal density function

$$p(u_n'|u_1',\ldots,u_{n-1}',E_i) = \varphi[u_n'|u_n' \geq h_i(u_1',\ldots,u_{n-1}')] \tag{5.20}$$

Using (5.19) and(5.20), the final form of the conditional density function is

$$p(\mathbf{u}|E_i) = \varphi(u_1',\ldots,u_{n-1}')\,\varphi[u_n'|u_n' \geq h_i(u_1',\ldots,u_{n-1}')]\frac{\Phi[-h_i(u_1',\ldots,u_{n-1}')]}{p_i} \tag{5.21}$$

It is seen that the conditional density function for a nonlinear problem has almost the same form as the one for a linear problem in (5.15). Compared to the latter, the reliability index β_i of the component has been replaced by the function $h_i(u_1',\cdots,u_{n-1}')$ to

account for the nonlinearity of the limit state surface. The factor $\Phi[-h_i(u'_1,\cdots,u'_{n-1})]/p_i$ multiplied at the end of (5.21) corrects the normal density function $\varphi(u'_1,\cdots,u'_{n-1})$ to the true conditional density function $p(u'_1,\cdots,u'_{n-1}|E_i)$. The exact probability p_i remains unknown, but it will drop out, as shown below.

Since the exact component probabilities are unknown, instead of (5.13), we use the normalized weight factors based on the FORM approximations

$$w_i = \frac{\Phi(-\beta_i)}{\sum_{j=1}^{n}\Phi(-\beta_j)}, \; i = 1, \ldots, n \tag{5.22}$$

Now suppose that a time-point component is randomly selected according to the weights in (5.22), and let $\mathbf{u}_i^*$, $\boldsymbol{\alpha}_i$ and β_i respectively denote its design point, unit direction vector and reliability index. We must generate a random $\mathbf{u}$ according to (5.21) and compute $q(\mathbf{u})$ from (5.14). Equivalently, we can generate $\mathbf{u}$ according to

$$p(\mathbf{u}|E_i) = \varphi(u'_1,\ldots,u'_{n-1})\,\varphi\left[u'_n \middle| u'_n \geq h_i(u'_1,\ldots,u'_{n-1})\right] \tag{5.23}$$

and compute $q(\mathbf{u})$ according to

$$q(\mathbf{u}) = \frac{\Phi[-h_i(u'_1,\ldots,u'_{n-1})]}{\sum_{j=1}^{n} I\left[-g_j(\mathbf{u})\right]} \frac{\sum_{j=1}^{n} p_j}{p_i} \tag{5.24}$$

Note that the product of (5.14) and (5.21) is identical to the product of (5.23) and(5.24). Also note that (5.23) is a valid probability density function.

We now introduce an approximation based on our second assumption above. Namely, we replace the ratio of the exact component probabilities in (5.24) by their first-order approximations, i.e.,

$$q(\mathbf{u}) \cong \frac{\Phi[-h_i(u'_1,\ldots,u'_{n-1})]}{\sum_{j=1}^{n} I\left[-g_j(\mathbf{u})\right]} \frac{\sum_{j=1}^{n}\Phi(-\beta_j)}{\Phi(-\beta_i)} \tag{5.25}$$

As mentioned earlier, this reformulation is exact for stationary processes. In fact, in that case, the ratio of the sum of component probabilities to the probability of component i

(the last quotient in (5.24) and (5.25)) equals the number of components n for both the exact and first-order probabilities. For non-stationary processes, the above reformulation may introduce an approximation, which for reasons described earlier is not expected to be critical for most practical applications.

Based on the above, the procedure for simulating a sample $\mathbf{u}_k$, $k = 1, \cdots, N$, for a nonlinear problem involving a nonlinear dynamical system, non-Gaussian excitation, or uncertain system properties can be stated as follows:

a) Compute the design point $\mathbf{u}_i^*$, the unit direction vector $\boldsymbol{\alpha}_i$, the reliability index β_i, and the FORM probability approximation $\Phi(-\beta_i)$ for each time-point component i, $i = 1, \cdots, n$. Efficient methods for finding the design point for nonlinear systems are described in Chapter 3 and Koo and Der Kiureghian (2001).

b) Randomly select a time-point component according to the discrete probabilities w_i, $i = 1, \cdots, n$, in (5.22). Suppose that the i-th component is selected with the corresponding unit direction vector $\boldsymbol{\alpha}_i$ and reliability index β_i.

c) Simulate a standard normal vector $u = (u_1, \cdots, u_n)$.

d) Project $\mathbf{u}$ onto the orthogonal plane $\boldsymbol{\alpha}_i^{\mathrm{T}}\mathbf{u} = 0$. The result, $\mathbf{u} - \boldsymbol{\alpha}_i^{\mathrm{T}}\mathbf{u}\boldsymbol{\alpha}_i$, is identical to the point $(u_1', \cdots, u_{n-1}', 0)$ in the $\mathbf{u}'$ space.

e) Determine the distance $h_i(u_1', \cdots, u_{n-1}')$ from the point $(u_1', \cdots, u_{n-1}', 0)$ to the limit-state surface $G_i(\mathbf{u}) = 0$ in the direction parallel to $\boldsymbol{\alpha}_i$.

f) Simulate a uniform variable U on [0,1] and compute

$$d = \Phi^{-1}\left[U + (1-U)\Phi(h_i)\right] \tag{5.26}$$

g) Compute

$$\begin{aligned} \mathbf{u}_k &= (\mathbf{u} - \boldsymbol{\alpha}_i^{\mathrm{T}}\mathbf{u}\boldsymbol{\alpha}_i) + d\boldsymbol{\alpha}_i \\ &= \mathbf{u} + (d - \boldsymbol{\alpha}_i^{\mathrm{T}}\mathbf{u})\boldsymbol{\alpha}_i \end{aligned} \tag{5.27}$$

The above simulation procedure is similar to that for linear systems described in the previous section, with the additional tasks being: (a) the design point $\mathbf{u}_i^*$ for each time-point component must be obtained by solving an optimization problem (see Koo and Der

Kiureghian 2001), (b) the distance $h_i(u'_1,\cdots,u'_{n-1})$ to the component limit-state surface must be computed for each point simulated in the orthogonal plane. This is typically done by a simple iterative scheme, such as bi-section analysis, involving a few computations of the component limit-state function.

5.5 Applications

Example 5.1

The two-degree-of-freedom Bouc-Wen structure in Example 4.8 (Section 4.5.4) is reconsidered. The system parameters and the excitation pattern are as before except the hysteretic parameters α_i, $i=1,2$. We consider three sets of values of the hysteretic parameters, i.e. $\alpha_1=\alpha_2=1$ for a linear system, $\alpha_1=\alpha_2=0.5$ for a mildly nonlinear system, and $\alpha_1=\alpha_2=0.1$ for a strongly nonlinear system.

The limit state function is set as $g=d_{20}-d_2(t)$, where d_{20} is a threshold, for which the three values $3\sigma_{d2o}$, $6\sigma_{d2o}$ and $9\sigma_{d2o}$ are considered. The first-excursion probability during the interval 5.5 – 14 seconds is considered, since owing to the modulating function in (4.19), the probability of an excursion before 5.5 seconds or after 14 seconds is negligible compared to that during the specified interval. This duration is discretized into 35 time-point components with equal interval of 0.25 seconds. The correlation coefficients between the neighboring time-point events range from 0.95 to 0.98.

Simulation for the first-excursion probability is performed using methods: (1) importance sampling with the proposed conditional distributions ("Proposed I.S."), (2) importance sampling with the conventional method of using normal densities centered at component design points ("Conv. I.S."), and (3) the crude Monte Carlo simulation method ("M.C."). The simulation results are listed in Table 5.1. Each simulation is carried out until the coefficient of variation of the probability estimate reaches 0.05. Listed in Table 5.1 are the mean estimates of the first-excursion probability and the required number of simulations. For the proposed method, the number of evaluations of

the limit-state function (typically 3 – 5 per simulation for finding the distance $h_i(u'_1,\cdots,u'_{n-1})$ to the component limit-state surface) is given in parenthesis. In some cases, it was not possible to achieve the target coefficient of variation with the M.C. method with one million simulations. These cases are indicated as "NC" (not converged).

It is seen in Table 5.1 that in all cases the proposed importance sampling method achieves faster convergence in terms of the number of simulations, as compared to the conventional importance sampling method and the Monte Carlo simulation method. For nonlinear problems, however, the proposed sampling method requires several evaluations of the limit-state function in order to find the point on the component limit-state surface for each sample, while the other two methods require only one evaluation of the limit-state function per simulation. When the numbers of evaluations of the limit-state functions are compared, the proposed sampling method is still more efficient than the other two methods for linear and mildly nonlinear problems. For strongly nonlinear problems, however, the computational efficiency of the proposed sampling method falls behind the conventional importance sampling method.

Examination of the results in Table 5.1 indicates that the number of required simulations in the proposed method is more sensitive to the nonlinearity of the problem than to the threshold level. Therefore, the proposed importance sampling method is particularly effective for problems with small-excursion probability.

Example 5.2

In this example, we consider the case with uncertainties in the system parameters. The system and the excitation are the same as before, except that we now consider the hysteretic parameters α_1 and α_2 as random variables. It is assumed that α_1 and α_2 are statistically independent and identically distributed random variables having the beta distribution within the interval (0, 1) with means equal to 0.5 and coefficients of variation equal to 0.1. The limit state function is as before, and for the threshold the three values $3\,\sigma_{d2o}$, $4\ \sigma_{d2o}$ and $5\,\sigma_{d2o}$ are considered. The results of the analysis are compared with the results of the case with deterministic parameters $\alpha_1 = \alpha_2 = 0.5$ in Table 5.2.

It is observed in Table 5.2 that, regardless of the threshold, the first-excursion probability of the uncertain system is greater than that of the deterministic system. As in the case with deterministic system parameters, the proposed importance sampling method is more efficient than the other two methods in the number of simulations. When the numbers of evaluations of the limit-state functions are compared, the overall efficiency of the proposed method is more or less similar to that of the conventional importance sampling method.

Table 5.1. Comparison of the simulation results of the first-excursion probability.

System	Threshold		Simulation method (c.o.v. = 0.05)		
			Proposed I.S.	Conv. I.S.	M.C.
Linear ($\alpha_1 = \alpha_2 = 1$)	$3\sigma_{d2o}$	P_T	4.37E–2	4.78E–2	4.71E–2
		N	127	932	8,097
	$6\sigma_{d2o}$	P_T	5.66E–7	5.90E–7	0
		N	237	2,980	NC
Mildly nonlinear ($\alpha_1 = \alpha_2 = 0.5$)	$3\sigma_{d2o}$	P_T	8.82E–2	8.44–2	8.58E–2
		N	134 (745)	948	4,266
	$6\sigma_{d2o}$	P_T	3.95E–5	3.64E–5	3.50E–5
		N	228 (960)	2,442	NC
Highly nonlinear ($\alpha_1 = \alpha_2 = 0.1$)	$3\sigma_{d2o}$	P_T	2.24E–1	2.48E–1	2.31E–1
		N	604 (2,524)	626	1,335
	$6\sigma_{d2o}$	P_T	1.16E–2	1.13E–2	1.10E–2
		N	955 (4,215)	1,930	36,388
	$9\sigma_{d2o}$	P_T	1.75E–4	1.85E–4	1.77E–4
		N	1,134 (4,956)	3,597	NC

Numbers in parentheses indicate the number of evaluations of the limit-state function in the proposed important sampling method.

Table 5.2. Comparison of the simulation results of the first-excursion probability for deterministic and uncertain systems.

Threshold	System		Simulation method (c.o.v. = 0.05)		
			Proposed I.S.	Conv. I.S.	M.C.
$3\sigma_{d2o}$	Deter-ministic	P_T	8.82E–2	8.44–2	8.58E–2
		N	134 (745)	948	4,266
	Random	P_T	9.30E–2	9.67E–2	9.18E–2
		N	258 (1,050)	1,094	3,964
$4\sigma_{d2o}$	Deter-ministic	P_T	9.73 E–3	1.10E–2	1.04E–2
		N	179 (744)	1,302	38,089
	Random	P_T	1.14E–2	1.24E–2	1.07E–2
		N	269 (1,533)	1,581	30,796
$5\sigma_{d2o}$	Deter-ministic	P_T	8.82E–4	8.37E–4	8.30E–4
		N	510 (2,456)	1,782	482,109
	Random	P_T	9.73E–4	9.97E–4	9.72E–4
		N	579 (2,378)	2,676	411,172

Numbers in parentheses indicate the number of evaluations of the limit-state function in the proposed important sampling method.

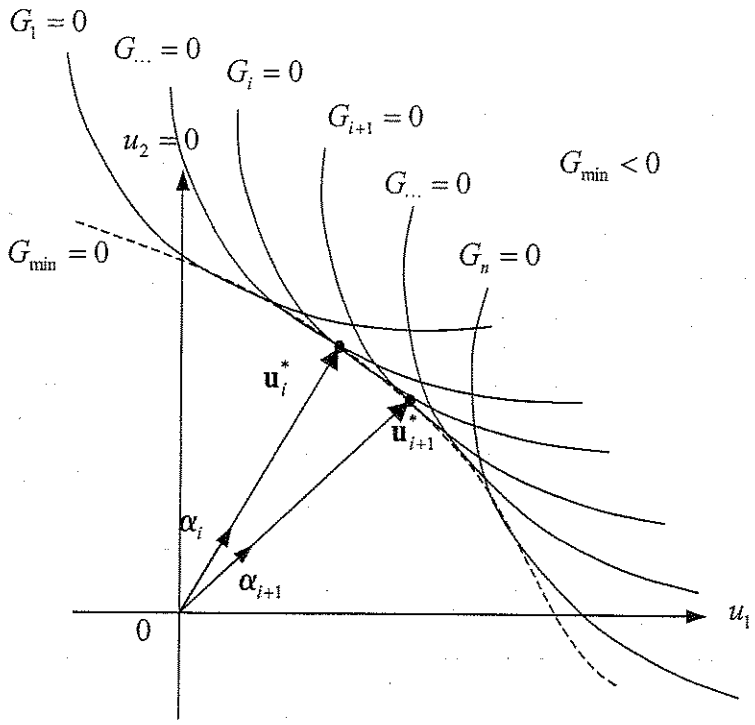

Figure 5.1. First-excursion probability as a series system.

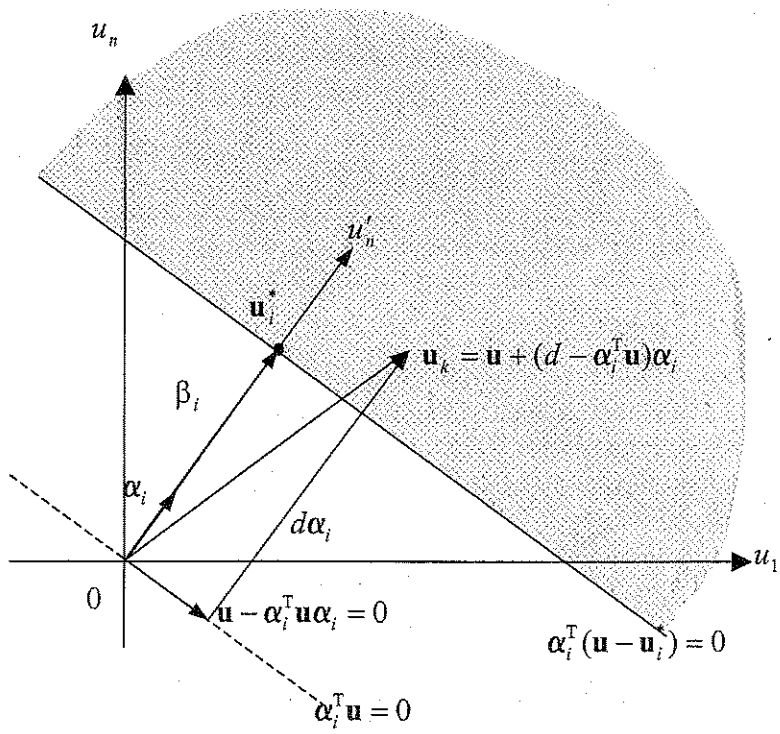

Figure 5.2. Simulation procedure for a linear system subjected to Gaussian excitation.

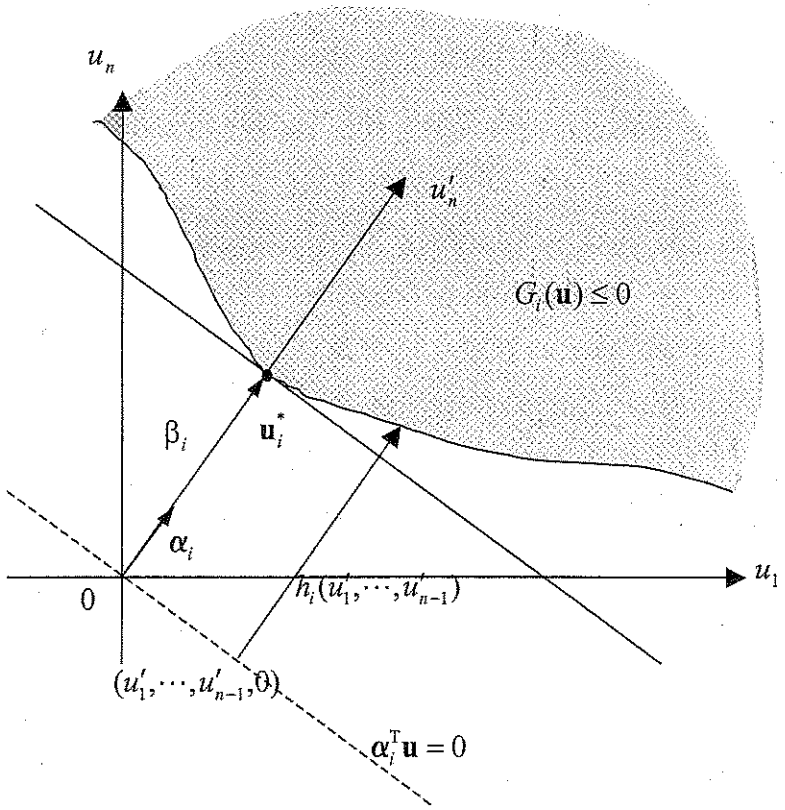

Figure 5.3. Simulation procedure for a nonlinear system.

6 Representation of Narrowband Process by Envelope and Phase Processes Using Nataf Distribution

6.1 Introduction

In solving random vibration problems, sometimes it is desired to represent a random process in a discrete form. For example, when using a simulation approach to solve a random vibration problem, the input process must be represented in terms of a set of random variables so it can be generated on a computer. Likewise, when a random-variable-based solution approach, such as FORM or SORM, is pursued, the input process must be represented in terms of random variables. There are a variety of ways to approximately represent a Gaussian random process as a linear function of a finite number of standard Gaussian random variables (see Der Kiureghian 2000). In general, the discrete representation is obtained by multiplying a vector of deterministic basis functions, itself discretized at a grid of time points, by a standard normal vector, where the basis functions depend on the correlation structure of the process. For any selection of discrete time points in the representation, the correlation matrix of the process must be positive definite in order to construct the basis functions.

In the case of a narrowband process, the correlation function tends to fluctuate nearly harmonically with an amplitude that decays slowly. As a result, in the discrete representation by the conventional methods, one often faces the difficulty that the correlation matrix of the process for the selected grid of time points is near singular. This situation is exasperated when the process has a high frequency content, in which case a large number of time points are necessary to properly represent the process. In this sense, representation of the narrowband process in a discrete form is a challenging task.

In this chapter, an alternative, approximate representation of a narrowband process is explored. The main idea is to discretize the envelope and phase processes, and then compute the corresponding realization of the process itself. This way, advantage is

taken of the slowly varying property of the envelope and phase processes, which enables us to take large time steps in the discretization. This approach not only is efficient in terms of the number of needed time points, but also avoids the near singularity problem associated with the correlation matrix of the process. The Nataf distribution model is employed to construct approximate non-Gaussian joint distributions of the envelope and phase vectors.

The findings of the study show that the method can efficiently generate a narrowband process with a relatively small size of the artificially generated random vector. Typically, the size of this vector can be 1/20 to 1/10 of that used in the conventional method. The Nataf distribution is found to be a convenient model to describe the joint distribution of the amplitude and phases processes at two selected points. However, the analysis also shows that this model of the joint distribution is not sufficiently accurate for reliability analysis, for which the description of the exact distribution in the tail region is essential. Therefore, the representation in terms of discretized envelope and phase processes may be considered useful for simulation purposes, as long as the interest is not in the tail region of the probability distributions. It is also determined that this discretization approach is not appropriate for FORM/SORM solution of random vibration problems.

6.2 Properties of a Narrowband Process

A process is narrowband when its power spectral density is zero, except for a narrow band of frequencies around a central (or average) frequency, ω_c. The sample function of a narrowband process shows a nearly harmonic behavior with slowly varying amplitude and phase. Based on this property, a narrowband random process $X(t)$ can be represented in the form (Rice 1944, 1945)

$$X(t) = A(t)\cos[\omega_c t + \Theta(t)] \tag{6.1}$$

where $A(t)$ is the envelope process and $\Theta(t)$ is the phase process.

Let $X(t)$ be a narrowband Gaussian process with zero mean. The envelope and phase processes can be defined as

$$A(t) = \sqrt{X(t)^2 + \hat{X}(t)^2} \tag{6.2}$$

$$\Theta(t) = \tan^{-1}\frac{\hat{X}(t)}{X(t)} - \omega_c t \tag{6.3}$$

where $\hat{X}(t)$ is a conjugate process of $X(t)$. Various definitions of the envelope result from alternative selections of $\hat{X}(t)$. The most popular definition of the envelope, known as the Cramer-Leadbetter envelope, is obtained when $\hat{X}(t)$ is defined as the Hilbert transform of $X(t)$ (Middleton 1960, Cramer and Leadbetter 1967). In that case, one can show that

$$\hat{X}(t) = A(t)\sin[\omega_c t + \Theta(t)] \tag{6.4}$$

Furthermore, $\hat{X}(t)$ is also zero-mean Gaussian and, for a given time t, $X(t)$ and $\hat{X}(t)$ are uncorrelated.

When a random process varies slowly, one can represent it in a discrete form with relatively large time steps. Since the envelope and phase processes of a narrowband process vary slowly, one can make a discrete representation of these processes with large time steps. Once the discrete representation of the envelope and phases processes is made, the corresponding realization of the narrowband process can be computed using (6.1) with an appropriate interpolation rule between the discrete time points.

For a discrete representation of a process, the joint distribution of the process at all time points is necessary. Unlike a Gaussian process, the higher-order joint distribution of a non-Gaussian process for multiple time points can be complicated and almost impossible to work with when the number of time points becomes large. The envelope and phase processes are no exception. For this reason, we make use of an approximate joint distribution for the discrete representation of these processes rather than the exact joint distribution. The Nataf distribution is particularly convenient for this purpose in the sense that it is closely related to the Gaussian distribution and that it can correctly match the correlation structure of the process. In the next section, we describe the joint distribution of the envelope and phase processes up to the second-order, which is sufficient for construction of the corresponding Nataf distributions.

6.3 Probability Distributions of Envelope and Phase Processes

The first-order joint probability density function of the Cramer-Leadbetter envelope and phase processes for a given time t is given by (Cramer and Leadbetter 1967)

$$f(a,\theta) = \frac{a}{2\pi\lambda_o}\exp\left[-\frac{1}{2}\frac{a^2}{\lambda_o}\right] \tag{6.5}$$

where $\lambda_o = \mathrm{E}[X^2(t)] = \sigma_X^2$ is the mean-square or variance of the original process $X(t)$ in (6.1). It is evident that, for a given time t, the envelope process $A(t)$ and the phase process $\Theta(t)$ are statistically independent. Furthermore, $A(t)$ has the Rayleigh distribution and $\Theta(t)$ has the uniform distribution.

In principle, the n-th order joint distribution of $A(t)$ and $\Theta(t)$ for any set of selected time points $t_1, \ldots, t_n$ can be derived by transformation of the random variables $X(t_i)$ and $\hat{X}(t_i)$, $i = 1, \ldots, n$, and the relations in (6.1) and (6.4). However, due to dependence of the random variables for different time steps and the non-Gaussianity of the envelope and phase processes, the joint density function quickly becomes complicated as the order n increases. However, the second-order distribution can be obtained relatively easily and solutions have been available since at least 1955 (see Price 1955, Davenport and Root 1958, Middleton 1960). Here, the solution for the second-order joint distribution and related properties are described.

Let $\mathbf{X} = [X(t_1), \hat{X}(t_1), X(t_2), \hat{X}(t_2)]^{\mathrm{T}} = [X_1, \hat{X}_1, X_2, \hat{X}_2]^{\mathrm{T}}$ denote the vector of random variables representing the stationary Gaussian narrowband process $X(t)$ and its conjugate $\hat{X}(t)$ at discrete time points t_1 and t_2. The joint distribution of $\mathbf{X}$ is given

$$f_{\mathbf{X}}(\mathbf{x}) = \frac{1}{(2\pi)^2\left|\det \boldsymbol{\Sigma}_{\mathbf{XX}}\right|}\exp\left[-\frac{1}{2}\mathbf{x}^{\mathrm{T}}\boldsymbol{\Sigma}_{\mathbf{xx}}^{-1}\mathbf{x}\right] \tag{6.6}$$

where

$$\boldsymbol{\Sigma}_{\mathbf{XX}} = \begin{bmatrix} \lambda_o & 0 & R(\tau) & \hat{R}(\tau) \\ 0 & \lambda_o & -\hat{R}(\tau) & R(\tau) \\ R(\tau) & -\hat{R}(\tau) & \lambda_o & 0 \\ \hat{R}(\tau) & R(\tau) & 0 & \lambda_o \end{bmatrix}; \tag{6.7}$$

and

$$\det \boldsymbol{\Sigma}_{XX} = \left[\lambda_o^2 - R(\tau)^2 - \hat{R}(\tau)^2\right]^2; \tag{6.8}$$

where $\lambda_o = \sigma_X^2$; $\tau = t_2 - t_1$, $R(\tau) = R_{XX}(\tau) = \mathrm{E}[X(t_1)X(t_2)]$; and $\hat{R}(\tau) = R_{X\hat{X}}(\tau)$ $= \mathrm{E}[X(t_1)\hat{X}(t_2)]$.

The corresponding joint distribution of the envelope and phase variables, $A(t_1)$, $A(t_2)$, $\Theta(t_1)$ and $\Theta(t_2)$, denoted $f(a_1, a_2, \theta_1, \theta_2)$, can be obtained by transformation of the random variables $\mathbf{X}$. Specifically,

$$f(a_1, \theta_1, a_2, \theta_2) = f(x_1, \hat{x}_1, x_2, \hat{x}_2)\left|\det \mathbf{J}_{(x_1,\hat{x}_1,x_2,\hat{x}_2),(a_1,a_2,\theta_1,\theta_2)}\right|$$

$$= \frac{a_1 a_2}{(2\pi)^2\sqrt{\left|\det \boldsymbol{\Sigma}_{XX}\right|}} \exp\left\{-\frac{\lambda_o}{2\sqrt{\left|\det \boldsymbol{\Sigma}_{XX}\right|}}\left[(a_1^2 + a_2^2) - 2a_1 a_2 \gamma\right]\right\} \tag{6.9}$$

$$0 \le a_1, a_2 < \infty \text{ and } 0 \le \theta_1, \theta_2 < 2\pi$$

where $\mathbf{J}_{(x_1,\hat{x}_1,x_2,\hat{x}_2),(a_1,a_2,\theta_1,\theta_2)}$ is the Jacobian of the transformation, whose elements are the partial derivatives of x_1, $\hat{x}_1$, x_2 and $\hat{x}_2$ with respect to a_1, θ_1, a_2 and θ_2, as derived from (6.1) and (6.4), and

$$\gamma = \frac{\kappa(\tau)}{\lambda_o}\cos(\omega_c \tau + \theta_2 - \theta_1 - \alpha) \tag{6.10}$$

where

$$\kappa(\tau) = \sqrt{R(\tau)^2 + \hat{R}(\tau)^2} \tag{6.11}$$

and

$$\alpha = \tan^{-1}\frac{\hat{R}(\tau)}{R(\tau)} \tag{6.12}$$

It is seen that the envelope and phase processes are not statistically independent, i.e., in general $f(a_1, a_2, \theta_1, \theta_2) \neq f(a_1, a_2) f(\theta_1, \theta_2)$. However, as $\tau \to \infty$, $\det \boldsymbol{\Sigma}_{XX} \to \lambda_o^4$ and $\kappa(\tau) \to 0$, and accordingly $\gamma \to 0$. Therefore, if the time lag τ is sufficiently large, the joint probability density function distribution becomes separable, i.e. $f(a_1, a_2, \theta_1, \theta_2) \to$ $f(a_1) f(a_2) f(\theta_1) f(\theta_2)$, and the envelope and phase random variables become

statistically independent, as expected. Obviously, the dependence of the random variables is a function of the time lag.

By integrating over one of the phase random variables, say θ_1, we obtain

$$f(a_1,a_2,\theta_2)=\frac{a_1a_2}{2\pi\sqrt{|\det\boldsymbol{\Sigma}_{XX}|}}I_o\left(\frac{a_1a_2\kappa(\tau)}{\sqrt{|\det\boldsymbol{\Sigma}_{XX}|}}\right)\exp\left[-\frac{1}{2\sqrt{|\det\boldsymbol{\Sigma}_{XX}|}}\lambda_o(a_1^2+a_2^2)\right] \tag{6.13}$$

where $I_o(\cdot)$ is the modified Bessel function of the first kind of order zero. We can see that the joint density function $f(a_1,a_2,\theta_2)$ can be written as $f(a_1,a_2)f(\theta_2)$. This implies $f(a_1,\theta_2) = f(a_1)f(\theta_2)$ and $f(a_2,\theta_1) = f(a_2)f(\theta_1)$. Thus, although the envelope process is not independent of the phase process, the envelope and phase at two distinct time points (including the same time point) are statistically independent. Further integration of (6.13) over the domain of the remaining phase angle gives the second-order joint probability density function of the envelope process as

$$f(a_1,a_2)=\frac{a_1a_2}{\sqrt{|\det\boldsymbol{\Sigma}_{XX}|}}I_o\left(\frac{a_1a_2\kappa(\tau)}{\sqrt{|\det\boldsymbol{\Sigma}_{XX}|}}\right)\exp\left[-\frac{1}{2\sqrt{|\det\boldsymbol{\Sigma}_{XX}|}}\lambda_o(a_1^2+a_2^2)\right] \tag{6.14}$$

It is seen that the envelope variables at two distinct time points are statistically dependent. However, as shown above, we can see that $\lim_{\tau\to\infty} f(a_1,a_2)=f(a_1)f(a_2)$.

Integration of $f(a_1,a_2,\theta_1,\theta_2)$ over the domains of a_1 and a_2 yields

$$f(\theta_1,\theta_2)=\frac{\sqrt{|\det\boldsymbol{\Sigma}_{XX}|}}{(2\pi)^2\lambda_o^2}\left[\frac{1}{1-\gamma^2}\left\{1+\frac{\gamma(\pi-\cos^{-1}\gamma)}{\sqrt{1-\gamma^2}}\right\}\right];\ 0\le\theta_1,\theta_2<2\pi \tag{6.15}$$

As in the case of the envelope process, we can see that the dependence between the phase angles at two time points decreases as the time lag increases.

Considering the complicated dependence structure between the envelope and phase processes and also the required high order of the joint probability density function needed for the discrete representation of these processes, it appears not to be practical to pursue the exact high-order distribution. Instead, as mentioned in the introduction, we explore the possibility of using the Nataf distribution model instead. For this purpose, the correlation functions of the envelope and phase processes are needed.

The correlation function of the envelope process, denoted $R_{AA}(\tau)$, has been derived by Uhlenbeck (1943):

$$R_{AA}(\tau) = \frac{\pi\lambda_o}{2} F\left(-\frac{1}{2}; -\frac{1}{2}; 1; \rho(\tau)^2\right) \tag{6.16}$$

In the above, $F(a;b;c;x)$ is the hyper-geometric function and

$$\rho(\tau) = \frac{\kappa(\tau)}{\lambda_o} \tag{6.17}$$

The correlation function of the phase process, denoted $R_{\Theta\Theta}(\tau)$, is given by Middleton (1960),

$$R_{\Theta\Theta}(\tau) = \pi^2\{1 + 2q - 4q^2 + \frac{1}{12}\Omega[\rho(\tau)]\} \tag{6.18}$$

where $q = (2\pi)^{-1}\sin^{-1}\rho(\tau)$, $\Omega(\rho(\tau)) = \frac{6}{\pi^2}\sum_{k=1}^{\infty}\frac{\rho(\tau)^{2k}}{k^2}$ and $\rho(\tau)$ is as in (6.17).

Using the above formulae, we can compare the correlation function of the original process with those of the envelope and phase processes. Figure 6.1 to 6.6 show the correlation coefficient functions and the corresponding power spectral densities for various selections of the correlation function $R_{XX}(\tau)$ or power spectral density $S_{XX}(\omega)$ of the process $X(t)$. For convenience, the spectral densities have been normalized such that the processes have unit variances. The processes in Figures 6.1, 6.2 and 6.4 are not narrowband processes, as can be seen by examining their spectral densities. For these processes, the rate of variation of the correlation functions of $X(t)$, $A(t)$ and $\Theta(t)$ are not significantly different. The processes in Figures 6.3, 6.5 and 6.6 are narrowband processes. For these processes, the spectral density function of $X(t)$ is concentrated in a narrow band around a central frequency. In contrast to the former, we see that the envelope and phase processes of the narrowband processes have correlation functions that exhibit much slower rate of change as compared to that of the parent process $X(t)$. This implies that much larger time increments can be used in discretizing the envelope and phase processes than discretizing the corresponding narrowband process.

6.4 Nataf Distribution of Envelope and Phase Processes

Consider a set of random variables $w=(w_1,\cdots,w_n)$ with marginal distributions $F(w_i)$, $i=1,\cdots,n$, and correlation coefficients $\rho_{ij}=\rho_{w_iw_j}$ between pairs of the random variables w_i and w_j, $i,j=1,\cdots,n$. The Nataf joint distribution of the random variables **w** is defined as

$$f(\mathbf{w})=f(w_1)\cdots f(w_n)\frac{\varphi_n(\mathbf{z},\mathbf{R})}{\varphi(z_1)\cdots\varphi(z_n)} \tag{6.19}$$

where $z=(z_1,\cdots,z_n)$ are jointly normal random variables with zero means, unit variances and correlation matrix $\mathbf{R}=[\rho_{o,ij}]$, $\varphi_n(\cdot,\cdot)$ denotes their n-variate normal density function, $\varphi(\cdot)$ denotes the uni-variate standard normal density function and $f(w_i)=dF(w_i)/dw_i$ are the probability density functions of w_i, $i=1,\ldots,n$. The random variables z_i are related to w_i by

$$z_i=\Phi^{-1}[F(w_i)] \quad i=1,\ldots,n \tag{6.20}$$

and the correlation coefficients $\rho_{o,ij}$ are related to ρ_{ij} by

$$\rho_{ij}=\int_{-\infty}^{\infty}\int_{-\infty}^{\infty}\left(\frac{w_i-\mu_i}{\sigma_i}\right)\left(\frac{w_j-\mu_j}{\sigma_j}\right)\varphi_2(z_i,z_j,\rho_{o,ij})dz_i dz_j \tag{6.21}$$

where μ_i and σ_i are the mean and standard deviation of w_i, respectively.

In the Nataf distribution, the dependence between the random variables **w** is described by the correlation structure of variables **z**. The difference between the two sets of correlation coefficients is usually small, except for strongly non-normal distributions. Closed form expressions of $\rho_{o,ij}$ in terms of ρ_{ij} have been given by Liu and Der Kiureghian (1986). For example, If w_i and w_j are Rayleigh random variables with the correlation coefficient ρ_{ij}, the correlation coefficient of the corresponding normal random variables z_i and z_j obtained from (6.20) is $\rho_{o,ij}=1.028\,\rho_{ij}-0.029\,\rho_{ij}^2$. For

uniform distribution w_i and w_j, the correlation coefficient of the jointly normal random variables z_i and z_j is given by $\rho_{o,ij} = 1.047\,\rho_{ij} - 0.047\,\rho_{ij}^3$.

Comparison of conditional probability density functions provides an indication of how well the Nataf distribution fits the exact joint distribution of two non-Gaussian random variables. Figure 6.7 compares the conditional density functions $f(a_2 \mid a_1)$ of the amplitudes $A(t_1)$ and $A(t_2)$ for $a_1 = \mathrm{E}[A(t_1)]$ at selected time lags, as obtained by the exact joint distribution in (6.14) and its Nataf approximation. Figure 6.8 compares the conditional density functions $f(\theta_2 \mid \theta_1)$ of the phases $\Theta(t_1)$ and $\Theta(t_2)$ for $\theta_1 = \mathrm{E}[\Theta(t_1)]$ at selected time lags, as obtained by the exact joint distribution in (6.15) and the Nataf approximation. It is seen that Nataf distribution fits quite well to the joint distribution of the amplitudes, but rather poorly to the joint distribution of the phases.

Figure 6.9 and 6.10 show the exact joint probability density function and its Nataf approximation of the amplitudes and phases for the time lag $\tau/T = 1$. For amplitudes, we can see that the overall shape of the Nataf distribution is similar to the exact joint distribution as in the conditional density function shown in Figure 6.7. For phases, in the exact density function, the mode is formed along the line $\theta_1 = \theta_2$ and $\theta_1 = \theta_2 \pm 2\pi$, and the density function rapidly dies out as the difference $|\theta_1 - \theta_2|$ increases. In the Nataf approximation, on the other hand, there are two sharp modes at $\theta_1 = \theta_2 = 0$ and $\theta_1 = \theta_2 = 2\pi$, and the line between the two modes forms a flat, curved ridge. The overall shape of the density function looks flatter than the exact one. The reason why Nataf distribution does not fit well for the phase variables is attributed to the strong non-Gaussian property of the uniform distribution.

6.5 Applications

So far, we have described the relation of the narrowband process with the envelope and phase processes, the second-order distributions of the amplitude and phase processes, and the Nataf distribution as a means for approximating the higher-order joint distributions of the envelope and phase processes. In this section, two possible applications are

considered, i.e., simulation of a narrowband random processes, and random vibration analysis by FORM for a narrowband input excitation.

6.5.1 Simulation of Envelope and Phase Processes

We wish to simulate a narrowband process by first simulating its envelope and phase processes, and then computing the corresponding realization of the process from (6.1). For simulation, a continuous random process must be represented in a discrete form, i.e., in terms of a vector of random variables. We need to use the joint distribution of the random vector. When the components of the random vector are non-Gaussian and dependent, as is the case with the envelope and phases processes, the simulation becomes exceedingly difficult. The inverse transform method, also known as the Rosenblatt transformation, is known to be a general method for simulation of a dependent random vector (Hohenbichler and Rackwitz 1981, Rubinstein 1981). Let $\mathbf{w} = (w_1, \cdots, w_n)$ denote the vector of non-Gaussian dependent random variables representing the process of interest and let $F(w_1, \ldots, w_n)$ denote their joint cumulative distribution function. The inverse transformation method uses the following formulae for the simulation of $\mathbf{w}$:

$$\begin{aligned} F_1(w_1) &= u_1 \\ F_2(w_2|w_1) &= u_2 \\ &\cdots \\ F_n(w_n|w_1, \cdots, w_{n-1}) &= u_n \end{aligned} \tag{6.22}$$

where $\mathbf{u} = (u_1, \cdots, u_n)$ are independent, uniformly distributed random variables in [0, 1] and $F_i(w_i|w_1, \cdots, w_{i-1})$ denotes the conditional distribution of w_i for given values of $w_1, \ldots, w_{i-1}$. For a random sample of $\mathbf{u}$, one can find the corresponding $\mathbf{w}$ by solving the set of equations (6.22). However, as the number of random variables increases, the conditional distribution, if it is known, becomes more complicated and it is harder to solve the set of equations (6.22). Therefore, this method is not practical for simulation of non-Gaussian random processes.

Simulation of a random process having the Nataf distribution is much simpler than that described above. In fact, the simulation of a non-Gaussian dependent vector

described by the Nataf distribution is as simple as that of a Gaussian vector. The only additional step is the marginal transformation (6.20), which must be computed for each simulated value. The steps of the simulation of a non-Gaussian, Nataf random process $w(t)$ with marginal cumulative distribution function $F(w)$ can be summarized as follows:

- Select a set of time points $t_1, \ldots, t_n$ and compute the corresponding correlation coefficients ρ_{ij}, $i, j = 1, \ldots, n$, of the process $w(t)$. Define $w_i = w(t_i)$.
- Using the formulae relating ρ_{ij} and $\rho_{o,ij}$ for the given marginal distribution, construct the corresponding correlation coefficient matrix $\mathbf{R} = [\rho_{o,ij}]$ and find $\mathbf{L}$ such that $\mathbf{R} = \mathbf{L}\mathbf{L}^T$ by Cholesky Decomposition. Note that the time points should be selected sufficiently apart so that $\mathbf{R}$ is not nearly singular.
- Simulate a set of standard normal variables $\mathbf{u} = (u_1, \cdots, u_n)$.
- Compute $\mathbf{z} \leftarrow \mathbf{L}\mathbf{u}$
- Compute $w_i = F^{-1}[\Phi(z_i)]$.
- Use an appropriate interpolation function to describe the values of the process between the time points values $w(t_i)$ and $w(t_{i+1})$.

The above is performed for the envelope and phase processes, $A(t)$ and $\Theta(t)$, respectively, and the resulting realization is used in (6.1) to compute the corresponding realization of the parent process $X(t)$.

Figure 6.11 shows one sample of a narrowband process simulated by the above procedure. The correlation function of the narrowband process is $R_{XX}(\tau) = \cos\omega_c\tau \dfrac{\sin b\tau/2}{b\tau/2}$ with $\omega_c = 2\pi$ rad/sec and b = 1 sec^{-1}. The time points have been selected at intervals of Δt = 2 sec for the envelope process and Δt = 4 sec for the phase process. Note that these intervals are even longer than the predominant period of the process, which is 1 sec. The dotted line in Figure 6.11 is the envelope process and the dashed line is the phase process. The corresponding narrowband process, shown as a solid line in Figure 6.11, is generated using (6.1). This realization of the process seems to be reasonable and consistent with what one expects of a narrowband process. However,

considering the approximation introduced by using the Nataf distribution, caution should be exercised in using this simulation method for the study of problems that deal with the tails of the distributions, e.g., the first-excursion probability above high thresholds.

6.5.2 Application to FORM

Consider a linear vibrating system subjected to a Gaussian excitation $f(t)$

$$\ddot{x}(t) + 2\zeta\omega\dot{x}(t) + \omega^2 x(t) = f(t) \tag{6.23}$$

where $f(t)$ is a narrowband Gaussian excitation with variance $\sigma^2 = 1$ and the correlation function $R(\tau) = \cos\omega_c\tau \dfrac{\sin b\tau/2}{b\tau/2}$ with $\omega_c = 2\pi$ rad/sec and $b = 1$ sec^{-1}. The system parameters are set as $\omega = 4\pi$ rad/sec and $\zeta = 0.05$. With the Gaussian excitation, the response of the linear system is also a Gaussian process, whose variance is estimated as $\sigma_x^2 \approx (0.00844)^2$ at the stationary state. We wish to compute the probability of the response exceeding a threshold x_0 at a given time.

We wish to solve the problem using the envelope and phase processes. We represent the narrowband excitation $f(t)$ as

$$f(t) = A(t)\cos[\omega_c t + \Theta(t)] \tag{6.24}$$

where $A(t)$ is the envelope process and $\Theta(t)$ is the phase process, as defined in Section 6.2. Recall that for a narrow-band process the correlation matrix obtained from a dense grid of time points is near singular. To avoid this problem, we discretize the envelope and phase processes instead of the process $f(t)$ itself.

Let $\mathbf{A} = [A_1, \cdots, A_n]^{\mathrm{T}}$ and $\boldsymbol{\Theta} = [\Theta_1, \cdots, \Theta_n]^{\mathrm{T}}$ denote vectors of random variables with elements $A_i = A(t_i)$ and $\Theta_i = \Theta(t_i)$, respectively, for a grid of time points t_i, $i = 1, \ldots, n$. We use a simple linear interpolation function to describe the processes $A(t)$ and $\Theta(t)$ between the time points. The continuous functions are then used in (6.24) to compute the corresponding description of the narrowband excitation. The response of the linear oscillator is thus completely defined by the set of random variables $\mathbf{A}$ and $\boldsymbol{\Theta}$. The

problem is now formulated as a FORM reliability problem, which requires the solution of the constrained optimization problem

$$\min \left\{ \|\mathbf{u}\| : G(\mathbf{u},t) = x_0 - x(\mathbf{u},t) \le 0 \right\} \tag{6.25}$$

where $\mathbf{u}$ is the standard normal vector obtained by transforming the variables $\mathbf{A}$ and Θ having the Nataf distribution.

The above reliability problem is nonlinear due to the nonlinear relation between the non-Gaussian variables $\mathbf{A}$ and Θ on one hand and the standard normal variables $\mathbf{u}$ on the other. The FORM solution can be obtained by the iterative method introduced in Section 2.2.2. For the FORM solution, we have set the target response time as $t_n = 6$ sec and have taken the time intervals of $\Delta t = 0.5$ sec for the envelope and phase processes. With a large time interval as taken above, we need only 26 random variables, i.e. 13 variables for the envelope process and 13 variables for the phase process, to represent the whole narrowband process. The time step for the corresponding narrowband process has been taken as one twentieth of Δt. The results of FORM analysis are listed in Table 6.1. We can see that the values of the FORM solutions are not satisfactory.

To investigate the reason for the poor result by FORM, we examine the shape of the limit-state function around the origin of the standard normal space. At the origin, we have a zero vector. Then, the normal counterparts z_i, $i = 1, \cdots, 2n$, are all zeros, and the corresponding envelope and phase vectors have the median values, say, $\mathbf{a} = [a_{0.5}, \cdots, a_{0.5}]^{\mathrm{T}}$ and $\boldsymbol{\theta} = [\theta_{0.5}, \cdots, \theta_{0.5}]^{\mathrm{T}}$. Under this condition, the system undergoes harmonic vibration with an amplitude approximately equal to $1.17\sigma_x$, as shown in Figure 6.12. By putting $x_0 = 1.17\sigma_x$ in the limit state function (6.25) and setting the target time t_n as the time of the system reaching the amplitude, we obtain $\|\mathbf{u}\| = 0$, i.e., $\beta = 0$ and $P_{f1} = 0.5$. Comparing with the exact solution $\beta = 1.17$ ($P_f = 0.12$), we can see that there is a large difference. One can understand the reason of this by examining the shape of the limit state surface, which is shown in Figure 6.13 along two axes. It is evident that the nonlinearity of the limit-state surface comes from the nonlinear relation of the envelope and phase variables with the standard normal variable.

Monte Carlo simulation was performed using the Nataf distribution for the envelope and phases processes. If the simulation shows results similar to the exact solution, we can conclude that the approximation by Nataf distribution works well and the error is due to the FORM approximation. As shown in Table 6.2, the results of the simulation are in close agreement with the exact solutions in Table 6.1 for low thresholds, but the agreement deteriorates at the high threshold. This suggests that the Nataf distribution performs well in the high probability density region and rather poorly in the tail region. Considering that the Nataf distribution fits the joint distribution up to the second-order moments, the poor performance in the tail region is not surprising. It is also clear that the large errors found in the comparison in Table 6.1 at low thresholds are mostly due to the FORM approximation, and less due to the Nataf approximation of the joint distribution of the envelope and the phase processes.

In summary, two major factors are contributed to the poor result of the FORM approximation in this problem. One is the nonlinear relation of the envelope and phase random variables with the standard normal random variables. This causes a strong nonlinearity of the limit-state surface in the standard normal space. The other is the approximate construction of the joint distribution by the Nataf approximation. This causes problems in the analysis for the tail region.

We conclude that this approach may not be appropriate for the FORM analysis of random vibrations due to the strong nonlinearity of the limit state surface. Considering that very few random variables are used to represent the continuous random process, however, this approach can be efficiently used for simulation of random vibration problems concerned with small thresholds having high probability density.

Table 6.1. FORM solution of random vibration problem by Nataf approximation of envelope and phase processes.

Threshold	Computed Reliability Index β	Exact Reliability Index β
$1\sigma_x$	–0.21	1.0
$2\sigma_x$	1.16	2.0
$3\sigma_x$	2.36	3.0

Table 6.2. Monte Carlo simulation of the random vibration problem using Nataf approximation of envelope and phase processes.

Threshold	Generalized Reliability Index β_G	No. of Simulations (c.o.v. = 0.1)
$1\sigma_x$	1.01 (p_f =1.56E–1)	544
$2\sigma_x$	1.91 (p_f =2.78E–2)	3,520
$3\sigma_x$	2.72(p_f =3.25E–3)	30,759

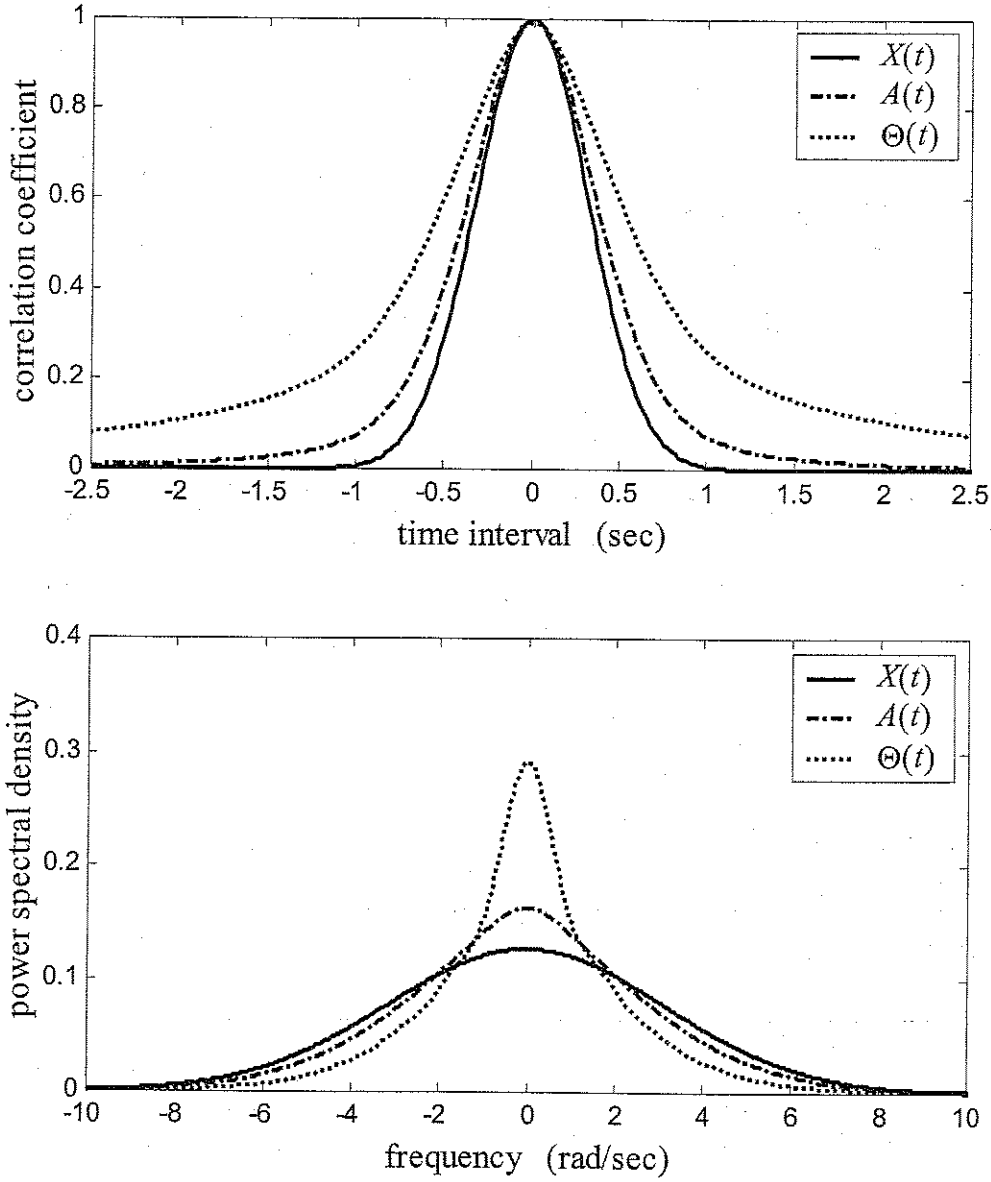

Figure 6.1. Comparison of correlation functions and spectral densities of the process $X(t)$, the envelope process $A(t)$, and the phase process $\Theta(t)$ for $R_{XX}(\tau) = \exp(-5\tau^2)$.

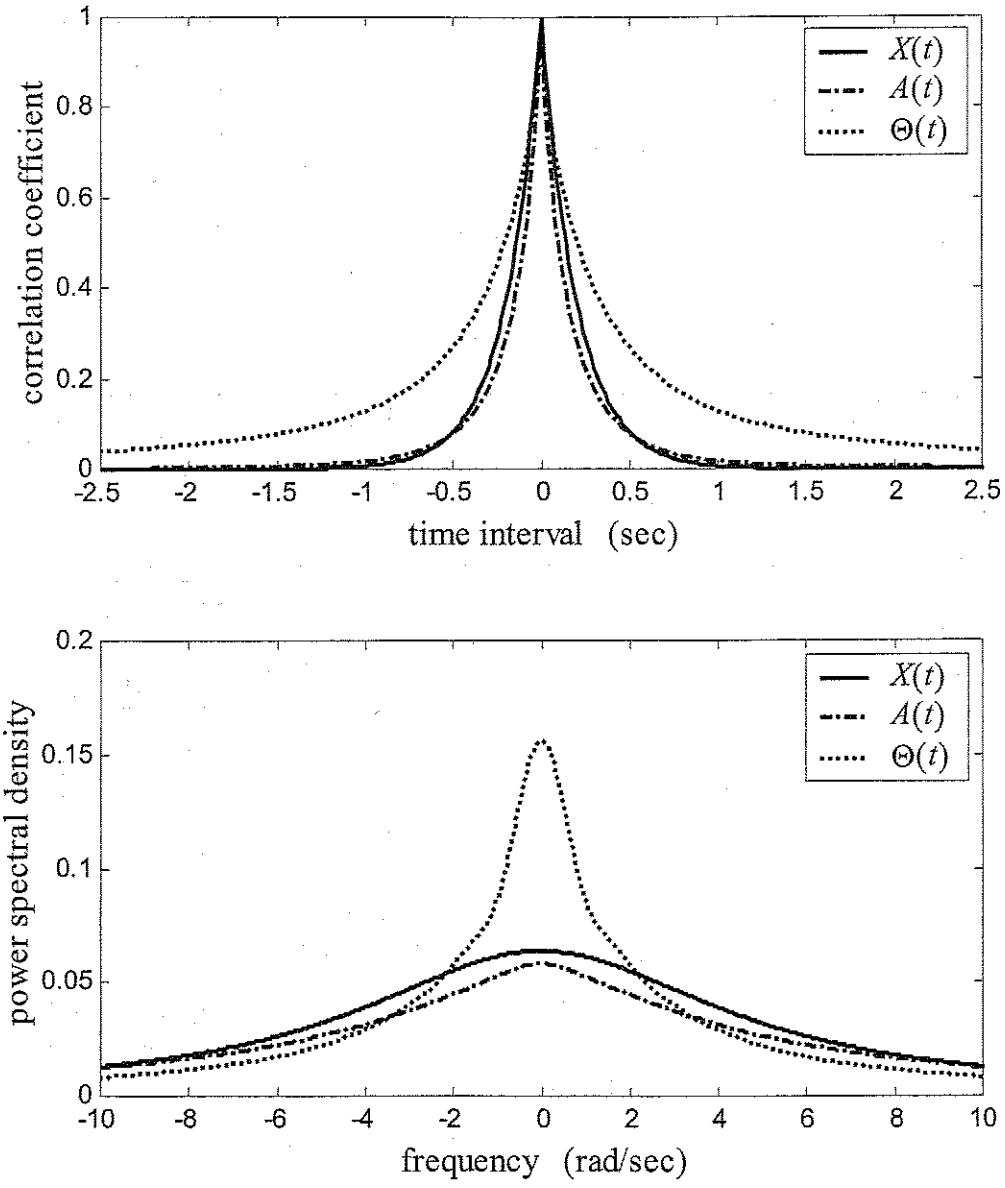

Figure 6.2. Comparison of correlation functions and spectral densities of the process $X(t)$, the envelope process $A(t)$, and the phase process $\Theta(t)$ for $R_{XX}(\tau) = \exp(-|\tau|)$.

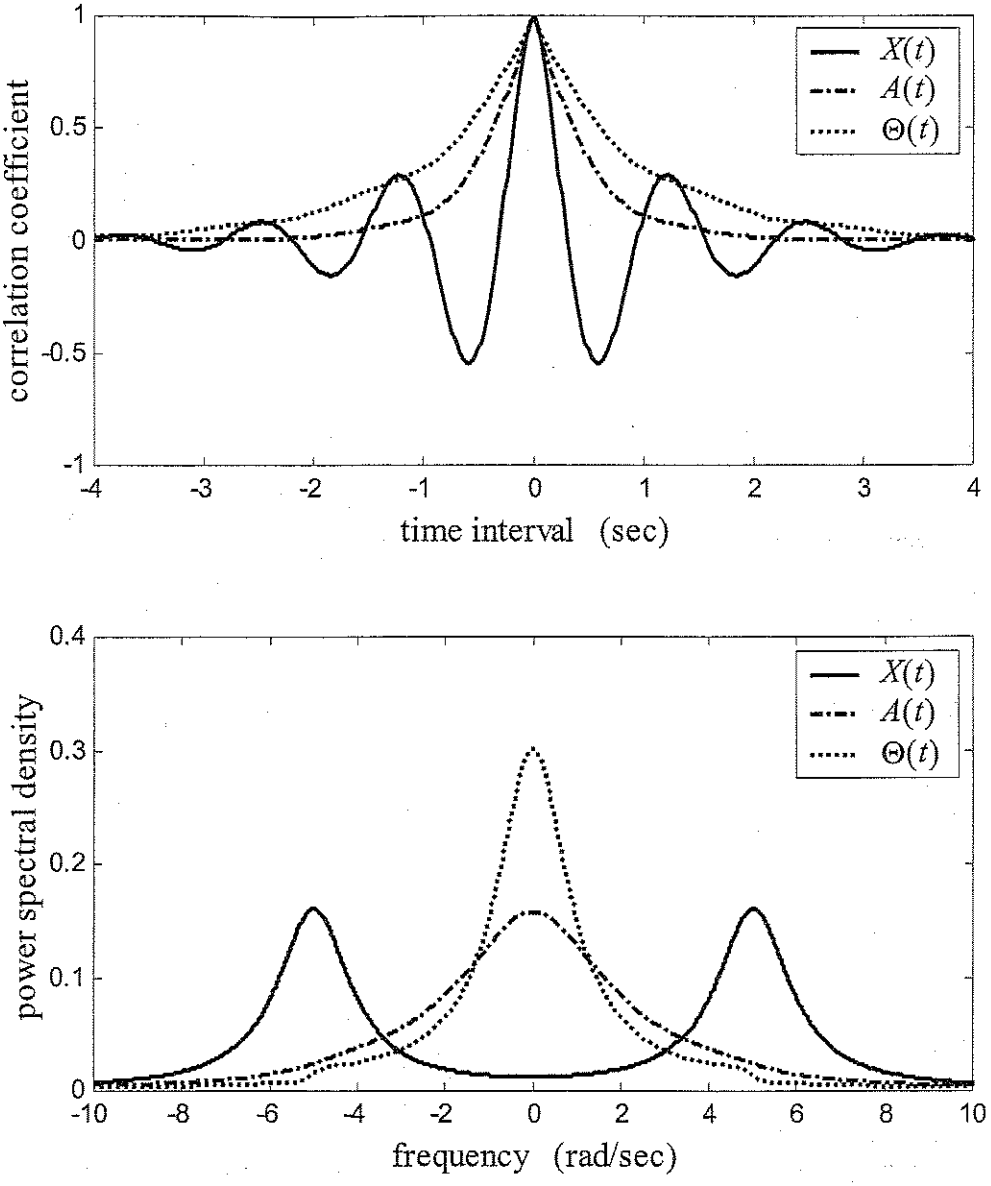

Figure 6.3. Comparison of correlation functions and spectral densities of the process $X(t)$, the envelope process $A(t)$, and the phase process $\Theta(t)$ for $R_{XX}(\tau) = \cos(5\tau)\exp(-|\tau|)$.

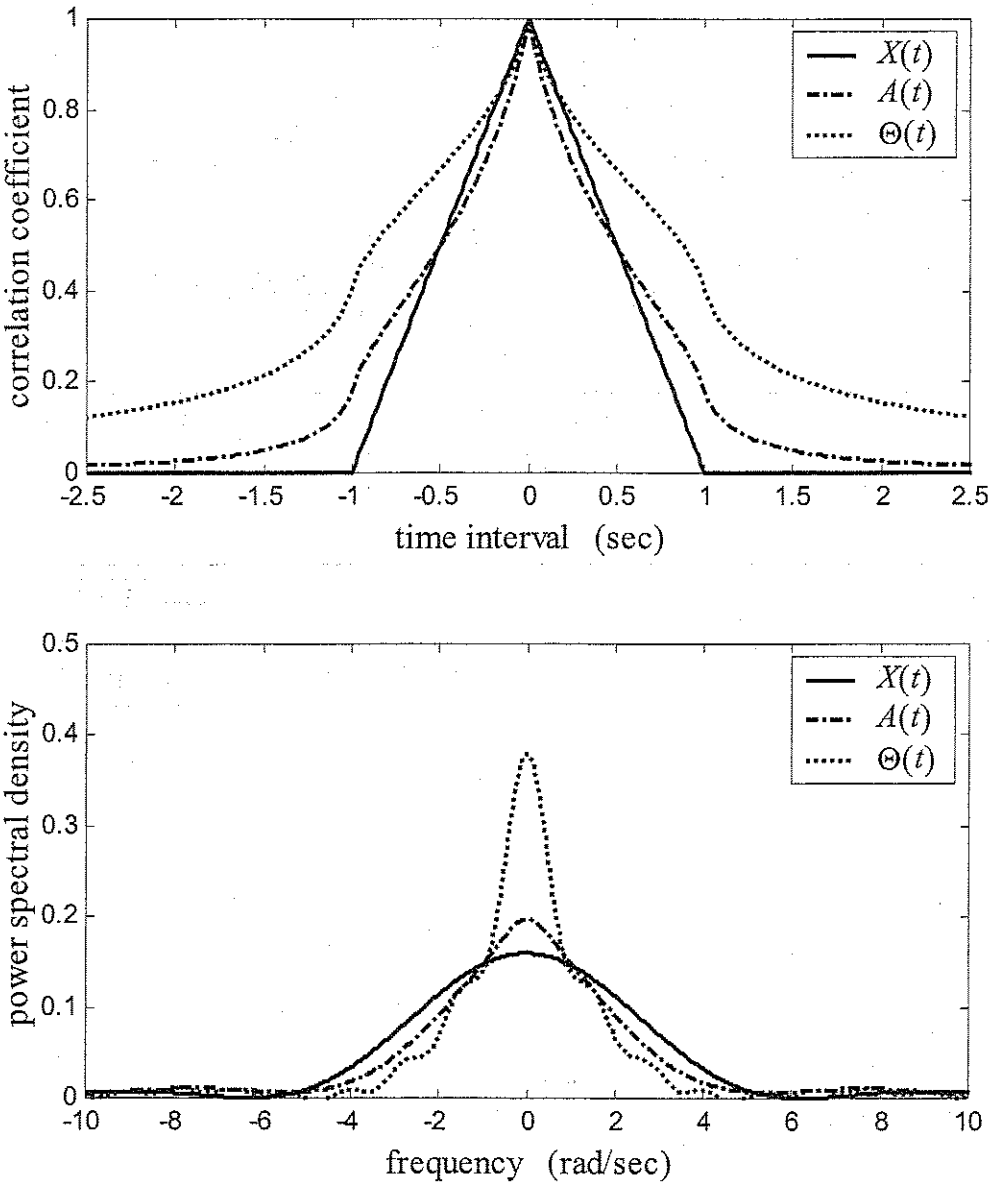

Figure 6.4. Comparison of correlation functions and spectral densities of the process $X(t)$, the envelope process $A(t)$, and the phase process $\Theta(t)$ for $R_{XX}(\tau) = 1 - |\tau|$.

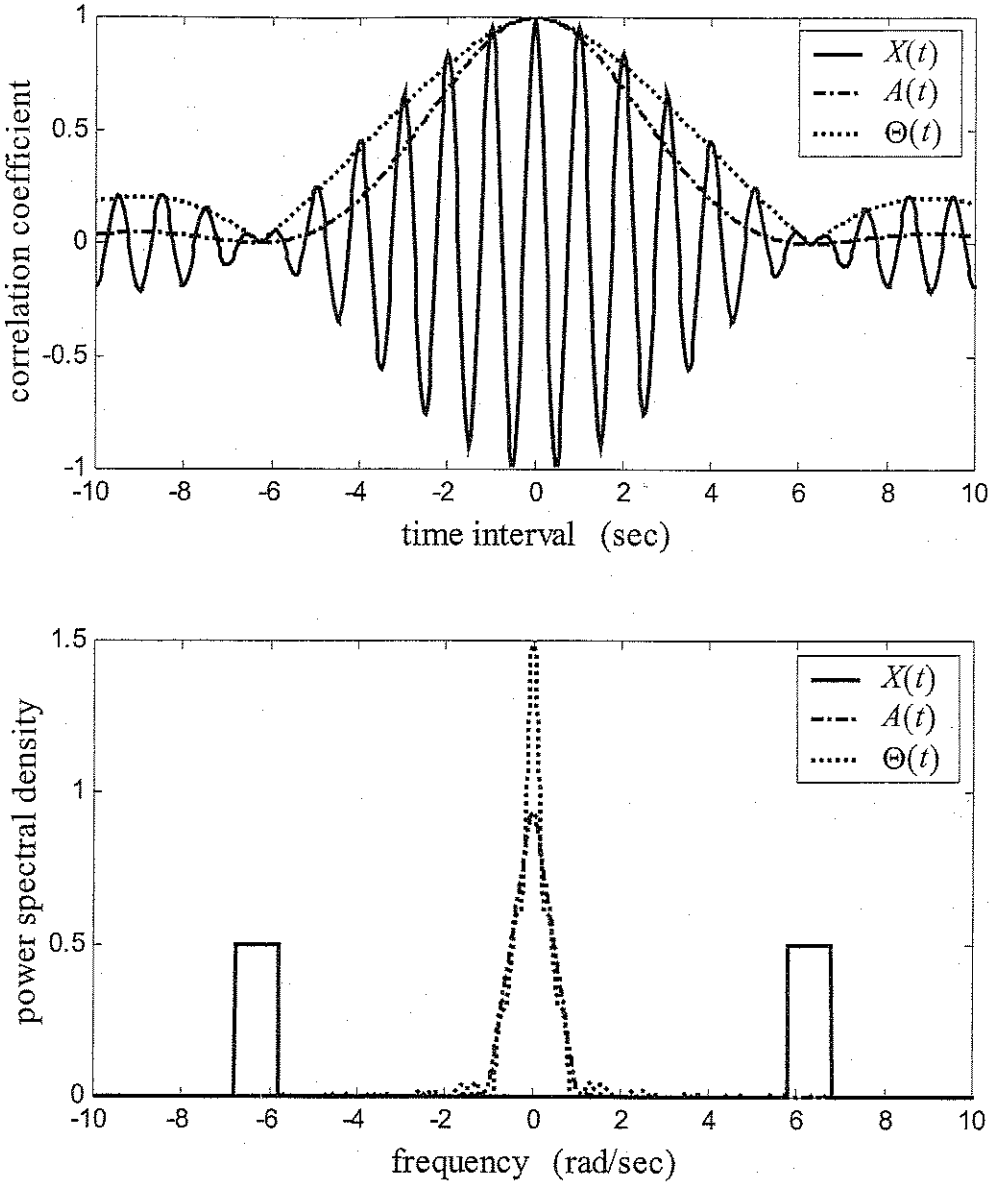

Figure 6.5. Comparison of correlation functions and spectral densities of the process $X(t)$, the envelope process $A(t)$, and the phase process $\Theta(t)$ for $R_{XX}(\tau) = \cos(2\pi\tau)\dfrac{\sin(\tau/2)}{\tau/2}$.

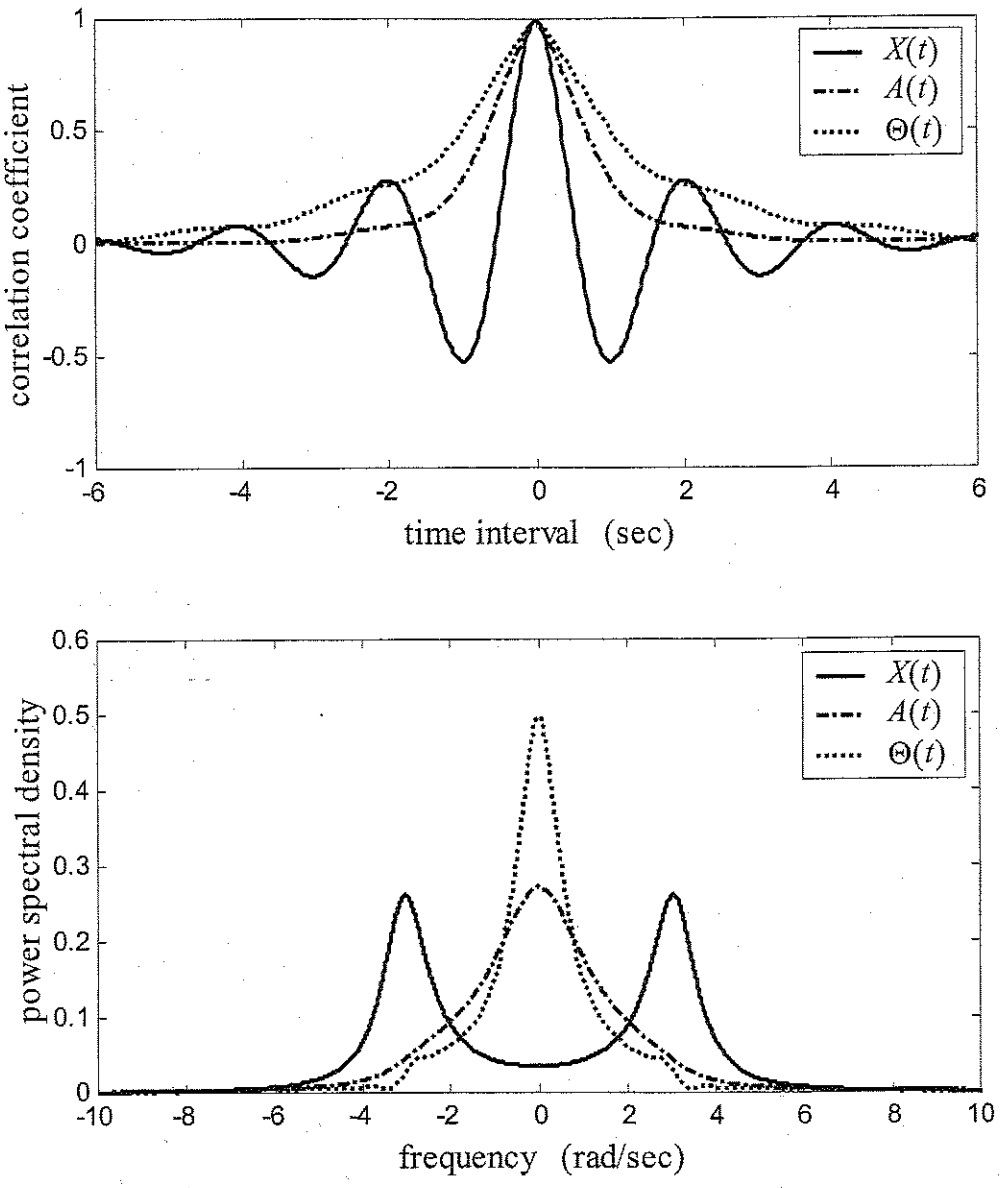

Figure 6.6. Comparison of correlation functions and spectral densities of the process $X(t)$, the envelope process $A(t)$, and the phase process $\Theta(t)$ for the Kanai-Tajimi filtered white noise with $\omega_c = \pi$ rad/sec and $\zeta = 0.2$.

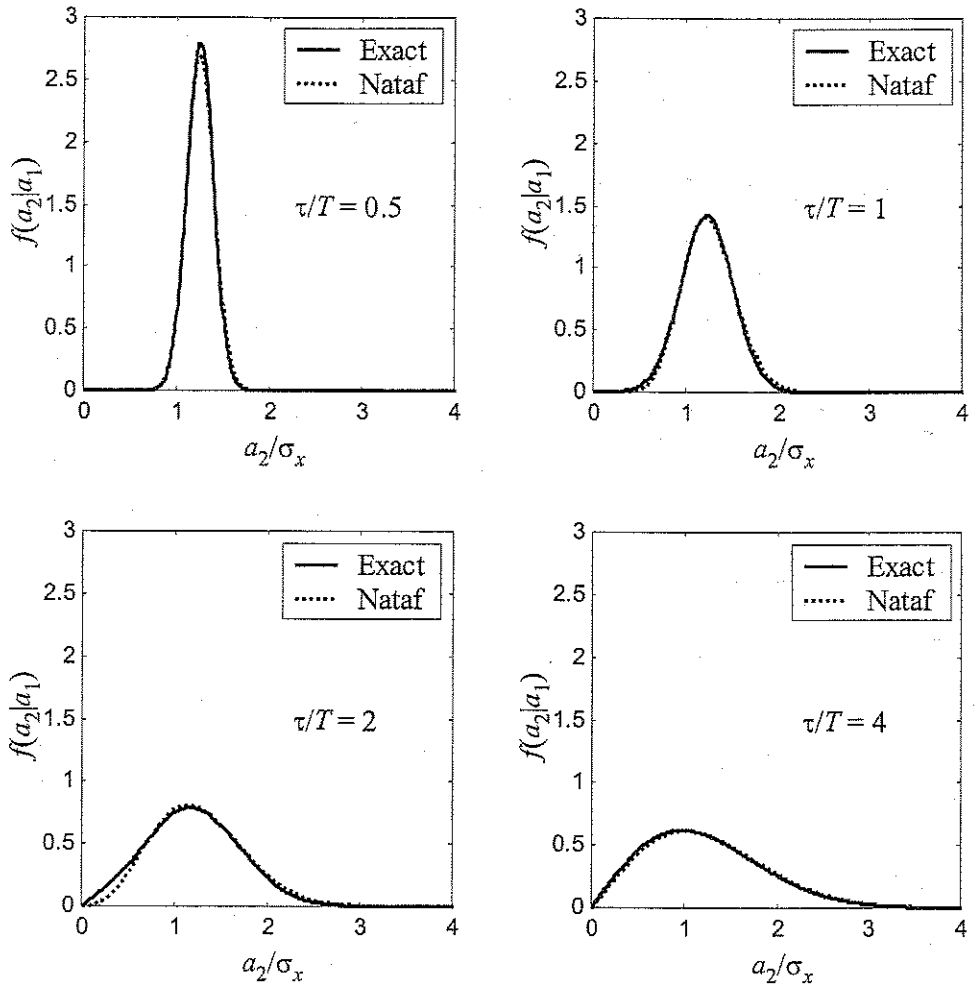

Figure 6.7. Comparison of the exact and Nataf-approximated conditional density functions of the envelope for $a_1 = \mathrm{E}[A(t_1)]$ at selected time lags.

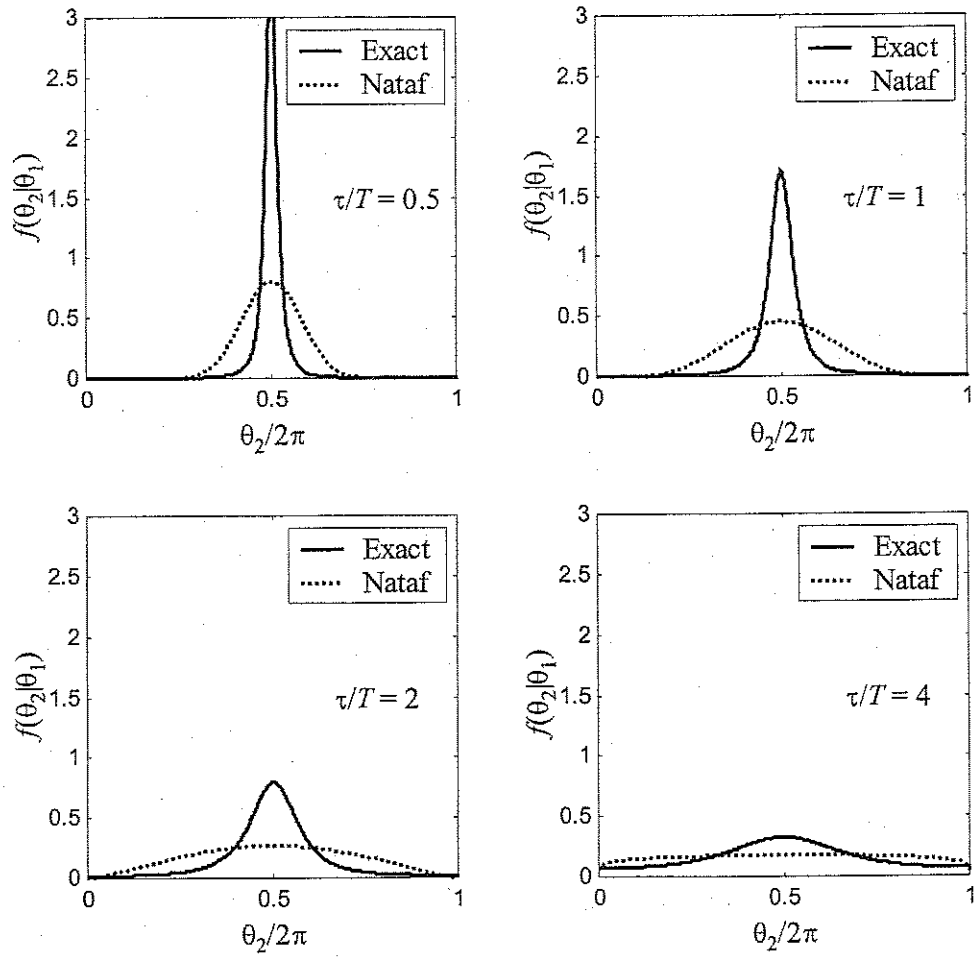

Figure 6.8. Comparison of the exact and Nataf-approximated conditional density functions of the phase for $\theta_1 = E[\Theta(t_1)]$ at selected time lags.

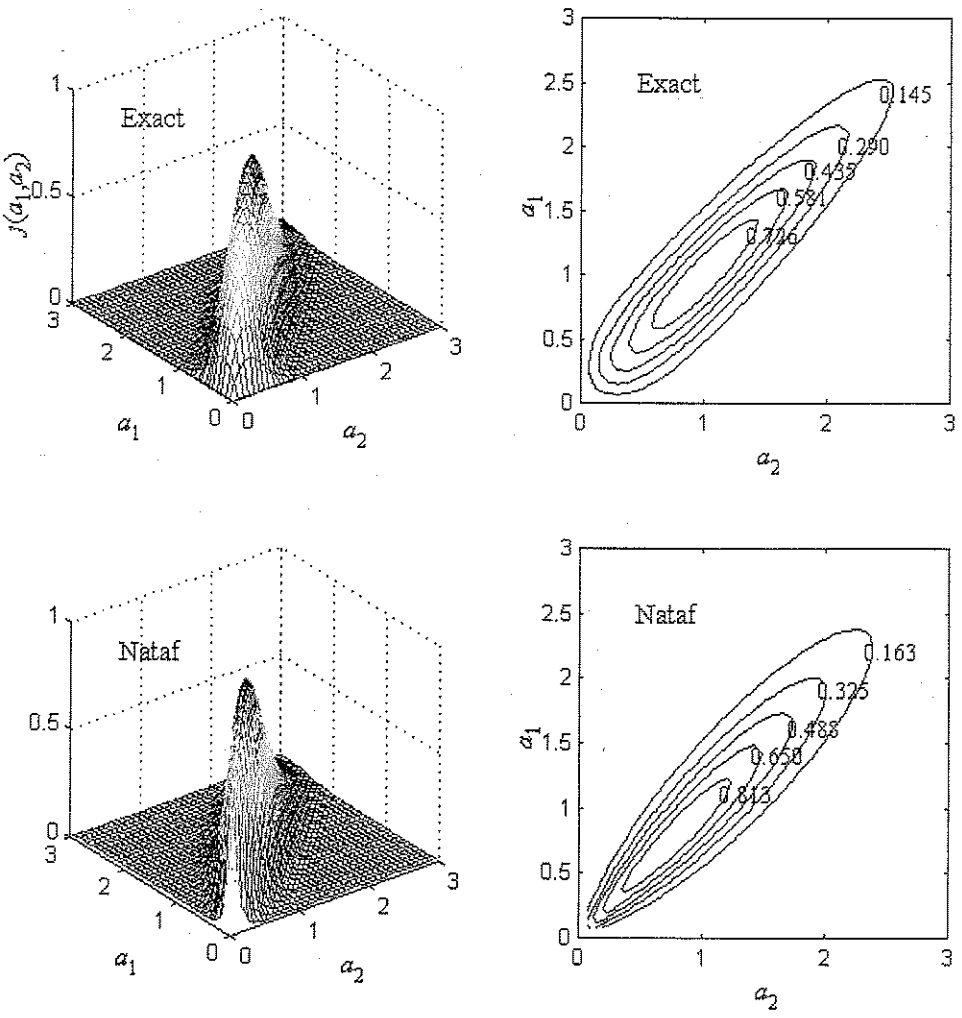

Figure 6.9. The exact joint distribution and Nataf distribution of the amplitudes for the time lag $\tau/T=1$.

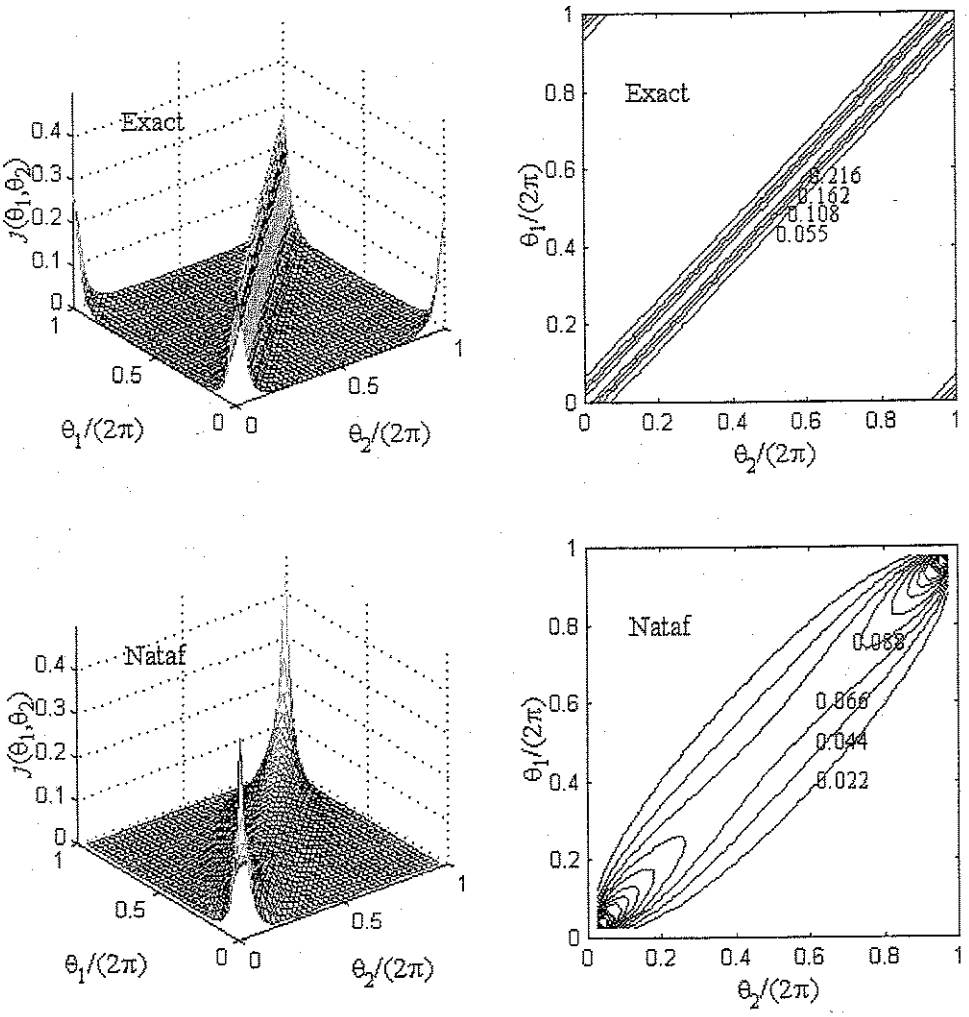

Figure 6.10. The exact joint distribution and Nataf distribution of the phases for the time lag $\tau/T=1$.

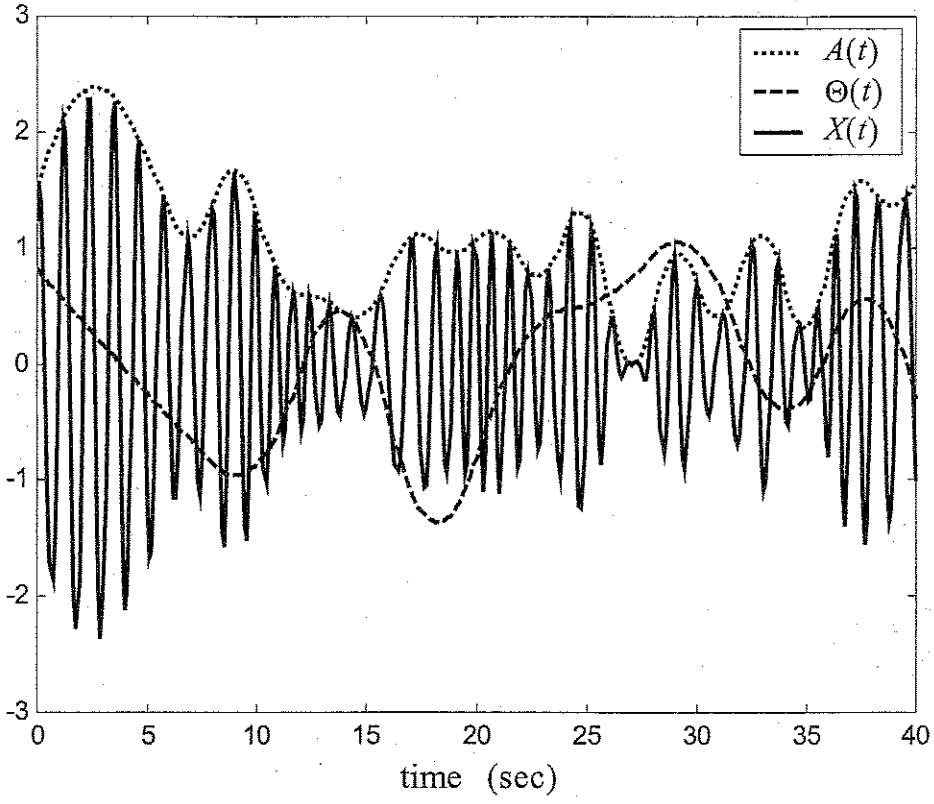

Figure 6.11. Simulated envelope and phase processes with corresponding realization of the parent process.

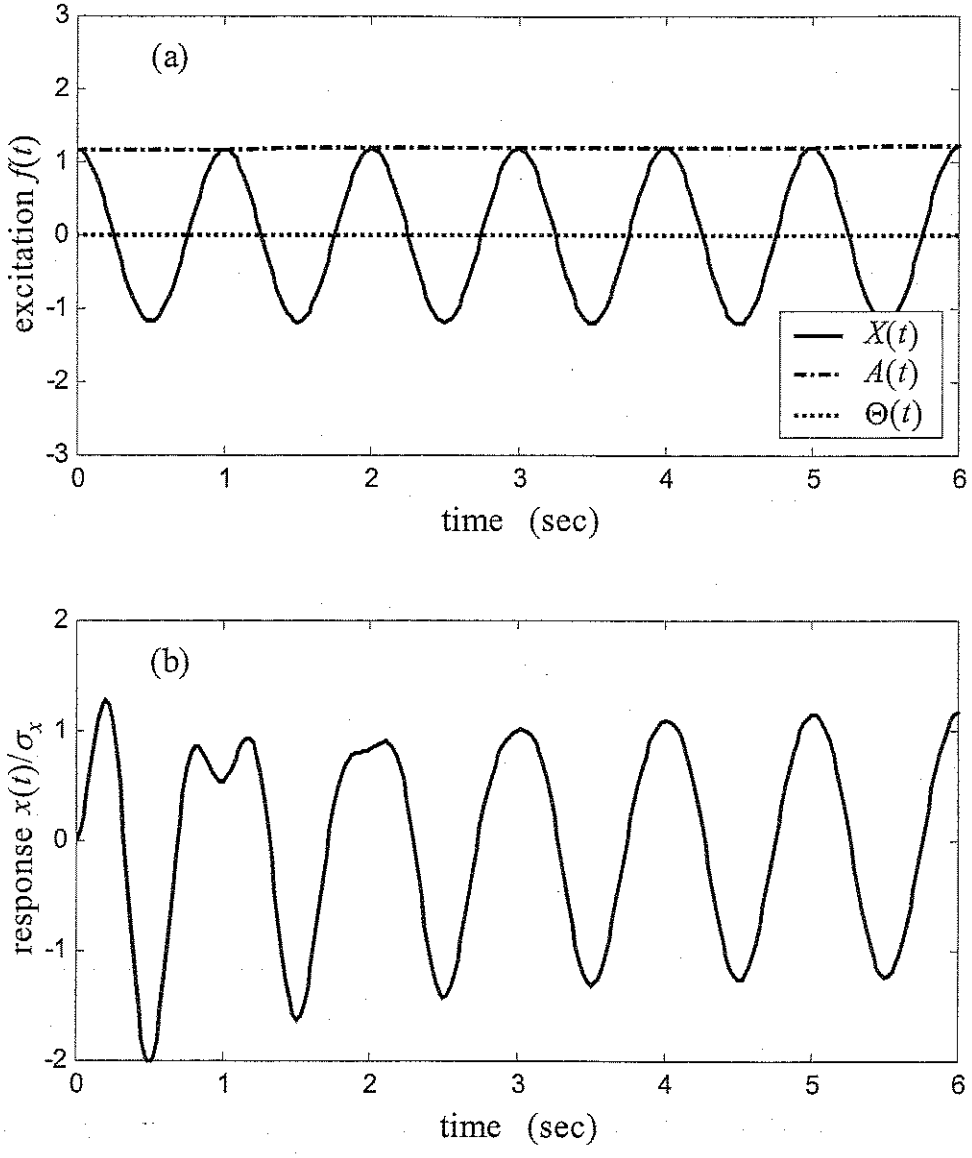

Figure 6.12. (a) Narrowband excitation $f(t)$ when all components of the envelope and phase random vectors are median values, i.e., $a_{i0.5}$ and $\theta_{i0.5}$, $i=1,\cdots,n$, and (b) the response of the linear system to the narrowband excitation.

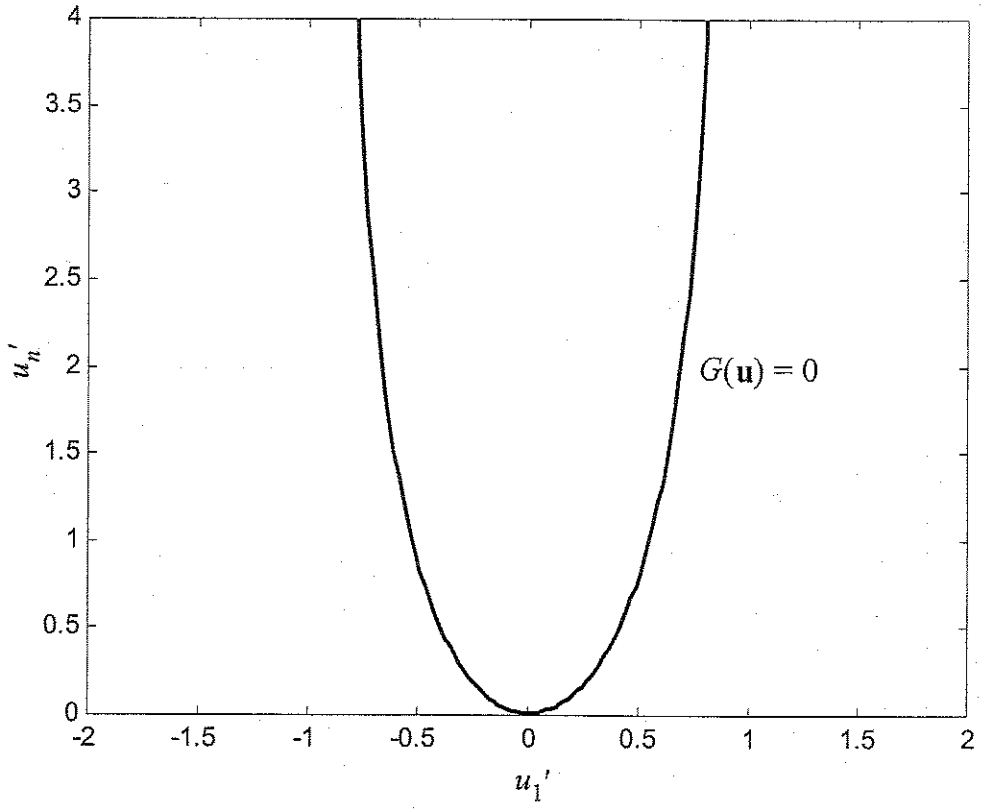

Figure 6.13. Limit-state surface $G(\mathbf{u}) = 0$ along principal axis u_1' for $x_0 = 1.17\sigma_x$.

7 Summary and Conclusions

7.1 Summary of Major Findings

Approximate solution methods for nonlinear random vibration problems are developed using the methods of time-invariant structural reliability. The approach requires a representation of the continuous-parameter input process in terms of a finite number of random variables, and a reformulation of the random vibration problem into one or more limit-state functions for each response statistic of interest. Considered statistics include the distribution of the response at a given time, the mean out-crossing rate, the first-excursion probability, the mean and variance of the cumulative excursion time, the mean duration of a single excursion, and the mean of the cumulative area of excursion. System uncertainties are easily accounted for by considering the system parameters as additional random variables. Standard structural reliability computation methods, such as FORM, SORM and various sampling techniques, are used to approximately estimate these statistics of the nonlinear random vibration response.

A key step in the proposed solution approach is finding the design point, which is the point on a limit-state surface that is nearest to the origin in a transformed standard normal space of the random variables. This involves solving a constrained nonlinear optimization problem, which generally requires iterative calculations of the dynamic response and its gradient for selected realizations of the random variables. Two factors contribute to making this problem challenging: (1) the large number of random variables resulting from the discretization of the input process, and (2) the nonlinear nature of the limit-state function, which may arise from nonlinearity in the system response, non-Gaussian nature of the input process, or uncertainty in the system characteristics. It is known that for a linear oscillator subjected to a Gaussian white noise input, the design-point excitation is proportional to the mirror image of the unit-impulse response function of the oscillator. Motivated by this finding, we investigate the dynamic characteristics of nonlinear oscillators by observing their free vibration and its mirror image. Specifically, the excitation that generates the mirror image of the free vibration is determined. It is

shown that for a nonlinear elastic oscillator subjected to a Gaussian white noise, the design point excitation is identical to the excitation that generates the mirror image of the free vibration response, when the oscillator is released from the target threshold. For more general nonlinear systems, including multi-degree-of-freedom systems, a similar approach leads to an approximate solution of the design point excitation. This solution can be used as a "warm" starting point in the optimization algorithm, thus significantly reducing the computational effort required for finding the exact design point.

Next, we investigate the accuracy and effectiveness of approximate reliability computation techniques, including FORM, SORM and sampling, for solving nonlinear random vibration problems. FORM approximates the limit-state surface by a tangential hyperplane at the design point. Though FORM is the simplest method among the methods investigated in this report, its accuracy is found to be fairly good for most moderately nonlinear random vibration problems. For several examples studied, the FORM approximation is found to be consistently superior to results obtained from the equivalent linearization method for high response thresholds that are of interest in reliability analysis.

SORM is usually used as a refinement tool to improve the accuracy of the FORM approximation. In SORM, the limit-state surface is approximated by a quadratic surface using the principal curvatures at the design points. While SORM usually requires second-derivative calculations, methods are available to compute the principal curvatures with large magnitude in an iterative way by use of the response gradients. However, investigations in this report revealed that for certain nonlinear random vibration problems the shape of the limit-state surface near the design point changes rapidly and, therefore, the curvatures estimated at the design point may not properly represent the shape of the limit-state surface away from the design point. As a result, estimates obtained by SORM may not be reliable. For this reason, SORM approximations are not pursued in this report.

Two sampling techniques are investigated in this report: importance sampling using design points, and sampling on the orthogonal plane. It is found that importance sampling using the design points is an efficient method for approximate solution of random vibration problems involving the distribution of the response. However, this approach is not effective for solving the mean out-crossing rate problem. It is also found

that the sampling on the orthogonal plane is better than or at least equivalent to the important sampling method in its efficiency. Furthermore, this sampling method is found to be effective for solving the mean out-crossing rate problem. Both methods are found to be significantly more efficient than the crude Monte Carlo simulation method.

The next topic of investigation is the first-excursion probability of nonlinear random vibration response. After discretizing the time axis, the first-excursion probability is represented as a series-system reliability problem. This formulation has been used recently to develop an efficient sampling method for computing the first-excursion probability of linear systems. In this report, importance sampling using design points and the sampling on the orthogonal plane methods are used to extend this series-system reliability approach to solving the first-excursion probability of nonlinear systems. Comparisons with the crude Monte Carlo simulation method demonstrate the efficiency and accuracy of the two sampling methods. It is found that the sampling on the orthogonal plane is at least as efficient as the sampling using design points method.

Lastly, an approximate representation of a narrowband Gaussian process in terms of discretized envelope and phase processes using the Nataf distribution model is explored. Second-order joint probability distributions of the envelope and phase processes are investigated and the Nataf distribution model is used to approximate the second- and higher-order joint distributions. With this formulation, it is possible to approximately represent the narrowband process with a relatively small number of random variables (compared to that required if the processes itself is discretized), which is convenient for FORM and sampling analysis. However, application of this method in conjunction with FORM does not produce sufficiently accurate results. Further analysis reveals that the error lies mostly in the Nataf approximation of the second- and higher-order joint distributions of the envelope and phase processes.

7.2 Recommendations for Future Study

Regarding the proposed approach as a solution method for nonlinear random vibration problems, several topics are recommended for future research to improve the efficiency of the solution procedure and the accuracy of the solution.

- Formulation of limit-state functions to describe response statistics of interest. In this report, a number of response statistics, including the distribution at a given time, the mean out-crossing rate, the mean and variance of cumulative excursion time, and the cumulative area of excursion, were formulated. Identification of other response statistics of interest and formulation of corresponding limit-state functions would broaden the scope of application of the proposed methodology.
- Development of a method for efficient representation of a continuous random process. In Chapter 6, we explored approximate generation of a narrowband process in terms of the envelope and phase processes using the Nataf distribution. Though the result is not sufficiently accurate for the reliability analysis, the method is far more efficient in terms of the number of random variables. There can be many other approaches for representation of a continuous random process. For example, one can use the frequency domain analysis to represent a continuous random process. More investigation on the effective representation of a continuous random process is desirable.
- Development of more efficient optimization algorithm to find the design point. In this report we developed an efficient approach to find the design point based on the dynamic characteristic of the oscillator. This approach may not be quite efficient for general nonstationary problems having spectral nonstationarity or strongly non-Gaussian input process. To deal with general problems efficiently, development of more efficient algorithm for finding the design point is necessary.
- Investigation of the geometry of the limit-state surface in high-dimensional standard normal space. When a random vibration problem is solved using the proposed approach, one inevitably has to deal with a large number of random variables. For a high-dimensional nonlinear problem, understanding of the geometry of the limit-state surface can help to develop more accurate solution tools, whether one uses analytical approaches or simulation techniques. Techniques to explore and map the surface in the standard normal space would be useful.

References

1. Abdelrahman, A.M., Yun, C.B., and Wang, P.C. (1978). Subcritical excitation and dynamic response of structures in frequency domain. *Computers & Structures*, 10(2), 761 – 771.

2. Abdo, T., and Rackwitz, R.(1990). A new b-point algorithm for large time-invariant and time-variant reliability problems, *Proceedings of the 3rd IFIP WG 7.5 working conference on reliability and optimization of structural systems,* Der Kiureghian, A. and Thoft-Christensen, P. editors. Springer-Verlag, Berlin, Germany. 26–28.

3. Atalik, T.S., and Utku, S. (1976). Stochastic linearization of multi-degree of freedom nonlinear systems. *Earthquake Engineering and Structural Dynamics*, 4, 411–420.

4. Au, S.K., and Beck, J.L. (2001). First excursion probabilities for linear systems by very efficient important sampling. *Probabilistic Engineering Mechanics*, 16(3), 193–207.

5. Ayyub, B.M., and Chia, C-Y. (1992). Generalized conditional expectation for structural reliability assessment. *Structural Safety*, 11, 131–146.

6. Baber, T.T., and Wen, Y.K. (1981) Random vibration of hysteretic degrading systems, *Journal of Engineering Mechanics*, ASCE, 107(6), 1069 – 1087.

7. Bjerager, P. (1988). Probability integration by directional simulation. *Journal of Engineering Mechanics*, ASCE, 114(8), 1285–1302

8. Bjerager,P., and Krenk, S. (1989). Parametric sensitivity in first-order reliability theory. *Journal of Engineering Mechanics*, ASCE, 115(7), 1577–1582

9. Bouc, R. (1963). Forced vibration of mechanical systems with hysteresis, Abstract, *Proceeding of 4th Conference on Nonlinear Oscillation*, Prague, Chechoslovakia.

10. Breitung, K. (1984). Asymptotic approximations for multi-normal integrals. *Journal of Engineering Mechanics*, ASCE, 110(3), 357–366

11. Butcher, C. (2000). An importance sampling technique for randomly excited systems discretized by finite elements. *Advances in Structural Dynamics*, Vol. II, Elsevier Science Ltd.

12. Caughey, T.K. (1963). Equivalent linearization techniques. *The Journal of the Acoustical Society of America*, 35, 1706–1711.

13. Caughey, T.K. (1971). Nonlinear theory of random vibration. *Advances in Applied Mechanics*, 11, 209–253.

14. Caughey, T.K. (1986). On response of nonlinear oscillators to stochastic excitation. *Probabilistic Engineering Mechanics*, 1(1), 2–4.

15. Caughey, T.K. and Ma, F. (1982). The exact steady-state solution of a class of non-linear stochastic systems. *International Journal of Nonlinear Mechanics*, 17(3), 137 – 142.

16. Chopra, A., (1995). *Dynamics of Structures*. Prentice Hall, Inc., New Jersey.

17. Cramer, H., and Leadbetter, M.R. (1967). *Stationary and Related Stochastic Processes*. New York, Wiley.

18. Crandall, S.H. (1963). Perturbation techniques for random vibrations of nonlinear systems. *Journal of Acoustical Society of America*, 35(14), 1700 – 1705.

19. Crandall, S.H. (1973). Correlation and spectra of nonlinear system response. *Nonlinear Vibration Problems*, Vol. 14. 39 – 53.

20. Crandall, S.H. (1980). Non-Gaussian closure for random vibration of nonlinear oscillators. *International Journal of Nonlinear Mechanics*, 15, 303 – 313.

21. Crandall, S.H. (1985). Non-Gaussian closure techniques for stationary random vibration. *International Journal of Nonlinear Mechanics*, 20(1), 1 – 8.

22. Davenport, W.B., and Root, W.L. (1958) *An Introduction to the Theory of Random Signals and Noise*, Mcgraw-Hill Book Company, Inc., New York.

23. Der Kiureghian, A., Lin, H.-Z., and Hwang, S.-J. (1987). Second-order reliability approximations. *Journal of Engineering Mechanics*, ASCE, 113(8), 1208–1225.

24. Der Kiureghian, A. and De Stefano, M. (1991). Efficient Algorithm for second order reliability analysis. *Journal of Engineering Mechanics*, ASCE, 117(12), 2904–2923.

25. Der Kiureghian, A. and Li, C-C. (1996a). A new method for seismic reliability assessment of nonlinear structures. Chapter 5 in "*Reliability-based optimal aseismic design of reinforced concrete buildings*", Ang, H-S., et al., Final Technical Report to CUREe, April.

26. Der Kiureghian, A. and Li, C-C. (1996b). Nonlinear random vibration analysis through optimization. *Proceedings of the 7th IFIP WG 7.5 working conference on reliability and optimization of structural systems*, Frangopol, D., Rackwitz, R., editors. Pergamon Press. 197 – 206.

27. Der Kiureghian, A. (2000). The geometry of random vibrations and solutions by FORM and SORM. *Probabilistic Engineering Mechanics*, 15(1), 81 – 90.

28. Ditlevsen, O. (1996). Dimension reduction and discretization in stochastic problems by regression method. Chapter 2 in *Mathematical Models for Structural reliability Analysis*, ed. Casciati, F. and Roberts, J.B. CRC, Florida.

29. Ditlevsen, O., and Madsen, H.O. (1996). *Structural Reliability Methods*. J. Wiley & Sons, New York, N.Y.

30. Drenick, R.F. (1970). Model-free design of aseismic structures. *Journal of Engineering Mechanics*, ASCE, 96(4), 483–493.

31. Drenick, R.F. (1973). Aseismic design by way of critical excitation. *Journal of Engineering Mechanics*, ASCE, 99(4), 649 – 667.

32. Drenick, R.F. (1977). The critical excitation of nonlinear systems. *Journal of Applied Mechanics*, ASME, 333–336.

33. Engelund, S and Rackwitz, R. (1993). A benchmark study on importance sampling techniques in structural reliability, *Structural Safety*, 12(4), 255–276.

34. Grigoriu, M. (1993). Simulation of nonstationary Gaussian processes by random trigonometric polynomials. *Journal of Engineering Mechanics*, ASCE, 119(2), 328–343.

35. Grigoriu, M. (1995). *Applied non-Gaussian processes*, PTR Prentice-Hall, Englewood Cliffs, NJ.

36. Hagen, O., and Tvedt, L. (1991). Vector Process out-crossing as parallel system sensitivity measure. *Journal of Engineering Mechanics*, ASCE, 117(10), 2201–2220.

37. Hampl, N.C. (1986). Non-Gaussian stochastic analysis of nonlinear systems. Casciati, F. and Favarelli, L(Eds.): *Preceedings of the 2nd International Workshop on Stochastic Methods in Structural Mechanics*, University Pavia, 243–254.

38. Hasofer, A.M. (1987). Distribution of the maximum of a Gaussian process by a Monte Carlo method, *Journal of Sound and Vibration*.112, 283–293.

39. Hohenbichler, M. and Rackwitz, R. (1981) Non-normal dependent vectors in structural reliability. *Journal of Engineering Mechanics*, ASCE, 107(6), 1227–1238.

40. Hohenbichler, M. and Rackwitz, R. (1988) Improvement of second-order reliability estimates by importance sampling. *Journal of Engineering Mechanics*, ASCE, 114(12), 2195 – 2199.

41. Iyengar, R.N., and Dash, P.K. (1978). Study of the random vibration of nonlinear systems by the Gaussian closure technique. *Journal of Applied Mechanics*, ASME, 45(6), 393 – 399.

42. Iyengar, R.N., and Manohar, C.S. (1987). Nonstationary random critical seismic excitations. *Journal of Engineering Mechanics*, ASCE, 113(4), 529 – 41.

43. Koo, H., and Der Kiureghian A. (2001). "Design point" excitation for stationary random vibrations. *Proceedings of the 8th International Conference On Structural Safety and Reliability*, Newport Beach, CA, June 2001 (CD-ROM).

44. Kraichnan, R.H. (1962). The closure problem of turbulence theory. *Symposium on Applied Mathematics*, American Mathematical Society, Providence, R.I., Vol. 13. 199 – 225.

45. Lambert, J.D. (1991) *Numerical Methods for Ordinary Differential Systems: Initial Value Problem*. John Wiley and Sons.

46. Li, C-C., and Der Kiureghian A. (1993). Optimal discretization of random fields. *Journal of Engineering Mechanics*, ASCE, 119(6), 1136–1154.

47. Li, C-C., and Der Kiureghian A. (1995). Mean out-crossing rate of nonlinear response to stochastic input. *Proceedings of 7th International Conference on Applications of Statistics and Probability (ICASP) in Civil Engineering Reliability and Risk Analysis*, Lemaire, M., Favre, J-L., and Mbarki, A, editors, Paris, France, 295-302.

48. Lin, Y.K. (1967). *Probabilistic theory of structural dynamics*, McGraw-Hill Inc., New York.

49. Lin, Y.K., and Cai, G.Q. (1995). *Probabilistic theory of structural dynamics - Advanced Theory and Applications*, McGraw-Hill Inc., New York.

50. Lin, A. (1988). *A Numerical evaluation of the method of equivalent nonlinearization*. Ph.D. Thesis, California Institute of Technology. Pasadena, CA.

51. Liu, P.-L., and Der Kiureghian, A. (1986). Multivariate distribution models with prescribed marginals and covariances. *Probabilistic Engineering Mechanics*, 1(2), 105–112.

52. Liu, P.-L., and Der Kiureghian, A. (1991). Optimization algorithms for structural reliability. *Structural Safety*, 9, 161–177.

53. Liu, P.-L., Lin, H.-Z., and Der Kiureghian, A. (1989). *CALREL User Manual*. Report No. UCB/SEMM-89/18, the Department of Civil Engineering, University of California, Berkeley, CA.

54. Lambert, J.D. (1991). *Numerical Methods for Ordinary Differential Systems: The initial Value Problem*. John Wiley and Sons.

55. Loève, M. (1977). *Probability theory*. Springer-Verlag, 4th Ed., New York.

56. Lutes, L.D. (1970). Approximate technique for treating random vibration of hysteretic systems. *Journal of Acoustical Society of America*, 48, 200–306

57. Lutes, L.D., and Sarkani S. (1997). *Stochastic analysis of structural and mechanical vibrations*. Prentice Hall, Inc., New Jersey.

58. Macke, M. (2000). Variance reduction in Monte Carlo simulation of dynamic systems. *Proceedings of 13th ASCE Engineering Mechanics Division Conference*, Melchers, R.E. and Stewart, M.G. editors. Sydney, Australia. 797 – 894.

59. Manohar, C.S., and Sarkar, A. (1995). Critical earthquake input power spectral density function models for engineering structures. *Earthquake Engineering and Structural Dynamics*, 24, 1549 – 1566.

60. Melchers, R.E. (1989). Importance sampling in structural systems. *Structural Safety*, 6, 3–10.

61. Middleton, D. (1960). *An Introduction to Statistical Communication Theory*, McGraw-hill Book Company, Inc. New York.

62. Newmark, N.M., (1959). A method of computation for structural dynamics. *Journal of Engineering Mechanics*, ASCE, 85, 67–94.

63. Nigam, N.C. (1983). *Introduction to Random Vibrations*, MIT Press, Cambridge, MA, 1983.

64. Price, R. (1955). *Some Results in the Study of Narrow-band Gaussian Noise*. Lincoln Laboratory, MIT, Lexington, Massachusetts.

65. Rice, S.O. (1944, 1945). Mathematical analysis of random noise. *The Bell System Technical Journal*, 23, 282–332 (1944), 24,46 – 156 (1945).

66. Roberts, J.B. (1981). Response of nonlinear mechanical systems to random excitation. *The Shock and Vibration Digest*, 13(4), 17 – 28, 13(5), 15 – 29.

67. Roberts, J.B. (1984). Techniques for nonlinear random vibration problems. *The Shock and Vibration Digest*, 16(9), 3 – 14.

68. Roberts, J.B. (1986). First passage probabilities for randomly excited systems: Diffusion methods. *Probabilistic Engineering Mechanics*, 1(2), 66 – 81.

69. Roberts, J.B., and Dunne, J.F. (1988). Nonlinear random vibration in mechanical systems. *The Shock and Vibration Digest*, 20(6), 16 – 25.

70. Roberts, J.B. (1989). *Averaging Methods in Random Vibration, Technical University of Denmark*, Lyngby, Denmark.

71. Roberts, J.B., and Spanos, P.D. (1986). *International Journal of Nonlinear Mechanics*, 21(2), 111 – 134.

72. Roberts, J.B., and Spanos, P.D. (1990). *Random vibration and statistical linearization*, John Wiley & Sons, Ltd. England.

73. Rubinstein, R.Y. (1981). *Simulation and the Monte Carlo Method.* John Wiley & Sons, New York.

74. Schueller, G.I., and Bucher, C.G. (1986). Nonlinear damping and its effects on the reliability estimates of structures. *Random Vibration: Status and Recent Developments*, Elishakoff, I. and Lyon, R.H. Editors. the Stephen Harry Crandall Festschrift, Amsterdam: Elsvier, 1986, 389 – 402.

75. Schueller, G.I., and Stix, R. (1987). Critical appraisal of methods to determine failure probabilities, *Structural Safety*, 4, 293–309.

76. Shinozuka, M. (1970). Maximum structural response to seismic excitations, *Journal of Engineering Mechanics*, ASCE, 96(5), 729–738

77. Shinozuka, M. (1972). Monte Carlo solution of structural dynamics, *Computers & Structures*, 2, 855–874.

78. Spanos, P.D., and Lutes, L.D. (1986). A primer of random vibration techniques in structural engineering, *The Shock and Vibration Digest*, 18, 3–10.

79. Soize, C. (1994) *The Fokker-Planck equation for stochastic dynamical systems and its explicit steady state solutions*, vol. 17. In: Advances in mathematics for applied sciences. World Scientific.

80. Soong, T.T., and Grigoriu, M. (1993). *Random Vibration of Mechanical and Structural Systems*. Prentice Hall, Englewood Cliffs, NJ.

81. Srinivasan, M., Ellingwood B., and Corotis, R. (1991). Critical base excitations of structural systems, *Journal of Engineering Mechanics*, ASCE, 117(6), 1403–1422.

82. Stratonovitch, R.L. (1964). *Topics in the Theory of Random Noise*, Vol 2. Gordon and Breach, NY.

83. Sudret, B., and Der Kiureghian, A. (2002). Comparison of finite element reliability methods, *Probabilistic Engineering Mechanics*, 17(4), 337 – 348.

84. Takewaki, I. (2002). Critical excitation for elastic-plastic structures via statistical equivalent linearization, *Probabilistic Engineering Mechanics*, 17, 73–84.

85. To, C.W.S. (2000) *Nonlinear random vibration – Analytical techniques and Applications*, Swets & Zeitlinger Publishers, the Netherlands, 2000.

86. Tsay, J.J., and Arora, J.S. (1990) Nonlinear structural design sensitivity analysis for path dependent problems. Part I: General theory. *Comp. Methods Appl. Mech. Eng.*,81,183–208

87. Tvedt, L. (1990). Distribution of quadratic forms in normal space – application to structural reliability, *Journal of Engineering Mechanics*, ASCE, 116(6), 1183–1197.

88. Uhlenbeck, G.E. (1943). *Theory of Random Process*. Radiation Laboratory, MIT, Lexington, Massachusetts.

89. Wang, P.C., and Yun, C.B. (1979). Site dependent critical design spectra. *Earthquake Engineering and Structural Dynamics*, 7(5), 569 – 578.

90. Wen, Y.K. (1976) Method for random vibration of hysteretic systems, *Journal of Engineering Mechanics*, ASCE, 102(4), 249–263.

91. Wen, Y.K. (1980) Equivalent linearization for hysteretic systems under random excitation, *Journal of Applied Mechanics*, ASME, 47(3), 150–154.

92. Zhang, Y., and Der Kiureghian A. (1993). Dynamic response sensitivity of inelastic structures. *Comp. Methods Appl. Mech. Eng.*, 108, 23–36.

93. Zhang, Y and Der Kiureghian A. (1994). Two improved algorithms for reliability analysis. *Proceedings of the 6th IFIP WG 7.5 working conference on reliability and optimization of structural systems,* Rackwitz R, Augusti G, Borri A, editors, Chapman and Hall, Assisi, Italy. 297–304.

94. Zhang, Y and Der Kiureghian A. (1997). *Finite Element Reliability Methods for Inelastic Structures.* U.C. Berkeley, Berkeley, California.

95. Zhang, Y and Ellingwood, B. (1994). Orthogonal series expansions of random fields in reliability analysis. *Journal of Engineering Mechanics*, ASCE, 120(12), 2660–2677

96. Zhu, W.Q. and Yu, J.S. (1989) The equivalent nonlinearization system method. *Journal of Sound and Vibration*, 129, 389–359.

Appendix A Formula for Bi-variate Normal Probability

Consider the bi-variate standard normal cumulative probability function with correlation coefficient ρ_{12}, defined by

$$\Phi_2(u_1,u_2,\rho_{12}) = \Phi(u_1)\Phi(u_2) + \int_0^{\rho_{12}} \varphi_2(u_1,u_2,\rho)d\rho \tag{A.1}$$

where $\varphi_2(u_1,u_2,\rho)$ is the bi-variate standard normal probability density function with zero means, unit variances and correlation coefficient ρ.

Our interest is in the special case where $u_2 = -u_1$ and $\rho_{12} = -1+\delta\rho$, where $\delta\rho > 0$ is close to zero. For this special case, the integral in (A.1) can be reduced into a simple expression, as shown below. First, observe that

$$\Phi_2(u_1,-u_1,-1) = 0 \tag{A.2}$$

It follows that

$$\lim_{\delta\rho\to 0} \int_0^{-1+\delta\rho} \varphi_2(u_1,-u_1,\rho)d\rho = -\Phi(u_1)\Phi(-u_1) \tag{A.3}$$

For our special case, (A.1) can be written as

$$\begin{aligned}
\Phi_2(u_1,-u_1,-1+\delta\rho) &= \Phi(u_1)\Phi(-u_1) + \int_0^{-1+\delta\rho} \varphi_2(u_1,-u_1,\rho)d\rho \\
&= \Phi(u_1)\Phi(-u_1) + \int_0^{-1} \varphi_2(u_1,-u_1,\rho)d\rho + \int_{-1}^{-1+\delta\rho} \varphi_2(u_1,-u_1,\rho)d\rho \\
&= \int_{-1}^{-1+\delta\rho} \varphi_2(u_1,-u_1,\rho)d\rho \\
&= \frac{1}{2\pi}\int_{-1}^{-1+\delta\rho} \frac{1}{\sqrt{1-\rho^2}} \exp\left(-\frac{u_1^2}{1-\rho}\right)d\rho
\end{aligned} \tag{A.4}$$

Considering that $\rho \approx -1$ in the narrow range of the integration, the exponential term is nearly constant and can be taken out of the integral, yielding the approximation

$$\Phi_2(u_1,-u_1,-1+\delta\rho) \approx \frac{1}{2\pi}\exp\left(-\frac{u_1^2}{2}\right)\int_{-1}^{-1+\delta\rho}\frac{1}{\sqrt{1-\rho^2}}d\rho$$

$$\approx \frac{1}{2\pi}\exp\left(-\frac{u_1^2}{2}\right)\left[\sin^{-1}(-1+\delta\rho)-\sin^{-1}(-1)\right] \qquad \text{(A.5)}$$

Table A.1 compares solutions obtained by the above formula with results obtained by numerical integration of (A.1) with a high level of accuracy. The comparison is made for a range of u_1 and $\delta\rho$ values that are of interest in the estimation of the mean out-crossing rate. It is seen that the simple expression in (A.5) for the bi-variate probability provides excellent accuracy for all the parameter values considered.

Table A.1. Comparison of the results of the numerical evaluation of (A.1) and the approximation formula (A.5).

$u_1 = -u_2$	δρ	Numerical Evaluation of (A.1)	Approximation Formula (A.5)
2	1E–2	3.03E–3	3.05E–3
	1E–3	9.52E–4	9.64E–4
	1E–4	2.93E–4	3.05E–4
	1E–5	8.51E–5	9.64E–5
3	1E–2	2.48E–4	2.50E–4
	1E–3	7.84E–5	7.91E–5
	1E–4	2.43E–5	2.50E–5
	1E–5	7.23E–6	7.91E–6
4	1E–2	7.44E–6	7.56E–6
	1E–3	2.37E–6	2.39E–6
	1E–4	7.39E–7	7.55E–7
	1E–5	2.23E–7	2.39E–7